DIETARY AND PROTEIN MODIFIERS OF COLITIS-ASSOCIATED CARCINOMA: SELENIUM, SELENOPROTEINS, AND MYELOID TRANSLOCATION GENES AND THEIR IMPACTS ON INFLAMMATION, STEM CELL PROPERTIES, AND OXIDATIVE STRESS

By

Caitlyn Whitten Barrett

Dissertation

Submitted to the Faculty of the

Graduate School of Vanderbilt University

in partial fulfillment of the requirements

for the degree of

DOCTOR OF PHILOSOPHY

in

Cancer Biology

December, 2013

Nashville, Tennessee

Dr. Christopher Williams, MD, PhD

Dr. Albert Reynolds, PhD

Dr. Raymond Burk, MD

Dr. Scott Hiebert, PhD

Dr. Barbara Fingleton, PhD

To my loving parents, both by blood and marriage,

Edward and Catherine Whitten and William and Linda Barrett

and

To my beloved husband, Paul, without whom none of this would be possible and our beautiful son Mason

ACKNOWLEDGEMENTS

This work would not have been possible without the financial support of the Cellular, Biochemical, and Molecular Sciences (CBMS) training grant (NIH T32 GM08554) and an F31 provided by the NIH for the project “Selenium and Selenoprotein P Modify Colorectal Tumorigenesis” (F31CA167920).

I gratefully acknowledge my advisor, Dr. Christopher Williams, for allowing me the opportunity to pursue my graduate career in his laboratory. I am especially grateful for his willingness to allow me to work on multiple projects in a wide range of topics and using an even broader range of techniques. There is no way that I could have obtained a better training experience than I have in the Williams Lab. Chris has allowed me the freedom to pursue topics that thrill me and has shared in my excitement about my projects and the methods we developed to answer the questions that arose within these projects. Dr. Williams has been an exceptional mentor and I feel honored to have been his first graduate student.

I would also like to thank the members of my committee for their dedication in overseeing me and encouraging me throughout the course of these projects. Each member has definitive fingerprints on all of my projects and the progression of my career as well as the expansion of my understanding has all been reliant on each of my committee members. Dr. Albert Reynolds, my chair, has been a wealth of knowledge regarding not only one of his many specialties Kaiso, but also tumorigenesis, mechanistic pathways, and WNT signaling. Moreover, he has always emphasized the importance of

mechanistic insight and the edification of my knowledge base in all areas of science. Dr. Raymond Burk came to me and Chris with the selenium and selenoprotein projects which have been the greatest successes in my career. Dr. Burk has been a constant support and has taught me more about a protein family that, until two years ago I had never heard of, than I know about any other group of proteins with which I have worked. It is because of Dr. Burk that I will continue my career at the University of Pittsburgh in a lab that studies selenoproteins in Parkinson's disease and that I will be able to ensure that this new lab performs selenium experiments correctly. I will never forget our long conversations about selenium metabolism, debates in the selenium field, and the exciting adventures that Ray had during his graduate and medical studies. Dr. Burk has been a true inspiration to me and I appreciate his passion for the proteins to which he has dedicated his entire scientific career. I am grateful to Dr. Scott Hiebert for his biochemical perspective without which I would be missing a good deal of my education. I am also immensely grateful for the days that I have spent in his lab discussing the MTGs as an equal. Dr. Hiebert has always approached scientific conversations with me as a way to both teach me and learn from me and I cannot begin to thank him enough for helping me develop confidence in my ability to explain my work and the skills that I will carry into my future regarding scientific thought. Last, but certainly not least, I am thankful for Dr. Barbara Fingleton. The only member of my committee without a vested interest in one of my proteins of interest, she has been able to introduce me to second and third dimensions within my projects. Her expertise in inflammation and the model system that I use has been invaluable and her willingness to teach me techniques, thought processes, and inflammatory pathways has

enriched my graduate school experience. Barbara has spent very large portions of her time with me and, in doing so, has taught me what it is to be a productive, compassionate, and fun scientist. Dr. Fingleton is the model for the scientist that I would one day like to become. She says that she needs to learn to say “no”, but I think that is what makes her one of the most successful scientists and people I have ever met.

I also owe a debt of gratitude to the Burk lab, specifically Dr. Kris Hill. Dr. Hill has spent countless hours patiently helping me understand the finer details of selenium metabolism and selenoprotein functions. Kris has read through all of my selenium manuscripts and helped me design several experiments to greatly enhance my work. I am also infinitely grateful for Amy Motley who has not only run all of my selenium measurement assays, but has been immensely supportive of me as I have navigated intricacies of selenium research. Teri Stevenson and Michelle Chatterton have been incredibly helpful with the provision of mice and help with genotyping protocols and, in general, the Burk lab has been incredibly generous with their time, reagents, and mice. The projects outlined in this thesis would not have been possible without the Burk lab.

I would like to thank members of the Williams lab for their support throughout my studies. I cannot think of a more dedicated, helpful, or fun lab and I am so grateful for the aid and kindness that each member, both past and present, has bestowed upon me. Hours in the procedure room and in conversation about our various projects has taught me the value of friendship within the lab. It will be impossible for another lab to take the place of the Williams Lab in my heart. I doubt I will ever be able to work with such a group

again, but I will strive to carry all that I have learned from each of you into my future career and interactions.

Finally, I would be remiss if I didn't recognize those that have supported me outside of the lab, insuring that I maintain balance in my life. During my first year in the IGP here at Vanderbilt, I met a man that would change my life. From day one, Paul Barrett has been my rock. He has supported me through the trials of science and life. When I spent 3 months trying to get enteroids to grow and when my grandmother passed away, he was there for me. He has edited all of my papers, watched every one of my presentations, and the day that I married him I made the best decision of my life. Paul also brought a supportive and loving family into my life. William and Linda Barrett are some of the most caring people I have ever known and their support has meant the world to me. I also have two new sisters who have welcomed me into their family with open arms. Ultimately, I must recognize the people who have seen me through the entirety of my life and gotten me to the place I am today. My parents and siblings are the greatest blessing in my life. They have trained me in who I should be and pushed me to be the best person possible. My mom, Catherine, has always been willing to listen to me and help me through difficult times and my father, Edward, has instilled in me the work ethic that has insured my graduate school success. My brother, Charlie, has been a constant inspiration. His music has moved me, and his company has taught me the value of close family. His living here in Nashville has truly made my experience exceptional. My sister, Carlyn, throughout the course of my life, has shown me that you absolutely have to do what you

love and love what you do. Her constant joy and bright disposition has helped me through many difficulties.

I have had the support of so many people during my graduate career and am infinitely thankful for each person that has touched my life.

TABLE OF CONTENTS

Page

LIST OF TABLES

LIST OF FIGURES

LIST OF ABBREVIATIONS

8-OHdG	8-Hydroxy-2'deoxyguanosine
ACF	Aberrant crypt foci
AML	Acute myeloid leukemia
AOM	Azoxymethane
APC	Adenomatous polyposis coli
ATF	Activating Transcription Factor
ATOX1	Antioxidant protein 1 homolog
Bcl-6	B-cell lymphoma 6
Bmp8b	Bone morphogenetic protein 8b
BOSS	Biomarkers of oxidative stress study
Ccl20	Chemokine (C-C motif) ligand 20
Ccl27	Chemokine (C-C motif) ligand 27
CD	Crohn's disease
CDKN2A	Cyclin-dependent kinase inhibitor 2A
ChIP	Chromatin immunoprecipitation
CI	Confidence interval
COX2	Cyclooxygenase 2
CRC	Colorectal cancer
CSDE1	Cold shock domain containing E1
CTCF	CTC-binding factor

CTF1	Cardiotrophin 1
Cxcl13	Chemokine (C-X-C) motif ligand 13
Cyp	Cytochrome P450
Cys	Cysteine
D1	Type 1 deiodinase
DKO	Double knockout
DSS	Dextran sodium sulfate
Dvl	Disheveled
EF	Elongation factor
Efn	Ephrin
EGF	Epidermal growth factor
EHT	Eto homologous on chromosome twenty (AKA MTGR1)
EMT	Epithelial-mesenchymal transition
ETO	Eight twenty-one (AKA MTG8)
F_2-IsoP	F_2-Isoprostane
Gdf1	Growth differentiation factor 1
Gfi1	Growth factor independent 1
Gpx	Glutathione peroxidase
GSH	Glutathione
GSTM2	Glutathione S-transferase M2
GSTτ1	Glutathione S-transferase theta 1
H_2O_2	Hydrogen peroxide

HDAC	Histone deacetylase
HEB	Human B-HLH factor
HNF-4α	Hepatocyte nuclear factor 4 alpha
HPF	High-powered field
HPRT	Hypoxanthine-guanine phosphoribosyltransferase
IBD	Inflammatory bowel disease
IFNγ	Interferon gamma
IFNκ	Interferon kappa
IGF1	Insulin-like growth factor 1
IHC	Immunohistochemistry
IL-17c	Interleukin 17c
IL-1β	Interleukin 1 beta
IL-23	Interleukin 23
IL-23a	Interleukin 23a
iNOS	Inducible nitrous oxide synthase
KBS	Kaiso binding site
LOH	Loss of heterozygosity
LPS	Lipopolysaccharide
LRH1	Liver receptor homolog 1
Lrig1	Leucine-rich repeats and immunoglobulin-like domains 1
MAPK	Mitogen-activated protein kinase
MCR1	Melanocortin 1 receptor

MEICS	Murine endoscopic index of colitis severity
MLH	MutL homolog
MMP	Matrix metalloproteinase
MTA2	Metastasis-associated 2
MTG16	Myeloid translocation gene on chromosome 16
MTG8	Myeloid translocation gene on chromosome 8
MTGR1	MTG-related protein 1
Mx1	Myxovirus (influenza virus) resistance 1
NCF2	Neutrophil cytosolic factor 2
N-CoR	Nuclear co-repressor (AKA SMRT)
NF-κB	Nuclear factor kappa B
NHR	Nervy homology region
NPC	Nutritional prevention of cancer trial
Nrf2	Nuclear Factor (Erythroid-Derived 2)-Like
Nrg4	Neuregulin 4
Nrx	Nucleoredoxin
OXSR1	Oxidative stress responsive 1
$p120^{ctn}$	p120-catenin
PDK1	Pyruvate dehydrogenase kinase isoenzyme-1
PI	Propidium iodide
PLZF	Promyelotic leukemia zinc finger
POZ-ZF	Pox virus and zinc finger-zinc finger

RNI	Reactive nitrogen intermediate
RNS	Reactive nitrogen species
ROS	Reactive oxygen species
SBP2	SECIS-binding protein 2
Se	Selenium
Sec (U)	Selenocysteine
SECIS	Selenocysteine insertion sequence
Sepp1	Selenoprotein P
SIR	Standardized incidence ratio
SNP	Single nucleotide polymorphism
SOD3	Superoxide dismutase 3
STAT3	Signal transducer and activator of transcription 3
t(16;21)	Translocation between the 16th and 21st chromosome
t(8;21)	Translocation between the 8th and 21st chromosome
TAF110	TBP-associated factor 110
TAL1	T-cell acute lymphocytic leukemia 1
TGFα	Transforming growth factor alpha
TGFβ	Transforming growth factor beta
TLR4	Toll-like receptor 4
TNFα	Tumor necrosis factor alpha
Tpo	Thyroid peroxidase
Trit1	$tRNA^{[Ser]Sec}$-isopentenyl-transferase

$tRNA^{[Ser]Sec}$	Selenocysteine-specific tRNA
TrxR1	Thioredoxin reductase 1
UC	Ulcerative colitis
UTR	Untranslated region
WT	Wild-type
ZBTB	Zinc finger and BTB domain containing

CHAPTER I

INTRODUCTION

Overview: Inflammatory bowel disease and colitis-associated carcinoma

Cancers of the digestive tract are a significant healthcare burden. In America in 2008 alone, more than 135,000 are estimated to have died of cancers of the digestive system (1). A large percentage of cancers of the digestive system arise because of chronic inflammation including hepatocellular carcinoma which can result from viral hepatitis, esophageal adenocarcinoma, which often arises from Barrett's esophagus, gastric cancer, frequently caused by *Helicobacter pylori*-induced gastritis, and colon cancer, which can result from inflammatory bowel disease (IBD) (2). IBD is comprised of two types of chronic inflammatory disorders of the intestine: Crohn's disease (CD) and ulcerative colitis (UC). IBD affects approximately 1.4 million Americans with typical onset occurring between 15 and 30 years of age (3). While the etiology of IBD is incompletely understood, evidence suggests that IBD is the result of inappropriate inflammatory responses to intestinal microbes which is dependent on genetic susceptibility in the host (4). In fact, prevailing thought presents the model that 1) microbes or other undefined environmental exposure, 2) genetic susceptibility, and 3) inappropriately sustained and severe autoimmune inflammatory response leads to repetitive inflammatory injury to the gastrointestinal tract.

There is constant debate in the field regarding the level of risk for colorectal cancer (CRC) in patients with IBD which is greatly dependent on the set-up and analysis of epidemiological data. A large single academic center study focused on histopathology of IBD patients and risk of CRC demonstrated that histologically severe inflammation was present in 41.4% of patients with dysplasia and 24.1% with CRC, but only 4.3% in controls. Moreover, annual risk for dysplasia or CRC was increased 4.5% with longer disease duration implicating disease severity and duration in risk of developing CRC (5). Patients with IBD (standardized incidence ratio (SIR), 2.2; 95% confidence interval (CI) 1.5-3.0) and long-standing extensive colitis (SIR, 7.0; 95% CI 4.4-10.5) are at increased risk for CRC, although the risk is lower among patients receiving thiopurine therapy (6) indicating that treatment should be taken into account when analyzing risk of CAC.

A meta-analysis of population-based data on cancer risk in CD revealed that there is an increased risk of CRC among people with CD (SIR, 1.9; 95% CI 1.4-2.5) (7) while a similar study analyzing UC revealed that men with UC have a greater risk of CRC (SIR, 2.6; 95% CI 2.2-3.0) than women (SIR, 1.9; 95% CI 1.5-2.3) and that young age at disease onset (SIR, 8.6; 95% CI 3.8-19.5) and extensive colitis (SIR, 4.8; 95% CI 3.9-5.9) were both risk factors for CRC (8) implicating sex, age, and extent of colitis in risk determination. The risks outlined in the above studies represent values that are lower than those historically noted for CAC risk in IBD, but the risk depends on age of IBD diagnosis, disease duration, disease severity, and efficacy of therapies and IBD management (9-13). Moreover, more effective anti-inflammatory treatment as well as more effective surveillance has likely led to the decrease in the observed association. Importantly, increased disease activity is

associated with increased risk so understanding modifiers of IBD severity and CAC risk factors are of paramount importance.

Unlike sporadic CRC there is no established genetic alteration associated with CRC predisposition in IBD. It is hypothesized that it is the chronic inflammation characteristic of IBD that causes cancer. In support of his hypothesis, CAC incidence increases with longer duration and greater extent of colitis, the concomitant presence of

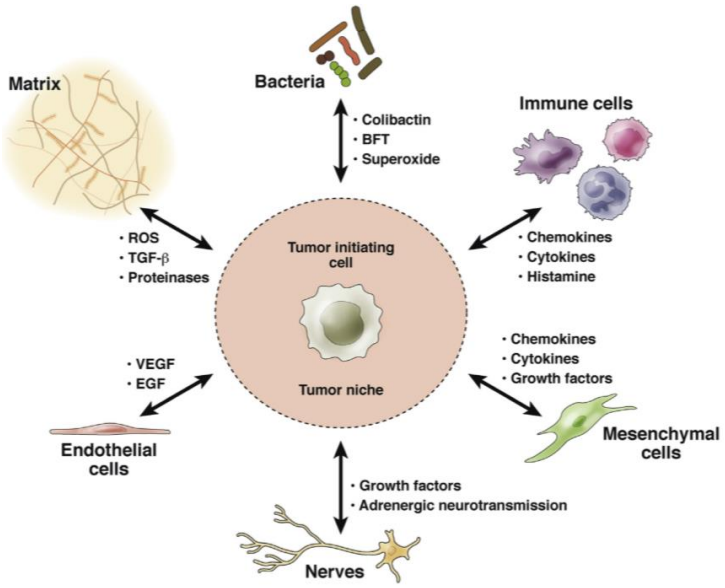

Figure 1.1 Tumor promotion by the tumor microenvironment. The cells within the tumor microenvironment form the niche for the tumor-initiating cells by producing tumor-promoting cytokines and chemokines. These create a supportive environment that supports the uncontrolled growth of initiated cells (promotion). The microbiota on the luminal side of the epithelium also contributes to the niche and is responsible for barrier defects and maintenance of chronic inflammation. The tumor microenvironment and epithelial cells interact with one another. Figure obtained from Quante et al (14).

inflammatory symptoms including primary sclerosing cholangitis, and CAC incidence decreases in response to anti-inflammatory treatment (5, 15). This inflammation likely contributes to tumorigenesis via cytokine and chemokine production by infiltrating

immune cells which support tumor initiation and promotion (Figure 1.1) (16). In fact, disruption of the NLRP3 inflammasome increases tumorigenesis in a mouse model of colitis-associated carcinoma (17). Cytokines and growth factors produced by immune cells can contribute to all stages of tumorigenesis, from initiation to progression and metastasis, by promoting tumor cell proliferation, inhibiting apoptosis, suppressing anti-tumor immunity and augmenting tumor blood vessel formation (14).

Inflammatory cells, including activated macrophages and neutrophils, produce reactive oxygen species (ROS) and reactive nitrogen intermediates (RNI), which are both highly reactive and mutagenic (18-21). As opposed to the early adenomatous polyposis coli (APC) mutations seen in sporadic CRC, early oncogenic events in CAC include p53 gene mutations. This occurs in both carcinoma and dysplasia, as well as in inflamed, but otherwise normal intestinal mucosa (22), suggesting that this mutation is an initiating event in development of CAC. Furthermore, epigenetic changes have been increasingly noted in relation to IBD and CAC. In fact, several groups have identified epigenetic modulation of histones and DNA within the loci of tumor suppressor genes including APC and p16(INK4a) and p19(ARF) as well as genes controlling DNA stability, such as MutL-homolog (MLH) (23-28). Indeed, most of the effects of inflammation discussed above, such as the ability to cause mutations and epigenetic changes and promotion of cellular regeneration in response to injury, continue to enhance oncogenesis during the tumor promotion stage. Accumulation of subsequent genetic and epigenetic changes including mutations in K-Ras and BRAF enhance tumorigenesis by reducing apoptosis, increasing proliferation, and reducing growth factor dependence (29). Furthermore, several crucial

signaling pathways in the promotion of tumorigenesis are activated in response to inflammation in IBD including NF-κB (30), TGFβ (31) STAT3 (32, 33), IL-23 (34, 35), COX2 (36), and IL-18 (37) to name a few.

Chronic inflammation present during CAC development can also influence metastatic dissemination (38, 39). The acquisition of a mesenchymal or dedifferentiated phenotype by tumor epithelial cells, known as epithelial-mesenchymal transition (EMT), apart from being controlled by TGFβ signaling, can also be enhanced by NF-κB and/or STAT3 signaling (40, 41). Additionally, TNF signaling stabilized the transcription factor Snail, which is pivotal for EMT (42). TNF also promoted survival and dissemination of single cancer cells in circulation as well as their successful extravasation and growth in the secondary site (43). Inflammation also regulates various proteases, whose activity was implicated in remodeling of extracellular matrix and in metastatic process (38, 44). Overexpression of various matrix metalloproteases (MMP), such as MMP7 and MMP9, is a hallmark of colon cancer (44), essential for tumor growth and progression. Thus, a more detailed understanding of modifiers of inflammation in IBD as well as factors that influence aberrantly regulated pathways in CAC is essential for the development of preventative strategies in patients with IBD at risk to develop CAC. The nutrients and proteins of focus in this work are strong targets for risk identification as well as treatment options in the progression from IBD to CAC.

Selenium, selenoproteins, and human health

In 1817, the element selenium (Se) was discovered by J.J. Berzelius (45). Initially considered toxic and later understood to be an essential micronutrient, it was not until the discovery of the first animal selenoprotein, glutathione peroxidase, in 1973 (46) that the Se mechanism of action began to be elucidated. Se is incorporated into proteins, known as selenoproteins, as selenocysteine (Sec) the twenty-first amino acid. Metabolic labeling studies reveal that 80% of bodily Se is incorporated into selenoproteins (47). To date, 25 genes encoding selenoproteins have been discovered within the human genome (48), the majority of which were discovered because Sec requires a very specialized mechanism for its incorporation into selenoproteins. Sec is encoded by a UGA codon in the selenoprotein mRNA. In most proteins, the UGA codon encodes a stop signal but *cis*-acting sequences in the selenoprotein mRNA recruit specialized *trans*-acting factors that are dedicated to Sec incorporation. As can be imagined, selenoprotein production is dependent upon availability of Se (49) and the importance of particular selenoproteins to human health can be hypothesized based on the hierarchy of selenoprotein expression that is reliant on this Se requirement. Se dietary intake depends on the bioavailability and content of Se in crop plants that is contingent on Se content in soil. As an essential micronutrient, Se plays a significant role in many human health processes and has even been linked to cancer suppression. In the subsequent chapter, a detailed explanation of Sec incorporation into selenoproteins as well as a broad description of the roles of Se and selenoproteins in human health will be discussed.

Selenium metabolism

Decoding of UGA as Sec is a well-conserved process, occurring in all three domains of life. The Sec incorporation mechanism has been largely worked out within prokaryotes. The Sec insertion site is identified by the presence of a stem-loop structure within the selenoprotein mRNA. This sequence is termed the selenocysteine insertion sequence (SECIS) and, in *Escherichia coli*, the SECIS resides directly downstream of the Sec UGA codon. In fact, movement of the SECIS by as few as three nucleotides can abolish Sec incorporation (50). In archea and eukarya, on the other hand, stem-loops are still required for the SECIS but sequence and structure requirements differ from prokaryotes. The SECIS is located within the 3' untranslated region (UTR) of the mRNA and can be located a significant distance from the Sec codon (49). This distance is required so that the single SECIS can recode multiple UGA codons as opposed to a single, contiguous UGA codon as is seen in prokaryotes (51, 52). In fact, a minimal spacing requirement of ~60 nucleotides must exist (53).

In addition to the *cis*-acting SECIS elements described above, Sec incorporation requires supplementary *trans*-acting factors including the selenocysteine-specific tRNA ($tRNA^{[Ser]Sec}$) (54) as well as the enzymes required for the biosynthesis of the Sec-charged tRNA, selenophosphate synthetase, phosphoseryl kinase, and selenocysteine synthase (55-57). Also required are an elongation factor (EF) specific for the tRNA and a SECIS-binding protein, SBP2, which recruits the EF to the selenoprotein mRNA (Figure 1.2) (58). Moreover, the recent discovery of mammalian Trit1 as a $tRNA^{[Ser]Sec}$- isopentenyl-transferase which is also indispensable for selenoprotein expression (59) demonstrates

that we are still learning about the complete mechanism of Sec incorporation into selenoproteins.

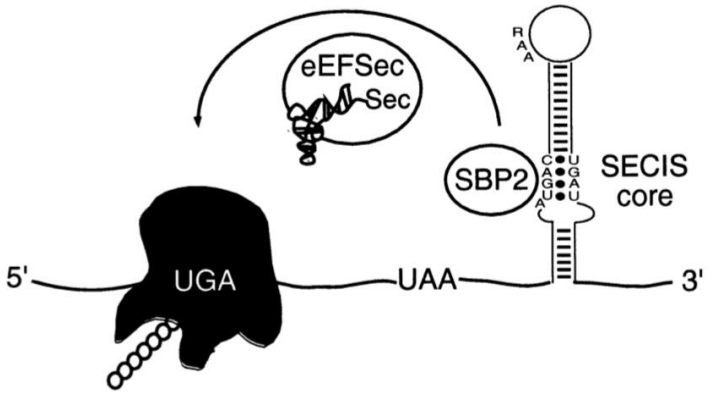

Figure 1.2 A schematic demonstrating Sec incorporation in eukaryotes. The model shows the hairpin structure of the SECIS as well as the trans-acting factors that are integral to Sec insertion including the elongation factor (eEFSec), Sec-binding protein 2 (SBP2) and the Sec-tRNA. Figure obtained from Driscoll et al (49).

Se metabolism takes place within the liver and ingested Se enters the liver via portal vein blood (60). Those selenoproteins synthesized by the liver include the Se transport protein selenoprotein P (Sepp1) which is exported to the circulation as well as selenoenzymes that support liver function (60). The liver also releases Se in the form of 1β-methylseleno-*N*-acetyl-D-galactosamine, which is the major urinary selenium metabolites and has been identified in rat liver and in rat and human urine (61). Finally, the liver produces methylated excretory forms (62) and non-specifically incorporates selenomethionine into proteins. Of those forms of Se produced by the liver, Sepp1 is important for the distribution of Se to other tissues and production of other selenoproteins.

Sepp1 has ten selenocysteines incorporated into its primary structure, nine of which exist within a putative Se transport domain of Sepp1. This Se-rich C-terminal domain is necessary for the delivery of Se to the brain and testis (63) via apoER2-mediated endocytosis of Sepp1 (64, 65) and to the kidney via megalin, a lipoprotein receptor localized to the proximal tubule epithelium (65). Knockout of Sepp1 in hepatocytes decreases plasma Sepp1 concentrations by 90%, thus decreasing whole-body and tissue Se concentrations, further validating a role for Sepp1 in Se transport to tissues besides the brain, testis, and kidneys. Moreover, ^{75}Se-labeled selenite tracing of metabolically available Se reveals that deletion of hepatocyte Sepp1 more than doubles ^{75}Se excretion in urine and increases liver ^{75}Se by 25% in mice lacking hepatic Sepp1 compared to controls, suggesting increased incorporation of metabolically available Se into liver selenoproteins consistent with there being competition for ^{75}Se between synthesis of Sepp1 and production of excretory metabolites (Figure 1.3) (66).

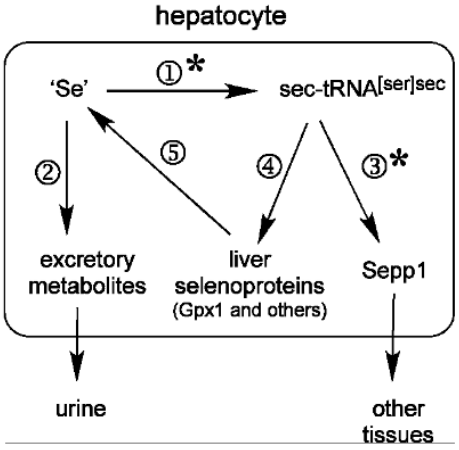

Figure 1.3 Model for the proposed fate of metabolically available Se. Hepatocytes can further metabolize several sources of Se. Synthesis of sec-tRNA$^{[ser]sec}$ ① competes with methylation reactions ② for Se and synthesis of Sepp1 ③ for export to the plasma competes with synthesis of intracellular selenoproteins ④. Furthermore, liver selenoproteins turn over ⑤ to release Se. The asterisks indicate the preferred path of Se during Se deficiency. Figure obtained from Hill et al (66).

Because Se is required for the production of selenoproteins, Se deficiency causes a substantial decrease in Sepp1 secretion. Moreover, Se deficiency also leads to decreased expression of other selenoproteins. During Se deficiency, mRNA stability contributes to the determination of what selenoproteins will be preferentially produced. The relative stability of mRNAs has been determined to be glutathione peroxidase-4 (*Gpx4*) > *Sepp1* > thioredoxin reductase 1 (*TrxR1*) > type I deiodinase (*D1*) > glutathione peroxidase-1 (*Gpx1*) (67). This hierarchy of mRNA expression likely relates to the relative importance of the selenoproteins in cellular homeostasis. Additionally, Se retention and selenoprotein expression are differentially regulated within different tissues, thus providing further hierarchical regulation of selenoprotein expression (68, 69).

Selenium in human health

The importance of Se to human health is most obvious when considering diseases common in areas of the world with Se-poor soil. Se deficiency has been identified as a factor in Keshan disease, a cardiomyopathy (70), which can be prevented by dietary Se supplementation. Se supplementation also prevents and treats Kashin-Beck disease, a deforming osteoarthritis (71). Both of these diseases are found in areas of China in which soil Se concentrations are low. The importance of selenoproteins to human health is demonstrated by humans with genetically impaired biosynthesis of selenoproteins who develop a multisystem disorder characterized by failure of the latter stages of spermatogenesis, axial muscular dystrophy, increased cutaneous ROS and susceptibility

to ultraviolet radiation-induced oxidative damage, impaired T lymphocyte proliferation, abnormal mononuclear cell cytokine secretion, and telomere shortening (72), giving some of the best evidence for the varied roles of selenoproteins in maintenance of human health.

Furthermore, epigenetic evidence reveals that low levels of Se are linked to a number of health problems including decreased survival in people infected with HIV (73), epileptic seizures (74) and age-associated neurological disorders (75). Moreover, dietary Se supplementation contributes to the prevention of neurodegenerative and cardiovascular diseases related to chronic oxidative stress as well as in the treatment of inflammatory disorders including autoimmune thyroid disease (76), viral diseases and sepsis (77-79), suggesting a link between Se and inflammation. In fact, a higher risk of CD was noted in individuals with low baseline Se levels.

While low Se status has been linked to several diseases, there is also risk associated with supranutritional Se status. At the most extreme, Se poisoning can result in hair loss, skin lesions, and deformities and as selenosis progresses, decreased cognitive function, weakness, paralysis, and ultimately death can occur (80). Se poisoning to this extent is rare, though, so it is the detrimental effects of slightly increased Se levels that are most worrisome. A secondary analysis of the Nutritional Prevention of Cancer (NPC) trial revealed that Se-enriched yeast supplemented individuals whose baseline plasma Se levels exceeded 122 ng/ml were at increased risk of developing type 2 diabetes compared to those assigned placebo (81). Though the mechanism of this increased risk is not clearly understood, the expression of selenoenzymes such as Gpx1, which act as antioxidants,

may interfere with insulin-regulated cellular pathways via hydrogen peroxide (H_2O_2) reduction (82), as H_2O_2 normally enhances the early insulin signaling cascade and stimulates insulin-induced glucose uptake (83, 84). Moreover, both Se compounds and Sepp1 are capable of attenuating insulin-induced phosphorylation of protein kinase B (Akt) (85, 86), and insulin downregulates hepatic biosynthesis of Sepp1 (85, 87), thus providing a potential feedback loop. Thus, there is a very small window in which Se supplementation is beneficial to human health, beyond which there are also detrimental effects.

Optimal recommended daily selenium intake

Se availability is the most important determinant for biosynthesis of selenoproteins. Therefore, optimized expression of selenoproteins through Se supplementation represents both a key objective and a biomarker of Se-replete status in intervention trials (88). As suggested in the previous section, there is a narrow target for beneficial Se supplementation. Animal studies demonstrated an inverted "U"-shaped curve of optimal Se intake where too little or too much Se can be detrimental to health (89). Further complicating matters, a number of studies designed to determine optimal Se supplementation arrived at very different conclusions based on the method of Se determination, study goals, and the population in which the study was conducted. In the U.S., where Se is available at sufficient levels in crops, the recommended dietary allowance for Se is 55 μg/day for healthy adults (90), while other studies have recommended that adequate Se intake ranges between 30 and 85 μg/day, with a

tolerable upper intake level of 300-450 μg/day (77, 91). These values have been determined based on various Se status parameters.

Traditionally, the Se content in hair, toenails or plasma has been measured; however, plasma levels of the two extracellular selenoproteins plasma glutathione peroxidase (Gpx3) and Sepp1 are considered to be preferable as biomarkers. Maximal Gpx3 activity is achieved at an intake of ~70 μg Se/day or plasma Se levels of 90 ng/ml (92). Sepp1 plasma levels plateau at ~105 μg Se/day and plasma Se levels of 124 ng/ml (93). As full expression of Sepp1 requires a greater Se intake than does Gpx3, it is the better indicator of Se nutritional status (94). On the basis of the Se intake needed for optimal Sepp1 expression based on the aforementioned parameters, ~75 μg Se/day is recommended for U.S. residents (95), but even this value comes with several stipulations. For instance, effects of Se-enriched milk protein and Se-yeast on rectal selenoprotein mRNA levels have been compared in Australians with adequate Se status (basal plasma Se levels of ~100 ng/ml) and while plasma Se levels increased similarly in both Se-supplemented groups, dairy-Se was more effective at stimulating selenoprotein expression (96), suggesting that the form of Se supplemented has an impact on the efficiency of incorporation.

Genetic polymorphisms also have a significant impact on Se utilization, meaning that the Se requirement for optimum human health can vary among individuals (97-102). Finally, the health process that is being modified by Se supplementation must be considered. For example, people with IBD demonstrate a decreased ability to absorb nutrients and thus have an increased risk of Se deficiency. Se supplementation in these

patients would need to be carefully monitored for Se biomarkers to insure adequate supplementation. Additionally, other diseases in which inflammation and ROS exceed the ability of the redox system to maintain balance might require higher levels of Se to insure proper maintenance of selenoptroteins.

In conclusion, when considering successful Se supplementation, four points should be considered: 1) the genetic and metabolic determinants that may affect efficiency of dietary Se supplementation, 2) differences in metabolization and, therefore, biological impact of the different Se compounds, 3) Se absorption and usage within individuals, and 4) potential adverse health effects of high Se intake (103).

Selenoproteins as modifiers of tumorigenesis

The vast majority of the characterized selenoproteins are enzymes that catalyze oxidation-reduction reactions and contain Sec in their active sites (104). Though Sec is structurally identical to cysteine (Cys) with the exception of a Se replacing the sulfur, the selenol group in Sec is more fully ionized than the thiol of Cys at physiological pH, making it a more potent antioxidant (105). Due to its antioxidant role as well as a plethora of epidemiological evidence pointing towards selenium as a suppressor of tumorigenesis, it is predicted that selenoproteins contribute to suppression of a multitude of cancer types. Within the following sections, the functions of selenoproteins as they relate to tumor modifying properties will be discussed with a particular focus on the two plasma selenoproteins, Gpx3 and Sepp1.

Selenium and selenoproteins in oxidative stress response and cancer

Populations with low Se status are at increased risk for several cancers including prostate, breast, lung, laryngeal and colorectal (106-108) and increased cancer-specific mortality has been seen in renal cancer patients (109). Moreover, animal models have demonstrated that Se supplementation can reduce the incidence and severity of liver, esophageal, pancreatic, prostatic, colon, and mammary carcinogenesis (110). In support of a potential role for Se in cancer suppression, several novel drugs are in development. Synthetic organoselenium compounds have been generated to promote anti-tumor activity (111), and encapsulated elemental Se nanoparticles are in production to increase anti-tumor efficacy and decrease toxicity compared to Se compounds commonly used in dietary supplements (112).

Interestingly, despite a consistent pattern in epidemiology, there are questions as to whether Se supplementation is of potential value in reducing cancer risk. An early intervention study of high-selenium yeast in humans demonstrated protection against prostate and other cancers (113, 114). The Wheat Bran Fiber Trial, the Polyp Prevention Trial, and the Polyp Prevention Study corroborated that variations in Se status may affect CRC risk as adenoma recurrences were significantly lower in the quartile with the highest plasma Se levels (150 ng/ml) versus the quartile with the lowest Se (113 ng/ml) (115). A Spanish study reported significantly lower serum Se levels in two groups of patients with large-size colorectal adenomas or CRC compared to healthy control subjects only for the age group ≤ 60 years (116), suggesting that age may be a confounding factor in several studies. Furthermore, a U.S. cancer screening trial identified a significant inverse

association between serum Se levels and the occurrence of advanced colorectal adenomas only among the high-risk group of recent smokers (117) implicating lifestyle decisions such as smoking as potential modifiers of study outcome.

In contrast, two larger U.S. case-control studies did not find any clear association between serum Se levels and the risk of recurrent CRC (118, 119), and a meta-analysis of intervention trials concluded that oral administration of antioxidants including Se were not effective in the prevention of colorectal neoplasia in the general population (120). As has been mentioned, though, there are limiting factors when considering Se supplementation in otherwise healthy people in areas like America where Se status is already sufficient for complete selenoprotein production. In support of this, in a meta-analysis of randomized controlled trials of Se supplements and cancer prevention, there was sufficient evidence to support the use of Se supplements in populations with high risk of cancer and *low baseline Se levels* (121).

There were several lines of evidence that point towards mechanisms for Se modification of tumorigenesis. Several intracellular selenoproteins metabolize reactive oxygen intermediates and thereby defend the cell against oxidative injury. In fact, it appears that over one third of all known selenoproteins are antioxidant in nature (122) and the antioxidant activity of selenoproteins is essential in minimizing the levels of hydroperoxides (123, 124). Thus, Se deficiency increases endogenous cytosolic oxidative stress (125). Rat models have shown that Se deficiency can lead to liver necrosis and lipid peroxidation in response to small doses of the redox-cycling compound diquat (126). Importantly, injection of Se ten hours prior to diquat injection prevents the injury via the

selenoprotein Sepp1 (127, 128). Alterations in oxidative stress have varied and far-reaching consequences in terms of tumor modulation. Most directly, high levels of ROS can promote cancer development through direct oxidative damage to DNA by species such as the hydroxyl radical (129). However, more recent evidence suggests that other actions of ROS, such as effects on p53, Nrf2, and Wnt signaling, cell proliferation, and invasiveness might be important to cancer susceptibility (130, 131).

As many intermediate steps in both the Nrf2 and Wnt pathways can be modulated by hydroperoxides, Se deficiency activates these pathways. In fact, the oxidation sensor Keap1, which maintains Nrf2 in the cytosol until its modification by hydroperoxides/electrophiles, is the link between Se and Nrf2 signaling. Wnt signaling, on the other hand, is activated by the oxidation sensor nucleoredoxin (Nrx), which is associated with disheveled (Dvl). Se deficiency results in oxidation of both sensors and the ultimate activation of both pathways (130), which are key players in the pathogenesis of cancer (132-134). Moreover, by a likely feedback mechanism, the selenoproteins Gpx2, TrxR2, and TrxR3 are regulated by Wnt signaling. Thus Se, which is essential for the biosynthesis of Wnt-dependent selenoproteins, is likely important during carcinogenesis (135).

As oxidative stress causes DNA damage, Se also impacts protection against DNA damage. Supplementation of either tissue culture media, animal or human diets with even moderate levels of Se compounds protect against the formation of DNA adducts, DNA/chromosome breakage, chromosome gain or loss, mitochondrial DNA damage, and telomere length and function alterations, and it is proposed that Se might do so through

more direct mechanisms than just reduction of hydroperoxides. Se has been proposed to enhance the DNA damage response, increase the activity of repair enzymes such as DNA glycosylases, and augment DNA damage repair pathways that involve p53, BRCA1 and Gadd45 (136).

Se is also thought to suppress tumor progression through inhibition of metastasis. Se has been linked to inhibition of angiogenesis, the formation of new blood vessels within and around a tumor through which metastatic cells can enter the blood stream, in mammary cancer. Se does so via inhibition of endothelial proliferation and survival as well as matrix degradation through enhancing production of Mmp7 (137). Moreover, other aspects of metastasis are inhibited by Se including cell motility, migration and invasion (138). Thus, Se not only inhibits tumor growth but also progression.

Experimentally, there is a plethora of evidence for a role of selenoproteins in protection from tumorigenic processes. In a murine model of chemically-induced hepatocarcinogenesis, tumorigenesis is increased in mice expressing a mutant Sec tRNA gene (*TrspA37G*) compared to wild-type mice (139), but Se supplementation decreased tumor size via augmentation of transforming growth factor-alpha (TGFα) signaling (140). Specific selenoproteins have also been tested for their impact on tumorigenesis in several models. For instance, in a mouse model of inflammation-associated carcinogenesis, glutathione peroxidase-2 (Gpx2) and Se decreased both inflammation and tumorigenesis (141) and knockout of the 15 kDa selenoprotein protected against aberrant crypt formation (ACF) during chemically-induced colorectal carcinogenesis (142). Moreover, epidemiological evidence exists for the involvement of selenoproteins in human

tumorigenesis. Loss of heterozygosity of the *GPX1* locus has been identified in breast, lung, head and neck, and colon cancers (143-145). A second glutathione peroxidase, Gpx3, is a biomarker for ovarian tumors and is frequently methylated in prostate cancer and esophageal adenocarcinoma arising in the setting of Barrett's esophagus (146, 147). Within the thioredoxin reductase system, both Trx and TrxR1 are overexpressed in non-small cell lung carcinoma, T-cell acute lymphoblastic leukemia, malignant pleural mesothelioma, colorectal cancer, breast carcinoma, hepatocellular carcinoma, gastric carcinoma, and cervical carcinoma. Moreover, increased cellular proliferation, decreased patient survival, and chemotherapeutic resistance are associated with overexpression of the thioredoxin system (148). Additionally, several selenoprotein single nucleotide polymorphisms (SNPs) have been associated with CRC (Figure 1.4). Of particular interest in their modification of cancer phenotypes are the plasma selenoproteins GPx3 and Sepp1 as they could potentially impact both intra- and extracellular redox activities.

Plasma glutathione peroxidase (Gpx3) in cancer

Gpx3 is expressed in a wide range of tissues, localizing to the cytoplasm and nuclei of cells and secreted into the blood stream (149). Due to its nuclear localization as well as its broad and unique substrate spectrum, including lipid and thymine hydroperoxides, Gpx3 is hypothesized to play an important role in Se-dependent chemoprevention. Gpx3 specifically reduces lipid peroxide concentrations in cell membranes and downregulates the eicosanoid biosynthesis pathway. This pathway increases inflammation, cancer growth, and metastasis suggesting that Gpx3 might inhibit tumorigenesis (150).

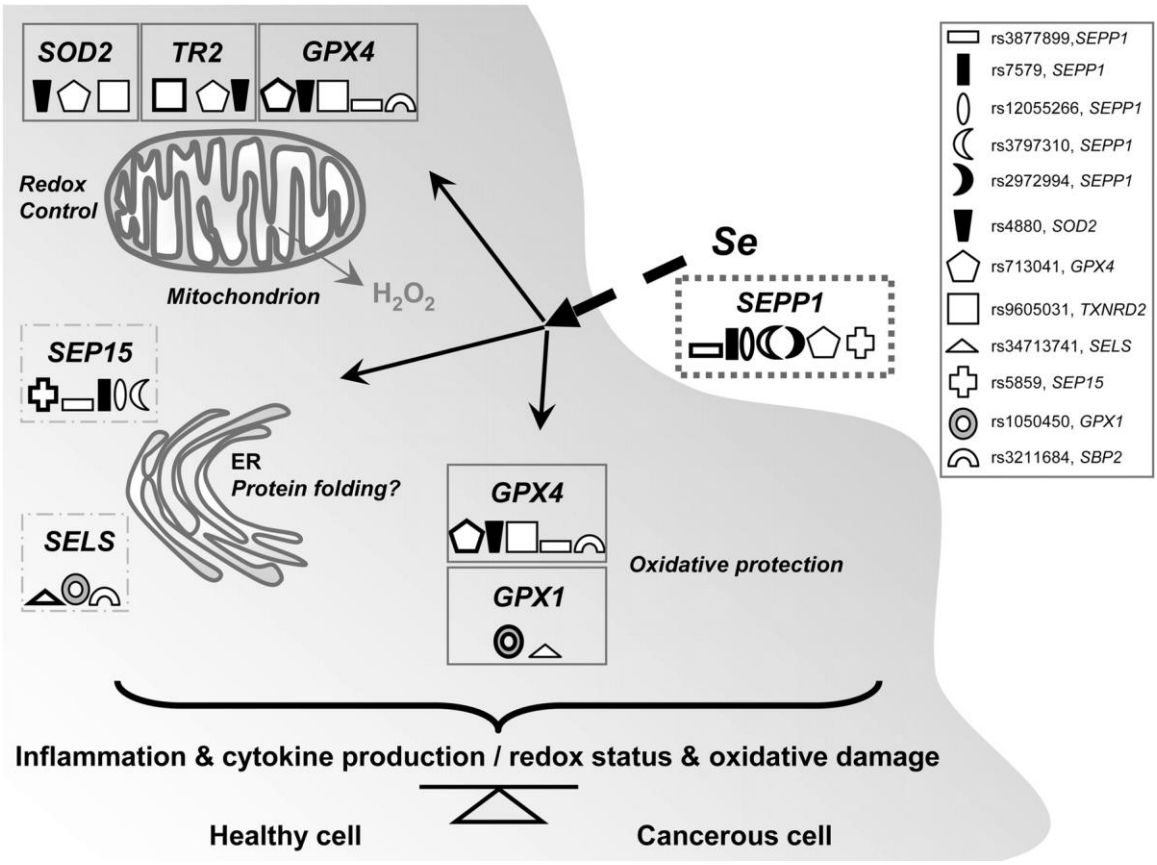

Figure 1.4 Colorectal functions modified by selenoproteins and their SNPs. The schematic shows the identified genetic interactions in the context of selenoprotein subcellular localization and biological function. Pictograms illustrate SNPs where rs numbers are defined in the legend in the upper right. Black arrows indicate the delivery of Se to the different selenoproteins. Figure obtained from Meplan et al (99).

There is inconsistent data regarding the roles of Gpx4 gene variants within the human population. The gene variant rs713041, which is located in the 3'UTR of *GPX3,* has been loosely associated with increased CRC risk (151). A second polymorphism in the *GPX3* gene causes a T-C substitution in the 3'UTR bordering the SECIS element (152). *In vitro*, the C variant promotes reporter gene expression to a greater extent than the T variant and competes more strongly for one or more proteins involved in Se incorporation,

possibly through modification of the structure of the 3'UTR in the vicinity of the SECIS (153). Likely due to these alterations in Gpx3 expression, the C variant has also been associated with increased mortality in breast cancer patients (154). Moreover, breast cancer patients have impaired basal Gpx3 gene expression and a reduced ability to induce Gpx3 expression in response to oxidative stress (155).

In perinatal mice *Gpx3* loss in the epidermis causes hyperplasia, dermal inflammatory infiltrate, dysmorphic hair follicles, and alopecia. These phenotypes are at least partially due to increased lipid peroxidation and COX2 levels (156). Moreover, ectopic Gpx3 expression in pancreatic tumor cell lines as well as L929 cells suppresses tumor progression by reducing proliferation, tumor growth in semisolid media and in orthotopic xenografts (157, 158). These data indicate that Gpx3 might suppress tumorigenesis, especially in the context of high inflammation and oxidative stress.

Selenoprotein P (Sepp1) in cancer

Based on its Sec location, Sepp1 has two domains. The first, and larger domain extends from the N-terminus through the residue just before the second Sec (residues 1-244). This N-terminal domain contains one Sec and seven Cys residues and the Sec exists within a UXXC motif that catalyzes the oxidation of glutathione (GSH) by a phosphatidylcholine hydroperoxide (159). The smaller domain extends from the second selenocysteine to the C-terminus (residues 245-366). It contains nine Sec and ten Cys residues (160) and serves as a Se transport domain (63).

Although Sepp1 is expressed almost ubiquitously in many tissues and cell lines (161), most research has focused on liver-secreted plasma Sepp1 (160). Interestingly, Sepp1 is abundantly expressed in normal colonic mucosa, and *SEPP1* mRNA and accompanying activity is significantly reduced in colon tumors (162). Similarly, it is dramatically reduced in human prostate tumors, mouse tumors, and in the androgen-dependent (LNCaP) and androgen-independent (PC-3) prostate cancer cell lines (163). Several SNPs have been identified in *SEPP1* that might contribute to decreased expression in tumors. For instance, there is an association between rs7579 genotype in *SEPP1* and prostate cancer risk (164). Furthermore, four variants in *SEPP1* were significantly associated with advanced colorectal adenoma risk including the variant *SEPP1 -4166G,* which exists within the promoter region, two loci in the 3' region of *SEPP1*, and a third locus in the 3' region of *SEPP1,* which was inversely associated with risk of colorectal adenoma (165). Also, though a novel $(TC)_3$ polymorphism within a complex $(A)_4$-C-$(A)_4$-GG-$(A)_8$-GCT-$(TC)_5$-$(T)_{17}$ (bp – 429 to bp – 477) repeat structure of the *SEPP1* promoter confers significantly reduced basal promoter activity, there is not a definitive link between this polymorphism and cancer risk. Additionally, genetic instability was observed within the $(T)_{17}$ repeat motif in CRC to the mutator phenotype. Thus, this *SEPP1* complex repeat structure may be of functional relevance to Sepp1 gene expression and thus modify tumorigenesis (98).

Experimentally, there is evidence supporting a role of Sepp1 downregulation in mechanisms of tumor promotion. *Sepp1* knockdown in Pr-111 cells resulted in increased ROS and subsequent cell growth inhibition upon H_2O_2 exposure. In support of Sepp1 loss

being the driver of these phenotypes, administration of exogenous Sepp1 was able to buffer ROS and rescue growth inhibition (166). Sepp1 has also been implicated in inflammatory processes that play substantial roles in tumorigenesis. The cytokine TGF-β_1 which is overexpressed in colon cancers (167) exerts an inhibitory effect on Sepp1 secretion as well as represses *Sepp1* transcription (168). Additionally, treatment of HepG2 cells with the cytokines interleukin 1β (IL-1β), tumor necrosis factor α (TNFα), and interferon γ (IFNY) repress promoter activity (169). These data suggest that Sepp1 is downregulated in response to inflammation and that this mechanism might contribute to Sepp1 downregulation during tumorigenesis. Another mechanism of Sepp1 regulation might depend on inhibition of Sepp1 transactivation by the glucocorticoid receptor which is increased during development, differentiation, and under conditions of critical illness (170).

Differentiation, a process often reversed during the course of tumorigenesis, is also influenced by Sepp1. During enterocytic differentiation, Sepp1 gene expression and secretion are both strongly upregulated through increased binding of hepatocyte nuclear factor-4α (HNF-4α) to an upstream promoter element in *Sepp1* (171). Additionally, knockdown of *Sepp1* in 3T3-L1 cells inhibits adipogenic differentiation, likely via concomitant upregulation of proinflammatory cytokines (172). These data suggest that Sepp1 promotes differentiation, a process that is generally associated with tumor progression. Thus, Sepp1 appears to be a contributor to suppression of tumorigenesis in multiple cancer types.

Transcriptional corepressors with functions in gut development and epithelial wound repair: Myeloid translocation genes

The analysis of translocation breakpoints in acute leukemia has identified several gene regulatory proteins that are critically involved in cellular proliferation, differentiation, apoptosis and stem cell properties; all processes that contribute to the leukemic phenotype (173). For example, the reciprocal translocation between the 8th and 21st chromosomes (t(8;21)) associated with acute myeloid leukemia (AML) has enabled the discovery of AML-1 on chromosome 21 and myeloid translocation gene 8 (*MTG8,* otherwise known as eight twenty-one; *ETO*) on chromosome 8 (174). t(8;21) retains the AML-1 DNA binding domain which is fused to the majority of the MTG8 protein. Knock-in of the AML-1/ETO translocation demonstrates that the fusion protein acts in a dominant manner to inhibit AML-1 targets (175). This suggests that MTG8 serves to form repression complexes which contribute to repression of targets bound by AML-1. In support of this, biochemical and molecular studies reveal a role for MTG8 as a component of histone deacetylase (HDAC) complexes which are recruited to AML-1 target genes (176-178).

After the discovery of MTG8, two other MTG family members were identified: myeloid translocation gene on chromosome 16 (MTG16) and myeloid translocation gene related protein-1 (MTGR1) (179-182). MTGR1 was characterized within the L-G murine myeloid cell line as an AML-1/ETO interacting protein. MTGR1 is an 85 kDa phosphoprotein that is recognized by MTG8 antibodies (182). Moreover, this gene was validated in randomly sequenced human cDNA (EST) database searches based on the MTG8 cDNA search probe. As such, MTGR1 is also termed ETO homologous on

chromosome twenty (*EHT*) (180). MTG16 is a second, less common, translocation involving chromosome 21, t(16;21), which was identified in therapy-related AML. Characterization of MTG16 cDNAs revealed a high degree of homology to MTG8 (181).

The MTG family of proteins are defined by four evolutionarily conserved domains called *nervy* homology regions (NHR) 1-4. The NHR1 and NHR2 domains are protein-interaction motifs (177, 183, 184). NHR1, homologous to the Drosophila transcriptional co-activator TBP-associated factor 110 (TAF110) (185), can positively or negatively regulate transcription through interaction with either co-repressors or transcriptional activators (186). The NHR2 domain contains a hydrophobic heptad repeat that mediates MTG dimerization as well as binding to the transcriptional co-repressor SIN3A (182, 187). The function of the NHR3 domain is not well understood but it is hypothesized that it may be involved in contacting certain co-repressors (188). The NHR4 domain contains a ring finger motif, which mediates protein interactions including those with N-CoR/SMRT (Figure 1.5) (176, 178, 189). The association of MTG family members with AML translocations and HDACs indicate that MTGs may be important in both normal physiology and pathology. The subsequent sections will explore the functions of MTGs and how they can be subverted in malignancy.

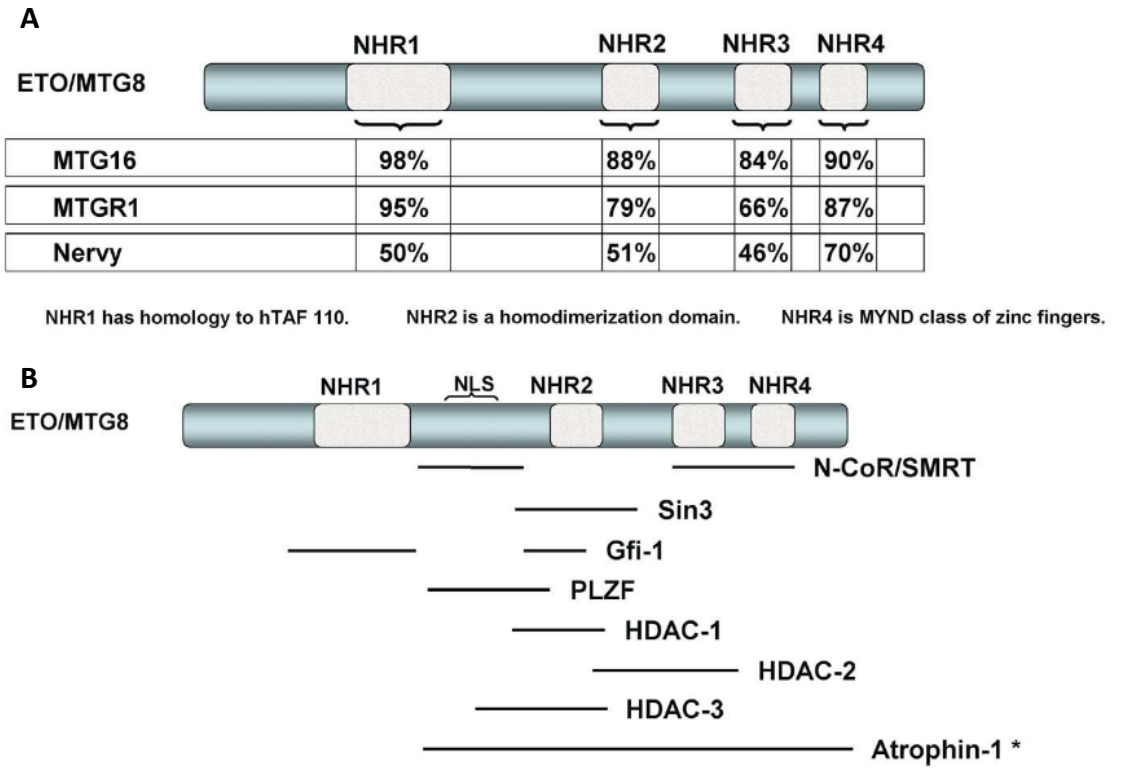

Figure 1.5 MTG8 family proteins are defined by their evolutionarily conserved domains, termed nervy homology regions. A) Schematic of MTG8 illustrating the positions of the NHR regions. Percentages represent the percent homology between MTG8, MTG16, MTGR1, and Drosophila nervy within each NHR. B) Schematic of MTG8 interaction domains and binding partners. Abbreviations: growth factor independence-1 (Gfi-1), promyelotic leukemia zinc-finger (PLZF), histone deacetylase (HDAC), nuclear co-repressor (N-CoR), silencing mediator of retinoic acid and thyroid hormone receptors (SMRT). The asterisk indicates that the binding domain for atrophin-1 has not been determined. Figure obtained from Davis et al (190).

Myeloid translocation genes in normal physiology

The MTG family is ubiquitously expressed, though individual members are expressed differentially, which may influence their activities within different tissues. *MTG8* is expressed in the human brain, heart, and peripheral blood as well as in the human hematopoietic cell line (HEL; human erythroleukemia) (191-194) and the $CD34^{+}$ compartment of human bone marrow cells (195). *MTG16*, on the other hand, is expressed

at high levels in the heart, pancreas, skeletal muscle, spleen, thymus, colon, and in peripheral blood leukocytes (181). Interestingly, substantially increased expression of MTG16 is observed during hematopoietic differentiation suggesting that its temporal regulation is important to the process of differentiation (196). MTGR1 is expressed in a vast number of human cell types including those within the adult heart, brain, skeletal muscle and to a lesser extent in placenta, kidney, pancreas, spleen, thymus, prostate, testis, ovary, small intestine, and colon (180, 197, 198).

The MTGs serve as scaffolding proteins upon which transcriptional repression complexes are built. Amongst those co-repressors recruited by MTG8 are N-CoR/SMRT, SIN3A, and HDACs -1, -2, and -3 (176, 178, 187-189). MTG16 also binds SIN3 as well as HDACs -1, -2, -3, -6, and -8 (187). As MTGs do not bind DNA directly, they must interact with DNA-binding transcription factors. Several MTG-recruiting proteins have been identified that illustrate the physiological processes in which MTGs are involved. MTG8, for example, is recruited by the promyleocytic leukemia zinc finger (PLZF) protein, which is involved in cell cycle progression and has been identified in translocations in acute promyelocytic leukemia. The PLZF and MTG8 proteins associate *in vivo* and *in vitro* and MTG8 enhances transcriptional repression by PLZF (192). This implicates MTG8 in yet another leukemia-associated interaction. In fact, the majority of proteins with which MTGs interact are involved in hematologic differentiation, proliferation, and malignancies. For instance, MTG8 and B cell lymphoma-6 (Bcl-6), a protein that is frequently translocated and hypermutated in diffuse large B cell lymphoma, are coexpressed in normal and malignant lymphoid tissue where they interact and colocalize.

MTG8 cooperates with Bcl-6 to repress the transcription of Bcl-6 targets via forming a complex on the promoters of Bcl-6 endogenous target genes (199). Furthermore, gene expression analysis indicates that Mtg16 is required for suppression of the cell-cycle regulating E protein *E2F2* (200) implicating Mtg16 in regulation of processes associated with cellular growth. Notch receptors are determinants of cell lineage allocation, commitment, and differentiation. Dysfunction of Notch signaling characterizes malignant conditions such as leukemias (201-206). MTG16 interacts with the intracellular domain of the Notch receptor, suggesting a role in the regulation of Notch-dependent lineage allocation in hematopoiesis (207).

MTGs also interact with proteins involved in non-hematopoietic malignancies. MTG16 overexpression leads to decreased transcription of genes involved in tumor cell metabolism including 6-phosphofructo-2-kinase/fructose-2,6-biphosphatase 3 and 4, and pyruvate dehydrogenase kinase isoenzyme 1 (PDK1). As a result of this downregulation, glycolytic metabolism is decreased while mitochondrial respiration and formation of ROS is increased, ultimately resulting in proliferation inhibition and decreased fraction of cells in the S-phase indicating that Mtg16 might serve as a tumor suppressor (208). Moreover, Mtgr1 interacts with TCF4 and can oppose β-catenin-dependent transcriptional activation leading to overexpression of the oncogene c-Myc (209), again potentially linking MTG family members to tumor modulation. One of the more interesting novel functions of MTG family members is in regulation of RNA-dependent effects on chromatin modification. There is increasing evidence that non-coding RNA plays a role in the epigenetic control of chromatin (210-212). Remarkably, all MTG proteins can bind RNA

through the zinc finger domains of the NHR4 domain and a short basic region upstream of the NHR2 domain resulting in a potential RNA component in MTG-mediated chromatin regulation (213).

Several functions of the MTG proteins have been elucidated by the analysis of genetic models of MTG gene deletion. For instance, mice carrying an inactivating insertion of LacZ in exon 2 of the *MTG8* locus demonstrate severely impaired viability as the result of failure in formation of the majority of the intestine, from the distal duodenum to the greater part of the colon. Of those *Mtg8*$^{-/-}$ pups that survive past 48 hours, 60% die by 21 days after birth and are 30-50% smaller than their littermates. The surviving *Mtg8*$^{-/-}$ mice are smaller than littermates but outwardly normal otherwise. Microscopic analysis of these mice, though, reveals small intestinal defects where marked intraluminal distention and blunted, disorganized villi are observed (214). Based on observations in these mice, Mtg8 seems to play an important role in the development of the midgut, likely due to effects on intestinal stem cell function.

The *Mtg16*$^{-/-}$ mouse is mildly anemic at birth with a predominance of the granulocyte/macrophage lineage at the expense of the megakaryocyte/erythroid lineages, as expected, linking Mtg16 to hematopoietic lineage allocation (215). Similar to Mtg8, *Mtg16*$^{-/-}$ mice display a gut phenotype. *Mtg16*$^{-/-}$ colons display increased enterocyte proliferation and augmented intestinal permeability. Similar to immune alterations identified in the whole body, the colon exhibits an increase in adaptive immune signatures with skewing towards Th1 responses (216).

Finally, *Mtgr1*$^{-/-}$ mice are smaller than their littermates throughout their lifespan but display no other overt phenotype. When analyzing the small intestine, though, a significant alteration is identified. *Mtgr1*$^{-/-}$ mice display a progressive reduction in the secretory cell lineage, including goblet, Paneth, and enteroendocrine cells beginning at weaning and continuing to 6-8 weeks of age. Moreover, there is a subtle colonic phenotype with increased proliferation and mild crypt expansion (217). Collectively, the gene knockout studies in *Mtg8*-, *Mtg16*-, and *Mtgr1*-deficient mice suggest that MTG transcriptional co-repressors play critical roles in intestinal biology and likely function in influencing stem cell behavior.

Myeloid translocation genes in pathology

As previously mentioned, *MTG8* and *MTG16* are both involved in chromosomal translocations that fuse them to the *AML-1* gene on the 21st chromosome. The *MTG8* translocation has been identified in 8-20% of all cases of AML and is even more prevalent in the French-American-British class M2 AML with a 30-50% occurrence. The t(16;21) is associated with therapy-related AML (181, 218-221). These translocations are non-random as breakpoints for both occur between exons 5 and 6 in *AML-1* and between exons 1 and 2 or 3 and 4 of MTG family members (181). MTGR1, on the other hand, maps to chromosome 20q11. This region is deleted in a small percentage of myelodysplastic syndromes and 3% of AML (180).

As transcription factors are frequently involved in hematologic malignancies, it is possible that many different molecular mechanisms lead to malignant transformation. As

such, some of these proteins might interact and mechanistically link different diseases. The members of the MTG family of transcriptional co-repressors are excellent candidates as such common factors because they are normally expressed in human hematopoietic cells, bind to HDACs, and interact with several proteins involved with hematological malignancies including PLZF, Bcl-6, PLZF/RARα, T-cell acute lymphocytic leukemia 1 (TAL1), growth factor independent 1 transcription repressor (Gfi1), and human B-HLH factor (HEB) (184, 199, 222, 223). MTG family members are likely involved in more tumorigenic processes than just those associated with hematologic malignancies.

In vitro, there is evidence for a role of MTG family members in malignancy. The ability of MTG8 to bind to HDACs probably plays a significant role in t(8;21)-containing leukemia (224). In fact, the addition of phenylbutyrate, an inhibitor of HDAC activity, to the t(8;21)-containing Kasumi cell line results in an increase in differentiated cells from 20% to 60% after 1 week (225). Moreover, the mouse models that were essential to developing an understanding of the physiological functions of the MTGs have been used to explore the pathology associated with absence of these proteins. Under conditions of hematopoietic stress, *Mtg16*$^{-/-}$ marrow demonstrates attenuated multi-lineage expansion capabilities resulting in an inability of *Mtg16*$^{-/-}$ marrow to form splenic colonies in recipient mice. Moreover, *Mtg16*$^{-/-}$ bone marrow fails to rescue radiation-induced marrow clearance in bone marrow transplant assays. Upon removal of bone marrow cells from knockout mice, *Mtg16*$^{-/-}$ stem cells continue to show defects in stem cell renewal assays (200). These observations implicate MTG16 in regulation of hematopoietic stem cell programs that are essential for lineage allocation (215).

Considering the gut phenotypes identified in MTG knockout mice at baseline, they were also stressed to uncover subsequent phenotypes. *Mtg16*$^{-/-}$ mice develop increased clinical symptoms including weight loss, diarrhea, mortality, and histological colitis as well as increased innate (Gr1^{+}, F4/80^{+}, CD11c^{+}, and MHCII^{+};CD11c^{+}) and Th1 adaptive (CD4^{+}) immune cells in response to dextran sodium sulfate (DSS) treatment. Additionally, there is an increase in apoptosis and compensatory increase in proliferation in DSS-treated mice. As another model of colonic injury, treatment of *Mtg16*$^{-/-}$ mice with *C. rodentium* results in augmented colitis and increased bacterial colonization. Finally, in support of more severe damage in response to injury, in human ulcerative colitis, *MTG16* mRNA levels are reduced (216).

Loss of *Mtgr1* also sensitizes the colonic epithelium to the effects of DSS, at least partially due to an increase in epithelial apoptosis rates. Significantly, *Mtgr1*$^{-/-}$ mice demonstrate impaired regeneration of colonic crypts, even ten weeks after a single DSS administration, suggesting a role for Mtgr1 in the colonic stem cell (226). When considering these knockout experiments in combination, these data suggest that MTG loss might contribute to increased tumorigenesis as well as severity of colitis. In support of this, *MTG16* has been mapped to the 16q24.3 breast cancer loss of heterozygosity (LOH) region. Moreover, the expression of *MTG16* is significantly reduced in a number of breast cancer cell lines and in primary breast tumors when compared to nontransformed breast epithelial cell lines and normal breast tissue and reintroduction of MTG16 into breast tumor cell lines with low MTG16 expression reduces colony growth on plastic and in soft agar (227). Furthermore, a genome-wide screen identified MTG8 as a candidate

cancer gene in CRC and breast cancer and four mutations within the NHR domains of MTG16 have been identified in CRC (228, 229). Taken together these data implicate MTG family member downregulation in tumor-promoting processes and indicate that loss of MTG family members might contribute to tumorigenesis.

A transcriptional repressor that modifies Wnt signaling: Kaiso

In mammalian genomes, transcriptional regulation relies on both a complex combinatorial interplay of transcription factors and epigenetic mechanisms. The former involve the building of protein complexes upon promoters of target genes based on specific DNA target sequences. The latter involve chromosomal and DNA structural alteration and are maintained within the progeny of a cell (230). DNA methylation is one of the epigenetic signatures common in regulation of gene expression. The transcription factor Kaiso not only binds to a consensus Kaiso binding site (KBS), TCCTGCNA (231), but also uses its three Krüppel-like C_2H_2 zinc fingers to bind methylated CpGs (232). Kaiso is a member of the zinc finger and BTB domain containing (ZBTB) protein family, within the broader poxvirus and zinc finger (POZ)-zinc finger (POZ-ZF) family. Two family members, ZBTB4 and ZBTB38 contain Kaiso-like zinc fingers and, like Kaiso, bind methylated DNA *in vitro* and *in vivo*, but unlike Kaiso, they can bind to single methylated CpGs (233). Kaiso and its family members have been implicated in cancer and development (234) and, as such, likely serve as targets for tumor modification. Interestingly, Kaiso is implicated in Wnt repression and shares several targets with the MTG family members described

previously suggesting that these two protein families might interact within a repression complex, which might serve as an important target for cancer therapeutics.

Kaiso targets and implications

Kaiso, like MTG16, is a component of an N-CoR complex. *In vitro*, the Kaiso/N-CoR complex is able to bind specific CpG-rich sequences in a methylation and sequence-specific manner. *In vivo*, Kaiso targets the N-CoR complex to several promoters including that of the metastasis-associated 2 (*MTA2*) gene in a methylation-dependent manner (235). Regulation of MTA2 is especially important as this protein is closely related to a protein that has been correlated with the metastatic potential of certain carcinomas (236) and MTA2, itself, represses p53 (237). Furthermore, Kaiso interacts with the CTC-binding factor (CTCF), a DNA binding protein that plays essential roles in regulating gene expression through its role as an enhancer blocker, through its POZ domain (238). CTCF modifies 3D chromatin architecture giving it a broad impact on a vast array of genes. Interestingly, CTCF has been identified as a tumor suppressor in breast cancer (239).

Perhaps one of the most well-studied roles of Kaiso is as a transcriptional repressor involved intimately in Wnt signaling. Wnt activation has been closely linked to colorectal tumorigenesis. Kaiso is a repressor of both canonical and non-canonical Wnt signals through both its methylated and sequence-specific DNA binding modalities. Kaiso regulates TCF/LEF1-activity by modulating HDAC1 and β-catenin-complex formation (240). Moreover, Kaiso associates with the Mmp7 promoter via its KBS ultimately allowing for the abrogation of β-catenin-mediated activation of the Mmp7 promoter upon Kaiso

binding (241). Mmp7 is a Wnt downstream effector protein that has been heavily implicated in the progression of many cancer types, especially CRC (242-244). Kaiso interacts with p120-catenin ($p120^{ctn}$), an E-cadherin-associated protein that affects E-cadherin function and stability. Interestingly, in response to Wnt3a, $p120^{ctn}$ is phosphorylated at two sites, Ser268 and Ser269, disrupting the interaction with E-cadherin resulting in enhanced binding of $p120^{ctn}$ to Kaiso and preventing Kaiso-mediated inhibition of the β-catenin-TCF4 transcriptional complex (245).

Kaiso in pathology

POZ-ZF proteins have been implicated in many biological processes, including but not limited to B cell fate determination, cell cycle progression, DNA damage responses and developmental events such as gastrulation, limb formation, and hematopoietic stem cell fate allocation (Table 1.1). As a result, dysfunction of POZ-ZF proteins such as Kaiso have been linked to developmental disorders and tumorigenesis (246). Both Kaiso and its closely-related family member ZBTB4 are downregulated in cancer (247, 248) and a study

Protein Name	Repressor, activator, or both?	Putative function(s)
PLZF	Repressor	Limb development; gene regulation in APL
Bcl-6	Repressor	Plasma cell fate; germinal center formation; germ cell apoptosis; gene regulation in B cell lymphoma
FAZF	Repressor	T cell proliferation; cytokine production; hematopoietic stem cell proliferation
MIZ-1	Both	Gastrulation; cell cycle progression; regulator of Myc-mediated gene regulation
HIC-1	Repressor	Tumor suppressor; craniofacial development; DNA damage responses; inhibition of Wnt signaling
ZBTB7	Repressor	Proto-oncogene; regualtor of oncogenesis; stimulator of HIV1 Tat activity
Kaiso	**Both**	**Gastrulation; canonical and non-canonical Wnt signaling; regulator of synapse formation**
BAZF	Repressor	Activation of naïve T cells
APM-1	Repressor	Possible tumor suppressor; cell growth inhibition; downregulated in cervical carcinoma cell lines
Nac-1	Repressor	Neuronal apoptosis; behavioral sensitization to cocaine; regulation of p53 levels
ZBTB38	Repressor	Expression in late postmitotic neurons; function unknown
ZBTB4	Repressor	Ubiquitous expression; function unknown

Table 1.1 Putative cellular roles of POZ-ZF family transcription factors. Here, Kaiso is bolded for its relevance to this work. Table adapted from Kelly et al (246).

to examine the expression pattern of Kaiso in human tumor tissue did not reveal an overt alteration in expression but did note a change in Kaiso localization. In human cancer tissues, Kaiso often localized to the cytosol rather than the nucleus. Interestingly, when cultured cells with nuclear Kaiso localization are xenografted into nude mice, localization of Kaiso shifts to the cytoplasm and, in some cells, Kaiso expression is completely abolished (249). Such expression and localization changes suggest that Kaiso expression is detrimental to tumorigenesis. In support of this hypothesis, increased $p120^{ctn}$ expression reduces Kaiso nuclear localization, which results in enhanced expression of Cyclin D1 ultimately leading to $p120^{ctn}$-dependent regulation of proliferation and cell cycle in lung cancer cells through Kaiso (250).

Interestingly, contrary to the aforementioned hypothesis, there are also instances in which increased Kaiso expression and/or nuclear localization are related to increased tumorigenic potential. For one, development of a *Kaiso*$^{-/-}$ mouse crossed with the well-characterized *Apc*$^{min/+}$ mouse that acquires intestinal polyps revealed that the absence of Kaiso leads to delayed polyposis (251). Moreover, Kaiso repressed methylated tumor suppressor genes, including the *CDKN2A* gene in human colon cancer cell lines. Significantly, knockdown of Kaiso induced tumor suppressor gene expression and increased susceptibility to cell cycle arrest and cell death in response to chemotherapy (247). Finally, nuclear localization of Kaiso has been identified as a risk factor in high-grade and triple-negative invasive breast cancer (252). Taken together, these data suggest that the impact of Kaiso on tumorigenesis is multifactorial and may depend on localization, cancer type, and cancer stage.

Experimental overview

The activities of each of the proteins outlined above are involved in pivotal roles in stem cell activity and inflammatory and injury response. Because colitis-associated carcinoma not only depends upon altered growth and differentiation properties within the cell, but is also reliant upon inflammatory injury, we predicted that selenoproteins, myeloid translocation genes, and Kaiso would modify development of colitis-associated carcinoma. In order to test this hypothesis, we take advantage of the murine azoxymethane (AOM), repeated dose dextran sodium sulfate (DSS) model of

inflammatory carcinogenesis to test the impact of loss of these proteins on tumor development as well as inflammatory injury.

Until 2003, inflammatory injury and subsequent tumorigenesis were modeled using the DSS injury model. DSS-induced colitis is characterized by pro-inflammatory cytokine and chemokine (IL-1, IL-6, KC, TNF-α, and IFNλ) induction (253, 254) and downregulation of anti-inflammatory cytokines such as IL-10 (254-257), likely at least in part due to induction of macrophage infiltration into the colonic epithelium (258). DSS induces colonic injury but its mechanism of action is only beginning to be understood. It has been demonstrated that DSS can cause inhibition of reverse transcriptase activities by competing with poly (U) ultimately resulting in the disruption of major cellular functions (259). Moreover, DSS inhibits ribonuclease activity disturbing mRNA translation (260, 261). It is thought that DSS penetrates epithelial cells of the colon by establishing linkages with medium-chain-length fatty acids such as dodecanoate which form nanometer-sized vesicles in the cytoplasm that activate intestinal inflammatory signaling pathways (262). The end result of DSS administration is inflammatory injury within the distal colon, which after several administrations over a long period of time leads to the development of colitis-related tumorigenesis, albeit, with low incidence and multiplicity (263). In 2003, though, Tanaka *et al.* combined the inflammatory injury resulting from DSS administration with initial injection of a potent carcinogen, AOM, to enhance tumorigenesis (264). When mice were given a low dose of AOM followed by one week of exposure to 2% DSS and 20 weeks of incubation, they developed adenocarcinomas with 100% penetrance and approximately 6 adenocarcinomas per mouse and adenomas with

38% incidence and less than one adenoma per mouse, and these neoplasias demonstrated positivity for β-catenin, COX2, and iNOS, but not p53 (264). This protocol has been modified, increasing DSS concentration administered as well as number of administrations and amount of AOM and has allowed for a deeper understanding of modifiers of inflammation and inflammation-related carcinogenesis (33, 265-267).

The AOM/DSS model for colitis-associated cancer is used in the subsequent chapters to determine the impact of altered dietary Se intake, loss of the plasma selenoproteins Gpx3 and Sepp1, loss of Mtgr1, and knockout of Kaiso in combination with Mtg16 on severity of inflammation and inflammatory carcinogenesis. Our modification of this protocol, to be used in the Se and selenoprotein experiments, involves injection with 12.5 mg/kg AOM intraperitoneally as described in (265, 268, 269). After a 3-day recovery period, the animals are started on the first of 3 cycles of 3% DSS *ad libitum*. Each cycle is 4 days in length and separated by a 16-day recovery period. After the last cycle, animals are sacrificed following 26 days of recovery. We note that, in response to the aforementioned protocol though, absence of Mtg16 results in a phenotype so severe that it leads to extremely high morbidity. For this reason, the Mtg16 and Kaiso protocols utilize 10 mg/kg AOM and two administrations of 2% DSS.

In addition to the inflammatory injury protocol employed, there are several experiments that are specific to the nutrient or protein being analyzed. In Chapter II, mice are depleted of selenium via dietary mechanisms and tested, not only for tumor burden effects, but also for response to DSS-induced injury as a single modality. Moreover, in order to determine alterations in reactive oxygen species in response to inflammation,

F_2-Isoprostanes are analyzed. Furthermore, cytokines and chemokines are analyzed to determine how selenium deficiency impacts extent of inflammation.

In Chapter III, because Gpx3 has been implicated in antioxidant activity, oxidative stress genes and oxidative DNA damage within tumors are analyzed. Caco2 cells are also utilized to test for ROS production, DNA damage, and apoptosis in response to Gpx3 knockdown and H_2O_2 administration as well as colony formation post-Gpx3 knockdown. In Chapter IV, a novel model of epithelial stem cell function, organoid culturing, is utilized to analyze the effects of Sepp1 loss on response to oxidative stress as well as baseline proliferation and stem cell phenotypes, establishing an epithelial cell-autonomous role for Sepp1 in protection from oxidative stress and alteration of Wnt tone. Furthermore, bone marrow macrophages are activated in order to determine how Sepp1 loss, either partial or complete, impacts macrophage polarization. In Chapter V, *in situ* hybridization is utilized to measure MTGR1 expression alterations in tumors compared to normal adjacent tissue. Bone marrow transplant is also employed to determine whether the *Mtgr1*$^{-/-}$ tumor effect is hematopoietic cell autonomous. Finally, in Chapter VI, an interaction between MTG16 and Kaiso is established via yeast two hybrid, immunofluorescent colocalization, and coimmunoprecipitation and the role of this interaction in the transcriptional repression of Mmp7 is established using luciferase reporter assays, chromatin immunoprecipitation, and expression analysis, ultimately suggesting that this interaction might influence inflammatory carcinogenesis resulting in the experiments performed in Chapter VII, which test the impact of either Mtg16 or Kaiso loss or absence of both proteins on inflammatory carcinogenesis. The experiments

described in this work have been performed with the goal to identify modifiers and potential therapeutic targets in the treatment of colitis-associated carcinoma.

CHAPTER II

DIETARY SELENIUM DEFICIENCY EXACERBATES DSS-INDUCED EPITHELIAL INJURY AND AOM/DSS-INDUCED TUMORIGENESIS[1]

Introduction

The essential micronutrient selenium (Se) is of fundamental importance to human health. Se, through selenoproteins, has antioxidant roles, influences immune activity, and its levels are inversely correlated with cancer risk (73) and inflammatory bowel disease (IBD) (270-272). In the case of IBD, red blood cell glutathione peroxidase activity (273), a Se-dependent activity and mRNA levels of Sepp1 (274), a selenoprotein, are reduced.

IBD is an autoimmune inflammatory disease of the GI tract affecting as many as 1.4 million people in the United States (275). IBD carries numerous and serious medical complications: stricture and fistula formation, infection, severe pain, anemia, and malnutrition (276-279). The pathophysiology of IBD is thought to be multifactorial in origin. Genetic, microbial, and environmental factors have all been implicated, but the fundamental etiology remains unclear. Nutritional deficiencies have been a major concern in the management of IBD for decades and numerous studies have documented decreased levels of Se in IBD compared to control patients (280-283). Moreover, as Se

[1] This work has been published under Caitlyn W. Barrett, Kshipra Singh, Amy K. Motley, Mary K. Lintel, Elena Matafonova, Amber M. Bradley, Wei Ning, Shenika V. Poindexter, Bobak Parang, Vishruth K. Reddy, Rupesh Chaturvedi, Barbara M. Fingleton, Mary K. Washington, Keith T. Wilson, Sean S. Davies, Kristina E. Hill, Raymond F. Burk, Christopher S. Williams. (2013) *Dietary selenium deficiency exacerbates DSS-induced epithelial injury and AOM/DSS-induced tumorigenesis*, PLoS One, 8, e67845 (7).

deficiencies are often seen in IBD, downregulation of several selenoproteins have also been identified. Serum selenoprotein P (Sepp1) levels are significantly lower in patients with Crohn's disease (274) and glutathione peroxidase 1 mRNA is significantly downregulated in mononuclear cells from patients with IBD (284). Defects in epithelial integrity contribute to IBD pathogenesis and understanding mechanisms affecting epithelial homeostasis is a priority (285). In this regard, Se has been directly linked to WNT signaling (286) and the intrinsic apoptosis pathway (287), suggesting that it may play a role in epithelial integrity in response to injury.

Several epidemiological studies suggest that Se status is inversely correlated with cancer incidence and mortality (288-291), but Se supplementation trials failed to show benefit, possibly due to the fact that the advantages of Se supplementation are dependent on several factors including baseline Se status, genetic background (e.g. the existence of polymorphisms in selenoprotein genes), type of cancer, as well as the metabolic conversion and dose of Se supplements (103). Furthermore, several selenoproteins have been correlated with cancer risk. Mutation of the selenocysteine transfer RNA gene which results in decreased expression of some selenoproteins results in reduction in murine colon cancer risk (292). More specifically, elevated glutathione peroxidase-2 (Gpx2) expression has been detected in colorectal adenomas (162, 293-295). Subsequently, double knockout of Gpx1 and Gpx2 leads to bacterial-induced intestinal inflammation and, ultimately, ileal tumor formation (296) and Gpx2 decreases inflammation and tumors in response to inflammatory carcinogenesis (297). Expression levels of selenoproteins including Gpx1, Gpx3, and Sepp1 are significantly decreased in

colorectal cancer, with lowered Sepp1 expression correlating most significantly with tumor stage (298). As such, we have shown that Gpx3 serves as a tumor suppressor in the AOM/DSS model of CAC (268). Thus, both Se and selenoproteins may play pivotal roles in tumor modulation, especially in the setting of inflammatory carcinogenesis.

There may be sub-populations of CRC patients who would benefit from Se supplementation. IBD may fall into this category as it is characterized by chronic inflammation and oxidative stress (299) and ulcerative colitis and Crohn's colitis patients are at increased risk for developing colon cancer (300). Experimental studies demonstrating that Se deficiency exacerbates intestinal injury and tumorigenesis are not definitive. The aim of these studies was to determine whether Se deficiency exacerbates colitis and promotes inflammation-associated carcinogenesis. Mice were rendered Se-deficient via maintenance on a tightly controlled Se-deficient diet. Se-deficient mice had exacerbated colitis after DSS injury, resulting in a pro-tumorigenic microenvironment with increased cytokines, oxidative stress, and DNA damage. Furthermore, when inflammatory carcinogenesis modeling was performed, Se-deficient mice had increased tumorigenicity and more advanced lesions compared to Se-sufficient cohorts. Thus, Se supplementation in Se-deficient IBD patients may protect from mucosal injury and malignant degeneration.

Materials and Methods

Ethics Statement. This study was performed in strict accordance with the recommendations in the Guide for the Care and Use of Laboratory Animals of the National Institutes of Health. The protocol was approved by the Institute of Animal Care and Use

Committee at Vanderbilt University (protocol number: M/10-355). Every effort was made to minimize suffering.

Murine DSS morbidity and inflammatory carcinogenesis modeling. Experimental diets were *Torula* yeast-based and identical except for their Se contents. The basal diet contained less than 0.01 mg Se per kg (Se-deficient) and the Se-sufficient diet was the same diet supplemented with 0.25 mg Se as sodium selenite per kg. Se-deficient and -sufficient diets were prepared and pelleted to our specifications (301) by Harlan-Teklad (Madison, WI, USA). Upon weaning, Wild-type (WT) C57BL/6 mice were maintained on the experimental diets for 12 weeks prior to initiation of DSS or AOM/DSS experiments to ensure Se deficiency.

DSS at a molecular weight of 40,000-50,000 was obtained from USB Corporation (Cleveland, OH, USA). A single lot was used for all experiments described in this publication. A 3% w/v DSS solution was made in distilled water and filtered through a 0.22 µm cellulose acetate filter. This solution was then substituted for animal drinking water and barriers were placed on the automatic watering systems within each cage.

For the DSS morbidity experiments, Se-sufficient (n=15) and Se-deficient (n=10) mice were treated with DSS (Figure 2.1A) until their weight loss reached 20% of their original weights, at which time they were sacrificed. Animals were weighed daily and stools were examined for consistency and the presence of blood. Stool consistency scores ranged from 0-2, with 0 = hard, normal stools, 1 = soft and spread, 2 = diarrhea-like. Presence of blood was scored with a 0 = no blood, 2 = blood present, 4 = copious amounts of blood. Values were added for each mouse.

For the murine inflammatory carcinogenesis protocol (results shown in Figures 5-6), Se-sufficient (n=18) or -deficient (n=20) C57BL/6 WT mice were injected with 12.5 mg/kg AOM (Sigma-Aldrich) intraperitoneally as described in (265, 268, 269). After a 3-day recovery period, the animals were started on the first of 3 cycles of 3% DSS *ad libitum* (see schematic in Figure 2.5A). Each cycle was 4 days in length and was separated by a 16-day recovery period. Eight days into each recovery period, murine endoscopy was performed to monitor colitis severity and tumor burden (302). After the last cycle, animals were sacrificed following 26 days of recovery. Mice were anesthetized with isofluorane prior to exsanguination from the inferior vena cava. Blood was treated with 15 µl of a 1 mg/ml solution of disodium EDTA to prevent coagulation and plasma was separated by centrifugation for 2 minutes at 12,000xg. The colon was removed, flushed with PBS, and opened longitudinally and gross tumor counts were conducted using a dissecting microscope at 15x magnification and size measurements obtained using digital calipers. Microscopic analysis was conducted by an experienced gastrointestinal pathologist (M.K. Washington) for dysplasia on H&E stained "Swiss rolled" colons (processed by the Vanderbilt Translational Pathology Shared Resource core). Low-grade dysplasia (LGD) refers to preinvasive pedunculated, sessile, or flat plaque-like lesions with simple glandular outlines, without loss of cellularity polarity. High-grade dysplasia (HGD) are adenomas with architectural complexity, increased cytologic atypia, and loss of tumor cell polarity (303, 304). Sections of tumor and normal adjacent colon were collected and stored in RNAlater (Qiagen, Valencia, Santa Clarita, California, USA) and a section of the most distal colon above the anus was collected and flash frozen in liquid nitrogen for

protein analysis and/or determination of Se content. The remainder of the colon was "Swiss Rolled", formalin fixed overnight, and sectioned for histological analysis.

Colonic selenium measurements. The determination of colonic Se was carried out using a modification of the fluorometric assay of Koh and Benson (305) and Sheehan and Gao (306). Briefly, tissue was digested in nitric and perchloric acids and Se was complexed with diaminonaphthalene. Selenium-diaminonaphthalene was extracted into cyclohexane and fluorescence was measured in a Perkin-Elmer LS 55 fluorometer.

Plasma glutathione peroxidase activity assay. Plasma collected from mice was subjected to a glutathione peroxidase (Gpx) activity assay using a modified protocol (307) based on the method of Paglia and Valentine (308). In short, 800 µl of reaction cocktail (50mmol/L potassium phosphate, pH 7.0, 1mmol/L EDTA, 1mmol/L NaN_3, 0.2mmol/L glutathione) was mixed with 10 µl plasma and 90 µl water in a clear plastic cuvette and incubated at room temperature for 5 minutes. Next, 100 µl of H_2O_2 substrate (0.25mmol/L H_2O_2 in H_2O) was added to the reaction mixture to initiate the reaction. Gpx activity was assessed by measuring the rate of change of A_{340} during the linear phase of the reaction. The rate of change was then converted to the number of µmoles of NADPH oxidized/minute using the extinction coefficient of 6.2×10^3 L mol^{-1} cm^{-1} for NADPH at 340 nm. Blank reactions with distilled water were subtracted from each assay.

F_2-Isoprostane analysis. DSS-treated mice (WT C57BL/6 fed Se-sufficient diets n=3, WT C57BL/6 fed Se-deficient diets n=3, 3% DSS *ad libitum* for 3 days) were housed in metabolic cages and urine was collected for 12 hours on days 0 and 3 of DSS administration. Urinary F_2-isoprostanes were measured by stable isotope dilution gas

chromatography mass spectrometry using [2H4]15-F2t-isoprostane as internal standard as previously described (309). Values were normalized to mg creatinine in urine.

Histological injury analysis. A colitis damage score was generated from digital images of H&E stained sections, by first measuring the distance around the intact muscularis using AVP Universal Desktop Ruler software (as performed by (272, 310)). The areas of ulceration were then measured and given scores of 1, 2, 3, or 4, where a score of 1 represents injury involving the lower 1/3 of the crypt, 2 equaling injury to the lower 2/3^{rds} of the crypt, 3 equaling total crypt loss however the epithelial lining remains intact and 4 equaling total crypt and complete epithelial loss. The ulceration score was then multiplied by the length of the involved colon, summed, and divided by the total colon length to give a measure of ulceration severity/colon length. Measurements were performed in a blinded fashion in all colons from mice subjected to the DSS morbidity protocol.

Cytokine array analysis. RNA from Se-sufficient or -deficient DSS morbidity colons (collected on day nine of DSS treatment) was isolated using the RNeasy Mini Kit (Qiagen, Valencia, Santa Clarita, California, USA). cDNA was synthesized using the iScript cDNA synthesis kit (Bio-rad, Hercules, California, USA) from 1 µg of total RNA. 1 µl of the 20 µl cDNA produced through the iScript reaction was used as a template in each subsequent PCR reaction. SYBR green qRT-PCR was performed using mouse cytokine array libraries I (Cat #: MCA-I) and II (Cat #: MCA-II) purchased from RealTimePrimers.com (Elkins Park, Pennsylvania, USA) according to manufacturer's instructions. Individual cytokines were analyzed using the delta-delta Ct method and normalized to Hypoxanthine-Guanine Phosphoribosyltransferase (*Hprt*). Those showing significant differences were plotted

using Graphpad Prism. In order to develop the heat map, data was incorporated into the free web-based PCR array analysis software provided by SABiosciences (Qiagen).

Immunohistochemistry and immunofluorescence staining. Five-micrometer sections were cut, dewaxed, and hydrated. Antigen retrieval was conducted using Antigen Unmasking Reagent (Vector Laboratories, Inc., Burlingame, California, USA) according to manufacturer's instructions. After blocking, primary antibody was added [α-Ki67 (NeoMarkers RB-1510-P, Fremont, California, USA), 1:1,000; α-8-hydroxy-2'deoxyguanosine (8-OHdG, Abcam ab26842, Cambridge, Massachusetts, USA) 1:50] and incubated overnight at 4°C. Isotype-matched antibodies were included as negative controls. Sections were then incubated for one hour at room temperature in secondary antibody (Ki67: Goat α-Rabbit-cy3, Invitrogen A10520; 8-OHdG: α-mouse-FITC, Sigma F-0257). Identification of apoptotic cells was conducted using the ApopTag Plus Peroxidase *In Situ* Apoptosis Kit (Chemicon, Temecula, California, USA) according to the manufacturer's protocol. Control slides were obtained by omitting the terminal transferase (TnT) enzyme. For immunofluorescence staining of proliferation and DNA damage, slides were counterstained and mounted with ProLong Gold antifade including 4',6-diamidino-2-phenylindole (DAPI, Invitrogen, Grand Island, New York, USA). DNA damage indices were generated by counting the number of positive cells per colon length within each high-powered field, with 5 high-powered fields counted per colon, starting at the most distal colon. Apoptosis, and proliferation indices were generated by counting either the number of positive cells per high-powered field (HPF; 40x objective) within each

tumor or the number of positive cells per longitudinal crypt section in 20 crypts per mouse by a blinded observer. The average score was then calculated for each Swiss-rolled colon. *Statistical methods*. Differences between Se-deficient and -sufficient mice were determined utilizing Graphpad Prism and analysis with the Student's t-test. The survival curve was analyzed using the Log-rank (Mantel-Cox) test. Differences in stool scores and percentage weight loss were determined using two-way ANOVA for repeated measurements over time. Urine F_2-isoprostane analysis of all four groups was analyzed using one-way ANOVA with a Newman-Keuls post-test to determine variances between columns. Finally, statistical analysis of high-grade dysplasia was performed using the Fisher's Exact test.

Results

Dietary selenium maintains epithelial integrity.

Se, through selenoproteins, has antioxidant roles, influences immune activity, and has been inversely correlated with IBD (272, 311) and cancer risk (73). Because oxidative stress compromises mucosal integrity (312), and Se deficiency has been shown to increase oxidative stress (125), we determined whether dietary Se deficiency influences the severity of colitis following treatment with 3% DSS *ad lib* (Figure 2.1A). Animals were fed either Se-sufficient or -deficient diets for 12 weeks, an extended period of time sufficient

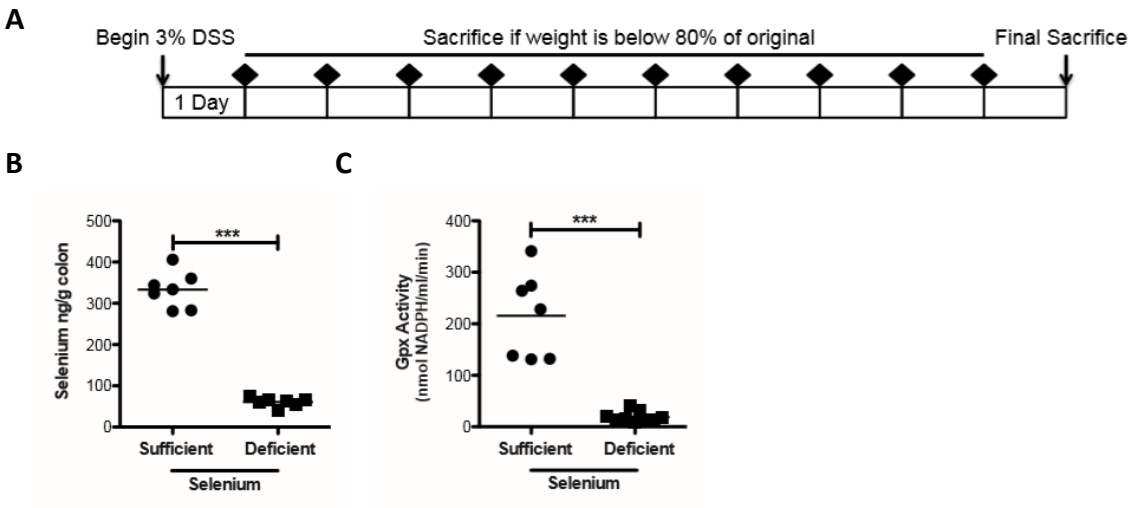

*<u>Figure 2.1</u> Dietary selenium depletion reduces colon selenium levels and plasma glutathione peroxidase activity. A. Schematic for the DSS morbidity protocol. At day 0, mice were weighed and then given a 3% DSS solution in lieu of drinking water. Each day, mice were weighed and stools were obtained for analysis of blood and stool consistency (weight and stool analyses times indicated by black diamonds). Individual mice were sacrificed if their weights fell below 80% of their original weights. B. Selenium sufficient (n=7) and deficient (n=7) colons were analyzed for selenium concentrations. ***P<0.0001. C. Plasma glutathione peroxidase activity is quantified. ***P<0.0001.*

to ensure Se deficiency which we confirmed via measurement of colonic mucosal Se levels at the end of the DSS experiment (333.1 ± 16.5 vs 60.6 ± 4.1 ng/g, *P*<0.0001, Figure 2.1B) and plasma glutathione peroxidase (Gpx) activity (215.4 ± 31.6 vs 18.9 ± 27.8 nmol NADPH/ml.min, *P*<0.0001, Figure 2.1C). In this experiment, mice were maintained on 3% DSS until their weight reached 80% of their original weights (survival endpoint). Se deficient mice median survival was 9 days in comparison to Se-sufficient whose median survival was 12 days (*P*=0.003, Figure 2.2A). Additionally, Se-deficient mice had worsened diarrhea and increased blood in stools (stool scores at day 9: 2.7 ± 0.7 vs 5.7 ± 0.3, *P*=0.02, Figure 2.2B), had accelerated weight loss (84.3 ± 1.2 vs 77.4 ± 1.2% of starting body weight at day 9, *P*=0.01, Figure 2.2C), and had more severe colitis/epithelial injury (2.1 ± 0.2 vs

2.9 ± 0.1, *P*=0.006, Figure 2.2D). These results indicate that Se is protective against DSS-induced colonic injury.

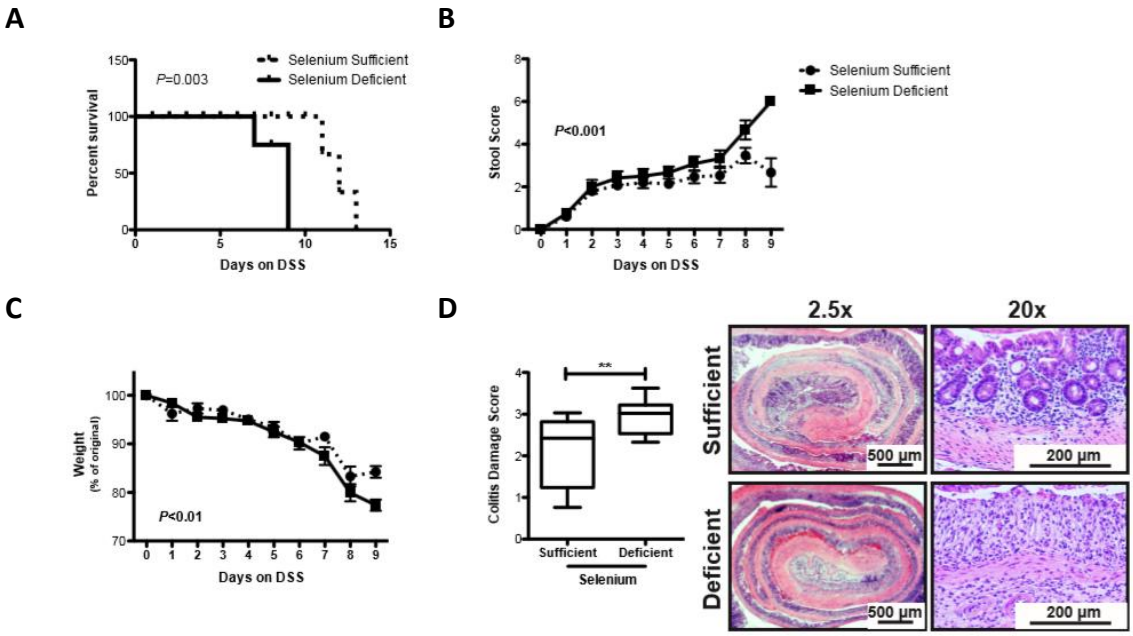

*Figure 2.2 Selenium deficiency exacerbates colonic injury after DSS treatment. A. Se-sufficient (n=15) and -deficient (n=10) mice were subjected to the DSS morbidity protocol (see Figure 1A) and percent survival was tracked. P=0.003, Log-rank (Mantel-Cox) test. B. Stool scores were analyzed for Se-sufficient and -deficient mice on the DSS morbidity protocol. The graph depicts the average stool score for each dietary group on each day of DSS administration. P<0.001, 2-way ANOVA. C. Percent of original weight averaged for each dietary group on each day of DSS administration. P<0.01, 2-way ANOVA. D. Colitis damage scores (described in Materials and Methods) for each dietary group analyzed at the completion of the experiment (left) and representative images of Swiss rolled colons from each group (right). Top and bottom of box 25th and 75th percentile, bar represents the median value, whiskers minimum and maximum values. **P=0.006, Students-t test.*

Pro-tumorigenic microenvironment is promoted by selenium deficiency.

Inflammation, a component of the epithelial and tumor microenvironment, is a contributing factor that predisposes to malignancy and, as we had observed increased injury in response to DSS administration in Se-deficient mice, we wanted to determine whether chemokine and cytokine signaling was aberrantly regulated in Se-deficient mice

in response to injury. Therefore, we analyzed Se-sufficient and -deficient colons for cytokine mRNA expression using a mouse cytokine array. Because the RNA isolated for analysis was isolated from whole colon, the source of these cytokines and chemokines would include epithelial and stromal components. This analysis yielded alterations in several chemokines and cytokines that are displayed as a heat map for all genes tested (Figure 2.3). Significantly altered cytokines were grouped according to function using

A

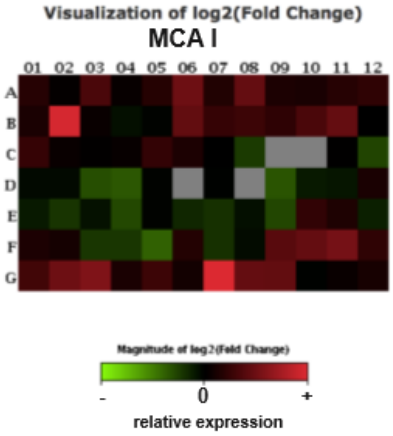

Layout	1	2	3	4	5	6	7	8	9	10	11	12
A	Il2	Il4	Il9	Il11	Il13	Il15	Il21	Tslp	Il5	Csf2	Il6	Il12a
B	Il12b	Il23a	Osm	Zfp91	Clc	Ctf1	Csf3	Lep	Epo	Gh	Tpo	Ifnb1
C	Ifnk	Ifne1	Il28	Ifng	Il10	Il19	Il20	Il24	Vegfa	Vegfb	Vegfc	Figf
D	Pdgfc	Pdgfd	Ngfb	Ntf3	Ntf5	Bdnf	Gdnf	Csf1	Fgf1	Fgf2	Fgf3	Fgf4
E	Fgf5	Fgf6	Fgf7	Fgf8	Fgf9	Fgf10	Fgf11	Fgf12	Fgf13	Fgf14	Fgf15	Fgf16
F	Fgf17	Fgf18	Fgf20	Fgf21	Fgf22	Fgf23	Nrg1	Nrg3	Nrg4	Igf1	Hgf	Egf
G	Efna1	Efna2	Efna3	Efna4	Efna5	EfnB1	EfnB2	EfnB3	Gas6	Angpt1	Angpt2	Angpt4

B

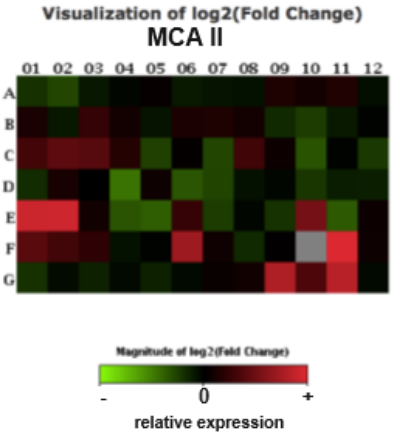

Layout	1	2	3	4	5	6	7	8	9	10	11	12
A	Tnf	Lta	Ltb	Tnfsf4	Cd40lg	Fasl	Cd70	Tnfsf8	Tnfsf9	Tnfsf10	Tnfsf11	Tnfsf12
B	Tnfsf13b	Tnfsf14	Tnfsf15	Tnfsf18	Eda	Il1a	Il1b	Il18	Il1f5	Il1f6	Il1f8	Il17b
C	Il17c	Il17d	Il17f	Bmp2	Bmp4	Bmp5	Bmp6	Bmp7	Bmp8a	Bmp8b	Gdf7	Gdf1
D	Gdf3	Bmp3	Gdf10	Nodal	Mstn	Gdf11	Gdf9	Bmp15	Inhba	Inhbb	Inhbc	Inhbe
E	Tgfb1	Tgfb2	Amh	Inha	Bmp1	Bmp10	Gdf15	Lefty1	Lefty2	Ccl2	Ccl3	Ccl4
F	Ccl5	Ccl7	Ccl8	Ccl11	Ccl19	Ccl20	Ccl21a	Ccl22	Ccl24	Ccl25	Ccl27	Ccl28
G	Cxcl1	Cxcl2	Cxcl3	Cxcl5	Cxcl9	Cxcl10	Cxcl11	Cxcl12	Cxcl13	Cxcl14	Cxcl16	Ppbp

Figure 2.3 Cytokines are aberrantly regulated in selenium-deficient mice subjected to DSS. A. Heat map of mouse cytokine library I and B. mouse cytokine library II gene expression in Se-deficient (n=4) versus -sufficient (control, n=4) colons post-DSS morbidity (left) and a chart of represented cytokines (right). Green=underexpression, Red=overexpression where intensity of color indicates increasing distance from 0; Grey=qRT-PCR yields were undetectable.

PANTHER Pathway Analysis software (313). Transforming growth factor beta (TGF-β) signaling was altered with increased *Tgf-β1* and *-β2* transcripts and decreased growth

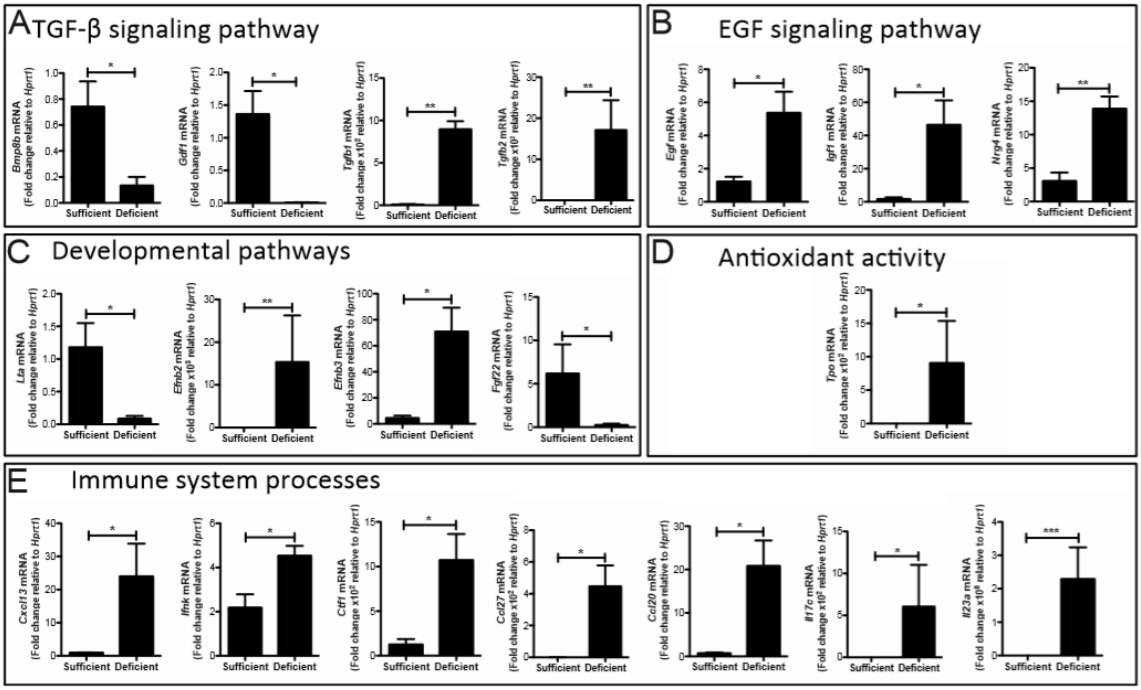

*<u>Figure 2.4</u> Cytokine expression is aberrantly regulated in selenium deficient mice post-DSS. A. mRNA expression changes in Se-sufficient (n=4) and -deficient (n=4) mice on from day nine of the DSS morbidity protocol. Genes were grouped based on pathways identified by PANTHER pathway analysis software. Expression was normalized to Hprt. A. TGF-β pathway alterations include Bmp8b=bone morphogenetic protein 8b, Gdf1=Growth differentiation factor-1, Tgfβ1=transforming growth factor beta-1, Tgfβ2=transforming growth factor beta-2. B. EGF pathway alterations include Egf=epidermal growth factor, Igf1=insulin-like growth factor 1, Nrg4=neuregulin 4. C. Developmental pathway alterations include expression changes in Lta=lymphotoxin alpha, Efnb2=ephrin-B2, Efnb3=ephrin-B3, Fgf22=fibroblast growth factor 22. D. The gene altered within the group titled antioxidant activity is Tpo=thyroid peroxidase. E. Immune system process alterations are demonstrated in Cxcl13=chemokine (C-X-C motif) ligand 13, Ifnk=interferon kappa, Ctf1=cardiotrophin 1, Ccl27=chemokine (C-C motif) ligand 27, Ccl20=chemokine (C-C motif) ligand 20, IL17c=interleukin 17c, IL23a=interleukin 23a. *P<0.05, **P<0.01, ***P<0.001.*

differentiation factor-1 (*Gdf1*) and bone morphogenetic protein 8b (*Bmp8b*) (Figure 2.4A). Additionally, the EGF pathway was altered (Figure 2.4B), as were components of developmental programs (Figure 2.4C). Levels of thyroid peroxidase (*Tpo*), PANTHER

classified as an antioxidant, was increased (0.01 ± 0.003 vs 9.1 ± 6.3 fold change, *P*=0.04, Figure 2.4D), consistent with a decrease in Se leading to aberrant regulation of thyroid hormone production (314). Supporting immune system process activation there was increased chemokine (C-X-C motif) ligand 13 (*Cxcl13*), interferon kappa (*Ifnk*), cardiotrophin 1 (*Ctf1*), chemokine (C-C motif) ligand 27 (*Ccl27*), chemokine (C-C motif) ligand 20 (*Ccl20*), interleukin 17c (*Il-17c*), and interleukin 23a (*Il-23a*) messenger RNA in Se-deficient states (Figure 2.4E). Collectively, multiple factors capable of promoting tumor development were upregulated after DSS treatment in a Se-deficient state.

Lipid peroxidation, a marker of oxidative stress, is increased in the urine of selenium-deficient mice after DSS induced colitis.

DSS administration in the drinking water causes colonic epithelial injury and a robust innate inflammatory response producing an environment enriched in reactive oxygen and nitrogen species (315). Oxidative injury is quantifiable by measuring F_2-isoprostanes (F_2-IsoPs), one of the most reliable measures of *in vivo* lipid peroxidation, a marker of oxidative stress (309, 316). We measured F_2-IsoPs using stable isotope dilution gas chromatography mass spectrometry methodology. F_2-IsoP levels were not different at baseline between Se-sufficient and -deficient mice (0 time point, Figure 2.5A). However, increased urine F_2-IsoPs were observed in mice fed a Se-deficient diet when compared to mice on a Se-sufficient diet, after 3 days of 3% DSS (6.0 ± 0.3 vs 9.1 ± 1.0 ng/mg creatinine, *P*=0.05, Figure 2.5A), indicating that Se protects from lipid peroxidation

in this model. Therefore, F_2-IsoPs effectively quantitate oxidative stress levels in the DSS model and Se-deficiency increases whole animal oxidative stress after DSS-induced injury.

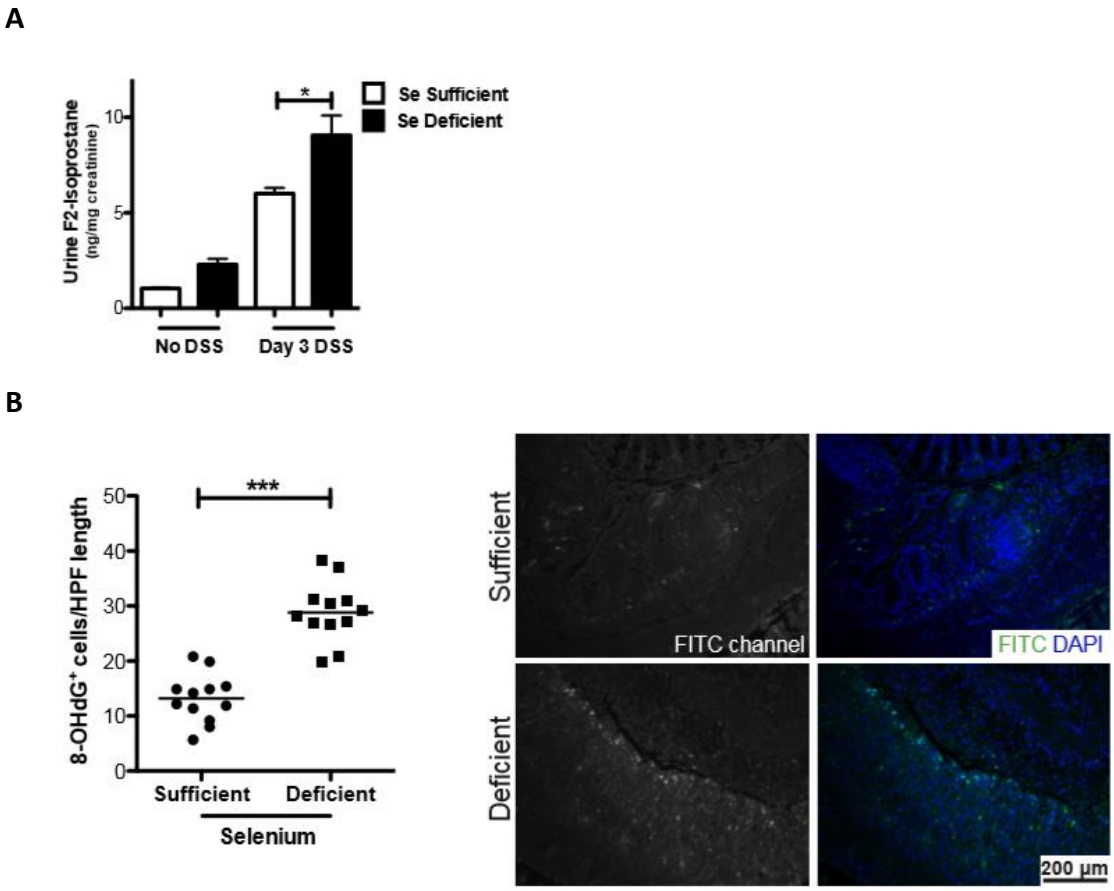

*Figure 2.5 Selenium deficiency induces oxidative stress as measured by F_2-isoprostanes and DNA damage A. Selenium-sufficient (n=3, white bars) and -deficient (n=3, black bars) mice were given 3% DSS ad lib. and maintained in metabolic cages. Urine was collected at days 0 and 3 of DSS administration and F_2-isoprostanes were measured and normalized to mg of creatinine. *P=0.05, 1-way ANOVA. B. 8-OHdG (FITC) staining was performed in Se-sufficient (n=12) and -deficient (n=12) mice post-DSS morbidity protocol and quantified based on number of positive cells per high-powered field (HPF, 40x) length (left). Representative staining is shown on the right. ***P<0.0001.*

DNA damage is increased in selenium-deficient mice in response to DSS.

As inflammatory injury and lipid peroxidation were upregulated in Se-deficient mice, and because Se has been linked with DNA damage repair (136, 317), we next determined whether DNA damage was increased in these mice. Colonic epithelial 8-OHdG

staining, which identifies oxidative damage to DNA, was significantly increased in Se-deficient mice after DSS injury (13.2 ± 1.3 vs 28.8 ± 1.6 8-OHdG$^+$ cells/HPF length, *P*<0.0001, Figure 2.5B). Thus, Se-deficiency exacerbated colitis and was associated with increased pro-inflammatory and pro-tumorigenic cytokines and increased DNA damage. These changes collectively produce a microenvironment primed for tumorigenesis.

Dietary selenium protects from inflammatory carcinogenesis.

Because Se deficiency promoted an activated pro-tumorigenic microenvironment and DNA damage after DSS treatment, we next determined if Se status modified inflammatory carcinogenesis. AOM is a procarcinogen that is metabolically activated to a potent alkylating agent forming O^6-methyl-guanine (318). Its oncogenic potential is markedly augmented in the setting of chronic inflammation, such as that induced by repeated cycles of DSS treatment (319, 320).

To determine if dietary Se modifies CAC, we modeled inflammatory carcinogenesis in Se-deficient or –sufficient C57BL/6 mice using AOM/DSS (Figure 2.6A). At necropsy, Se-deficient mice demonstrated increased tumor multiplicity (3.4 ± 0.4 vs 7.6 ± 0.9 tumors/mouse, *P*=0.0002, Figure 2.6B) as well as a higher degree of dysplasia (*P*<0.0001, Figure 2.6C) compared to Se-sufficient mice. Consistent with the morbidity

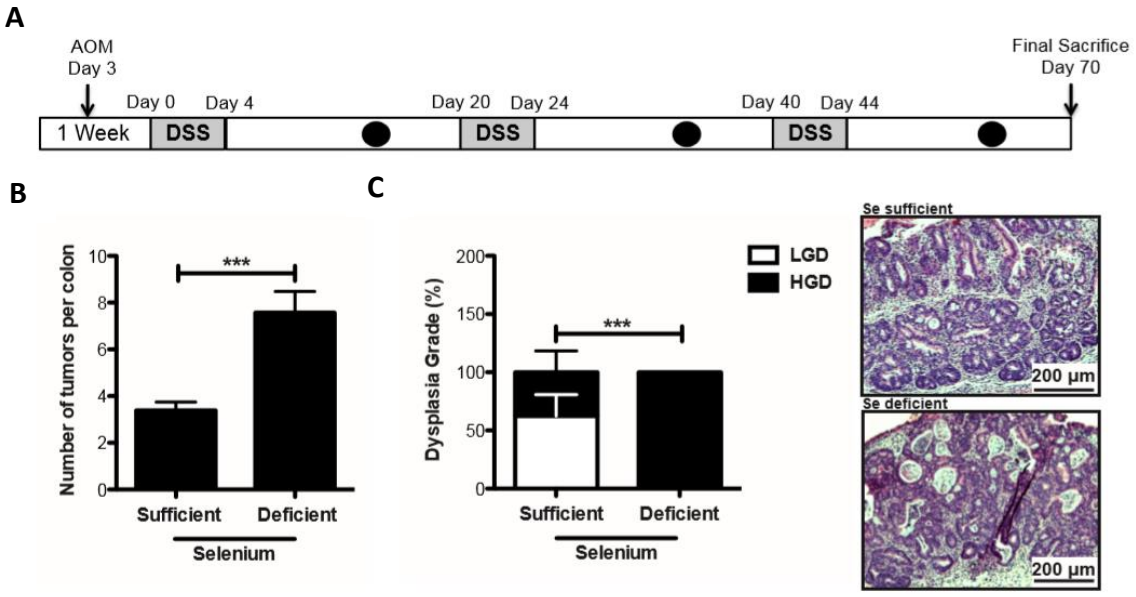

*Figure 2.6 Selenium protects against tumor initiation and progression in inflammatory carcinogenesis. A. Schematic of the AOM/DSS CAC protocol. Mice are injected with AOM 4 days prior to beginning the first of three 4-day cycles of DSS. There are 16 days between each DSS cycle and mice are sacrificed 26 days after their last cycle of DSS. Black circles indicate periods at which mice are endoscopically analyzed. B. Selenium sufficient (n=18) and deficient (n=20) mice were subjected to the AOM/DSS protocol and tumor number was analyzed. ***P=0.0002. C. Tumors were analyzed (by pathologist M.K. Washington) for dysplasia grade (LGD=low-grade dysplasia, HGD=high-grade dysplasia) and quantified based on percent of tumors demonstrating each grade (left, HGD ***P<0.0001, Fisher's exact test). Representative H&E stained colons are displayed on the right.*

studies (Figure 2.2), there was an increase in morbidity in Se-deficient mice in response to the AOM/DSS protocol (Figure 2.7A), though this difference was not statistically significant. We did not detect alterations in colon weight or length, however, suggesting that Se-deficient mice did not sustain chronic inflammatory changes in response to the AOM/DSS protocol (Supplementary Figure 2.7B and C), at least when evaluated after the 26-day recovery period. Taken together, these data suggest that Se serves as a tumor suppressor that exerts its influence at the levels of tumor initiation and progression.

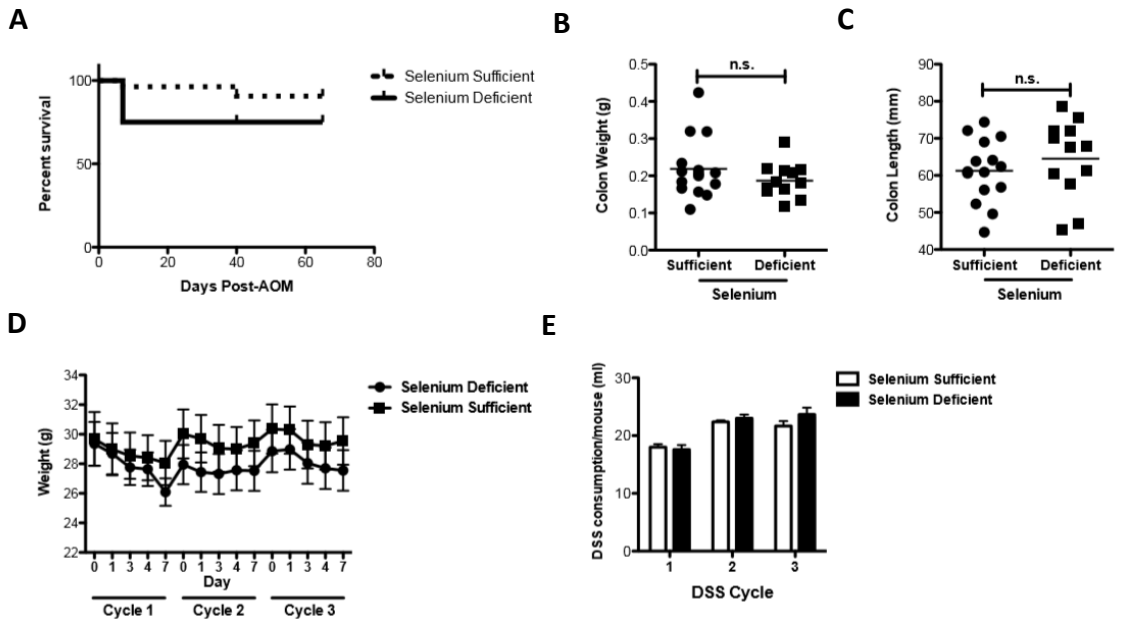

Figure 2.7 Selenium levels do not significantly impact survival, colon weight, colon length, or mouse weight in response to AOM/DSS. A. Survival curve of Se-deficient and -sufficient mice in response to the AOM/DSS protocol. B. Colon weight (g) and C. colon length (mm) post-AOM/DSS protocol. D. Mouse weight (g) throughout the AOM/DSS protocol measured on days 0, 1, 3, 4, and 7 of DSS administration during each DSS cycle. E. DSS consumption/mouse during the four days of DSS administration.

Selenium deficiency results in increased intratumoral proliferation and a general increase in DNA damage.

Several selenoproteins have been identified as direct WNT targets (135) and Se deficiency activates WNT signaling (286), implicating Se deficiency in a proliferation pathway that is aberrantly regulated in colorectal cancer. Furthermore, mitochondrial selenoproteins have been implicated in the regulation of mitochondrial-dependent cell death (287). As we noted an increase in tumor number in Se-deficient mice, we determined whether cellular proliferation or apoptosis indices were altered. Proliferation, as measured by Ki67 staining, was increased in the tumors of Se-deficient

mice (26.0 ± 1.9 vs 39.5 ± 2.9 Ki67^{+} cells/tumor HPF, *P*=0.0008, Figure 2.8A). Apoptosis was quantified by TUNEL staining and no difference was seen between the two groups.

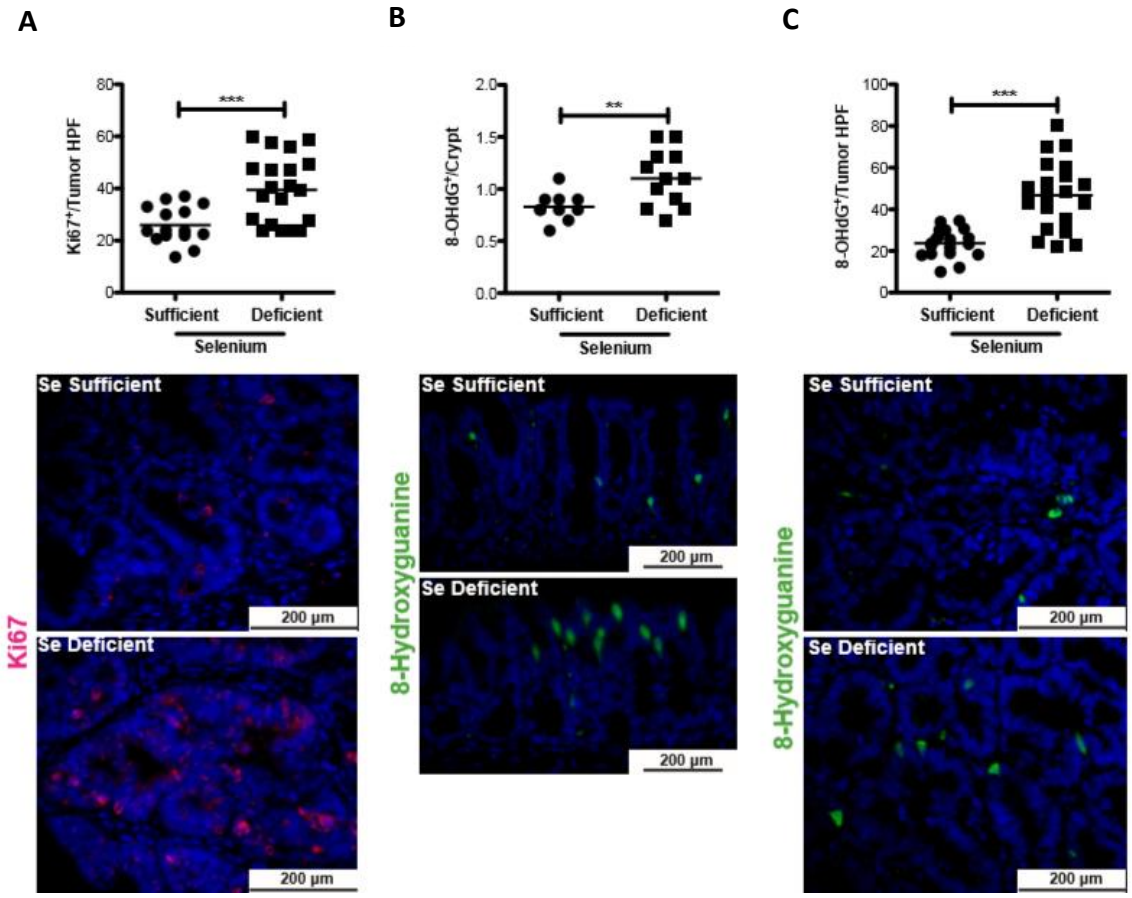

*<u>Figure 2.8</u> Selenium deficient colons demonstrate increased intratumoral proliferation and DNA damage in response to inflammatory carcinogenesis. Swiss-rolled colons of Se-sufficient and –deficient mice post-AOM/DSS protocol were analyzed for proliferation and DNA damage. A. Ki67 immunohistochemistry was conducted to identify actively proliferating cells. Intratumoral proliferation index calculated from number of Ki67-positive cells per HPF (top, Se-sufficient n=15, Se-deficient n=20, 40x). B. Immunofluorescence for 8-OHdG was conducted according to Materials and Methods. Staining is quantified per longitudinal crypt section in 20 crypts of each mouse (top) and representative images are shown (bottom). C. 8-OHdG staining is quantified per tumor HPF (top, Se-sufficient n=19, Se-deficient n=20, 40x) and representative images are shown (bottom). **P=0.009, ***P<0.0001.*

Interestingly, an increase in intratumoral proliferation is generally associated with an increase in tumor size and not number. For this reason, and due to the fact that DSS

results in DNA damage (268, 321) which can lead to changes in the initiation frequency, we stained crypts and tumors of Se-sufficient and -deficient mice with 8-OHdG. Consistent with what was observed in the DSS morbidity study, Se deficiency led to a significant increase in DNA damage within crypts (0.83 ± 0.04 vs 1.1 ± 0.08 8-OHdG$^+$/crypt, P=0.009, Figure 2.8B), as well as tumors (23.7 ± 1.5 vs 46.8 ± 3.7 8-OHdG$^+$/tumor HPF, P<0.0001, Figure 2.8C). Indicating augmented DNA damage, potentially contributing to the increased tumorigenesis observed in Se-deficient mice.

Discussion

The essential trace element Se may be useful for the prevention and/or abrogation of several diseases related to oxidative stress including neurodegenerative, cardiovascular diseases (78). In these diseases, Se deficiency is uncommon and thus therapeutic approaches targeting Se would require supranutritional amounts of Se for treatment. This point is important because harmful side-effects of supranutritional Se have been identified including increased risk for diabetes (81). In contrast, IBD is a disease characterized by chronic inflammation, high oxidative stress and Se deficiency making it a potential target for Se supplementation, with the goal being to restore Se nutritional status to the normal range. In support of this concept, our results demonstrate that, in fact, Se sufficiency protects against DSS-induced injury when compared to Se deficiency as morbidity, weight loss, and mucosal injury in response to DSS were all significantly increased in mice fed a Se-deficient diet. Moreover, Se may protect against mucosal injury by decreasing expression of pro-inflammatory cytokines; as such we detected increased

mRNA expression of the B cell chemoattractant chemokine (C-X-C motif) ligand 13 (*Cxcl13*), the T cell inflammation associated Chemokine (C-C motif) ligand 27 (*Ccl27*), the lymphocyte chemoattractant Chemokine (C-C motif) ligand 20 (*Ccl20*), as well as interleukin *(Il)-17c* which can promote Th17 cell responses (322). Of particular interest is the upregulation of *Il-23a*, as Il-23 has been shown to be a pro-inflammatory factor and target protein for inhibitory therapy in Crohn's disease, since it has major effects on Th17 cell differentiation (323). These data suggest that restoration of normal Se levels may be a therapeutic option in IBD.

DSS-induced colonic injury, like ulcerative colitis, results in increased oxidative stress, which is at least partly attributable to immune cell infiltration and the release of inflammatory mediators (324, 325). One method to quantify oxidative injury is to assess lipid peroxidation via measurement of F_2-isoprostanes (F_2-IsoPs), non-enzymatic derivatives of arachidonic acid (309). It is important to note that, although lipid peroxidation is an indirect measure of oxidative stress, the Biomarkers of Oxidative Stress Study (BOSS) identified F_2-IsoPs as the most reliable index of *in vivo* oxidative stress when compared against other known biomarkers (316). Other labs have demonstrated increased F_2-IsoPs in response to DSS using the Cayman assay (326, 327). We utilized stable isotope dilution gas chromatography mass spectrometry analysis of F_2-IsoPs to demonstrate that Se deficiency further augments the effects of DSS, indicating that DSS-induced lipid peroxidation, an indicator of oxidative injury, is increased in response to Se deficiency upon DSS administration and implicating Se in protection from lipid peroxidation in the DSS model.

Chronic inflammation and cyclic epithelial injury characteristic of IBD results in increased cancer risk, although the magnitude of this risk is unclear (300). In our studies we found that Se deficiency leads to increased colonic injury and inflammation. Additionally, several TGF-β signaling components were aberrantly expressed in Se-deficient mice after DSS treatment. Transcripts for bone morphogenetic protein 8b (*Bmp8b*), which important for primordial germ cell determination (328), and a second TGF-β family member, growth differentiation factor 1 (*Gdf1*), were downregulated in DSS-treated Se-deficient mice. Gdf1 is correspondingly underexpressed in salivary gland adenoid cystic carcinoma (329) suggesting a potential role as a tumor suppressor. Furthermore, *Tgf-β1* gene expression is upregulated in Se-deficient mice and has been implicated in the pathogenesis of colorectal neoplasia and several polymorphisms have been identified in colorectal adenoma which lead to *Tgf-β1* overexpression (330, 331). *Tgf-β2*, also identified as overexpressed in Se-deficient mice, has been linked with tumor promotion as it is upregulated in colorectal, breast, pancreatic, and brain cancer (332).

Transcripts of the EGF pathway are also upregulated in Se-deficient mice with pathway members including epidermal growth factor (*Egf*), insulin-like growth factor 1 (*Igf1*) and neuregulin 4 (*Nrg4*) all demonstrating increased expression in Se-deficient compared to -sufficient mice subjected to the DSS morbidity protocol. EGF is upregulated nearly 3-fold in colorectal carcinoma (333) and the EGF signaling pathway is intimately linked to promotion of solid tumor growth (334). These data coupled with the fact that we also see increased expression of the ephrins *Efnb2* and *Efnb3*, which are known to contribute to tumor promotion as well as progression (335), suggest that the signaling

cascades and inflammation resulting from Se deficiency after DSS injury may result in increased cancer risk.

Beyond activation of oncogenic signaling pathways, Se deficiency may promote tumorigenesis via affecting genomic integrity (129). Supplementation with moderate levels of Se compounds both *in vivo* and *in vitro* is thought to protect against the formation of DNA adducts and maintain chromosomal stability and telomere length and function (136). In support of this we found that Se deficiency did, in fact, increase DNA adduct formation, a marker of DNA damage, after DSS-induced colonic stress, suggesting another mechanism by which Se might inhibit tumorigenesis in CAC.

Two prior studies report on the effects of reduced dietary Se in inflammatory colon tumorigenesis. Both have demonstrated a subtle, non-significant, increase in tumorigenesis with decreased dietary selenium (141). There are several potential explanations for why we observed a significant increase in tumor burden in our studies; 1) Differences in model selection, 2) strain of mice studied, and 3) degree and magnitude of Se deficiency. Our mice were fed Se-deficient diets (less than 0.01 mg Se/kg) for 12 weeks prior to the initiation of our protocols. This extensive time-frame was selected because our group has previously determined that this will ensure Se deficiency (336). In our current studies we confirmed Se deficiency by measuring plasma Gpx activity and colonic Se levels. In contrast, the prior studies used low Se diets (0.02 and 0.086 mg Se/kg, respectively) for shorter time periods before protocol initiation. Our AOM/DSS protocol employs a single injection of AOM followed by cyclical administration of 3% DSS. Using this protocol, we achieved a tumor penetrance of 100% revealing a significant role of Se

deficiency in inflammatory carcinogenesis. Furthermore, our data suggest that Se may also protect from tumor progression as more advanced lesions occurred in the setting of Se deficiency.

There is considerable epidemiological evidence indicating that Se levels and cancer are inversely correlated (103, 288, 290, 337). Dietary intervention studies targeting Se have been inconsistent, however. Our findings suggest that Se supplementation, as a therapeutic intervention, should be targeted to patient populations, or individual patients, with demonstrable Se deficiency. Importantly, our data indicate that patients with IBD, a disease in which Se deficiency occurs, might benefit from Se supplementation to prevent CAC. Beyond IBD and CAC, there needs to be a concerted effort towards fully understanding the molecular basis for how Se protects from tumorigenesis, in what cancers Se is important, at what dietary levels Se is most beneficial, and in which patient populations selenium supplementation might have a beneficial impact.

Acknowledgments

This work was supported by the National Institutes of Health grants DK080221 (CSW), R01DK82813 (RFB), P50CA095103 (MKW), R01AT004821 (KTW), R01AT004821-S1 (KTW), R01DK053620 (KTW), P01CA028842 (KTW), P01CA116087 (KTW), 1F31CA167920 (CWB), and P30 DK058404 (Vanderbilt Digestive Disease Center), Merit Review Grants from the Office of Medical Research, Department of Veterans Affairs 1I01BX001426 (CSW) and 1I01BX001453 (KTW), and ACS-RSG 116552 (CSW). The funders had no role in study design, data collection and analysis, decision to publish, or preparation of the manuscript.

This work was supported by an NCI T-32 Supplement T32CA009592-26. This publication was also supported in part by the NCI Cancer Center Support Grant P30CA068485 utilizing the Translational Pathology shared resource, which provided tissue processing and staining services. The content is solely the responsibility of the authors and does not necessarily represent the official views of the NCI or the NIH. The authors thank Teri Stevenson and Michelle Chatterton for help with animal husbandry, members of the Williams and Burk laboratories for thoughtful discussions about this research project.

CHAPTER III

TUMOR SUPPRESSOR FUNCTION OF THE PLASMA GLUTATHIONE PEROXIDASE GPX3 IN COLITIS-ASSOCIATED CARCINOMA[2]

Introduction

Inflammatory bowel disease (IBD), which affects 1 in 600 Americans, is characterized by severe and chronic inflammation. Such inflammation is a known contributor to cancer as it promotes an environment rich in chemokines, cytokines, and reactive oxygen species (ROS) influencing epithelial proliferation and survival programs and impacting genomic integrity (15, 299). For example, patients with IBD demonstrate increased nitric oxide production via activated macrophages and granulocytes and increased plasma levels of the marker for DNA damage 8-hydroxydeoxyguanosine (299, 338). As such, the risk for cancer is increased 6-fold in patients with IBD compared with the general population, and cancer, or risk thereof, is a cause of significant morbidity in IBD (300).

Selenium is a necessary trace element that is present in the primary structure of selenoproteins as selenocysteine. Several epidemiological studies have inversely correlated nutritional selenium status with colon and prostate cancer risk, although this is somewhat controversial. The effect of selenium status in IBD has not been definitively

[2] This work has been published under *Caitlyn W. Barrett, *Wei Ning, Xi Chen, J. Joshua Smith, Mary K. Washington, Kristina E. Hill, Lori A. Coburn, Richard M. Peek, Rupesh Chaturvedi, Keith T. Wilson, Raymond F. Burk, Christopher S. Williams (2013) Tumor suppression function of the plasma glutathione peroxidase Gpx3 in colitis-associated carcinoma, Cancer Research, 73, 1245-55 (3).

evaluated. It is proposed that the effect of selenium on carcinogenesis is realized by the selenoproteins into which it is incorporated. In support of this, mouse models with impaired selenoprotein expression demonstrate increased aberrant crypt foci, a preneoplastic colon lesion, and breast cancer incidence (292, 339). The selenocysteine present in the catalytic triad of glutathione peroxidases is optimized by hydrogen bonding with glutamine and tryptophan residues, enhancing its activity and, in the case of certain glutathione peroxidases such as GPX1, this allows it to exert antioxidant activity (68, 340). One mechanism, though by no means the only, by which glutathione peroxidases may reduce cancer risk is by blunting the tumor-promoting effects of oxidative stress.

Gpx3, or plasma glutathione peroxidase, is the only known selenocysteine-containing extracellular form of glutathione peroxidase (Gpx) and accounts for nearly all of the glutathione peroxidase activity in plasma (341). *Gpx3* mRNA is expressed in a tissue-specific manner by the kidney, heart, lung, liver, brain, adipose tissue, breast, and gastrointestinal tract, but the majority of plasma Gpx3 is kidney-derived (342-344). It is likely that other organs contribute to plasma Gpx3 as nephrectomized rats retain 30% of original glutathione peroxidase activity (345). Gpx3 is transported via circulation where it binds to the basement membranes of epithelial cells such as those in the gastrointestinal tract (346). Gpx3 promoter hypermethylation and downregulation is commonly seen in human cancer (298, 347-349). In prostate cancer, hemizygous and homozygous deletions as well as methylation of the first exon of Gpx3 frequently occur (349). Promoter hypermethylation insures decreased expression of Gpx3 in gastric, cervical, thyroid, head and neck, and lung cancers, and in melanoma (347, 348) suggesting that Gpx3 serves as a

tumor suppressor in these cancers. Genetic evidence supports a role for GPX enzymes in IBD with Gpx1;Gpx2 double knockout mice developing spontaneous ileocolitis (350) and intestinal carcinoma that is associated with bacteria-induced inflammation (351). In fact, Gpx2 alone may have a protective role in inflammatory carcinogenesis (141). The role of Gpx3 in these processes has never been directly tested.

We hypothesized that loss of Gpx3 would enhance tumorigenesis in inflammatory carcinogenesis, a process rich in ROS production and chemokine/cytokine driven pro-proliferative stromal signals (15, 299, 352-354). In order to test this we applied the azoxymethane/dextran sodium sulfate (AOM/DSS) murine inflammatory carcinogenesis model to *Gpx3*$^{-/-}$ mice. This model has been used to identify modifiers of colitis-associated carcinoma including NF-κB (265), TLR4 (266), TNFα (355), and Mtgr1 (269), as well as innate immune responses (33) and intestinal microflora (356). We found a striking increase in tumor number in the absence of Gpx3, indicating a direct impact of Gpx3 on tumor initiation. In support of an initiating role, *Gpx3*$^{-/-}$ mice demonstrated increased DNA damage. Tumors in *Gpx3*$^{-/-}$ mice demonstrated increased inflammation as well as increased infiltration of M2 macrophages, proliferation, and nuclear β-catenin. *Gpx3*$^{-/-}$ tumors were also more advanced. As expected, knockdown of Gpx3 in the human colon cancer cell line Caco2 resulted in increased ROS production and DNA damage. Thus we provide genetic evidence that Gpx3 behaves as a potent tumor suppressor during inflammatory carcinogenesis *in vivo* likely by decreasing the ROS and DNA damage that lead to tumor initiation.

Materials and Methods

Murine Inflammatory Carcinogenesis and Chronic Colitis Protocols. 7-8 week old C57Bl/6 WT (n=17) or congenic *Gpx3*$^{-/-}$ (n=20) mice were injected with 12.5 mg/kg of AOM (Sigma-Aldrich) intraperitoneally as described in Greten, *et al* (265). After a three-day recovery period the animals were started on the first of four cycles of 3% DSS *ad libitum* (see Schematic in Figure 3.1A). Each cycle lasted 5 days and was separated by a 16-day recovery period. A second DSS-only control arm was included for C57Bl/6 WT (n=14) and *Gpx3*$^{-/-}$ (n=19) that followed the same protocol outlined above excluding the AOM injection. After the last cycle, animals were sacrificed following a 26-day recovery period. Tumor counts and measurements were performed in a blinded fashion under a stereo dissecting microscope. Each colon was then bisected longitudinally and half was Swiss rolled for microscopic analysis and the other half was partitioned into normal and tumor tissue and saved for protein and RNA analysis. Microscopic analysis was performed by a gastrointestinal pathologist (MKW) for severity of inflammation (357) and dysplasia on haematoxylin and eosin (H&E) stained "Swiss rolled" colons (processed by the Vanderbilt Translational Pathology Shared Resource core). Four days after the third cycle of DSS, murine endoscopy was utilized in order to monitor colitis severity (358) and tumor burden. All *in vivo* procedures were carried out in accordance with protocols approved by the Vanderbilt Institutional Animal Care and Use Committee.

Plasma Glutathione Peroxidase Activity Assay. Blood was collected from mice via the vena cava and plasma was separated from erythrocytes (K_3EDTA) by centrifugation at 12,000 rpm for 1 minute. Glutathione peroxidase activity was determined according to a

modified protocol (307) based on the method of Paglia and Valentine (308). Briefly, 800 μl reaction cocktail (50 mM potassium phosphate, pH 7.0, 1 mM EDTA, 1 mM NaN_3, 0.2 mM NADPH, 1 E.U./ml GSSG-reductase, and 1mM GSH) was mixed with 20 μl plasma and 80 μl water in a clear plastic cuvette and incubated at room temperature for 5 minutes. 100 μl hydrogen peroxide (H_2O_2) substrate (0.25 mM H_2O_2 in H_2O) was added to the reaction mixture to initiate reaction. Gpx activity was assessed by measuring the rate of change of A_{340} per minute over a 3 minute time period after the addition of H_2O_2 to the reaction mixture. The enzymatic reaction is linear during this time period. The rate of change was then converted to the number of μmol NADPH oxidized per minute using the extinction coefficient of 6.2×10^3 L mol^{-1} cm^{-1} for NADPH at 340 nm. Blank reactions with plasma replaced by distilled water were subtracted from each assay.

Oxidative stress gene RT-PCR. RNA was made from 30 mg WT water treated colons and normal adjacent tissue from AOM/DSS colons using the RNeasy Mini kit (Qiagen), according to the manufacturer's directions. cDNA was then made using the SuperScript cDNA kit (Invitrogen). RT-PCR was then performed using an oxidative stress primer library (HOSL-1, Realtimeprimers.com). Reactions were performed according to the manufacturer's recommendations. Analysis was performed using the delta-delta-Ct method.

Immunohistochemistry and immunofluorescence. Five-micrometer sections were cut, dewaxed, hydrated and endogenous peroxidase activity quenched with 0.03% hydrogen peroxide in MeOH. Antigen retrieval was performed using the boiling sodium citrate method in a microwave (20 mmol sodium citrate pH 6.5) for 16 minutes at 30% power.

After blocking, primary antibody was added (α-Ki67, (NeoMarkers), 1:1000; α-8-hydroxy-2’ deoxyguanosine (Abcam) 1:50; α-β-catenin, (BD Transduction Laboratories), 1:1000; α-arginase I (Arg1), (Santa Cruz), 1:500; α-IL-1β, (R&D Systems), 1:50; FITC-α-F4/80 (eBioscience), 1:1000) and incubated overnight at 4°C. Isotype-matched antibodies were included as negative controls. The Vectastain ABC Elite System (Vector Labs) was used to visualize staining for immunohistochemistry. Identification of intratumoral apoptotic cells was performed using the ApopTag Plus Peroxidase in situ Apoptosis Kit (Chemicon) according to the manufacturer's protocol. Control stains were obtained by omitting the terminal transferase (TnT) enzyme. For immunofluorescence staining of macrophage markers and DNA damage, slides were counterstained and mounted with ProLong Gold antifade including DAPI (Invitrogen). Gpx3 staining was performed as described (346). Immune cell, apoptosis, and proliferation indices were generated by counting the number of positive cells per high-powered field (HPF; 40× objective) within each tumor by a blinded observer. A β-catenin index was employed, as previously reported (269). This index is generated by multiplying the staining intensity (on a scale of 1-4) by percentage of the cells demonstrating nuclear staining. The average score was then calculated for each Swiss rolled colon.

Cell Culture and shRNA Knockdown. Caco2 human colon tumor cells were obtained from ATCC (HTB-37) and had morphologic characteristics consistent with their known identity. Formal authentication was not performed. Caco2 cells were maintained in DMEM supplemented with 10% FBS and penicillin/streptomycin (P/S). HEK293T cells were maintained in RPMI1640 supplemented with 10% FBS and P/S. HEK293T packaging cells

were transfected with Mission shRNA constructs (Sigma-Aldrich) specific for human Gpx3 (clone ID: TRCN0000273651-NM, TRCN0000273684, and TRCN0000008678) as well as the PAX2 and pMD2.G plasmids using the Calcium Phosphate transfection method. Twenty-four hours post-transfection, medium was removed from the HEK293T cells and passed through a 0.45 μM filter. 4 μg/ml Polybrene (Millipore) was added to the filtered media. Growth medium was removed from Caco2 cells and replaced with infection medium. After 6 hours, the infection medium was replaced with normal growth medium and the infection process was repeated 24 hours later. Cells were selected for knockdown using 5 μg/ml Puromycin (Invitrogen) over a 3-day period. Knockdown was analyzed by the delta-delta-CT method following RT-PCR using Gpx3-specific Taqman probes (Invitrogen) and by Western blotting using rabbit anti-mouse Gpx3 8096 (dilution 1:5000; custom-made by Rockland).

ROS Determination. Caco2 cells infected with either scrambled or Gpx3-specific shRNA were pre-treated with 500 U/ml PEGylated catalase (PEG-CAT, Sigma) one hour prior to 1.5 hour treatment with 200 μM H_2O_2. Either ROS detection reagent 6-carboxy-2',7'-dichlorodihydrofluorescein diacetate, di(acetoxymethyl ester) (DCFH2, Invitrogen) or the oxidation insensitive analog of DCFH2 (DCF, Invitrogen) was used to stain treated cells according to the manufacturer's protocol for flow cytometry analysis. In short, cells plated on a 6-well plate in phenol red-free medium were washed with 500 μl PBS. Cells were then resuspended in 1 μM DCFH2 or 0.5 μM DCF in pre-warmed PBS and incubated for either 20 minutes or 5 minutes at 37°C, respectively. Cells were then washed twice with

PBS and centrifuged at 1600 rpm for 6 minutes between washes. Cells were analyzed for positivity by flow cytometry.

Detection of DNA Damage and Active Caspase-3 by Flow Cytometry. Caco2 (sh-scrambled) and Caco2 (sh-hGpx3) cells were treated with H_2O_2 (100 μM) for 4 hours and washed with PBS, fixed in 0.1% paraformaldehyde, and permeabilized with 100% methanol on ice. Levels of DNA damage and active caspase-3 were assessed as described previously (359). In brief, cells were incubated with rabbit anti-active caspase-3 antibody conjugated with phycoerythrin (PE; dilution 1:50; BD Biosciences) and 8-oxoguanosine–binding peptide conjugated with fluorescein isothiocyanate (dilution 1:100) for 30 minutes at room temperature. Cells were acquired with a BD LSRII system (BD Biosciences) and analyzed using FlowJo software (Star tree, Ashland, OR).

Matrigel Colony Formation Assay. The day prior to Matrigel plating, Matrigel (BD, 354234) at 9 mg/ml was thawed overnight in ice at 4°C. For each well of a 48-well plate, 50 µl ice cold Caco2 media (DMEM supplemented with 10% FBS and pen/strep) was mixed with 50 µl Matrigel. Plates were then allowed to solidify at 37°C for thirty minutes. Caco2 cells were trypsinized, washed with PBS, and diluted to 10,000 cells/ml in 2 ml media. A 1:1 mixture of cells and Matrigel was added to the wells in the prepared 48-well plate and incubated at 37°C for thirty minutes. To avoid drying, 200 µl complete Caco2 media was added to each Matrigel-filled well. Cells were maintained at their normal growth conditions and media was changed every 2-3 days. On day 22, cells were counted using GelCount (Oxford Optronix, Oxford, UK).

Results

Glutathione peroxidase activity is decreased and oxidative stress is increased in AOM/DSS-treated mice.

Gpx3 is often downregulated in cancer (298, 347-349) and we sought to determine whether its expression or activity was altered in the AOM/DSS model of inflammatory carcinogenesis. For these experiments, 7-8 week old mice were injected with AOM and treated with 4 cycles of DSS as defined in the Methods section and shown in Figure 3.1A. During the course of this protocol, six *Gpx3*$^{-/-}$ mice died (lost over 20% of original body weight and were sacrificed), two after cycle 1, two after cycle 2, and two during cycle 4 of DSS. Whereas, as is typical with this protocol, two WT mice died, both after cycle 4, a time when we usually see mortality. These mice were not included in the final analysis. This increased morbidity suggests that Gpx3 may protect the mucosa from DSS induced injury.

As decreased Gpx3 levels are commonly seen in cancer, we first tested plasma Gpx3 activity in mice receiving water only versus mice post the AOM/DSS protocol to determine if Gpx3 activity might be altered. Measurement of oxidation of NADPH allowed us to determine that AOM/DSS leads to diminished plasma glutathione peroxidase activity (497.7 ± 56.9 versus 239.4 ± 40.8 nmol NADPH oxidized/ml plasma/min, P=0.0013, Fig. 3.1B). We next wanted to determine if local Gpx3 mRNA levels were affected in AOM/DSS tumorigenesis. There was no difference in *Gpx3* mRNA expression between matched tumor and adjacent normal mucosa samples, but other oxidative stress

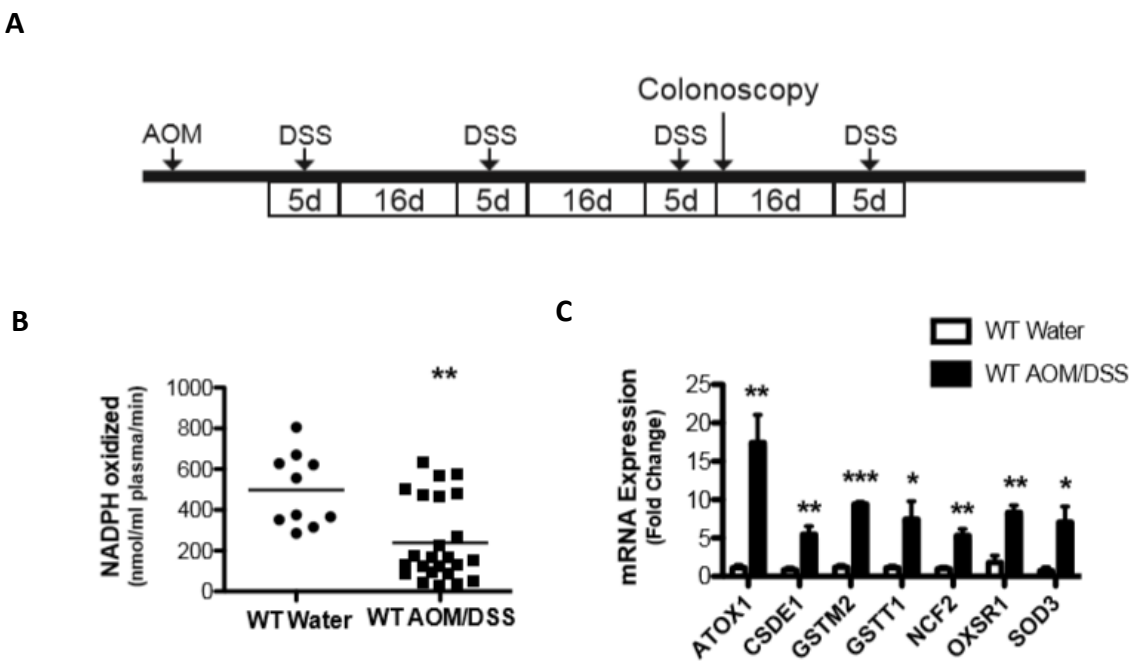

*Figure 3.1 Plasma Gpx3 activity is decreased and oxidative stress genes are increased in mice subjected to the AOM/DSS protocol. A, schematic of the AOM/DSS protocol. Animals injected with 12.5 mg/kg AOM at day 0 followed by 4 cycles of 3% DSS ad libitum separated by 16 days of recovery on water. B, plasma glutathione peroxidase activity determined after the completion of the AOM/DSS protocol. WT water treated, N = 10; WT AOM/DSS, N = 11; **, P = 0.0013. C, tumor tissue mRNA expression of oxidative stress genes (ATOX1, ATX1 antioxidant protein 1 homolog; CSDE1, cold shock domain containing E1, RNA binding; GSTM2, glutathione S-transferase M2, muscle; GSTT1, glutathione S-transferase theta 1; NCF2, neutrophil cytosolic factor 2; OXSR1, oxidative-stress responsive 1; SOD3, superoxide dismutase 3, extracellular) in WT water treated (N = 4) vs. WT AOM/DSS (N = 4); ***, P < 0.001; **, P < 0.01; *, P < 0.05.*

response genes were upregulated in normal adjacent colon tissue from AOM/DSS mice (Fig. 3.1C) suggesting an increase in oxidant stress resulting from the protocol. Finally, we wanted to determine if *GPX3* expression varied in a large colorectal cancer expression array dataset, and in this case *GPX3* was markedly and consistently underexpressed as early as the adenoma stage (Fig. 3.2A). We confirmed this observation with 10 matched normal/colon cancer samples by qRT-PCR, and in a second set of 10 matched samples by protein analysis, finding reduced *GPX3* levels in 80% of the samples (Fig. 3.2B & C). These

results support previous studies (298) and suggest that GPX3 may serve as a tumor suppressor in colorectal cancer.

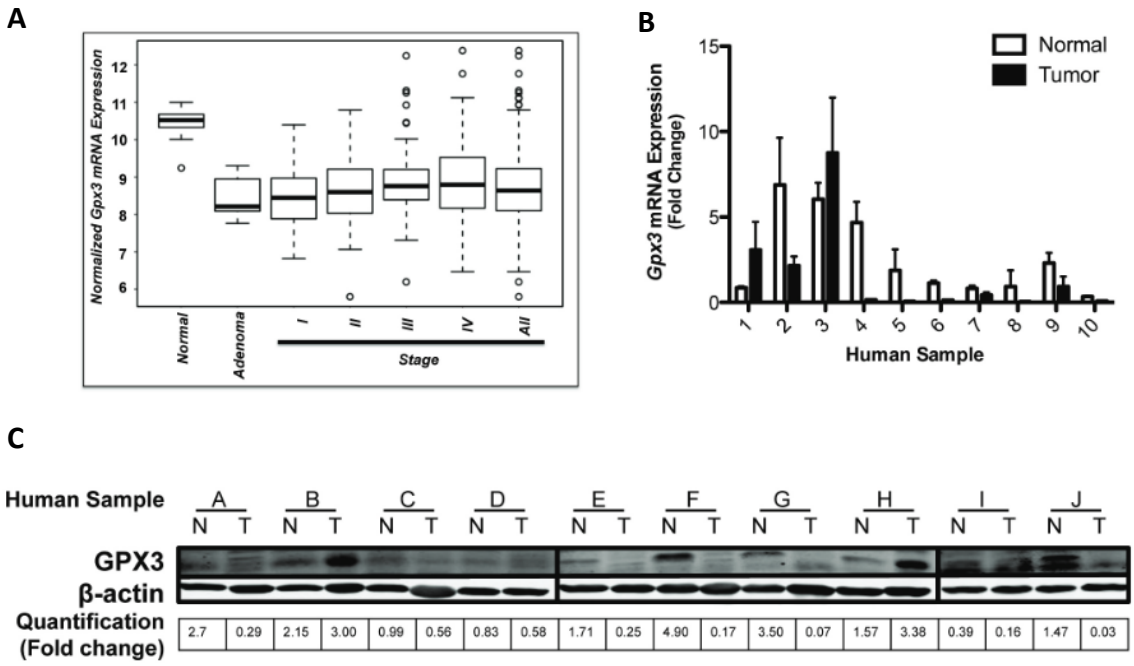

*Figure 3.2 Gpx3 expression is downregulated in human colon cancer samples. A) GPX3 expression is significantly downregulated in adenomas and colorectal cancer patients compared with normal adjacent colon tissues. **P<0.01 for each stage relative to normal. B) GPX3 expression in matched human normal and tumor samples. Error bars represent standard deviation of samples performed in duplicate. C) Western blot of GPX3 protein expression in matched human normal and tumor samples. Quantification is presented as fold change intensity controlled for β-actin.*

Gpx3 is a tumor suppressor in inflammatory tumorigenesis.

Utilizing the *Gpx3*$^{-/-}$ mouse, we directly tested whether Gpx3 was a tumor suppressor in the AOM/DSS model. 7-8 week old WT or *Gpx3*$^{-/-}$ mice were placed on the AOM/DSS protocol (Fig. 3.1A). As expected, mice lost weight and had looser stools as the result of DSS administration in both the DSS and AOM/DSS arms of the experiment,

though there was no significant difference between genotypes in these parameters. Gpx3 protein is normally seen in the colon binding the basement membrane on the basolateral

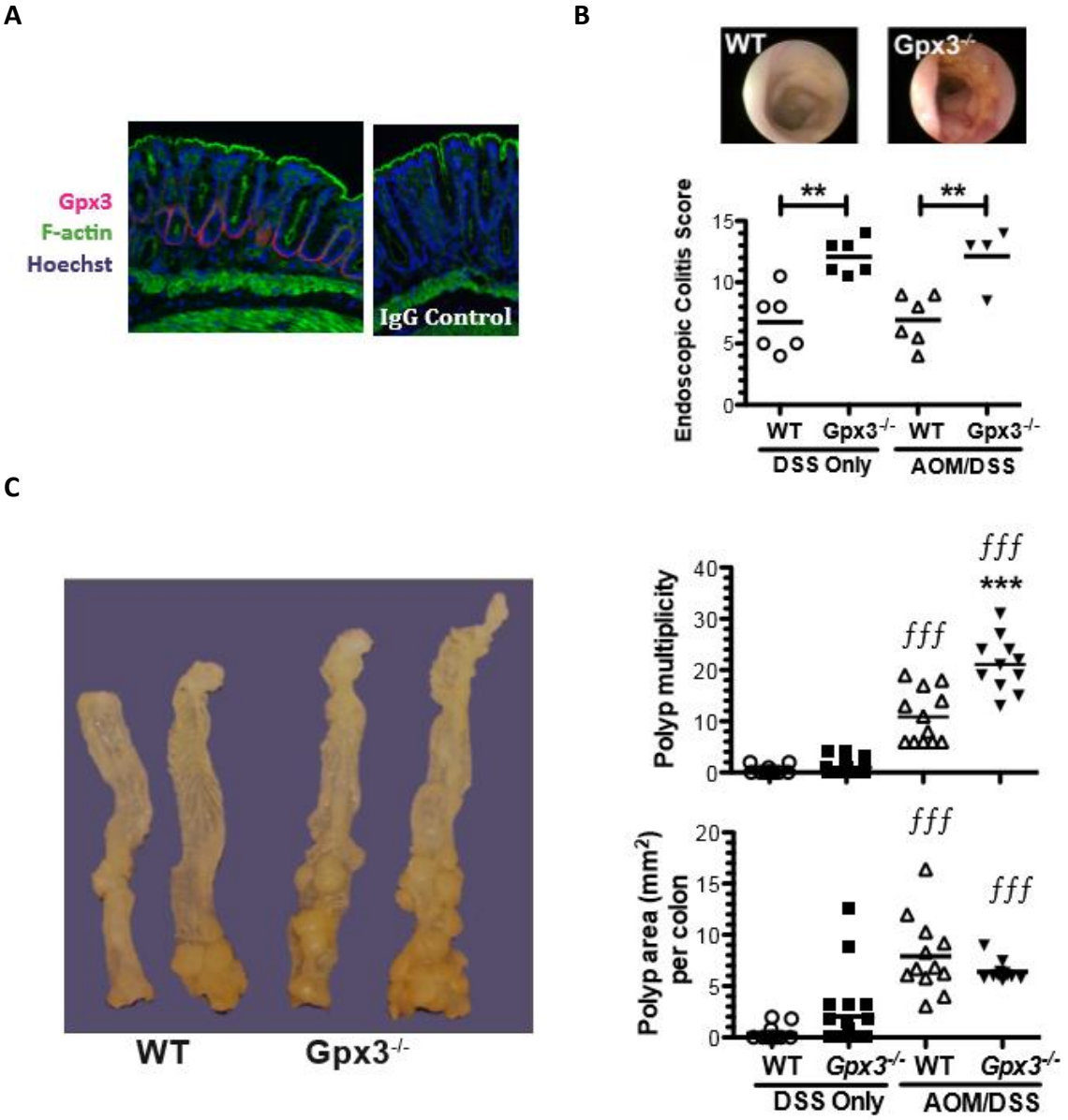

*Figure 3.3 Gpx3 functions as a tumor suppressor in inflammatory carcinogenesis. A, immunofluorescence staining of normal WT colon. Gpx3 (red), F-actin (phalloidin, green), and Hoescht (blue) staining is shown (left). Immunoglobulin G (IgG) control is shown on the right (×60 magnification). B, representative colonoscopic images from WT (top left) or Gpx3$^{-/-}$ (top right) mice after 3 cycles of DSS and murine endoscopic colitis scoring using the murine endoscopic index of colitis severity. **, P < 0.01. C, representative gross specimens from the indicated genotype (left). Tumor multiplicity (top right) and polyp burden (bottom right) are shown; results were determined via calculation of the combined surface area (Σ_{itot} $SA_i = L_i \times W_i$) of all lesions in each colon. DSS only WT, N = 13; Gpx3$^{-/-}$, N = 18, AOM/DSS WT, N = 12; Gpx3$^{-/-}$, N = 11. ***, P < 0.001 between WT and Gpx3$^{-/-}$. ^{fff}, P < 0.001 DSS only versus AOM/DSS groups.*

surface (346) (Fig. 3.3A). *Gpx3*$^{-/-}$ mice demonstrated an increased endoscopic colitis score (302) during both DSS and AOM/DSS protocols (Fig. 3.3B) with colonic thickening, vascular changes, evidence of fibrin, increased granularity, and softer stools than wild type mice (DSS: 12.1 ± 1.4 N=6 versus 6.8 ± 1.0, N=6; AOM/DSS: 12.1 ± 1.2, N=4 versus 6.9 ± 0.8; N=6, P<0.01 for both comparisons). Twenty-six days after the last DSS cycle the animals were sacrificed. Consistent with a role for Gpx3 in tumor suppression, quantification of tumor number in AOM/DSS mice demonstrated increased tumor multiplicity in *Gpx3*$^{-/-}$ mice (21.1 ± 1.6 tumors/mouse N=11 versus 10.8 ± 1.5 tumors/mouse N=12, P<0.0001). In addition, there was a trend towards increased tumor number and size in *Gpx3*$^{-/-}$ mice receiving DSS only without AOM when compared to wild-type mice (1.0 ± 0.3 tumors/mouse N=18 versus 0.4 ± 0.2 tumors/mouse, N=13, P=0.1, Fig. 3.3C).

Histologic examination by a gastrointestinal pathologist (MKW) of H&E stained sections from colons prepared as "Swiss Rolls" revealed increased injury severity based on a multi-parameter histologic injury score (357) in *Gpx3*$^{-/-}$ AOM/DSS mice (16.2 ± 2.6 N=14 versus 7.8 ± 0.92 N=16, P=0.003, Fig. 3.4A & B) with significant increases in inflammation, inflammation extent, and crypt damage/regeneration (Fig. 3.4C). Tumors were also analyzed for grade and *Gpx3*$^{-/-}$ adenomas demonstrated increased propensity for high-grade dysplasia characterized by loss of polarity and a more complex tumor growth pattern than WT tumors (Fig. 3.4D). In fact, one *Gpx3*$^{-/-}$ tumor demonstrated local invasion (Fig. 3.4A & D), a property rarely seen in response to AOM/DSS. These results suggest that Gpx3 loss results in increased colonic injury and inflammation and

contributes to tumor promotion and progression in the AOM/DSS model of inflammatory carcinogenesis.

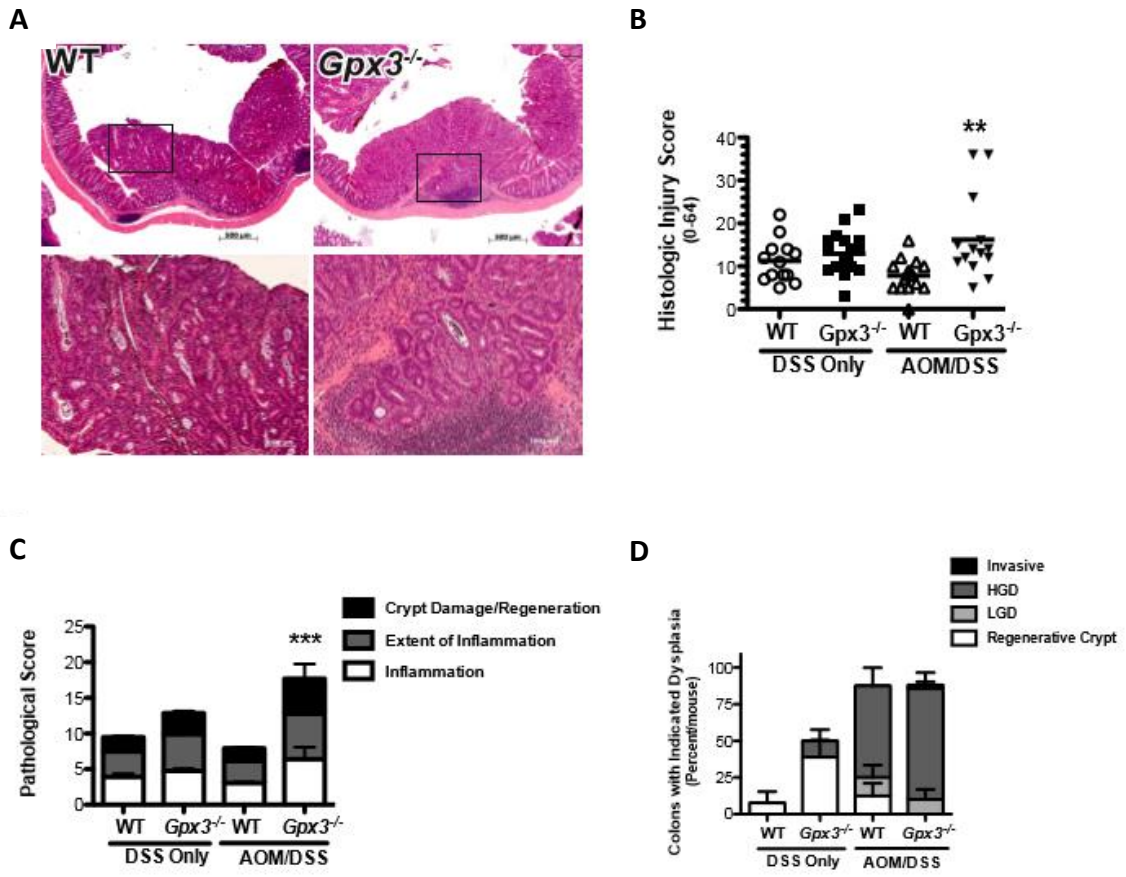

*Figure 3.4 Increased histologic injury in Gpx3$^{-/-}$ colons. A, representative H&E staining from WT (×10 top, ×20 bottom left) or Gpx3$^{-/-}$ (×10 top, ×20 bottom right) colons. There is evidence for invasive adenocarcinoma in the Gpx3$^{-/-}$ tumor. B, histologic injury score for DSS only or AOM/DSS tissues. **, P < 0.01. C, division of the histologic injury scores from B into pathologic inflammation, extent, and crypt damage/regeneration scores for DSS only or AOM/DSS tissues. ***, P < 0.001. D, dysplasia grading (conducted by M.K. Washington) in WT and Gpx3$^{-/-}$ tumors expressed as invasive, high-grade dysplasia (HGD), low-grade dysplasia (LGD), or regenerative crypt. Results represent percentage of total tumors for each group within each grade*.

Altered intratumoral proliferation in the absence of Gpx3.

Tumor number may be modified by increased cellular proliferation and/or survival or decreased apoptosis of transformed cells. Intratumoral proliferation rates were analyzed using *in situ* Ki67 staining. *Gpx3*$^{-/-}$ mice demonstrated an average of 163.9 ± 14.1

Ki67^{+} cells/tumor high-powered field (HPF). WT mice, on the other hand, displayed 73.9 ± 15.1 Ki67^{+} cells/tumor HPF (*P*=0.0003, Fig. 3.5A & B) indicating a significant increase in proliferation in *Gpx3*$^{-/-}$ tumors. No differences were seen in apoptotic indices as determined by TUNEL staining.

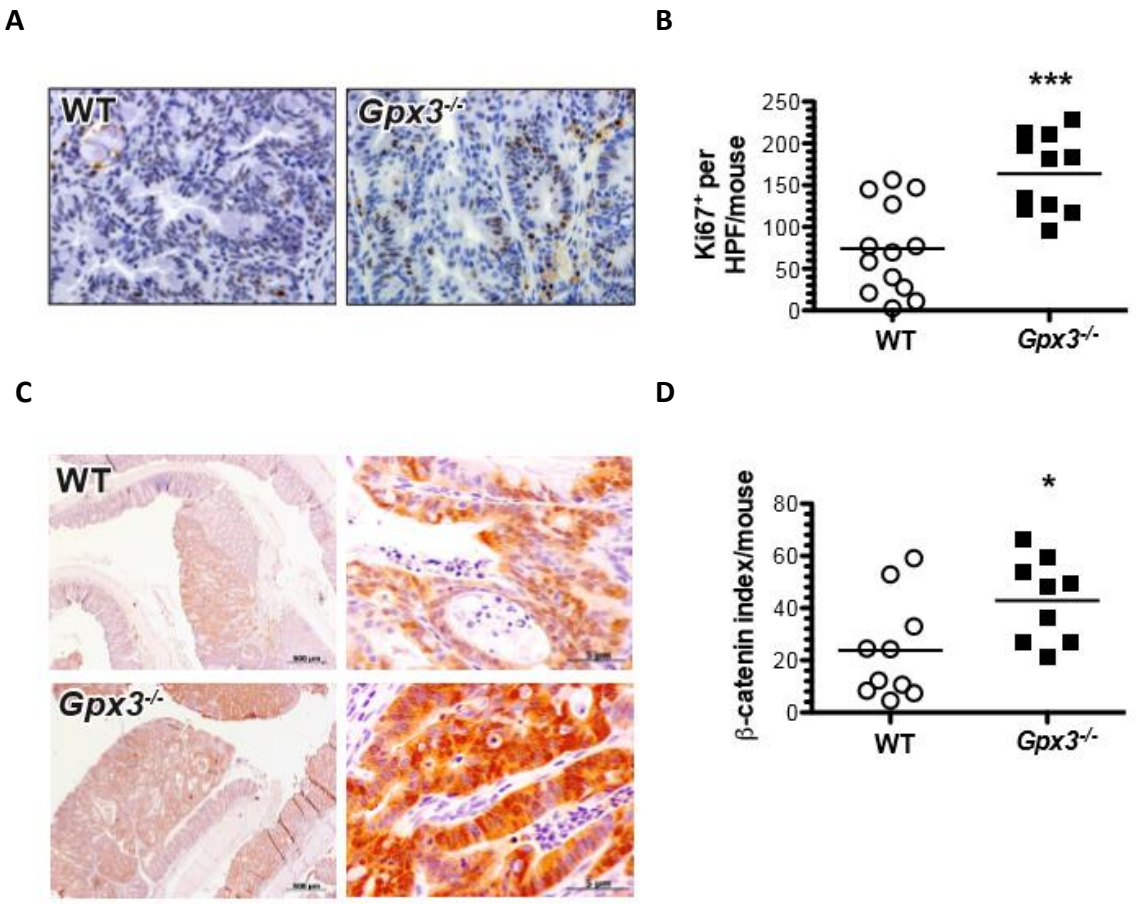

*Figure 3.5 Increased intratumoral proliferation and nuclear β-catenin in Gpx3$^{-/-}$ tumors. α-Ki67 immunohistochemistry was conducted to identify actively proliferating cells. A, representative images of Ki67 staining in WT or Gpx3$^{-/-}$ tumors (×40 magnification). B, intratumoral proliferation index calculated from number of Ki67-positive cells per HPF in 20 HPF per mouse. *** P = 0.0003. C, β-catenin expression and localization was determined via immunohistochemistry with β-catenin as per Materials and Methods (Gpx3$^{-/-}$, N = 10, WT, N = 10 tumors). Representative staining for β-catenin from WT or Gpx3$^{-/-}$ tumors (left, ×10 magnification; right, ×40 magnification). D, intratumoral β-catenin index calculated as described in Materials and Methods. * P = 0.03.*

Increased nuclear and total β-catenin in Gpx3$^{-/-}$ tumors.

Selenium deficiency in mice is predicted to stimulate the Wnt pathway (286). As the Wnt pathway is known to drive pro-proliferative and survival processes and is often hyperactive in the AOM/DSS model (264), we hypothesized that Wnt signaling, as evidenced by altered β-catenin localization, might be further perturbed in the absence of Gpx3. Therefore, we stained *Gpx3*$^{-/-}$ tumors for β-catenin localization. *Gpx3*$^{-/-}$ tumors demonstrated a significant increase in both nuclear and total β-catenin, suggesting that the Wnt pathway is upregulated in these mice, even above that typically seen in AOM/DSS tumors (Fig. 3.5C & D, *P*=0.03).

Increased M2 macrophage infiltrate and DNA damage in Gpx3$^{-/-}$ tumors.

Macrophages are major modifiers of inflammation and resolution in response to injury. Their activity and motility is also significantly modified by selenium and selenoprotein modulation (360). Since *Gpx3*$^{-/-}$ mice demonstrate increased injury and inflammation in response to AOM and DSS (Fig. 3.3B & C), Gpx3 loss may influence intratumoral macrophage composition. *Gpx3*$^{-/-}$ tumors demonstrated increased F4/80^{+} and Arg1^{+} pro-tumorigenic M2 macrophages (17.1 ± 1.7 versus 9.7 ± 1.5 F4/80^{+}/Arg1^{+} cells/tumor HPF, *P*=0.005; Fig. 3.6A & B, bottom) and decreased F4/80^{+} and IL-1β^{+} anti-tumorigenic M1 macrophages (10.1 ± 1.7 versus 18.6 ± 1.8 F4/80^{+}/IL-1β^{+} cells/tumor HPF, *P*=0.003; Fig. 3.6A & B, top) compared to WT mice, suggesting that Gpx3 may have an impact on macrophage polarization, promoting a skewing towards pro-tumorigenic macrophage distribution.

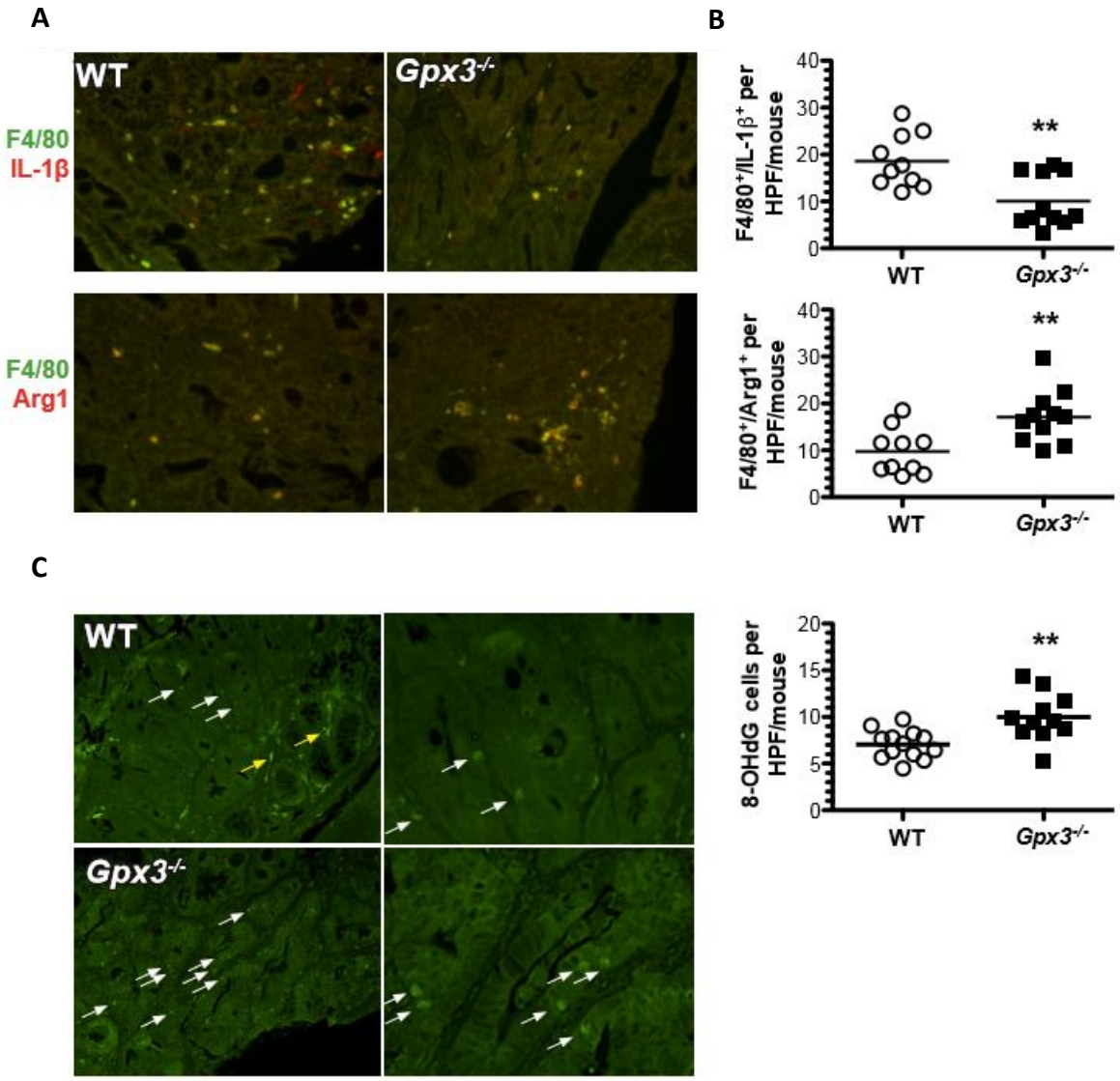

*Figure 3.6 Increased M2 macrophages and evidence for oxidative DNA damage in Gpx3$^{-/-}$ tumors. Immunofluorescence for M1 (IL-1β^{+}, F4/80^{+}) and M2 (Arg1^{+}, F4/80^{+}) macrophage markers and 8-OHdG was conducted according to Materials and Methods. A, example images from WT top row or Gpx3$^{-/-}$ tumors. B, quantification of M1 (top) or M2 (bottom) macrophages per tumor HPF. ** P < 0.01. C, example images from WT (top row) or Gpx3$^{-/-}$ (bottom row) tumors. White arrow indicates positive staining in epithelial cells, yellow arrow indicates nonspecific staining. D, 8-OHdG quantification. **P < 0.01. All images taken at ×40 magnification.*

ROS is produced during the AOM/DSS protocol as evidenced by increased expression of oxidative stress response genes (Fig. 3.1C and (361)). Because ROS can

directly induce DNA damage via oxidation and deamination of DNA bases (362), and because DNA damage is an indicator of tumorigenesis risk, we wanted to determine whether loss of Gpx3 would lead to increased DNA damage. 8-hydroxyguanine (8-OHdG) staining was performed to determine intratumoral DNA damage. In fact, *Gpx3*$^{-/-}$ tumors demonstrated evidence for increased DNA damage compared to WT tumors (10.0 ± 0.8 versus 7.1 ± 0.4 8-OHdG^{+} cells/HPF, *P*=0.002, Fig. 3.6C).

GPX3 knockdown in vitro leads to increased ROS levels and DNA damage.

To determine whether knockdown of *GPX3 in vitro* would recapitulate results seen *in vivo* we used shRNA to *GPX3* in the human colon cancer cell line Caco2. Caco2 cells were used as a model cell line because they express high levels of endogenous *GPX3* compared to other colon cancer cell lines. shRNA-mediated knockdown resulted in decreased *GPX3* expression both at the mRNA and protein levels (Fig. 3.7A). At baseline, knockdown of *GPX3* had no impact on ROS production or DNA damage, though stimulation with hydrogen peroxide (H_2O_2) resulted in a significant increase in ROS (16.1% versus 7.3%, *P*=0.0019), which was abolished with pre-treatment with the H_2O_2 scavenger PEG-CAT. Furthermore, GPX3 knockdown had no effect on the activity of the oxidation-insensitive DCFH2^{+} analog, DCF^{+} (Figure 3.7B, right graph, compare white to black bars), indicating the results obtained with DCFH2^{+} were due to changes in hydrogen peroxide concentrations as opposed to changes in uptake, ester cleavage, or efflux of the probe. There was also a concomitant increase in DNA damage (1401 versus 766 8-oxoguanosine

MFUs, $P<0.05$, Fig. 3.7C) in *GPX3* knockdown cells, consistent with data seen in tumors of *Gpx3*$^{-/-}$ mice. Thus, GPX3 does not seem to impact baseline oxidant parameters *in vitro*

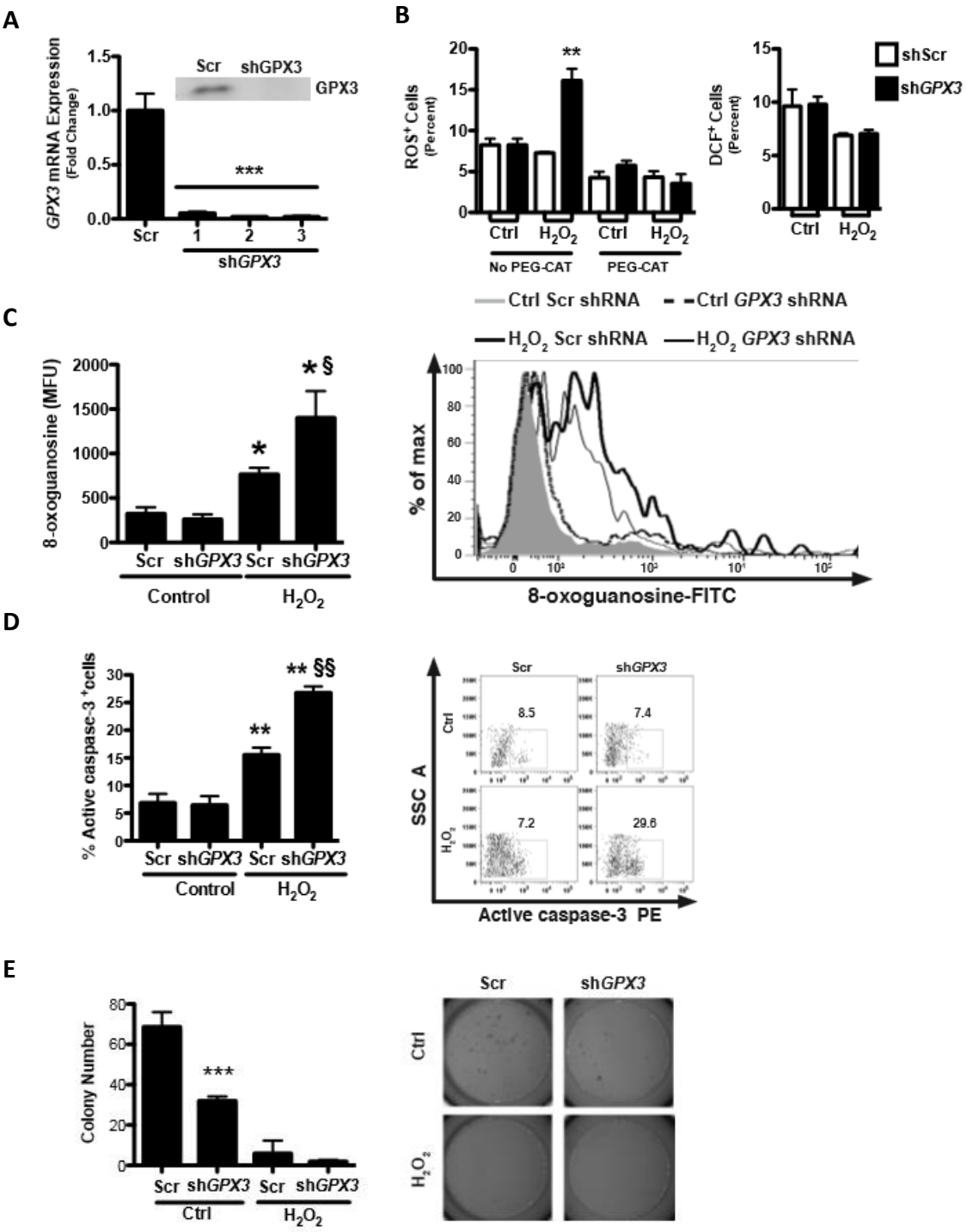
A
GPX3 mRNA Expression (Fold Change)
Scr
shGPX3
GPX3
***
Scr
1
2
3
shGPX3
B
ROS+ Cells (Percent)
**
Ctrl
H2O2
Ctrl
H2O2
No PEG-CAT
PEG-CAT
DCF+ Cells (Percent)
shScr
shGPX3
Ctrl
H2O2
C
Ctrl Scr shRNA
Ctrl GPX3 shRNA
H2O2 Scr shRNA
H2O2 GPX3 shRNA
8-oxoguanosine (MFU)
* §
*
Scr shGPX3 Scr shGPX3
Control
H2O2
% of max
8-oxoguanosine-FITC
D
% Active caspase-3 +cells
** §§
**
Scr shGPX3 Scr shGPX3
Control
H2O2
Scr
shGPX3
Ctrl
H2O2
8.5
7.4
7.2
29.6
SSC A
Active caspase-3 PE
E
Colony Number
***
Scr shGPX3 Scr shGPX3
Ctrl
H2O2
Scr
shGPX3
Ctrl
H2O2

*Figure 3.7 Increased ROS, DNA damage, and apoptosis and decreased soft agar colony formation post-GPX3 knockdown. A, GPX3 mRNA and protein (inset) expression after knockdown with GPX3-specific shRNA constructs in Caco2 cells. **, P < 0.01. B, quantification of percentage of ROS-positive cells ($DCFH2^+$) post-GPX3 knockdown in untreated or 200 µmol/L H_2O_2-treated Caco2 cells after pretreatment with the H_2O_2 scavenger PEG-CAT (left). **, P < 0.01. Quantification of percentage of DCF^+ (oxidation-insensitive analog) cells post-Gpx3 knockdown in untreated or H_2O_2-treated Caco2 cells (right). C, DNA damage as measured by 8-oxoguanosine–FITC flow cytometry in cells treated with scrambled or Gpx3-specific shRNAs and with or without H_2O_2 treatment. *, P < 0.05; [f], P < 0.05. D, apoptosis, assessed as staining for active caspase-3 by flow cytometry (side-scatter-A; SSC-A). The percentage positive cells are shown. **, P < 0.01; [ff], P < 0.01. E, colony formation assay in Matrigel in Gpx3 knockdown and scrambled control Caco2 cells with and without H_2O_2 treatment. ***, P < 0.001 Scr versus shGPX3 control.*

without application of a stressor, suggesting that its primary role is to buffer excessive hydrogen peroxide concentrations.

Knockdown of GPX3 in vitro leads to increased apoptosis and decreased contact-independent growth.

Because our data suggest that Gpx3 functions as a tumor suppressor in colitis-associated carcinoma (CAC) *in vivo*, we wanted to determine whether it modified cellular growth properties *in vitro* in the acute setting in an established colon cancer cell line. In contrast to *in vivo* modeling where there was no effect of *Gpx3* deletion on apoptosis, knockdown of *GPX3* in Caco2 cells led to increased apoptosis (26.8% versus 15.6%, *P*<0.001, Fig. 3.7D) and no difference in proliferation when exposed to the stressor H_2O_2. Also of note, knockdown of GPX3 led to decreased contact-independent growth in Matrigel colony formation assays (7.3 versus 16.1 colonies, *P*<0.001, Fig. 3.7E), indicating the potential for a dual role for Gpx3 as a tumor suppressor in chronic inflammatory carcinogenesis while its loss in already established tumor cells (such as Caco2 cells) is detrimental to them.

Discussion

Chronic inflammation, as seen in ulcerative colitis and Crohn's colitis, predisposes to malignancy (15). In fact, the risk for cancer is increased 6-fold in patients with IBD compared with the general population (300). Although the relationship between chronic inflammation and carcinogenesis is complicated and imprecisely understood, it is hypothesized that the excess ROS and reactive nitrogen species (RNS) accompanying inflammation contribute to malignancy. During chronic inflammation superoxide is produced at rates that overwhelm antioxidant systems (363, 364). When reactive oxygen and nitrogen species are not cleared efficiently, they begin to react with lipids, proteins, and DNA (365). More specifically, oxidative DNA damage leads to C/G base pair mutations which lead to an increased frequency of C:G→T:A transversion (366), a mutation which is most frequently observed in mutated proto-oncogenes and tumor suppressor genes (367). GPX3 is an extracellular glutathione peroxidase that is able to abrogate ROS and is postulated to protect from carcinogenesis via these activities, although this has up to now not been rigorously tested using reverse genetics. We applied this approach to define the role of Gpx3 in inflammatory carcinogenesis and now demonstrate that Gpx3 is indeed a potent inhibitor of tumor promotion and progression. The impact of Gpx3 loss on tumorigenesis is likely mediated by increased inflammation and DNA damage as well as increased intratumoral proliferation that probably results from an increase in β-catenin nuclear translocation and Wnt stimulation. Loss of Gpx3 in the AOM/DSS CAC model leads to increased tumor number, but not size. *Gpx3*$^{-/-}$ tumors also demonstrated increased

tumor staging suggesting that its loss also contributes to progression. In fact, one *Gpx3*$^{-/-}$ tumor demonstrated local invasion, a characteristic that is not normally seen as the result of the AOM/DSS protocol. This is significant because it supports epidemiological data that demonstrates that throughout the course of colorectal cancer progression, GPX3 expression is decreased (298).

While the *in vivo* reverse genetic experiments using the *Gpx3*$^{-/-}$ mice in the AOM/DSS protocol model allowed us to decipher the cumulative effects of the absence of *Gpx3* throughout the full spectrum of transformation from normal cells to tumor cells, *in vitro* experiments were conducted in established cancer cells (Caco2) to isolate the contribution of GPX3 to maintenance or promotion. As noted *in vivo*, GPX3 loss resulted in increased DNA damage. Of interest, knockdown of GPX3 in Caco2 cells resulted in a decrease in contact independent growth and increase in apoptosis in response to H_2O_2, indicating that the acute absence of Gpx3 is detrimental to established carcinoma growth.

Our data show that there is increased inflammation and crypt damage and regeneration in *Gpx3*$^{-/-}$ AOM/DSS mice compared to WT mice. Further, this inflammation occurred despite a decrease in M1 and increase in M2 macrophages. It is theorized that M1 macrophages, which normally serve as pro-inflammatory cells, are tumoricidal and downregulated during cancer development while M2 macrophages, which normally aid in the resolution of the inflammatory response, are pro-tumorigenic and upregulated within the tumor microenvironment (368). Thus Gpx3 loss likely contributes to differential macrophage activation or recruitment that further supports tumor growth and survival. This is an interesting finding as selenoprotein deficiency leads to diminished macrophage

migration (360) and selenium enhances the capacity of a host to generate cytotoxic lymphocytes and macrophages to destroy tumor cells (369, 370). Thus, our data suggest that at least part of the immune cell modifying properties of selenium are actuated by Gpx3.

Thus far, our data support a tumor suppressor role for Gpx3 via clearance of ROS. Upon knockdown of Gpx3 in the human colorectal cancer cell line Caco2, we saw an induction of ROS as well as an increase in DNA damage resulting from hydrogen peroxide treatment that supports our *in vivo* data. Contrary to what was originally expected, knockdown of Gpx3 did not alter proliferation at baseline or during stress as was seen *in vivo*. Instead, apoptosis was increased in response to H_2O_2 administration, a result that would be expected in cells that do not harbor the capacity to deal with oxidative stress due to the loss of the antioxidant Gpx3. Even at baseline, knockdown of Gpx3 in Caco2 cells resulted in a decrease in contact-independent cell growth, a marker of tumorigenicity. This is contrary to our *in vivo* findings in which Gpx3 served as a tumor suppressor. Though initially surprising, we hypothesize that the tumor suppressive role of Gpx3 exists in its ability to prevent the initiation and malignant transformation *in vivo*, but in cells that are already malignant, Gpx3 is able to promote tumorigenesis by protecting them from apoptosis. This also likely explains why, despite having higher proliferation rates, the tumors of *Gpx3*$^{-/-}$ mice are not larger than those of WT mice. It may be that, upon the application of a stressor such as DSS, malignant cells in *Gpx3*$^{-/-}$ mice are dying more rapidly than those in WT mice and stabilizing the tumor size.

In conclusion, we demonstrate that removal of Gpx3 enhances inflammation and injury, proliferation, nuclear β-catenin, and DNA damage in tumors of mice subjected to an inflammatory carcinogenesis protocol. The net effect of these changes leads to an increase in tumor promotion in response to Gpx3 loss. Thus, Gpx3 appears to serve as a tumor suppressor in CAC. These studies provide insight into disease pathogenesis and indicate that at least one of the selenoproteins that modifies carcinogenesis is Gpx3 and that it may serve as a substrate for translational investigations in colitis-associated carcinoma.

Acknowledgements

This work was supported by the National Institutes of Health grants DK080221 (CSW), R01 DK82813 (RFB), P50CA095103 (MKW), AT004821 (KTW), AT004821-S1 (KTW), DK053620 (KTW), and 1F31CA167920 (CWB), Merit Review Grants from the Office of Medical Research, Department of Veterans Affairs 1I01BX001426 (CSW) and 1I01BX001453-01 (KTW), and ACS-RSG 116552 (CSW). We thank Teri Stevenson for help with animal husbandry. We would also like to thank members of the Williams and Burk labs for thoughtful discussions regarding this research project. Finally, we thank Virginia Winfrey for her help with immunofluorescent staining and imaging.

CHAPTER IV

ABSENCE OF SELENOPROTEIN P PROMOTES STEM CELL PROPERTIES, AUGMENTS ROS-INDUCED DAMAGE AND PROMOTES COLITIS-ASSOCIATED TUMORIGENESIS

Introduction

Selenium is a trace mineral that is incorporated into proteins as selenocysteine encoded by a UGA codon in the selenoprotein mRNA. UGA is normally read as a stop codon so selenocysteine incorporation relies on a *cis*-acting sequence within the mRNA (selenocysteine insertion sequence) and *trans*-acting factors dedicated to selenocysteine incorporation (such as selenocysteine-charged tRNA) (49). Selenoprotein synthesis is dependent on Se levels resulting in a hierarchy of selenoprotein expression during times of Se deficit. Even under conditions of severe Se deficiency, the majority of Se is used to synthesize selenoprotein P (Sepp1) (160). In fact, the bulk of Se is released into the plasma from the liver in two specific forms, Sepp1 and 1β-methylseleno-N-acetyl-D-galactosamine, but *Sepp1* is also expressed by a wide range of tissues (371). Sepp1 has two proposed main roles: the first is to supply various tissues with selenium and the second is an antioxidant function. The transport role is thought to be carried out by the C-terminal domain of Sepp1 which contains nine selenocysteine residues (372). *Sepp1* deletion in mice results in severe depletion of Se within the brain and testis as well as in other organs to a lesser extent (336). The antioxidant role is proposed to be carried out by a single selenocysteine within a UxxC redox motif in the N-terminal domain (160).

Two enzymatic activities have been described for the N-terminal selenocysteine: phospholipid hydroperoxide glutathione peroxidase and peroxynitrite reductase (159, 373). As such, Sepp1 is an effective reductant of reactive oxygen species enabling it to prevent damage of cellular lipids, proteins, and nucleic acids (79). Its antioxidant role suggests that Sepp1 could play a significant role in cancer prevention, particularly in the context of inflammatory cancers characterized by increased oxidant stress such as colitis-associated carcinoma (299). Several epidemiological studies have inversely correlated nutritional Se status and cancer risk, particularly in colon cancer (374). Sepp1 is downregulated in colorectal cancers (162) and single nucleotide polymorphisms (SNPs) in the selenoprotein P gene (*SEPP1*) are significantly associated with advanced adenoma risk (165).

Se deficiency can result in stimulation of the Wnt and Nrf2 pathways (125, 130, 286) which are known to be essential in the pathogenesis of colon cancer (132-134). Because Sepp1 serves as the major selenium transport protein, it is likely that it contributes to localized Wnt and Nrf2 signaling in target tissues. Furthermore, as the gastrointestinal tract is susceptible to oxidative damage resulting from direct contact of the colonic epithelium with microbial and food-derived reactive oxygen species, loss of Sepp1 might prime the colonic epithelium for increased oxidative damage-induced tumor initiation. This potential damage is augmented in the context of inflammatory bowel disease (IBD) during which oxidative stress plays a major role (299). The majority of oxidative species generated by the reaction of cellular substrates with nitric oxide during IBD result in elevated expression of the inducible form of nitric oxide synthase (NOS2)

(338). NOS2 has been shown to downregulate expression of *Sepp1* in a mouse model of chronic colitis (171). Sepp1 has also been identified as an IL-10-dependent, alternatively activated macrophage-associated gene, linking Sepp1 to a pro-tumorigenic microenvironment (375). Thus, not only through reduction of oxidative species, but also via modulation of the immune system and Wnt signaling, Sepp1 potentially plays a critical role in stem cell pathways and the development of tumors during colitis-associated carcinoma.

The vast majority of Sepp1 is produced by the liver and it is proposed that Sepp1 activity is solely extracellular in nature. To date, it is unknown whether Sepp1 made within and secreted from extrahepatic cells plays a significant role in antioxidant defense. During mouse development spatiotemporal expression of Sepp1 is observed in the intestine and is predicted to play a role in both Se transport and antioxidant defense during embryogenesis (376). Sepp1 expression is also regulated in response to inflammation (171) and negatively regulated by the glucocorticoid receptor (170), suggesting that its cell-specific regulation is important. Of particular interest, cell culture studies in adipocytes have determined that loss of SEPP1 expression results in the upregulation of inflammatory cytokines MCP-1 and IL-6 in preadipocytes, leading to the inhibition of adipocyte differentiation (172); for the first time implicating extrahepatic Sepp1 in the regulation of inflammatory response and differentiation. These data suggest that epithelial-derived Sepp1 might also contribute to cellular phenotypes.

Due to the roles of Sepp1 in Wnt and Nrf2 modulation as well as antioxidant defense, we hypothesized that Sepp1 would contribute to stem cell phenotypes, protect

from reactive oxygen species, and modify colitis-associated carcinogenesis. In order to first establish epithelial cell-autonomous roles for Sepp1 in a closed system, we isolated small intestinal organoids (enteroids) from *WT* and *Sepp1*$^{-/-}$ mice and analyzed them for stem cell properties including plating efficiency, percentage of branching enteroids and stem spheroids, and average number of branches within each branching enteroid. Concurrent with a role in Wnt signaling, *Sepp1*$^{-/-}$ enteroids demonstrated increased stem cell properties. Moreover, treatment of enteroids with hydrogen peroxide resulted in an increase in reactive oxygen species as well as an increase in proliferation which is also seen at baseline. Finally, survival is decreased in *Sepp1*$^{-/-}$ enteroids when treated with multiple administrations of hydrogen peroxide over a 4-day period. Because of the enteroid stem cell properties and responses to hydrogen peroxide, we wanted to test whether *Sepp1*$^{-/-}$ mice would demonstrate increased inflammatory tumorigenesis. *WT*, *Sepp1*$^{+/-}$, and *Sepp1*$^{-/-}$ mice were subjected to the azoxymethane, repeated dose dextran sodium sulfate (AOM/DSS) protocol to model colitis-associated carcinoma. *Sepp1*$^{+/-}$ mice demonstrated increased tumorigenesis compared to *WT* mice, but surprisingly, *Sepp1*$^{-/-}$ mice displayed decreased tumorigenesis. We hypothesized that this decrease in tumorigenesis was due to decreased survival of initiated epithelial cells because of augmented inflammatory damage upon complete Sepp1 loss. In support of this hypothesis, *Sepp1*$^{-/-}$ mice subjected to AOM administration alone demonstrated increased tumorigenesis and chronic DSS administration resulted in increased mucosal injury. Moreover, homozygous loss of either the Se-rich C-terminal region or mutation of the N-terminal UXXC redox motif resulted in increased tumorigenesis, suggesting that

both domains contribute to the Sepp1 tumor phenotype but when both are lost concurrently the stressed placed on the initiated epithelium during the CAC protocol is significant enough to kill initiated cells.

Finally, because absence of Sepp1 in enteroids leads to increased stem cell phenotypes and reduced ability to deal with oxidative stress in an epithelial cell autonomous manner, we predicted that liver-derived Sepp1 might not contribute significantly to the *Sepp1*$^{-/-}$ tumor phenotype. Conditional knockout of liver Sepp1 (*Sepp1*$^{Fl/Fl}$*;Alb-cre*) did not alter tumorigenesis in response to the AOM/DSS protocol indicating that plasma Sepp1 does not contribute significantly to the *Sepp1*$^{-/-}$ phenotype. This report is the first to utilize enteroids to establish the epithelial cell autonomous responses to Sepp1 loss and map the domains of Sepp1 necessary for tumor modification in an inflammatory carcinogenesis model. Finally, this study reports that liver-derived Sepp1 is not required for the effect that Sepp1 has on tumor modification.

Materials and methods

Ethics Statement. This study was performed in strict accordance with the recommendations in the Guide for the Care and Use of Laboratory Animals of the National Institutes of Health. The protocol was approved by the Institute of Animal Care and Use Committee at Vanderbilt University (protocol number: M/10-355). Every effort was made to minimize suffering.

Murine Inflammatory Carcinogenesis Protocol: Because *Sepp1*$^{-/-}$ mice exhibit decreased survival when not fed a selenium-supplemented diet (301), mice were maintained on

diets that were Torula yeast-based and supplemented with 1.0 mg Se as sodium selenite per kg. This diet was prepared and pelleted to our specifications (301) by Harlan-Teklad (Madison, WI, USA). Eight- to twelve-week old C57BL/6 wild type (*WT*) (n=13), *Sepp1*$^{+/-}$ (n=9), or *Sepp1*$^{-/-}$ (n=11) mice (336, 372) (constitutional knockout experiments), *WT* (n=16) or *Sepp1*$^{\Delta 240\text{-}361/\Delta 240\text{-}361}$ (n=14) mice (63) (truncation experiments), WT (n=12) or Sepp1U40S/U40S (n=15) (redox motif mutant experiments), or *Sepp1*$^{FL/FL}$ (n=16) or *Sepp1*$^{FL/FL}$*;Alb-cre* (n=17) mice (66) (liver-specific knockout experiments) (Figure 4.1A) were injected with 12.5 mg/kg of AOM (Sigma-Aldrich, St. Louis, MO, USA) intraperitoneally. Three days post-injection, the animals were started on the first of three cycles of 3% DSS *ad libitum* (Figure 4.1B). Each cycle lasted 5 days and was followed by a 16-day recovery period. During each cycle of recovery, twelve days post-DSS administration, colonoscopy (Karl Storz veterinary endoscopy) was performed to assess injury, tumor multiplicity, and tumor grade (358). Injury was evaluated based on the murine endoscopic index of colitis severity (MEICS) which grades mucosal thickening, vasculature pattern, granularity, exudate, and stool consistency (358). Mice were subsequently sacrificed on day 70. Tumor counts and measurements were performed in a blinded fashion under stereo-dissecting microscope. Histologic analysis was performed in a blinded fashion for severity of inflammation (357) and dysplasia on hematoxylin and eosin (H&E) stained "Swiss rolled" colons by a gastrointestinal pathologist (MKW). All *in vivo* procedures were carried out in accordance with protocols approved by the Vanderbilt Institutional Animal Care and Use Committee.

Immunohistochemistry and immunofluorescence staining. For Sepp1 and phalloidin staining, mice were exsanguinated and colons and small intestines flash frozen in liquid nitrogen. Five-micrometer frozen sections were cut and Sepp1 staining was performed as described previously (377).For all other staining, five-micrometer sections of paraffin-embedded colons were cut and haematoxylin and eosin (H&E) staining was performed by the Vanderbilt University Translational Pathology Shared Resource. Cut sections were dewaxed, hydrated, and quenched of endogenous peroxidase activity with 0.03% hydrogen peroxide in methanol. Antigen retrieval was conducted using Antigen Unmasking Reagent (Vector Laboratories, Inc., Burlingame, California, USA) according to manufacturer's instructions. After blocking, primary antibody was added [α-Ki67 (NeoMarkers), 1:1,000; α-arginase I (ARG1, Santa Cruz), 1:500; α-IL-1β (R&D Systems), 1:40; α-F4/80 (ABd Serotec) 1:1000; α-8-OHdG (Santa Cruz), 1:500] and incubated overnight at 4°C. Isotype-matched antibodies were included as negative controls. Identification of intratumoral apoptotic cells was conducted using the ApopTag Plus Peroxidase In Situ Apoptosis Kit (Chemicon, Temecula, California, USA) according to the manufacturer's protocol. Control slides were obtained by omitting the terminal transferase (TnT) enzyme. For immunofluorescence staining of proliferation, macrophages, and DNA damage, slides were counterstained and mounted with ProLong Gold antifade including 4',6-diamidino-2-phenylindole (DAPI, Invitrogen, Grand Island, New York, USA). Apoptosis, proliferation, DNA damage, and M1 and M2 macrophage indices were generated by counting either the number of positive cells per high-powered field (HPF; 40x objective) within each tumor or the number of positive cells per crypt in

20 crypts per mouse by a blinded observer. The average score was then calculated for each Swiss-rolled colon.

Colonic selenium measurements. The determination of colonic selenium was carried out using a modification of the fluorometric assay of Koh and Benson (305) and Sheehan and Gao (306). Briefly, tissue was digested in nitric and perchloric acids and Se was complexed with diaminonaphthalene. Selenium-diaminonaphthalene was extracted into cyclohexane and fluorescence was measured in a Perkin-Elmer LS 55 fluorometer.

Western blot analysis of apoptosis and WNT pathway proteins. Flash-frozen sections of colon (n=6 for each genotype) were lysed in RIPA buffer including 1x protease inhibitor cocktail (Sigma) using a rotor homogenizer (Janke & Kunkel IKA-Labortechnik Ultra-Turrax T25). Protein quantification was performed using a Pierce BCA Protein Assay Kit (Thermo) according to manufacturer's instructions. Samples were treated with loading buffer, boiled, and 40 µg was run on an SDS-PAGE gel for western blot detection. The Apoptosis Antibody Sampler (mouse preferred, #9930) and Wnt signaling Antibody Sampler (#2915) kits (Cell Signaling Technology, Danvers, MA, USA) were used according to manufacturers' protocol and analyzed using Odyssey imaging software. In short, Western blots were run and transferred onto nitrocellulose. Blots were blocked with Odyssey Blocking Buffer (LI-COR Biosciences, Lincoln, NE, USA) for 1 hour at room temperature with rocking. Blots were incubated with primary antibodies from each kit diluted 1:1000 in Odyssey Blocking Buffer overnight at 4°C with rocking. Blots were washed three times for five minutes each with PBST and then incubated at room temperature for 1 hour in secondary antibody (IRDye® 680LT Infrared Dye conjugated to antibodies against either mouse or rabbit)

diluted 1:1000 in Odyssey Blocking Buffer. Blots were washed three times for five minutes each with PBST, rinsed with PBS, and imaged using the Odyssey quantitative fluorescence imaging system. Quantification was performed using Odyssey Imaging Software and normalized either to total caspase or β-actin.

Bone marrow macrophage polarization and analysis. Bone marrow macrophages were isolated and activated as has been previously published (378, 379). For the production of classically activated macrophages, bone marrow macrophages were primed with 150 U/ml IFNλ for 6 hours and subsequently stimulated with 10 ng/ml LPS. For the production of alternatively activated macrophages, bone marrow macrophages were treated with 20 U/ml IL13 for 12 hours. Six hours prior to activation of both macrophage types, RNA was isolated using the RNEasy MiniKit (Qiagen, Valencia, CA, USA). 1 µg RNA was utilized to perform reverse transcription PCR using the iScript cDNA synthesis kit (Bio-Rad, Hercules, CA, USA). 1 µl of the subsequent cDNA was used for quantitative RT-PCR analysis of the targets iNOS, IL-1β, and Ym1 using primers purchased from RealTimePrimers.com.

Plasma Sepp1 protein determination. Plasma Sepp1 was measured by ELISA. Plasma samples were prepared prior to assay by dilution in PBST (PBS with 0.05% Tween-20) containing 2% rat plasma cleared of Sepp1 by monoclonal antibody 8F11 (380) immunoaffinity purification. 0.1 µl of normal mouse plasma was used in the ELISA assay. The monoclonal antibody 9S4 was used as the capture antibody, and the polyclonal antibody preparation 695, obtained from a rabbit immunized with rat Sepp1, was used as the detection antibody. Wells of a microtiter plate were coated with 9S4 (0.1 µg/well) and blocked with Block Ace (Serotec, Ltd., Raleigh, NC, USA). After washing, the plate was

incubated with sample (50 µl of pre-prepared plasma) and purified antibody preparation 695 (50 µl of 1 µg/ml) at 37 °C for 30 min. Horseradish peroxidase-conjugated goat anti-rabbit IgG was used to detect the amount of 695 bound to Sepp1 captured by 9S4. The TMB Microwell Peroxidase Substrate System (KPL, Gaithersburg, MD, USA) was used for color development followed by treatment with the stop solution 1 N H_2SO_4. The developed color was measured at 450 nm with a Multiskan Spectrum plate reader (ThermoElectron Corporation, Vantaa, Finland). Each assay plate contained a standard curve built with 9S4 immunoaffinity-purified mouse Sepp1 (0–7.5 ng).

Small intestinal organoid culturing. Four inches of the distal small intestine were dissected. The small intestinal section was flushed with ice cold PBS and cut open lengthwise and dissected into 1cm pieces then transferred into 5ml ice cold PBS. Small intestine was vortexed for 3 seconds to pull off loose villi. PBS was removed with a pipettor and the villus wash was repeated. Tissue was transferred to 5ml chelation buffer (1mM EDTA, made fresh in DPBS) and rocked for 10 minutes at 4°C. Chelation buffer was removed from the tissue with a pipettor and tissue was washed twice with 10 ml PBS. 5 ml PBS was added and shaken gently for 2 minutes. The supernatant from the first shake was poured off. 5 ml PBS was added and the shake was repeated for 2 minutes then supernatant was poured off. 5 ml fresh chelation buffer was added and chelation was performed for 10 minutes at 4°C with rocking. The small intestinal segments were washed twice with PBS and then 5 ml PBS PBS was added for 2 minutes of shaking. The supernatant was poured off and the shake was repeated with a new aliquot of PBS. Crypts were filtered through a 70 µm filter into a pre-chilled 50 ml tube. The filter was rinsed

with 5 ml cold shaking buffer (PBS with 43.3mM sucrose and 54.9mM Sorbitol). Complete crypts were counted and enough volume was transferred for 1200 crypts to a pre-chilled 5 ml round-bottomed tube. Crypts were centrifuged at 150 xG for 10 minutes at 4°C. Shaking buffer was aspirated being careful not to disturb the pellet. Using pre-chilled pipette tips, crypts were resuspended in 50 µl of Matrigel (BD Bioscience #356237, San Jose, CA, USA), per well, containing 50 ng/ml EGF (R&D Systems #2028-EG-200, Minneapolis, MN, USA), 100 ng/ml Noggin (R&D Systems #1967-NG-025/CF), 500 ng/ml R-Spondin: 500ng/ml (R&D Systems #3474-RS-050), and 50ug/ml Wnt3a (Millipore #GF-160, Billerica, MA, USA). Using pre-chilled pipette tips, 50 µl Matrigel per well was plated with growth factors into 12-well cell culture plates so that the Matrigel formed a mounded dome. The plate was placed in an incubator at 37°C for 30 minutes to allow Matrigel to polymerize fully. Matrigel was overlayed with 500 µl Minigut culture media (Advanced DMEM/F12 (Invitrogen #12634-010, Carlsbad, CA, USA), L-Glutamine (Invitrogen #25030), Pen-Strep (Invitrogen #15140-148), Hepes (Mediatech #25-060-CI), N2 Supplement (R&D Systems #390155), B27 Supplement (Invitrogen #17504044). Every 4 days, media was replaced with fresh Minigut media plus growth factors.

Whole-mount 6-carboxy-2',7'-dichlorodihydrofluorescein diacetate (Carboxy-H_2DCFDA) enteroid staining. Enteroids were grown to full maturity, at least 4 days post-plating. The morning of hydrogen peroxide treatment, enteroid media was replaced with fresh Minigut. Either 0 µM, 400 µM, or 800 µM hydrogen peroxide was added directly to media. Two hours post-hydrogen peroxide treatment, growth media was removed from cells. Cells were treated with pre- warmed DPBS containing either the probe carboxy-H_2DCFDA

(Invitrogen #mp-36103) or, as a negative control, carboxy-DCFDA to provide a final working concentration of 5 mM. Enteroids were incubated at 37°C in a cell culture incubator for 1 hour. Loading buffer was removed and cells were returned to pre-warmed Minigut media. Cells were incubated at 37°C for 15 minutes. Media was removed and enteroids were fixed overnight at 4°C in 2% formaldehyde with gentle rocking. Fixative was removed and enteroids were washed twice with DPBS. Enteroids were imaged with a LSM 510 Confocal microscope using the same specifications for imaging of all enteroids. Reactive oxygen species were quantified as staining intensity using ImageJ Image Analysis software. The graph represents the fold change intensity relative to *WT* enteroids treated with 0 µM hydrogen peroxide. Error bars represent the standard error of the mean for three separate experiments performed in duplicate.

Whole-mount enteroid proliferation staining. Proliferation was determined using the Click-iT EdU cell proliferation assay (Invitrogen #C-10337) according to manufacturers' instructions. In short, enteroids were grown to full maturity, at least 4 days post-plating. The morning of hydrogen peroxide treatment, enteroid media was replaced with fresh Minigut. Either 0 µM or 800 µM hydrogen peroxide was added directly to media. Two hours post-hydrogen peroxide treatment, media was replaced with fresh Minigut media and a 10 µM working solution of EdU was added to each well of the plate. Enteroids were incubated for 15 minutes under normal growth conditions. After incubation, media was removed and 1 ml of 2% formaldehyde in PBS was added to each well and incubated overnight at 4°C. The fixative was removed and enteroids were washed twice with 1 ml 3% BSA in PBS. Wash buffer was removed and 1 ml of 0.5% Triton X-100 in PBS was added

to each well and incubated at room temperature for 20 minutes. Click-iT reaction cocktail was prepared and 0.5 ml was added to each well. The plate was incubated for 30 minutes at room temperature, protected from light. The reaction cocktail was removed and enteroids were washed once with 1 ml 3% BSA in PBS. The wash solution was removed and enteroids were stained with TO-PRO-3 (1:500 in PBS for 15 minutes at room temperature). Enteroids were washed twice with 1 ml of PBS for 30 minutes. Enteroids were imaged with a LSM 510 Confocal microscope using the same specifications for imaging of all enteroids. Proliferation was quantified as EdU^+ cells/crypt area where crypt area was determined using ImageJ Image Analysis software. The graph represents the fold change intensity relative to *WT* enteroids treated with 0 μM hydrogen peroxide. Error bars represent the standard error of the mean for three separate experiments performed in duplicate.

RNAseq assay and analysis. Tumors were dissected from *WT* and *Sepp1*$^{-/-}$ mice and RNA was isolated using the RNEasy MiniKit (Qiagen, Valencia, CA, USA). RNA integrity was determined using Experion RNA StdSens Analysis Kit (Bio-Rad, Hercules, CA, USA). All RNA samples had RNA integrity numbers (RINs) >8 and were deemed suitable for hybridization. A total of 10 mg of cRNA was used in the second cycle of first strand synthesis to generate the correct sense for target hybridization. Mouse gene 1.0 ST arrays (Affymetrix, Santa Clara, CA, USA) were scanned the next day. CEL files were imported into Partek Express (Partek, St Louis, MI, USA) and Robust Multichip Average (RMA) was run across all eight samples. Pivot data was exported and posted. A t-test was run between the *Sepp1*$^{-/-}$ and *WT* sample groups in Partek. The P-value was multiple testing

corrected with Bonferroni and Stepup. Expression array analysis was performed hybrizing cRNA to the Mouse gene 1.0 ST chip (Affymetrix). Differentially expressed genes were classified using the Ingenuity Pathway Analysis Program (http://www.ingenuity.com/products/ipa, Qiagen).

Statistical Methods: Analyses comparing two groups were analyzed using the Student's t-test. One-way ANOVA and Newman-Keuls post-test was used to compare multiple groups. Data is presented as the mean +/- the standard error of the mean (SEM) in bar graphs and a line identifying the mean is shown when all data points are plotted. Percentages of mice displaying altered dysplasia grade were determined using Chi-square contingency analysis for each grade. All of these analyses were performed using GraphPad Prism®5.0c (San Diego, CA, USA).

Results

Selenoprotein P is a haploinsufficient tumor suppressor.

Because Sepp1 has been heavily implicated in protection from reactive oxygen species, we hypothesized that *Sepp1*$^{+/-}$ and *Sepp1*$^{-/-}$ mice would display increased inflammatory tumorigenesis. The inflammatory tumorigenesis model that we used to test this hypothesis was the azoxymethane, repeated dose dextran sodium sulfate (AOM/DSS)

A

Nomenclature	Mouse Description
WT	Wild-type N10 C57/BL6
Sepp1$^{+/-}$	Heterozygous selenoprotein P knockout (C57/BL6)
Sepp1$^{-/-}$	Homozygous selenoprotein P knockout (C57/BL6)
Sepp1$^{\Delta 240\text{-}361/\Delta 240\text{-}361}$	Homozygous deletion of Sepp1 amino acids 240-361 (C57/BL6)
Sepp1$^{U40S/U40S}$	Homozygous mutation of position 40 selenocysteine to serine (C57/BL6)
Sepp1$^{c/c}$*/alb-cre*$^{+/-}$	Conditional knockout of liver-derived selenoprotein P (C57/BL6)

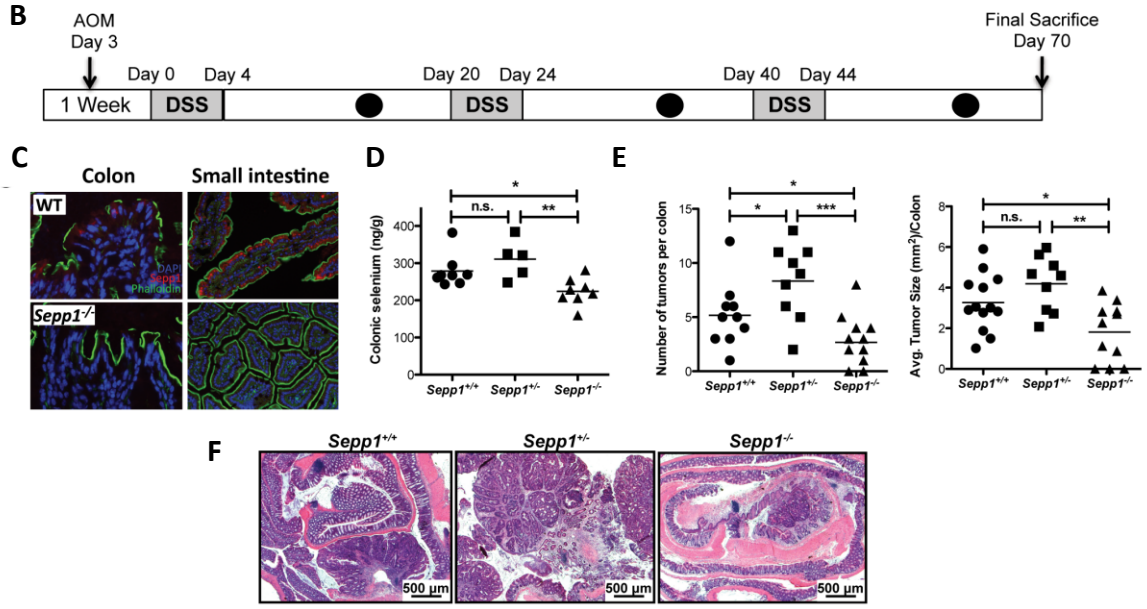

Figure 4.1 Sepp1 haploinsufficiency results in increased inflammatory tumorigenesis in response to the AOM/DSS model. A) Table describing the genotypes subjected to the AOM/DSS protocol and the symbols used for each genotype. B) Schematic of the AOM/DSS protocol utilized. Mice are injected with azoxymethane (AOM) and started on the first of three four-day cycles of DSS administration three days post-AOM injection. Mice are analyzed by endoscopy twelve days after each DSS administration for tumor burden and injury (black circles). Mice are sacrificed at day 70. C) Immunofluorescence staining of Sepp1 (red) within the colon and small intestine of WT and Sepp1$^{-/-}$ mice (100x magnification). D) Quantification of colonic selenium in WT, Sepp1$^{+/-}$, and Sepp1$^{-/-}$ mice. E) Tumor number (tumors/mouse, left) and average tumor size (mm^2, right) within each mouse and F) representative images of Swiss rolled colons from each mouse (25x magnification).

colitis-associated carcinoma model (Figure 4.1B). AOM is a procarcinogen that is metabolically activated to a potent alkylating agent forming O^6-methyl-guanine (318). Its oncogenic potential is augmented in the setting of chronic inflammation, which is induced

by repeated cycles of DSS treatment (319). Importantly, Sepp1 expression is seen in the colon and small intestine of *WT* mice (Figure 4.1C), indicating that it exhibits function within these tissues. *WT*, *Sepp1*$^{+/-}$, and *Sepp1*$^{-/-}$ mice were subjected to the AOM/DSS protocol and, upon sacrifice, analyzed for tumor burden. As expected, complete loss of Sepp1 led to a decrease in colonic Se (Figure 4.1D), though surprisingly, this decrease was not severe, indicating that Sepp1 is not the only mechanism of Se transport into the colon. Partial loss of Sepp1 led to an increase in tumor number (5.2 ± 0.8 vs 8.3 ± 1.2 tumors/mouse, *P*=0.03, Figure 4.1E, left) but no change in tumor size. Unexpectedly, complete knockout of Sepp1 led to a decrease in tumor number (2.7 ± 0.7, *P*=0.02, Figure 4.1E, left) and size (3.3 ± 0.4 vs 1.8 ± 0.4 mm^2, *P*=0.02, Figure 4.1E, right). As this decrease in tumorigenesis was concomitant with increased apoptosis as measured by TUNEL staining (34.3 ± 3.1 vs 74.4 ± 10.9 TUNEL$^+$ cells/tumor high-powered field, P<0.01, Figure 4.2A) and western blotting for markers within the intrinsic apoptosis pathway (Figure 4.2D), we hypothesized that this decrease might be caused by clearance of initiated cells due to oxidative injury beyond that which total Sepp1 loss could compensate. Moreover, proliferation was increased in *Sepp1*$^{+/-}$ tumors (55.6 ± 2.8 vs 85.9 ± 2.9 Ki67$^+$ cells/tumor HPF, *P*<0.0001, Figure 4.2B) and decreased in *Sepp1*$^{-/-}$ tumors (55.6 ± 2.8 vs 19.0 ± 6.9 Ki67$^+$ cells/tumor HPF, *P*<0.0001, Figure 4.2B), further supporting a role of clearance of initiated cells in the *Sepp1*$^{-/-}$ tumor phenotype.

In order to determine whether Sepp1 absence promotes tumorigenesis utilizing either AOM or DSS as single modalities and, thus, understand the impact of Sepp1 on

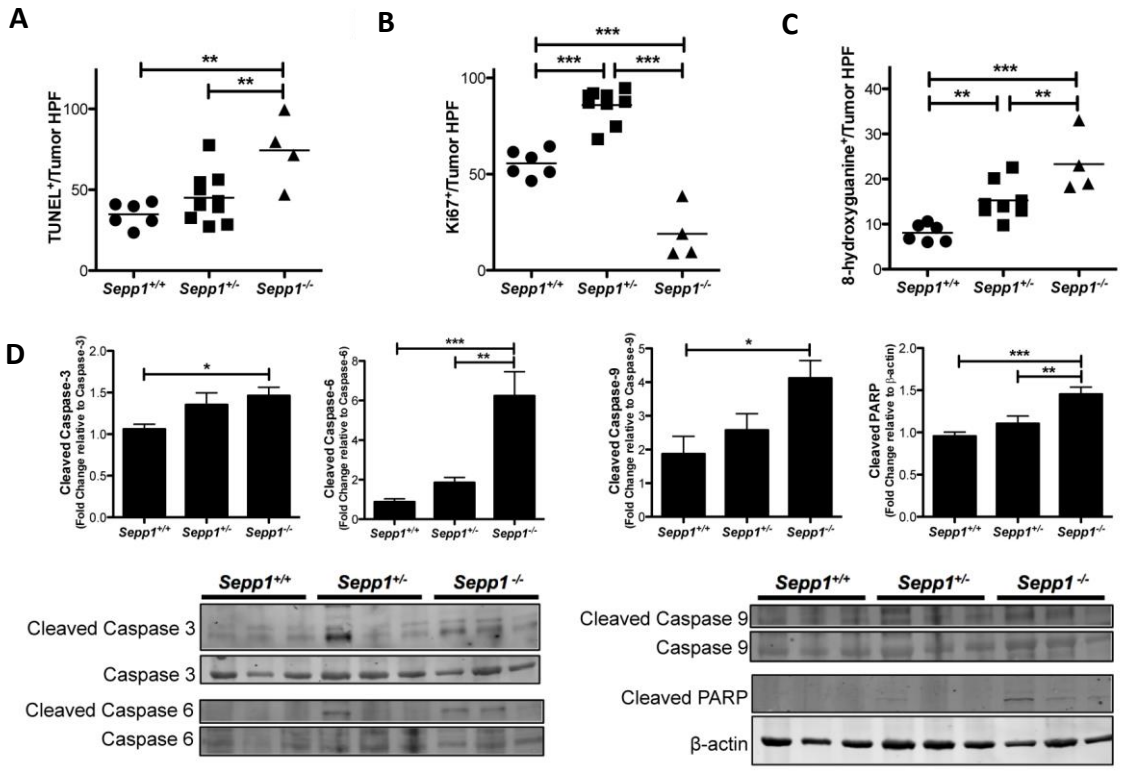

*Figure 4.2 Intratumoral apoptosis and DNA damage are increased in response to complete Sepp1 knockout and proliferation is increased in Sepp1$^{+/-}$ tumors. A) Quantification of intratumoral apoptosis as determined by TUNEL^{+} cells/tumor high-powered field (HPF, 40x magnification). B) Quantification of intratumoral proliferation as determined by Ki67^{+} cells/tumor HPF. C) Quantification of intratumoral DNA damage as measured by 8-hydroxyguanine^{+} cells/tumor HPF. D) Quantification of intratumoral canonical apoptosis targets cleaved caspase-3, cleaved caspase-6, cleaved caspase-9, and cleaved PARP relative to total caspase-3, caspase-6, caspase-9, and β-actin, respectively. Quantification is shown as fold change relative to WT (top) and representative images of blots from three individual tumors from each genotype (bottom). *P<0.05, **P<0.01, ***P<0.001.*

tumorigenesis without the possibility of initiated cell clearance in response to injury, we assessed ACF and tumor production as well as injury in response to AOM or DSS administration. Endoscopic analysis of tumor burden 15 weeks post-AOM administration revealed an increase in tumor number in *Sepp1*$^{-/-}$ mice compared to WT mice (3.7 ± 0.6 vs 7.7 ± 2.2 tumors/colon, Figure 4.3A). Moreover, endoscopic injury analysis using the MEICS scoring system (302) post-DSS administration revealed increased injury in response

to DSS (4.1 ± 0.5 vs 8.1 ± 0.4 MEICS score, P<0.0001, Figure 4.3B). Because tumorigenesis is increased in *Sepp1*$^{-/-}$ mice subjected to AOM alone and injury is increased in *Sepp1*$^{-/-}$ mice subjected to DSS, we suspect that Seep1 loss leads to increased tumorigenic potential that is lost when initiated cells are cleared by the increased DSS-induced injury in *Sepp1*$^{-/-}$ mice.

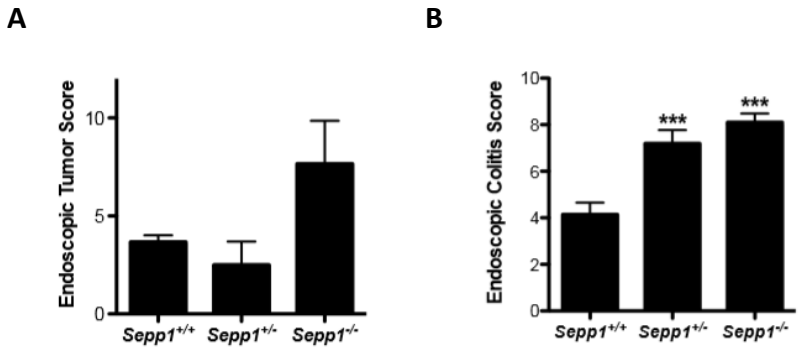

Figure 4.3 Sepp1$^{-/-}$ *mice demonstrate increased tumorigenesis and injury in response to AOM and DSS as sole agents, respectively. A) Endoscopic tumor score in mice treated with AOM alone. B) Endoscopic colitis score (MEICS) in mice treated with DSS alone.*

Intratumoral DNA damage increases in a dose-dependent manner with decreased Sepp1 expression.

Se has been identified as a potential contributor to the maintenance of genomic stability (129, 136), however the role of selenoprotein P in DNA damage repair is unknown. We wanted to test the impact of Sepp1 deficiency on crypt and intratumoral DNA damage. 8-hydroxyguanine staining, a measure of oxidative DNA damage, in fact, demonstrated that intratumoral DNA damage increases with decreased Sepp1 expression (*WT*: 8.1 ± 0.8, *Sepp1*$^{+/-}$: 15.3 ± 1.5, P=0.002, *Sepp1*$^{-/-}$: 23.3 ± 3.4 8-hydroxyguanine^{+} cells/tumor HPF, P=0.0007, Figure 2.2C) though crypt DNA damage was not altered when

compared to *WT* mice in response to Sepp1 deficiency. These data suggest that, within the tumor microenvironment, decreasing Sepp1 expression leads to an increase in oxidative DNA damage.

Pro-tumorigenic M2 macrophage polarization is increased in Sepp1$^{+/-}$ tumors.

The most significantly induced gene in response to polarization of macrophages to the M2 phenotype is selenoprotein P (375, 381, 382). Moreover, proinflammatory cytokines induce NOS2 resulting in down-regulation of Sepp1 (171) indicating that Sepp1 may play a role in macrophage polarization and inflammation. We, therefore, wanted to analyze tumors from *WT*, *Sepp1*$^{+/-}$ and *Sepp1*$^{-/-}$ mice post-AOM/DSS for macrophage polarization. Staining for the pan-macrophage marker F4/80 and either the M1 macrophage marker IL-1β revealed an increase of total macrophages (*WT*: 13.1 ± 1.3, *Sepp1*$^{+/-}$: 23.2 ± 3.0, $P<0.01$, *Sepp1*$^{-/-}$: 13.1 ± 0.8 F4/80^{+} cells/tumor HPF, Figure 4.4A) resulting from unaltered M1 macrophages (Figure 4.4B) but increased M2 macrophage recruitment (*WT*: 8.4 ± 0.8, *Sepp1*$^{+/-}$: 18.0 ± 3.9, *Sepp1*$^{-/-}$: 8.3 ± 1.1 F4/80^{+}/Arginase I^{+} cells/tumor HPF, Figure 4.4C) in *Sepp1*$^{+/-}$ tumors. Interestingly, *Sepp1*$^{-/-}$ tumors did not demonstrate this increase in M2 polarized macrophage infiltration. In order to determine whether this was a recruitment or polarization effect, we isolated bone marrow macrophages from *WT*, *Sepp1*$^{+/-}$, and *Sepp1*$^{-/-}$ mice and activated them to either the M1 or M2 polarizations using IFNλ and LPS to polarize to the M1 and IL-13 to polarize to the M2 phenotype. Analysis of M1 markers *iNOS* and *IL-1β* demonstrated decreased M1 polarization in *Sepp1*$^{+/-}$ macrophages (iNOS: 19494 ± 593.8 vs 14961 ± 782.3 fold change,

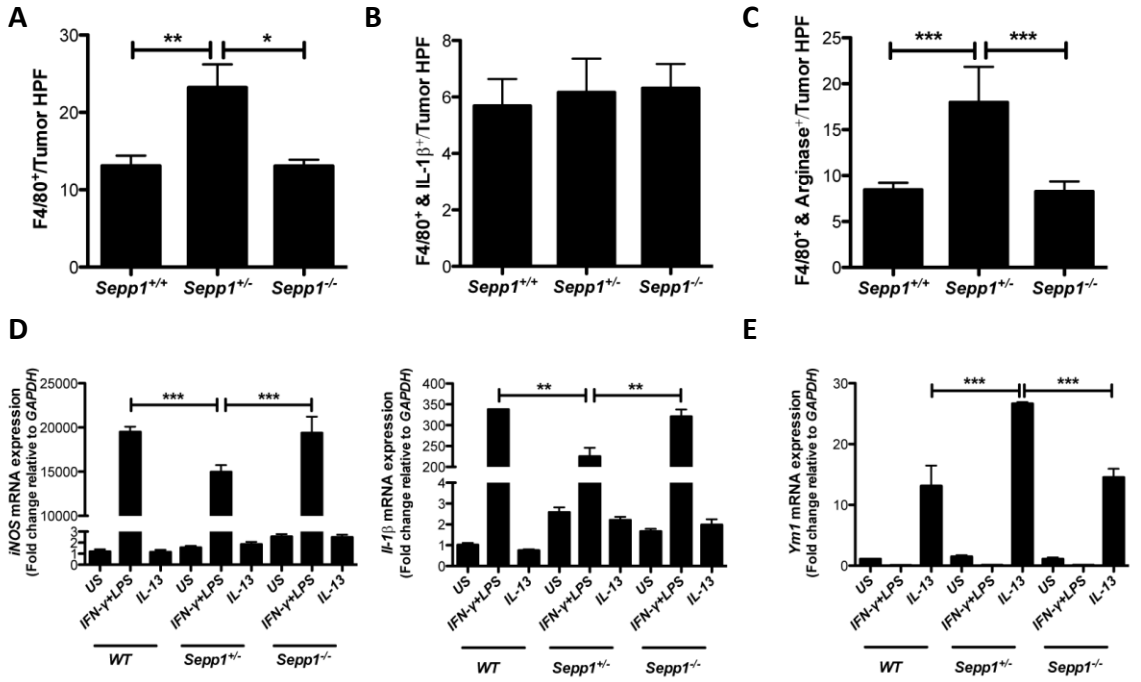

*Figure 4.4 Sepp1 regulates pro-tumorigenic M2 macrophage polarization. Quantification of A) intratumoral total macrophage staining as determined by F4/80⁺ cells/tumor HPF, B) M1 macrophage staining as determined by F4/80⁺/IL-1β⁺ cells/tumor HPF, and C) M2 macrophage staining as determined by F4/80⁺/Arginase I⁺ cells/tumor HPF. D) iNOS (left) and IL-1β (right) and E) Ym1 mRNA expression in WT, Sepp1⁺/⁻, and Sepp1⁻/⁻ in vitro-activated bone marrow macrophages. Graphs demonstrate fold change in expression relative to unstimulated (US) WT macrophages normalized to GAPDH. *P<0.05, **P<0.01, ***P<0.001.*

P<0.001, IL-1β: 337.6 ± 0.78 vs 225.1 ± 20.66 fold change, *P*<0.001, Figure 4.4D) while the M2 marker *Ym1* demonstrated increased polarization to M2 (13.1 ± 3.3 vs 26.6 ± 0.3, *P*<0.001, Figure 4.4E). Though this is not a complete polarization defect, this data indicates that Sepp1 haploinsufficiency may lead to improper macrophage response to directed stimulation suggesting that the macrophage phenotype seen in *Sepp1*$^{+/-}$ tumors may be due to increased polarization to the M2 phenotype.

Loss of the selenium-rich C-terminal domain of selenoprotein P promotes inflammatory tumorigenesis.

Selenoprotein P is considered the primary Se transport protein as deletion of the Se-rich C-terminal domain (*Sepp1*$^{\Delta 240\text{-}361/\Delta 240\text{-}361}$) results in severe Se deficiency in the brain and testis of mice (63). In fact we see that, to a lesser extent, loss of this domain leads to decreased colonic Se (394.5 ± 19.6 vs 260.2 ± 10.6 ng selenium/g colon, *P*=0.0001, Figure 4.5A) as well suggesting that selenoprotein P contributes to Se delivery to the colon but is not the sole source. Because of the role of Se in DNA damage repair, Wnt and Nrf2 signaling, and links to modification of several cancer types including colorectal, lung, laryngeal, hepatic, and prostate (108, 139, 164, 383) to name a few, we wanted to determine whether the loss of the Se-rich domain of selenoprotein P would contribute to tumorigenesis. We subjected *WT* and *Sepp1*$^{\Delta 240\text{-}361/\Delta 240\text{-}361}$ mice to the AOM/DSS protocol and analyzed them for tumor burden. We discovered that Sepp1 truncation leads to an increase in tumor number (3.9 ± 0.7 vs 7.9 ± 1.4 tumors/mouse, *P*=0.02, Figure 4.5B). Also, because we have established a role for dietary Se in dysplasia grade (384), we submitted H&E stained "Swiss rolled" colons to a gastrointestinal pathologist to determine tumor grade and determined that Sepp1 truncation also leads to an increase in tumors displaying high-grade dysplasia (*P*<0.05, Figure 4.5C).

Concomitant with an increase in tumor number was an increase in intratumoral proliferation (13.4 ± 1.7 vs 20.3 ± 2.2 Ki67^{+} cells/tumor HPF, *P*=0.04, Figure 4.5D) but no change in crypt proliferation or crypt or tumor apoptosis. Consistent with a role of Se in

DNA damage repair, crypt (0.7 ± 0.04 vs 1.0 ± 0.08 8-OHdG$^+$ cells/crypt, *P*=0.02, Figure 4.5E) and intratumoral (17.1 ± 2.7 vs 29.8 ± 2.8 8-OHdG$^+$ cells/tumor HPF,

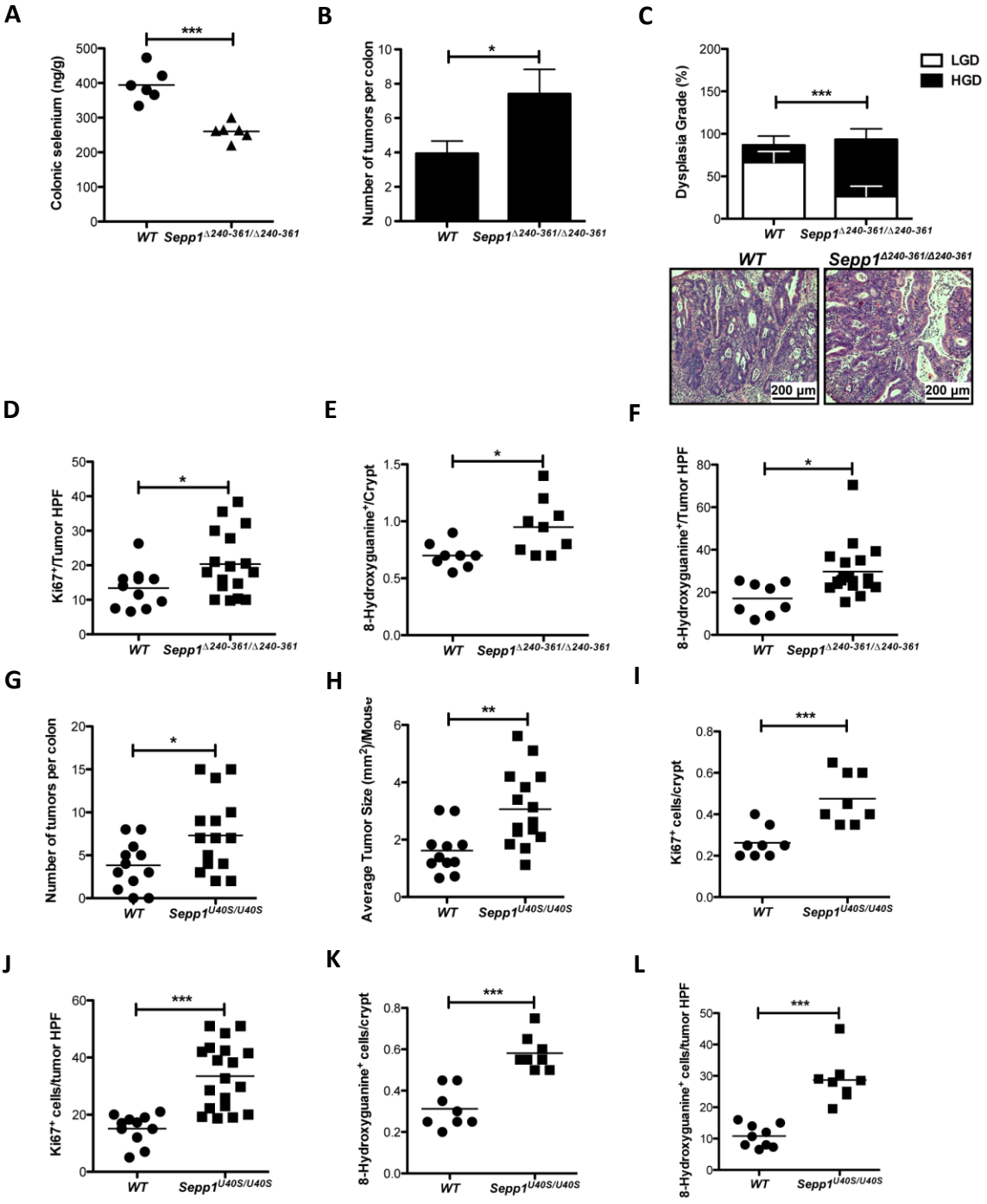

Figure 4.5 *Both the selenium-rich region and putative antioxidant domain of selenoprotein P protect from inflammatory tumorigenesis. A) Quantification of colonic selenium in WT and Sepp1$^{\Delta 240\text{-}361/\Delta 240\text{-}361}$ mice. B) Number of tumors within each mouse and C) percentage of total tumors for each genotype with either high grade dysplasia (HGD, black) or low grade dysplasia (LGD, white) (top) and representative images from tumors of the given genotypes (40x magnification, bottom). D) Quantification of intratumoral proliferation as measured by Ki67^{+} cells/tumor HPF, E) crypt DNA damage as measured by 8-hydroxyguanine^{+} cells/crypt averaged from 20 crypts within each mouse, and F) intratumoral DNA damage as measured by 8-hydroxyguanine^{+} cells/tumor HPF. G) Number of tumors and H) average tumor size within either WT or Sepp1$^{U40S/U40S}$ mice. I) Quantification of crypt proliferation as measured by Ki67+ cells/crypt averaged from 20 crypts within each mouse, J) intratumoral proliferation as measured by Ki67^{+} cells/tumor HPF, K) crypt DNA damage as measured by 8-hydroxyguanine^{+} cells/crypt averaged from 20 crypts within each mouse, and L) intratumoral DNA damage as measured by 8-hydroxyguanine^{+} cells/tumor HPF. *P<0.05, **P<0.01, ***P<0.001.*

P=0.01, Figure 4.5F) DNA damage indices are increased in mice lacking the Se-rich C-terminal domain. These data suggest that the Se-rich domain of Sepp1 might protect from tumor initiation by reducing DNA damage in response to AOM and DSS administration.

Mutation of the redox active selenocysteine in Selenoprotein P promotes inflammatory tumorigenesis.

Within the N-terminal domain of selenoprotein P, residues 40-43, exists a UXXC redox motif which possesses phospholipid hydroperoxide glutathione peroxidase activity (160). As such, it may be that selenoprotein P is able to contribute to antioxidant activity within mice challenged with DSS. In order to test whether loss of this antioxidant domain would lead to alterations in tumorigenesis, we subjected Sepp1 mice in which the selenocysteine (U) at amino acid 40 was mutated to an enzymatically dead serine (S) (Sepp1$^{U40S/U40S}$) to the AOM/DSS protocol. In response to this inflammatory carcinogenesis protocol, Sepp1 mutated mice displayed increased tumor number (3.8 ± 0.7 vs 7.3 ± 1.1 tumors/mouse, *P*=0.02, Figure 4.5G) and tumor size (1.6 ± 0.2 vs 3.1 ± 0.3

mm^2, *P*=0.002, Figure 4.5H). This increase in tumorigenesis was likely at least partially dependent upon an increase in crypt (0.3 ± 0.02 vs 0.5 ± 0.04 $Ki67^+$ cells/crypt, *P*=0.0009, Figure 4.5I) and intratumoral (15.2 ± 1.6 vs 33.5 ± 2.6 $Ki67^+$ cells/tumor HPF, *P*<0.0001, Figure 4.5J) proliferation despite no change in apoptosis. We did note an increase in crypt (0.3 ± 0.03 vs 0.6 ± 0.02 8-$OHdG^+$ cells/crypt, *P*<0.0001, Figure 4.5K) and intratumoral (10.8 ± 1.2 vs 28.7 ± 2.6 8-$OHdG^+$ cells/tumor HPF, *P*<0.0001, Figure 4.5L) DNA damage, suggesting that the redox site of Sepp1 contributes to protection from DNA damage.

Hepatic Sepp1 does not contribute to the $Sepp1^{-/-}$ tumorigenic phenotype.

Hepatic selenoprotein P expression is essential for Se homeostasis (66) and restoration of hepatic Sepp1 can reverse neurological and reproductive phenotypes of *$Sepp1^{-/-}$* mice (385) indicating that Sepp1 produced by and transported from the liver is able to supplement Sepp1 loss in the brain and testes. We wanted to test whether liver-derived Sepp1 is the major driver of the tumorigenic protection in response to inflammatory carcinogenesis. We, therefore, crossed floxed Sepp1 mice with mice expressing albumin-driven cre (*$Sepp1^{c/c}$;alb-$cre^{+/-}$*) and subjected these mice to the AOM/DSS protocol. As would be expected upon liver-specific knockout of Sepp1, plasma levels of Sepp1 were severely reduced compared to those seen in *WT* mice (31.4 ± 2.1 vs 3.9 ± 0.6 µg Sepp1/mg plasma, *P*<0.0001, Figure 4.6A). Despite this decrease in plasma Sepp1, tumor number (7.1 ± 1.0 vs 6.5 ± 0.7 tumors/mouse, *P*=0.6, Figure 4.6B) and size (2.4 ± 0.3 vs 2.3 ± 0.2 mm^2, *P*=0.9, Figure 4.6C) were similar between *WT* and

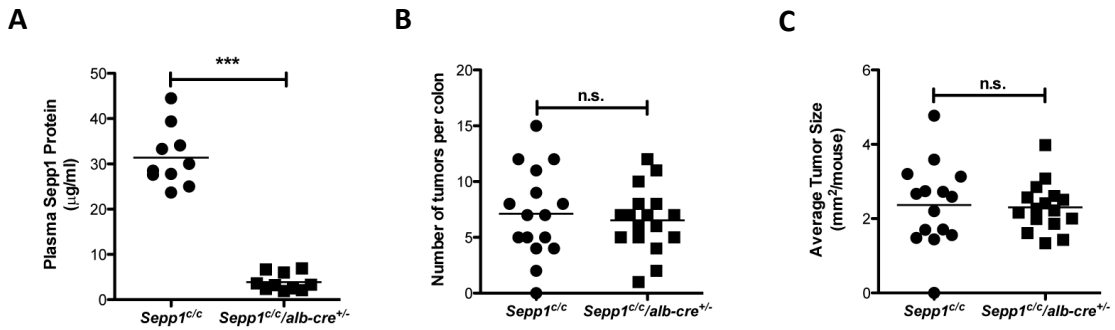

*Figure 4.6 Liver-derived Sepp1 does not modify colitis-associated carcinoma. A) Quantification of Sepp1 protein within the plasma of either WT or Sepp1$^{c/c}$/alb-cre$^{+/-}$ mice. B) Number of tumors and C) average tumor size within each mouse (mm^2). ***P<0.001.*

Sepp1$^{c/c}$;alb-cre$^{+/-}$ mice indicating that loss of liver-derived Sepp1 does not impact the tumorigenic phenotype that is seen upon complete Sepp1 knockout. This is especially important because it indicates that there is an important function for non-plasma Sepp1 in anti-tumor properties.

Absence of Selenoprotein P augments stem cell properties and reduces the ability of enteroids to survive in response to hydrogen peroxide.

Selenoprotein P regulates oxidative stress and toxicity (373, 386) and, consistent with a function in Wnt signaling, has been shown to play a role in differentiation and stem cell properties (172, 387). Interestingly, we noted that liver-derived Sepp1 does not contribute to tumorigenesis in our mouse model, suggesting a potential epithelial influence of Sepp1. Of interest, though Sepp1 is not expressed in the colon or enteroids to the extent of that in the liver, there is expression which, upon loss, could contribute to epithelial phenotypes (Figure 4.7A). We, therefore, wanted to determine whether selenoprotein P contributed to epithelial growth and stem cell properties at baseline as

well as whether hydrogen peroxide treatment would alter ROS production and survival within the epithelial compartment. Recently, a model for epithelial crypt growth has been established based on the isolation of stem cells from the small intestinal crypt. From single crypts, complex structures can be grown *in vitro* that closely resemble their *in vivo* counterparts (388). We utilized this model system to determine how the small intestinal epithelial compartment responds to selenoprotein P knockout.

Enteroids can be grown from a single stem cell or complete crypts (389) and the "stemness" of an enteroid can be measured by several growth properties displayed by the enteroid. For instance, augmented stem cell survival can be measured by an increase in the number of crypts that survive plating versus the total number of crypts plated (plating efficiency). Furthermore, the percentage of branching enteroids or stem spheroids at a certain time point can establish the capabilities of the stem cells to differentiate and the extent of stem cell signaling, respectively. Finally, the number of branches within each enteroid exhibit the ability of the stem cells to self-propagate and establish new crypts. We analyzed *Sepp1*$^{-/-}$ enteroids for each of these properties (plating efficiency: 96.5 ± 2.4 % enteroids of total crypts plated, branching enteroids: 61.5 ± 1.8 % branching enteroids, stem spheroids: 14.5 ± 0.2 % stem spheroids, number of branches: 3.2 ± 0.2 number of branches per branching enteroid, Figure 4.7B) and discovered an increased stem cell fitness and growth abilities compared to *WT* enteroids (plating efficiency: 65.5 ± 2.0 % enteroids of total crypts plated, $P<0.0001$, branching enteroids: 42.1 ± 2.4 % branching enteroids, $P=0.02$, stem spheroids: 7.6 ± 0.9 % stem spheroids,

P=0.002, number of branches: 1.9 ± 0.1, *P*=0.003, Figure 4.7B). We next wanted to determine the response of *Sepp1*$^{-/-}$ enteroids to hydrogen peroxide treatment. Analysis

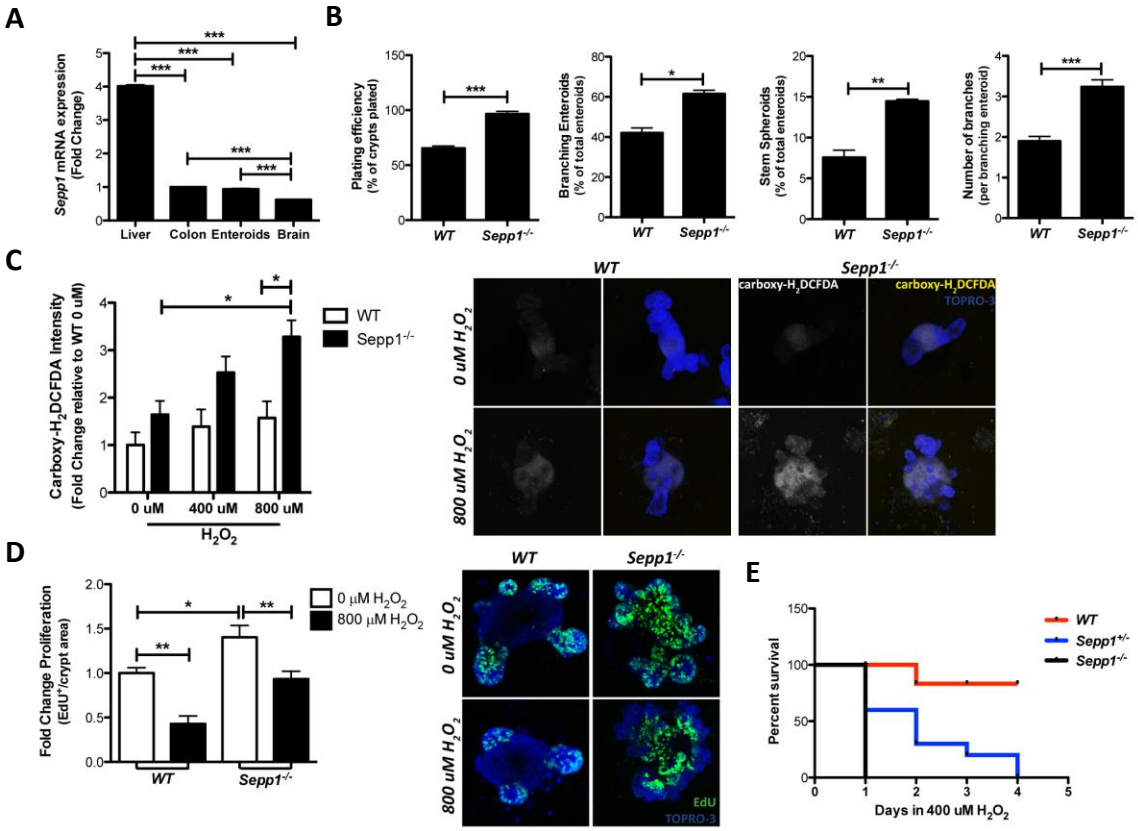

Figure 4.7 Sepp1$^{-/-}$ *enteroids display an increase in stem cell characteristics and increased ROS production, proliferation, and decreased survival in response to hydrogen peroxide administration. A) Relative Sepp1 mRNA expression in the liver, colon, brain, and enteroids isolated from WT mice. The graph displays fold change expression normalized to GAPDH and relative to colonic Sepp1 expression. B) Enteroid stem cell properties determined based on plating efficiency as measured by percentage of surviving enteroids one day post-plating compared to total crypts plated, percent of branching enteroids and stem spheroids relative to total enteroids counted three days post-plating, and average number of branches per branching enteroid at four days post-plating. C) ROS quantification as determined by carboxy-H₂DCFDA staining intensity measured after 2 hours of treatment with 0 µM, 400 µM, and 800 µM hydrogen peroxide. The quantification is displayed as the fold change in intensity relative to WT enteroids treated with 0 µM hydrogen peroxide (left). Representative images of the single carboxy-H₂DCFDA channel and merged carboxy-H₂DCFDA and TO-PRO3 channels in WT and Sepp1*$^{-/-}$ *enteroids treated with either 0 µM or 800 µM hydrogen peroxide (100x magnification, right). C) Proliferation quantification as determined by EdU*$^{+}$ *cells per crypt area within WT and Sepp1*$^{-/-}$ *enteroids after two hours of treatment with either 0 µM or 800 µM hydrogen peroxide (left) and representative images of EdU staining in WT and Sepp1*$^{-/-}$ *enteroids post-treatment with either 0 µM or 800 µM hydrogen peroxide (100x magnification, right). D) Survival curves for WT (red), Sepp1*$^{+/-}$ *(blue), and Sepp1*$^{-/-}$ *(black) enteroids after daily treatment with 400 µM hydrogen peroxide. *P<0.05, **P<0.01, ***P<0.001.*

of reactive oxygen species (ROS) produced after treatment with hydrogen peroxide revealed a decreased ability of *Sepp1*$^{-/-}$ mice to respond to oxidative stress as carboxy-H_2DCFDA staining intensity was increased (800 µM H_2O_2: 1.6 ± 0.4 vs 3.3 ± 0.4 fold-change intensity relative to 0 µM H_2O_2 *WT*, *P*=0.04, Figure 4.7C) though there was no change in staining intensity of the oxidative-insensitive analogue carboxy-DCFDA. Moreover, baseline proliferation was increased in *Sepp1*$^{-/-}$ enteroids (1.0 ± 0.06 vs 1.4 ± 0.1 fold-change EdU^+ cells/crypt area relative to 0 µM H_2O_2 *WT*, *P*<0.05, Figure 4.7D) and treatment with hydrogen peroxide resulted in decreased *Sepp1*$^{-/-}$ proliferation compared to untreated null enteroids (1.4 ± 0.1 vs 0.9 ± 0.09 fold-change EdU^+ cells/crypt area relative to 0 µM H_2O_2 *WT*, *P*<0.01, Figure 4.7D), but *Sepp1*$^{-/-}$ enteroids retained increased proliferation compared to *WT* enteroids (0.4 ± 0.09 vs 0.9 ± 0.09 fold-change EdU^+ cells/crypt area relative to 0 µM H_2O_2 *WT*, *P*<0.05, Figure 4.7D). Finally, *Sepp1*$^{-/-}$ enteroids demonstrated decreased survival in response to multiple daily administrations of hydrogen peroxide (*P*=0.005, Figure 4.7E). These data indicate that absence of Sepp1 increases baseline stem phenotypes and proliferation but decreases the antioxidant potential of enteroids. These data are important because they indicate an epithelial cell-autonomous role for Sepp1 in processes that would likely contribute to tumorigenesis in CAC, a cancer characterized by increased oxidative stress.

Wnt signaling and oxidative stress gene signatures are altered in Sepp1$^{-/-}$ epithelium.

Enteroids rely on the addition of growth factors EGF, Noggin, and R-spondin in order to properly grow and differentiate. As Sepp1 null enteroids demonstrate increased stem cell properties and fitness, we wanted to determine whether absence of signaling down one of the three pathways required for enteroid establishment and growth would reverse the baseline enteroid phenotype. Depletion of EGF, Noggin, and R-spondin resulted in similar decreases in survival in all three genotypes indicating that all three pathways are important for enteroid persistence (Figure 4.8A), but absence of R-spondin is the only condition in which both heterozygous and null enteroids displayed decreased survival compared to WT enteroids, though this difference was not statistically significant (Figure 4.8A). These data indicate that the stem phenotypes seen upon Sepp1 knockout are most dependent on Wnt signaling.

In order to acquire an unbiased understanding of gene changes within tumors of *Sepp1*$^{-/-}$ tumors, we performed RNAseq analysis of tumors from *WT* and *Sepp1*$^{-/-}$ mice subjected to the AOM/DSS protocol. Ingenuity pathway analysis indicates that Wnt signaling is altered in *Sepp1*$^{-/-}$ tumors with increases in TGFβR3, APPL2, SFRP-4 and -5, and Cdh-2 expression and obvious pathway abnormalities (Figure 4.8B), thus validating results seen in enteroids. As further validation of altered Wnt signaling in these tumors, protein analysis demonstrates increased expression of the Wnt targets Lef-1, Cyclin D1, and Mmp7 upon loss of Sepp1 expression (Figure 4.8C). We also wanted to determine whether alterations could be determined within oxidative stress genes. First, we looked

for changes in expression of other selenoproteins to determine if compensation was taking place and found that expression of selenoproteins were not significantly different

A

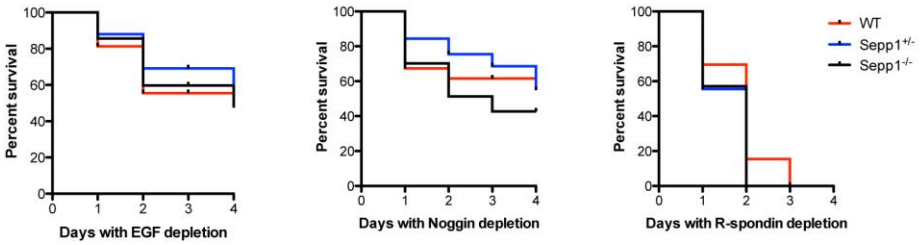

B

Gene Symbol	Gene Name	Fold Change	P-value
TGFβR3	Transforming growth factor beta-3	3.4	5.00E-05
APPL2	Adapter protein containing PH domain, PTB domain and leucine zipper motif 2	2.4	0.0015
SFRP4	Secreted frizzled-related protein 4	2.7	0.00015
SFRP5	Secreted frizzled-related protein 5	2.9	5.00E-05
Cdh-2	Cadherin-2	2.1	0.00035

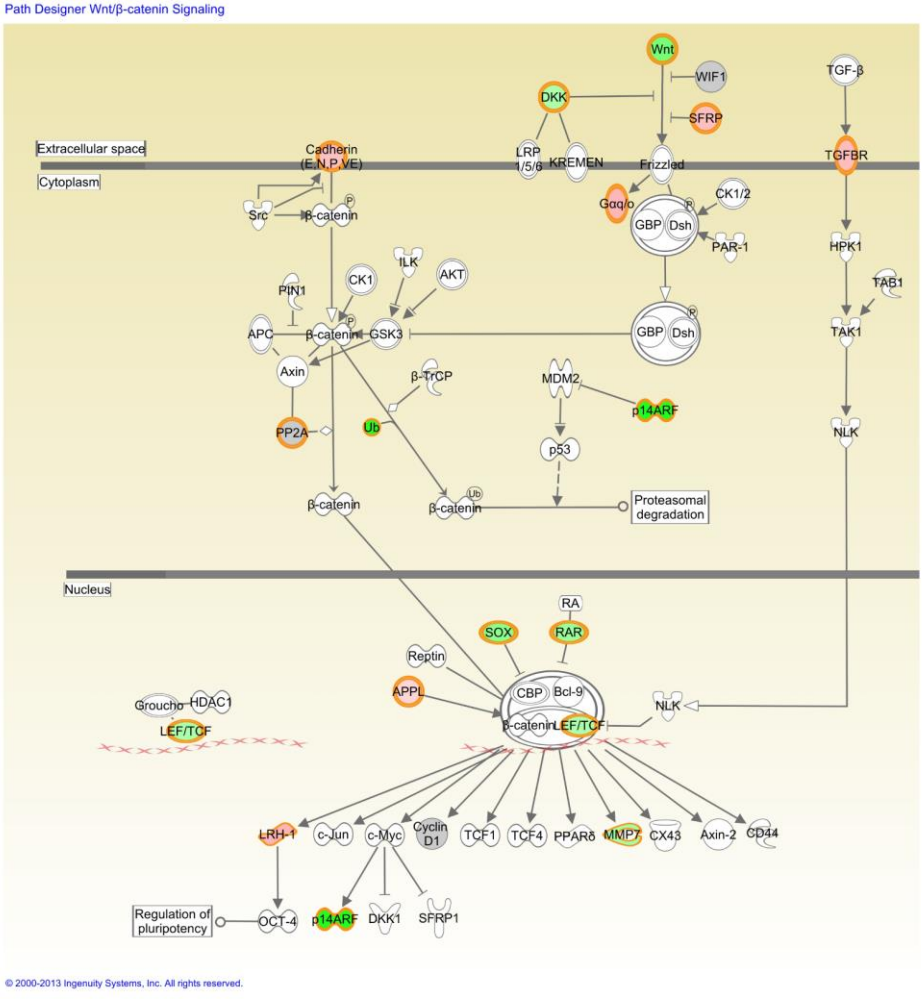

C

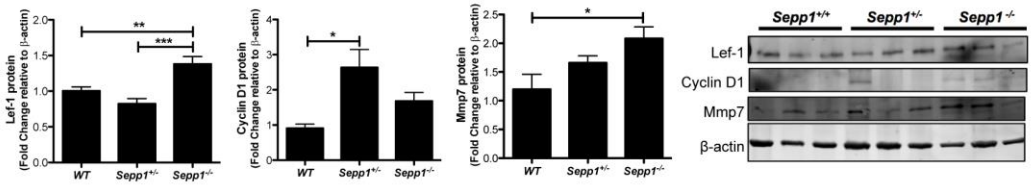

Figure 4.8 *Wnt signaling plays a pivotal role in the Sepp1$^{-/-}$ phenotype. A) Survival curves in response to growth factor depletion in WT, Sepp1$^{+/-}$, and Sepp1$^{-/-}$ enteroids. B) Ingenuity pathway analysis of Sepp1$^{-/-}$ tumor RNAseq data relative to WT data. Select genes from the WNT signaling pathway that are overexpressed in Sepp1-/- tumors (top) and WNT pathway alterations demonstrated in a pathway map (bottom). Genes highlighted with red are overexpressed and genes highlighted with green are suppressed. Intensity of color indicates extent of expression where darker color indicates a greater expression change. C) Quantification of WNT proteins Lef-1, Cyclin D1, and Mmp7 normalized to β-actin. Quantification is shown as fold change relative to WT (top) and representative images of blots from three individual tumors from each genotype (bottom).*

between *WT* and *Sepp1$^{-/-}$* tumors. We did note significant alterations in several cytochrome P450 gene family members as well as beta-hydroxysteroid dehydrogenase genes (Table 4.1) suggesting that other antioxidant genes are upregulated to attempt to compensate for Sepp1 loss.

Gene Symbol	Gene Name	Enzymatic Activity	Fold Change	P-value
Cyp2b10	Cytochrome P450 2B10	oxidoreductase activity	-2.1	0.0001
Aldh1a1	Retinal dehydrogenase 1	oxidoreductase activity	2	5.00E-05
Hpd	4-hydroxyphenylpyruvate dioxygenase	oxidoreductase activity	2.1	5.00E-05
Hsd3b2	3 beta-hydroxysteroid dehydrogenase/Delta 5-->4-isomerase type 2	oxidoreductase activity	2.2	5.00E-05
Cyp2d9	Cytochrome P450 2D9	oxidoreductase activity	2.2	5.00E-05
Fmo2	Dimethylaniline monooxygenase [N-oxide-forming] 2	oxidoreductase activity	2.2	5.00E-05
Hsd17b13	17-beta-hydroxysteroid dehydrogenase 13	oxidoreductase activity	2.2	5.00E-05
Nos1	Nitric oxide synthase, brain	oxidoreductase activity	2.2	5.00E-05
Cyp2c65	Cytochrome P450, family 2, subfamily c, polypeptide 65	oxidoreductase activity	2.3	5.00E-05
Cyp4b1	Cytochrome P450 4B1	oxidoreductase activity	2.3	0.00065
Cyp4f14	Leukotriene-B4 omega-hydroxylase 3	oxidoreductase activity	2.34	5.00E-05
Hao2	Hydroxyacid oxidase 2	oxidoreductase activity	2.4	5.00E-05
Nrxn2	Protein Nrxn2	oxidoreductase activity	2.5	0.00025
Ddo	D-aspartate oxidase	oxidoreductase activity	2.5	0.00035
Dpyd	Dihydropyrimidine dehydrogenase [NADP(+)]	oxidoreductase activity	2.6	5.00E-05
Hsd3b3	3 beta-hydroxysteroid dehydrogenase/Delta 5-->4-isomerase type 3	oxidoreductase activity	2.6	5.00E-05
Cyp2c55	Cytochrome P450 2C55	oxidoreductase activity	2.7	5.00E-05
Cd163	Scavenger receptor cysteine-rich type 1 protein M130	oxidoreductase activity	3.2	5.00E-05
Cyp2d12	Cytochrome P450, family 2, subfamily d, polypeptide 12	oxidoreductase activity	3.7	5.00E-05
Clvs2	Clavesin-2	oxidoreductase activity	3.8	0.0011
Cyp2e1	Cytochrome P450 2E1	oxidoreductase activity	4.1	5.00E-05

Table 4.1 *Significantly up- or down-regulated oxidative stress response genes in Sepp1$^{-/-}$ tumors compared to WT tumors.*

Discussion

Selenoprotein P mRNA levels are significantly decreased in colorectal cancer tissue relative to normal mucosa (162) and association studies have identified multiple SNPs in *SEPP1* that are linked to colorectal cancer incidence or risk (99, 165). Perhaps most importantly for the purpose of this study, expression of Sepp1 is also significantly decreased during progression in tumors resulting from ulcerative colitis (390). This link may be dependent upon the role of selenoprotein P in antioxidant activity as it has been shown to be a hydroperoxide-reducing enzyme (159) and oxidative stress is a characteristic of inflammatory bowel disease (299). This possibility is supported by the fact that selenoprotein P is also downregulated in prostate cancer and results in decreased protection against oxidative damage (164, 166) and *in vitro*, Sepp1 protects astrocytes (391) and keratinocytes (386) from oxidative damage. These data suggest that Sepp1 may protect from colitis-associated carcinoma and its antioxidant activities might contribute to this protection. Thus, Sepp1 may serve as a therapeutic target in the prevention of CAC in patients with IBD.

In support of this proposed role, partial loss of Sepp1 leads to increased tumorigenesis concomitant with increased DNA damage, proliferation, and pro-tumorigenic M2 macrophage infiltration. Interestingly, the macrophage phenotype appears to result from improper polarization as activation of *Sepp1*$^{+/-}$ bone marrow macrophages also leads to increase prevalence of M2 characteristics suggesting that decreased Sepp1 expression alters macrophage polarization. Moreover, truncation of the selenium-rich domain of Sepp1 or mutation of the N-terminal redox active selenocysteine

also resulted in increased tumorigenesis, suggesting that both functional domains of Sepp1 contribute to protection from inflammatory tumorigenesis. Interestingly, despite the fact that the liver produces the majority of Sepp1 which is distributed via the blood stream, we present evidence here that implicates epithelial-derived Sepp1 in protection from oxidative stress and tumorigenesis. For one, small intestinal organoids isolated from *Sepp1*$^{-/-}$ mice display increased stemness and proliferation, two properties closely linked with tumorigenesis. Moreover, they demonstrate a decreased ability to deal with oxidative stress as hydrogen peroxide treatment leads to increased ROS production and decreased survival. Finally, absence of liver-derived Sepp1 does not alter tumorigenesis. While this does not directly implicate epithelial Sepp1 in the *Sepp1*$^{-/-}$ tumor phenotype, coupled with enteroid data, the liver-specific knockout data suggest that epithelial Sepp1 at least plays a contribution to the phenotype. Additionally, the Se-rich C-terminal domain of Sepp1 is considered to primarily function as a Se transport domain but the *Sepp1*$^{c/c}$*;alb-cre*$^{+/-}$ and *Sepp1*$^{\Delta 240\text{-}361/\Delta 240\text{-}361}$ phenotypes do not phenocopy one another suggesting that there may be a role for the C-terminal domain of Sepp1 beyond selenium transport. Future experiments should focus on epithelial-specific knockout models in order to confirm this hypothesis.

Induction of several signaling pathways have been linked to Se depletion including Nrf2 (125) and Wnt (130), there is little known about the contribution of Sepp1 to these pathway alterations or others which might be specific to Sepp1. We, therefore, performed an unbiased RNAseq analysis of tumors from *WT* and *Sepp1*$^{-/-}$ mice post-AOM/DSS protocol. Amongst the most severely altered pathways in response to Sepp1

loss was the Wnt pathway. While genes were both up- and down-regulated in this pathway, some of particular importance including the Wnt ligand, the transcriptional effector LEF/TCF, and the Wnt targets Mmp7, which we also validated at the protein level, and p14ARF were all decreased at the mRNA level. Genes that demonstrated increases in expression included the TGF-β receptor, E-cadherin, and the liver receptor homologue- 1 (LRH-1) which is important for maintaining stem cell pluripotence during development (392). Importantly, Ingenuity analysis identified the Wnt/β-catenin signaling pathway as being stimulated in *Sepp1*$^{-/-}$ tumors despite those genes that were downregulated. This is important because Sepp1 is a Se transporter and Se deficiency leads to an increase in Wnt signaling suggesting that Sepp1's selenium transport function may contribute to Wnt modulation.

We also wanted to survey *Sepp1*$^{-/-}$ tumors for alterations in redox gene regulation. Interestingly, we did not note increased expression of other selenoproteins, indicating that there was not compensation upon Sepp1 loss. Amongst some of the most significantly upregulated redox genes in response to Sepp1 deficiency in the AOM/DSS model were members of the cytochrome P450 family of oxidoreductases. The cytochrome P450 (Cyp) superfamily is a group of enzymes that catalyze the oxidation of organic substances (393). One Cyp identified, Cyp2e1, can reduce oxygen to produce pro-oxidant species, which can create oxidative stress particularly when antioxidant reserves are depleted (394) as would be seen with Sepp1 deficiency. This upregulation of the Cyp gene family likely results from the increased oxidative stress resulting from Sepp1

absence and ultimately results in augmentation of the already high oxidative load seen in *Sepp1*$^{-/-}$ mice.

We demonstrate that Sepp1 deficiency leads to protumorigenic phenotypes both within small intestinal epithelial cells and in response to the AOM/DSS inflammatory carcinogenesis protocol. These data utilize a novel stem cell model system as well as genetic models of Sepp1 modulation to show that Sepp1 would likely serve as a therapeutic target in the prevention and treatment of colitis-associated carcinoma, a cancer characterized by high oxidative stress.

Acknowledgments

Core Services performed through Vanderbilt University Medical Center's Digestive Disease Research Center supported by NIH grant P30DK058404 Core Scholarship. This publication was also supported in part by the NCI Cancer Center Support Grant P30CA068485 utilizing the Translational Pathology shared resource, which provided tissue processing and staining services. Support was also supplied by the National Center for Research Resources, Grant UL1 RR024975-01, and is now at the National Center for Advancing Translational Sciences, Grant 2 UL1 TR000445-06. The content is solely the responsibility of the authors and does not necessarily represent the official views of the NIH. The authors thank Teri Stevenson and Michelle Chatterton for help with animal husbandry, members of the Williams and Burk laboratories for thoughtful discussions about this research project.

CHAPTER V

MTGR1 IS REQUIRED FOR TUMORIGENESIS IN THE MURINE AOM/DSS COLITIS-ASSOCIATED CARCINOMA MODEL[3]

Introduction

MTGR1 (Myeloid Translocation Gene, Related-1, CBFA2T2), MTG8 (RUNX1T1) and MTG16 (CBFA2T3) are members of a gene family (MTGs) in which MTG8 and MTG16 were originally identified as targets of chromosomal translocations in acute myeloid leukemia (AML) (178, 190). Translocations involved in cancer identify master regulatory genes often affecting cellular proliferation, differentiation and apoptosis. MTGs are transcriptional co-repressors lacking both enzymatic activity and DNA binding capabilities, and act as scaffolding proteins upon which other transcriptional co-repressors (mSin3a, N-CoR, SMRT), histone deacetylases, and transcription factors assemble, thus directing promoter-specific targeting of repressor complexes (178, 190). The aggregate effect of these complexes is chromatin remodeling via post-translational histone modifications.

In addition to their pivotal role in AML, MTG8 and MTG16 have been implicated in epithelial malignancies, with the identification of multiple non-synonymous mutations in MTG8 and MTG16 in colorectal carcinoma (228, 229) and more recently additional mutations in MTG8 identified in breast and lung cancer (395). Furthermore, MTG16 is

[3] This work has been published under Caitlyn W. Barrett, Barbara Fingleton, Amanda Williams, Wei Ning, Melissa Steapleton, Mary K. Washington, Rupesh Chaturvedi, Keith T. Wilson, Scott W. Hiebert, Christopher S. Williams (2011) Mtgr1 is required for tumorigenesis in the murine AOM/DSS colitis-associated carcinoma model, *Cancer Research*, 71, 1302-12 (4).

proposed to function as a tumor suppressor in breast cancer (227). Recently, it has been demonstrated that MTGs bind to TCF4 and repress its transcriptional activity, thus linking MTGs with a stem cell regulatory pathway critical for epithelial homeostasis that is frequently targeted in malignancy (209). The role in tumorigenesis of MTGR1, the third MTG family member, has yet to be determined.

Observations made in *Mtgr1*$^{-/-}$ and *Mtg8*$^{-/-}$ mice have identified MTGs as participating in intestinal developmental and differentiation programs. Roughly a third of *Mtg8*$^{-/-}$ mice demonstrate a complete deletion of the midgut (214). *Mtg16*$^{-/-}$ mice revealed that MTG16 is required for hematopoietic progenitor cell fate decisions and early progenitor differentiation (396). *Mtgr1*$^{-/-}$ mice have increased intestinal proliferation and the progressive depletion of the secretory lineage in the small intestine, indicating that MTGR1 regulates intestinal proliferation and differentiation programs (217). Additionally, *Mtgr1*$^{-/-}$ mice are sensitive to DSS-induced colitis and exhibit chronic architectural changes with this type of injury implicating MTGR1 in epithelial repair programs (226). Collectively, the genetic evidence suggests that MTG proteins play key roles in intestinal biologic processes and could influence intestinal tumorigenesis.

Chronic inflammation, as in Ulcerative Colitis and Crohn's Colitis, predisposes malignancy (15, 397, 398), but with an extended latency. While inflammation can be linked to tumorigenesis, the long latency makes the molecular basis of these links less clear. Moreover, in certain malignancies inflammation may impair tumor growth. This is termed "tumor immunoediting" and represents the dynamic nature between the anti-

tumoral and pro-tumoral activities of immunity (399). Thus it is difficult to predict the impact a particular gene or pathway may have on tumorigenesis *a priori*.

We hypothesized that MTGR1 could modify inflammatory carcinogenesis, but whether this would be stimulatory or inhibitory was unclear. In order to test this hypothesis, we applied the azoxymethane/dextran sodium sulfate (AOM/DSS) murine inflammatory colitis model to *Mtgr1*$^{-/-}$ mice. This model has been employed to dissect NF-kB (400), TLR4 (266), and TNFα (401) signaling, innate immune responses (402), and the role of intestinal microflora (403) in inflammatory carcinogenesis. We found a striking decrease in tumor formation in the absence of MTGR1 coupled with increased intra-tumoral apoptosis. This phenotype required injury and was non-hematopoietic cell autonomous; however, global gene expression analysis revealed that members of WNT networks were decreased and genes associated with innate and adaptive immune networks upregulated in *Mtgr1*$^{-/-}$ tumors, implicating tumor immunity as a potential mechanism of tumor clearance. Supporting this concept, we observed decreased nuclear β-catenin and increased CD3^{+}, B220^{+}, NKp46^{+}, and F4/80^{+} infiltrates in *Mtgr1*$^{-/-}$ tumors. Thus, MTGR1 is required for efficient AOM/DSS-induced tumorigenesis and may promote survival of initiated colonocytes perhaps by its influence on suppressing tumor immunity.

Materials and Methods

Murine Inflammatory Carcinogenesis Protocol: 8-10 week old C57BL/6/129 mixed background WT (n=22) or *Mtgr1*$^{-/-}$ (n=19) mice were injected with 12.5 mg/kg of AOM (Sigma-Aldrich) intraperitoneally as described in Greten, *et al* (265). After a three-day

recovery period the animals were started on the first of four cycles of 3% DSS *ad libitum* (See Schematic in Figure 5.1A). Each cycle lasted 5 days and was separated by a 16-day recovery period. After the last cycle, animals were sacrificed following a 26-day recovery period. Tumor counts and measurements were performed in a blinded fashion under a stereo-dissecting microscope. Microscopic analysis was performed for severity of inflammation (357) and dysplasia on (H&E) stained "Swiss rolled" colons by a gastrointestinal pathologist (MKW). All *in vivo* procedures were carried out in accordance with protocols approved by the Vanderbilt Institutional Animal Care and Use Committee.

Mtgr1 expression: Tumors and adjacent non-tumor tissue from four colons were dissected from WT mice and RNA was isolated using the RNEasy MiniKit (Qiagen). SYBR Green (Bio-Rad) qRT-PCR using *Mtgr1* and GAPDH specific primers was performed in triplicate as previously described (226). Analysis of fold-change was performed using the $^{\Delta\Delta}$Ct method.

In situ hybridization: The MTGR1-1699T and MTGR1-2020B probe set and protocol of Amann *et al*. were used (217). Images were taken on a Zeiss Axioskope under identical conditions.

Immunohistochemistry: 2-h prior to sacrifice, animals were injected with 16.7 mg/kg bromodeoxyuridine. 5-micron sections were cut, dewaxed, hydrated and endogenous peroxidase activity quenched with 0.03% hydrogen peroxide in MeOH. Antigen retrieval was performed using the boiling sodium citrate method in a microwave (20mM sodium citrate pH 6.5) for 16 min at 30% power. After blocking, primary antibody added (α-β-catenin, (BD Transduction Laboratories), 1:1000; α-CD3, (Serotec), 1:1000; α-CD45r, (BD

Pharmingen), 1:40, monoclonal α-BrdU (Accurate Labs) 1:2000), α-arginase I (ARG1), (Santa Cruz), 1:500; α-IL-1β, (R&D Systems), 1:50; α-NKp46, (Santa Cruz), 1:500; α-matrilysin 338 (404), diluted 1:500) overnight at 4°C. Isotype-matched antibodies were included as negative controls. The Vectastain ABC Elite System (Vector Labs) was used to visualize staining for IHC. For immunofluorescence slides were counterstained with DAPI (Invitrogen) and mounted with ProLong Gold antifade (Invitrogen). Identification of intra-tumoral apoptotic cells was performed using the ApopTag® Plus Peroxidase *in situ* Apoptosis Kit (Chemicon) according to the manufacturers protocol. Control stains were obtained by omitting the terminal transferase (TnT) enzyme. Immune cell, apoptosis, and proliferation indices were generated by counting the number of positive cells per high-powered field (HPF; 40x objective) within each tumor (15 *Mtgr1*$^{-/-}$ 42 WT tumors) from 9 *Mtgr1*$^{-/-}$ and 14 WT tumor bearing mice. A total of 82 *Mtgr1*$^{-/-}$ and 319 WT high-powered fields were examined and the mean positive cells per HPF was calculated. A crypt apoptosis and proliferation index was generated by counting twenty crypts per mouse. This is presented as the mean number of TUNEL^{+} or BrdU^{+} cells per crypt.

Cell Culture and siRNA transfection: HCT116 cells were obtained from Dr. Robert Coffey and have morphologic characteristics consistent with their known identity. Formal authentication was not performed. One day prior to siRNA transfection, cells were plated at 2x10^{5} cells per well in a 6-well plate. Cells were then transfected with ON-TARGETplus SMARTpool siRNA for *Mtgr1*/CBFA2T2 (Thermo Scientific) using RNAiMax (Invitrogen) according to the manufacturer's protocol. 6 h after transfection, the transfection mixture was replaced with complete media. The next day, cells were starved overnight with media

containing 1% BSA and the next morning cells were washed and complete media was added. After harvesting, cells were analyzed for apoptosis using the TACS Annexin V-FITC flow cytometry kit (R&D Systems). Cells were analyzed on the 5-laser BD LSRII analyzer and unstained controls were used to establish proper gating. Presented are the average percentage of annexin V positive cells per 10,000 cells over three different trials.

Expression Array Assays: Tumors were dissected from WT and *Mtgr1*$^{-/-}$ mice and RNA was isolated using the RNEasy MiniKit (Qiagen). RNA integrity was determined using an Agilent 2100 Bioanalyzer (Agilent Technologies, Santa Clara, CA). All RNA samples had RNA integrity numbers (RINs) >8 and were deemed suitable for hybridization. A total of 10 mg of cRNA was used in the second cycle of first strand synthesis to generate the correct sense for target hybridization. Mouse gene 1.0 ST arrays (Affymetrix) were scanned the next day. CEL files were imported into Partek Express (Partek) and Robust Multichip Average (RMA) was run across all 8 samples. Pivot data was exported and posted. A t-test was run between the *Mtgr1*$^{-/-}$ and WT sample groups in Partek. The *P*-value was multiple testing corrected with Bonferroni and Step-up. Expression array analysis was performed hybrizing cRNA to the Mouse gene 1.0 ST chip (Affymetrix). Differentially expressed genes were classified using the PANTHER (Protein Analysis THrough Evolutionary Relationships) classification system (www.pantherdb.org/gen).

Bone Marrow Transplant: A single cell suspension of bone marrow cells was obtained from the tibia and femur of two *Mtgr1*$^{-/-}$ and four WT 6-week old donor mice, and the red blood cells were lysed with erythrocyte lysis buffer (Buffer EL, Qiagen). 0.85 x 10^6 bone marrow cells were injected via the tail vein into 15 *Mtgr1*$^{-/-}$ and 17 WT lethally irradiated

(900 rads) 8 to 12-week old recipient mice. The mice were then fed acidified water (0.015% HCl in autoclaved water) supplemented with 1.1 g/L neomycin sulfate and 125 mg/L polymyxin B sulfate for two weeks post transplantation (modified from Cotta et al. (405)). Eight weeks post-transplantation the mice were placed on the Murine Inflammatory Carcinogenesis Protocol.

Statistical Methods: Apoptosis, proliferation, and immune cell indices as well as the tumor and burden counts were analyzed using the Student's-t test using Graphpad Prism® 5.0c, unless otherwise indicated.

Results

Mtgr1 is overexpressed in AOM/DSS tumors.

Proteins regulating intestinal proliferation and differentiation pathways often contribute to oncogenesis. Given the newly discovered role of MTGR1 in regulating these processes coupled with the observation that loss of MTGR1 results in sensitization to gut injury, we hypothesized that *Mtgr1* expression maybe altered in AOM/DSS tumors. For these experiments, 8-10 week old mice were injected with AOM and treated with 4 cycles of DSS as defined in the Methods and shown in Figure 5.1A. Tumors and adjacent tissue were harvested and both qRT-PCR and *in situ* hybridization for *Mtgr1* mRNA expression was performed. A 10.7-fold increase ($P<0.001$) in *Mtgr1* mRNA expression was demonstrated in tumors compared to adjacent mucosa (Fig. 5.1B) and this expression was localized to a majority of the epithelial cells within the tumor whereas in adjacent histologically normal appearing colonic crypts it was expressed in only a small population

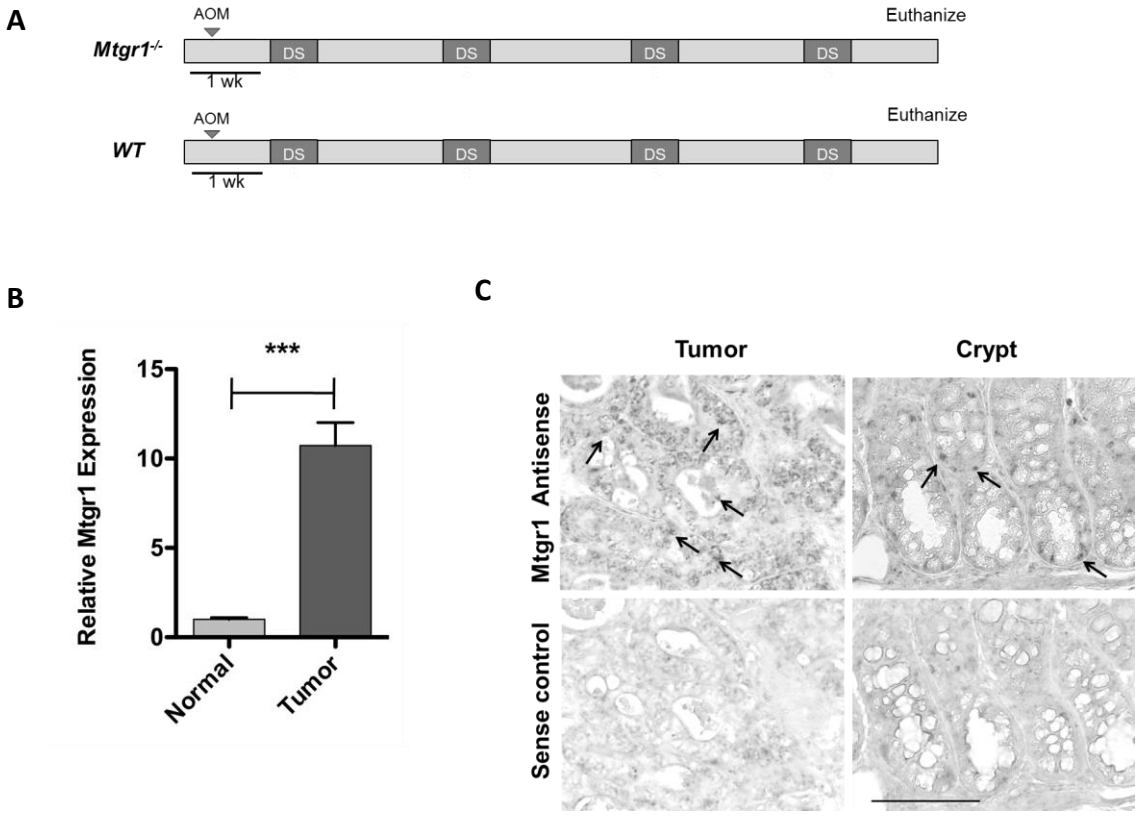

*Figure 5.1 Mtgr1 expression is increased in tumors resulting from AOM/DSS colitis-associated carcinoma. A, schematic of the AOM/DSS protocol. B, polyps and adjacent normal tissue subjected to Taqman qRT-PCR analysis via the delta-delta C_T method demonstrated a 10.73-fold increase in Mtgr1 expression in tumor versus normal tissue (***P<0.001). Error bar represents the standard error for four biological replicates performed in triplicate. C, Mtgr1 in situ hybridization of colonic "Swiss Rolls" obtained from WT AOM/DSS. Arrows indicate positive signal within the base of the crypt. Scale bar is 5 μm.*

of epithelial cells within the lower crypt region, consistent with the published expression pattern (Fig. 5.1C) (217). We next wanted to determine if *MTGR1* levels varied in human colon cancer. We were unable to obtain human colitis associated carcinoma samples therefore we performed qRT-PCR for *MTGR1* on two colorectal cancer sample groups. The first consisted of non-matched normal and colorectal carcinoma (CRC) tissues. In this group we observed a 2.3 fold increase in *MTGR1* expression in the CRC samples (P<0.05) (Fig. 5.2A). We then looked at 9 matched normal/colon cancer samples and found

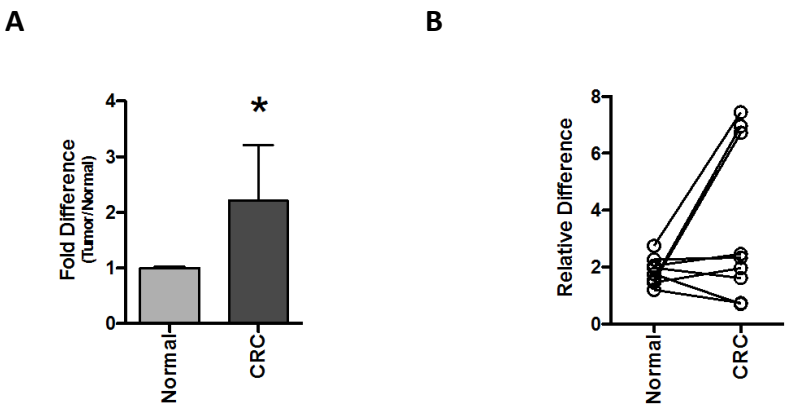

*Figure 5.2 MTGR1 is overexpressed in human colorectal cancer. A) Mtgr1 RNA levels in normal colon vs. CRC samples. (left) average of 3 normals vs 8 CRC samples, *P<0.05. B) Relationship plot of Mtgr1 RNA levels in nine matched normal and CRC samples indicating heterogeneity in Mtgr1 expression.*

heterogeneity in MTGR1 expression, however, 55% of the CRC samples demonstrated an increase in *MTGR1* expression (Fig. 5.2B). These results suggest that MTGR1 may contribute to inflammatory carcinogenesis in the colon and we postulated that deletion of MTGR1 may prevent tumor formation.

Mtgr1 is required for efficient inflammatory tumorigenesis.

Using genetic manipulation in the mouse, we tested whether MTGR1 was required for tumorigenesis in the AOM/DSS model. 8-10 week old WT or *Mtgr1*$^{-/-}$ mice were placed on the AOM/DSS protocol (Fig. 5.1A). Consistent with our prior report (226) *Mtgr1*$^{-/-}$ mice experienced greater weight loss in comparison to WT animals with each DSS treatment. Looser stool was evident in both groups, with frank blood frequently seen in the *Mtgr1*$^{-/-}$ mice. Four weeks after the last DSS cycle the animals were sacrificed. Despite the increased sensitivity to colitis, the *Mtgr1*$^{-/-}$ mice actually had significantly fewer polyps

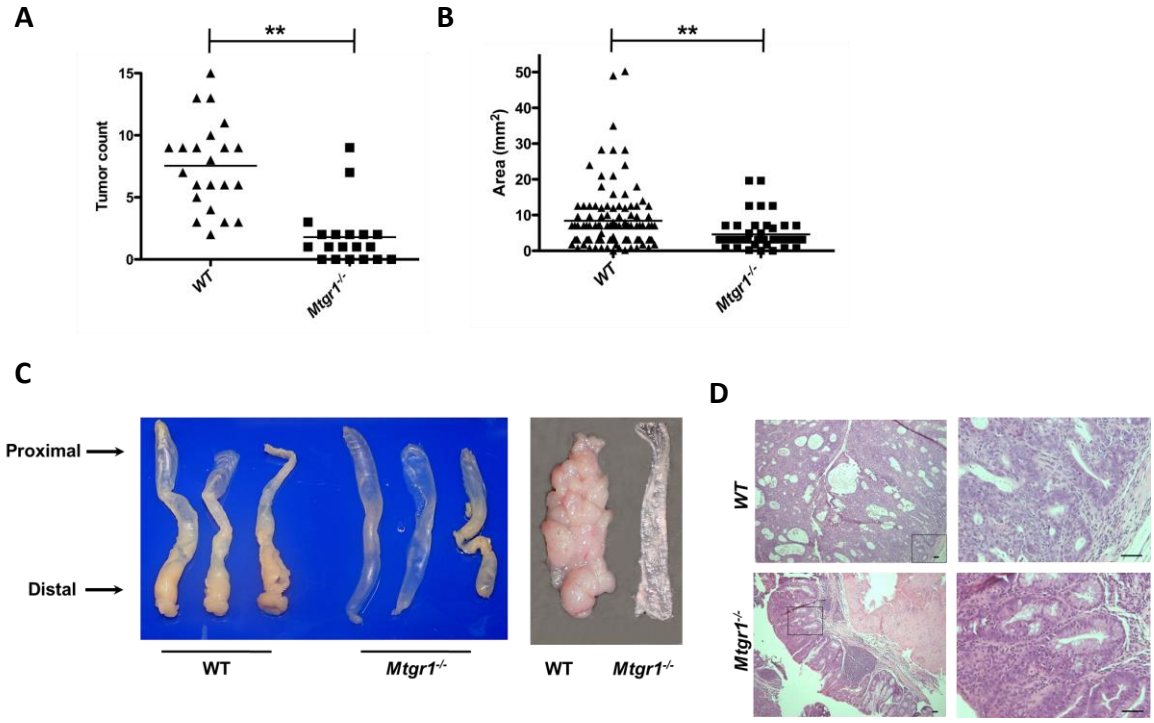

*Figure 5.3 Mtgr1 functions as a tumor promoter in the murine AOM/DSS inflammatory carcinogenesis model. A) polyp frequency and B) polyp size as determined via calculation of the surface area of each lesion in each mouse (**P<0.01). C) representative gross specimens from three WT and Mtgr1$^{-/-}$ AOM/DSS treated mice with longitudinally opened colons on the far right. D) representative H&E demonstrating tumors from WT and Mtgr1$^{-/-}$ mice. Overall, WT tumors were larger and displayed more dysplasia than those from Mtgr1$^{-/-}$ mice. Scale bar is 5 μm.*

compared to WT mice (1.8 ±0.5 vs 7.5 ±0.8, Fig. 5.3A) and decreased tumor size (4.6 ±0.62 mm^2 vs 8.4 ±0.83 mm^2, Fig. 5.3), which was apparent upon gross inspection (representative colons, Fig. 5.3C). Histologic examination of H&E stained sections from colons prepared as "Swiss Rolls" revealed adenomas with high grade dysplasia characterized by loss of epithelial polarity and a more complex tumor growth pattern frequently present in WT tumors, whereas the adenomas observed in the *Mtgr1*$^{-/-}$ colons (Fig. 5.3D) more often showed only low grade dysplastic changes. WT or *Mtgr1*$^{-/-}$ mice

treated either with AOM as a single modality, or with multiple exposures to DSS in the absence of AOM, did not develop tumors over this time frame (data not shown).

A decrease in tumor multiplicity in *Mtgr1*$^{-/-}$ mice suggested that MTGR1 may be playing a role in initiated or early tumor progenitor cell survival after injury, as opposed to influencing tumor promotion, in which case similar numbers of tumors, but smaller tumors would be expected. To determine if epithelial injury was required for this effect, we treated animals with AOM as a single agent (12.5 mg/kg IP) and assessed effects 48 weeks later. At necropsy, there was no difference in polyp or aberrant crypt foci (ACF) formation between WT and *Mtgr1*$^{-/-}$ mice (polyps, 3.5 ±0.2 vs 4.1 ±0.5, *P*=0.40; ACF, 23.4 ±0.1 vs 27.0 ±2.0, *P*=0.21, Fig. 5.4A, B). These data indicate that alterations in epithelial

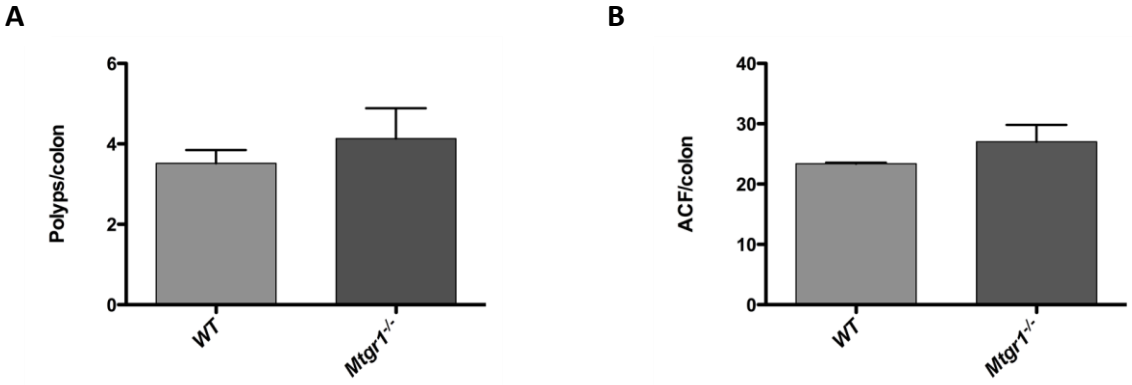

Figure 5.4 AOM-only experiments demonstrate no difference in polyp burden or ACF. A) mice treated with AOM and aged for 48 weeks had similar polyp and B) ACF burdens.

injury, either due to DSS itself or to inflammatory infiltration was required for the different AOM/DSS phenotype in *Mtgr1*$^{-/-}$ versus WT mice. Collectively, these experiments suggest that MTGR1 could protect early tumor progenitor cells from clearance after enterocyte injury.

Altered intratumoral apoptosis in the absence of MTGR1.

Variations in proliferation or apoptosis may account for the difference in tumor burden between *Mtgr1*$^{-/-}$ and WT mice. Intra-tumoral apoptosis rates were assessed using

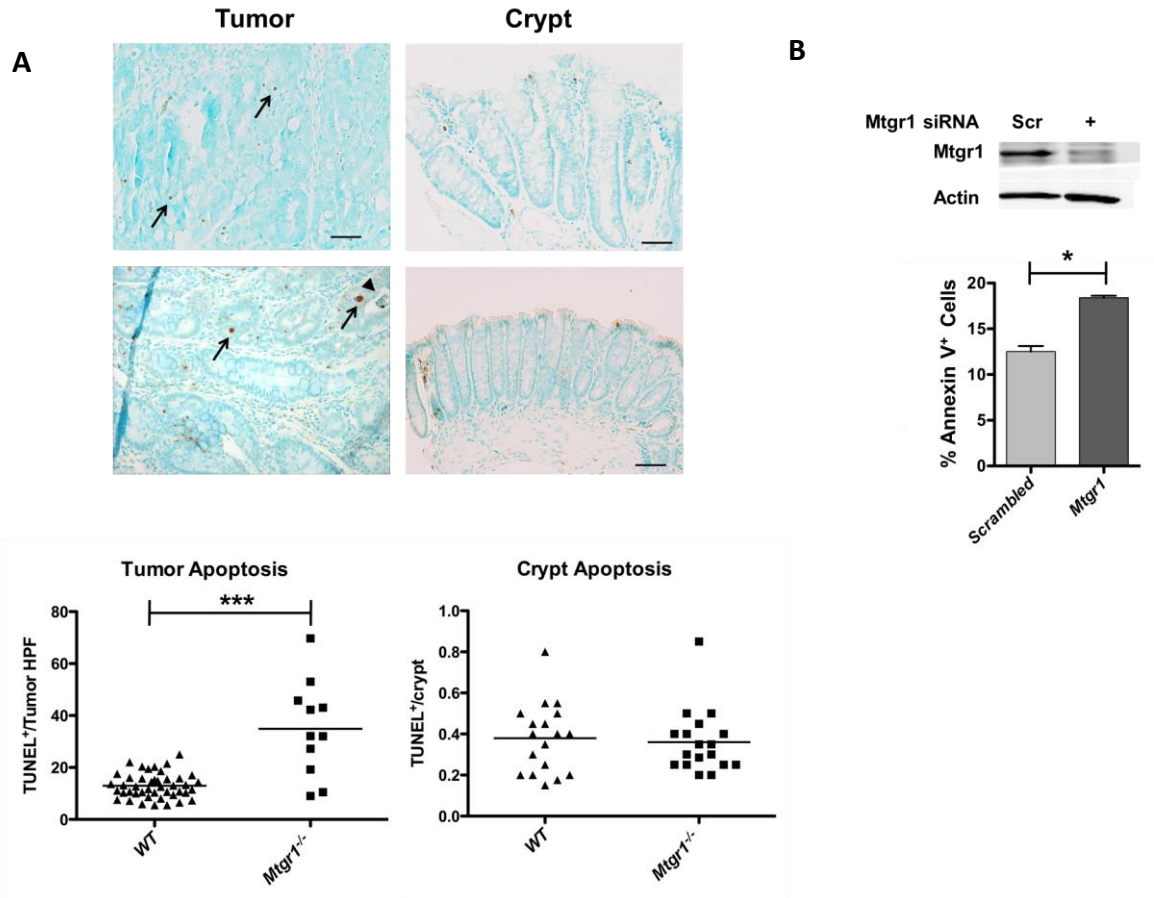

Figure 5.5 Mtgr1$^{-/-}$ *polyps demonstrate increased apoptosis. Colons were isolated from mice after completion of the AOM/DSS protocol. A) apoptosis was measured via TUNEL staining of Swiss rolled colons from all tumor bearing mice. Mtrg1*$^{-/-}$ *polyps, on average, have higher apoptotic cell counts than WT polyps (***P<0.001) but there is no difference in apoptosis within crypts. B) siRNA knockdown of Mtgr1 in the colon carcinoma line, HCT116, resulted in increased apoptosis compared to scrambled siRNA control (*P<0.05). Error bar represents the standard deviation for three biological replicates.*

in situ TUNEL staining. *Mtgr1*$^{-/-}$ mice demonstrated an average of 32.0 ±5.1 TUNEL^{+} cells/tumor high-power field (HPF). WT mice, on the other hand, displayed 12.9 ±0.9 TUNEL^{+} cells/tumor HPF (*P*<0.001, Fig. 5.5A), while no differences were seen in apoptotic

indices within crypts. To investigate whether there is a direct link between loss of MTGR1 and induction of apoptosis, we utilized a cell culture model using the human colon cancer cell line HCT116. Knockdown of MTGR1 by siRNA resulted in increased apoptosis as measured by annexin V and propidium iodide (PI) flow cytometry (Fig. 5.5B), but no change in proliferation (data not shown).

Next, to analyze proliferation rates, BrdU immunohistochemistry (IHC) was performed. BrdU positive cells/crypt were counted and averaged. As observed previously (226), non-tumorigenic *Mtgr1*$^{-/-}$ colonic epithelium showed a modest increase in proliferation compared to WT mice. However, intra-tumoral proliferation rates were similar between WT and *Mtgr1*$^{-/-}$ mice, suggesting that the difference in tumor formation and/or size was not a function of differences in epithelial proliferation rates between WT and *Mtgr1*$^{-/-}$ animals, but more likely due to differences in intratumoral apoptosis.

Decreased nuclear and total β-catenin in Mtgr1$^{-/-}$ *tumors.*

All three MTG family members (MTGR1, MTG16, and MTG8) are capable of competing with β-catenin for TCF4 occupancy and can repress TCF4 mediated transcriptional activity (209). Based on this observation, we stained WT or *Mtgr1*$^{-/-}$ tumors with a β-catenin specific antibody to determine the levels of β-catenin expression and its localization. We derived a β-catenin staining index, which incorporates the intensity of staining and percentage of nuclear β-catenin^{+} cells/HPF. We found uniformly high nuclear and cytoplasmic staining in the WT tumors (252.4 ±24.9, Fig. 5.6A, B). However, the

Mtgr1$^{-/-}$ tumors contained lower levels of nuclear β-catenin and there was a more heterogeneous staining pattern within the tumor (101.2 ±23.6, Fig. 5.6A, B).

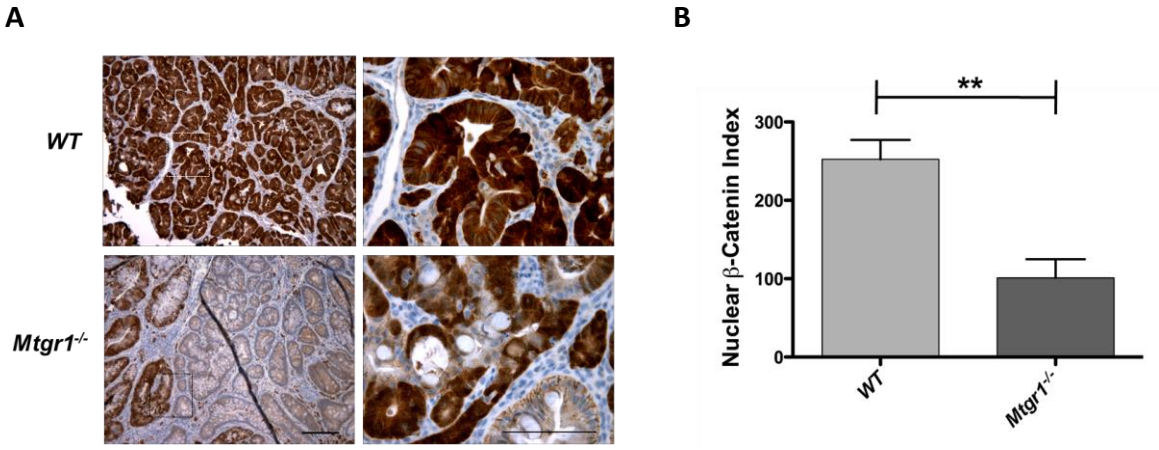

Figure 5.6 Decreased expression and heterogeneous distribution of nuclear β-catenin in Mtgr1$^{-/-}$ *tumors. β-catenin expression and localization was determined via immunohistochemistry with β-catenin as per Methods section. A) representative staining for β-catenin from WT or Mtgr1*$^{-/-}$ *tumors, B) β-catenin index (Percentage of tumor with nuclear β-catenin x expression intensity, (N=10 mice, each genotype) **P<0.01). Error bar represents the standard deviation and scale bar is 5 μm.*

Transcriptional network alterations in Mtgr1$^{-/-}$ *tumors.*

To address the mechanism by which MTGR1 might act during tumorigenesis, RNA was isolated from WT and *Mtgr1*$^{-/-}$ tumors and hybridized to Affymetrix Mouse Gene 1.0 ST arrays. After data normalization, expression profiles were uploaded to the PANTHER platform (313). Significant decreases in both Wnt (*P*=.001) and Cadherin (*P*=.0001) pathways in the *Mtgr1*$^{-/-}$ tumors was evident with the most significant reductions in the

Gene	Fold decrease in *Mtgr1*$^{-/-}$
Pnliprp1	-30x
Pnliprp2	-20x
Wif1	-17.9x
Dkk2	-7.6x
Lgr5	-8.9x
Axin2	-3.8x
Defensins (2,5,20,22,23)	-3.5x→-10x
Mmps (7,12,13,14)	-3.3x→-6.9x

Gene	Fold increase in *Mtgr1*$^{-/-}$
Cyp2c55	6x
Car4	4.8x
Hao3	4.7x
Slc26a3	3.8x
Aqp8	3.4x

Table 5.1 Differential expression of genes in Mtgr1$^{-/-}$ tumors. Tumors were developed according to the Murine Inflammatory Carcinogenesis Protocol and dissected from WT and Mtgr1$^{-/-}$ mice. Isolated RNA was hybridized to the Mouse gene 1.0 ST arrays and CEL files were imported into Partek for differential expression of genes. Among other genes,
Mmp7 was shown to be downregulated in Mtgr1$^{-/-}$ tumors.

Wnt target *Lgr5* (-8.95 fold), consistent with decreased Wnt signaling tone in the *Mtgr1*$^{-/-}$ tumors. Paradoxically, repressors of Wnt signaling (*Wif1* -17.9x, *Dkk2* -7.6x and *Axin2* -3.8x, Table 5.1) were also down-regulated. Levels of expression of the matrix metalloproteinases (*Mmp-7* 6.8x, *Mmp-13* 3.9x, *Mmp-12* 3.5x, and *Mmp-14* 3.4x) were also decreased in *Mtgr1*$^{-/-}$ tumors (Table 5.1). MMP7 is a known target gene of the Wnt pathway (244) and its overexpression has been associated with colon cancer (406). We therefore assessed MMP7 at the protein level by immunofluorescence, and observed not only decreased expression but also decreased secretion of MMP7 from colonic polyps in

the *Mtgr1*$^{-/-}$ versus WT mice (Fig. 5.7A, B). These findings suggest that decreases in WNT signaling and MMP expression may contribute to decreased tumor size in *Mtgr1*$^{-/-}$ mice.

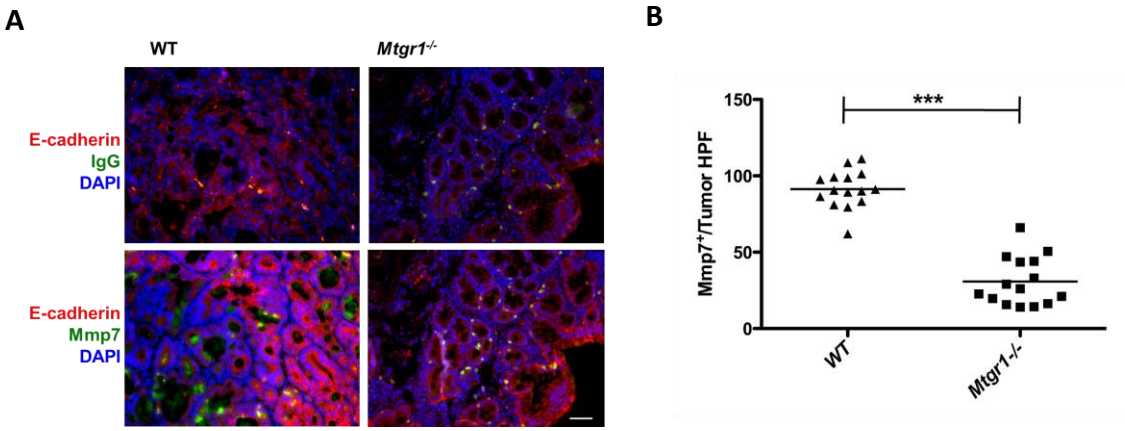

Figure 5.7 Decreased expression and secretion of Mmp7. A) immunofluorescence for Mmp7 demonstrated a decrease in Mmp7 production and secretion. E-cadherin, a downstream target of Mmp7 is shown in red. B) Mmp7^{+} *cells were counted per 40x HPF in tumors from WT and Mtgr1*$^{-/-}$ *mice (***P<0.001). Scale bar is 5 μm.*

Immune pathways are upregulated in Mtgr1$^{-/-}$ *tumors.*

PANTHER analysis of the changes in gene expression also revealed increased MHC-I (*P*=.001), MHC-II (*P*=.003), T-cell (*P*=6.8x10^{-11}), and B-cell mediated immunity pathways (*P*=.007), indicating that these gene classes are overrepresented in the *Mtgr1*$^{-/-}$ tumors (Table 5.2). To both confirm and extend these observations we performed immunohistochemistry on WT and *Mtgr1*$^{-/-}$ tumors to classify intratumoral inflammation. In *Mtgr1*$^{-/-}$ vs WT tumors (Fig. 5.8A, B), there were increased CD3^{+} T-lymphocytes (13.6 ±2.5/tumor HPF vs 49.4 ±5.6, *P* <0.001), B220/CD45r^{+} B-lymphocytes (15.8 ±2.3 vs 6.0 ±0.8/tumor HPF, *P* <0.001), and NKp46^{+} natural killer cells (51.0 ±3.7 vs 36.0 ±3.1/tumor HPF, *P*=0.004). Because *Mtgr1*$^{-/-}$ tumors were smaller than WT tumors and mononuclear phagocytes can exert anti-tumor activity by directly killing tumor cells and eliciting tissue

disruptive reactions (407), we used F4/80 and IL-1β co-staining and observed increased M1 macrophages in *Mtgr1*$^{-/-}$ tumors (29.1 ±3.0 positive cells/tumor HPF vs 11.6 ±1.6,

Panther Biologic Processes

(*Mtgr1*$^{-/-}$ relative to WT)

Increased

	Biological Function	p-value
Immunity subset	**B-cell and antibody-mediated immunity**	**$6.8x10^{-3}$**
	MHCII mediated immunity	**$3.5x10^{-3}$**
	MHCI mediated immunity	**$1.8x10^{-3}$**
	T-cell mediated immunity	**$6.9x10^{-11}$**
	Immunity and defense	**$1.4x10^{-6}$**
	Oxidative phosphorylation	$9.2x10^{-10}$
	Transport	$1.6x10^{-8}$
	Cation transport	$6.1x10^{-8}$
	Electron transport	$6.8x10^{-8}$
	Ion transport	$1.8x10^{-7}$
	Carbohydrate metabolism	$7.3x10^{-6}$
	Lipid, fatty acid and steroid metabolism	$6.2x10^{-5}$
	Muscle development	$3.6x10^{-4}$
	Muscle contraction	$4.7x10^{-4}$
	Neuronal activities	$1.1x10^{-3}$
	Blood circulation and gas exchange	$1.8x10^{-2}$
	Phosphate metabolism	$7.0x10^{-2}$
	Other receptor mediated signaling pathway	$9.2x10^{-2}$
	Fatty acid metabolism	$1.1x10^{-1}$
	Homeostasis	$1.2x10^{-1}$
	Regulation of vasoconstriction, dilation	$1.3x10^{-1}$
	Steroid hormone-mediated signaling	$1.6x10^{-1}$
	Carbohydrate transport	$2.0x10^{-1}$
	Synaptic transmission	$2.9x10^{-1}$
	Extracellular transport and import	$3.8x10^{-1}$
	Amino acid metabolism	$6.8x10^{-1}$
	Other neuronal activity	$8.3x10^{-1}$
	Other homeostasis activities	$8.7x10^{-1}$
	Other immune and defense	$9.7x10^{-1}$

Decreased

Biological Function	p-value
Pre-mRNA processing	$4.2x10^{-13}$
Nucleotide and nucleic acid metabolism	$9.9x10^{-10}$
mRNA splicing	$4.2x10^{-10}$
Pheromone response	$1.9x10^{-4}$
Nuclear transport	$3.8x10^{-4}$
mRNA transcription initiation	$8.4x10^{-4}$
rRNA metabolism	$9.0x10^{-4}$
Protein metabolism and modification	$1.0x10^{-3}$
Intracellular protein traffic	$1.8x10^{-3}$
Protein folding	$3.6x10^{-3}$
Cell cycle	$4.2x10^{-3}$
tRNA metabolism	$7.9x10^{-3}$
DNA metabolism	$8.6x10^{-3}$
DNA replication	$5.3x10^{-2}$
Proteolysis	$6.2x10^{-2}$
General mRNA transcription activities	$1.9x10^{-1}$
Protein targeting and localization	$1.9x10^{-1}$
DNA repair	$2.1x10^{-1}$
Stress response	$4.9x10^{-1}$
Mitosis	$5.0x10^{-1}$
RNA localization	$7.5x10^{-1}$

Table 5.2 Mtgr1$^{-/-}$ *tumors have increased adaptive and innate immunologic transcriptional networks. Post-normalized expression data was analyzed via PANTHER to map biologic process categories. Significant increases in B-, T-cell, MHCII and MHCI were identified in Mtgr1*$^{-/-}$ *tumors.*

P<0.001). Because M2 macrophages are generally considered pro-tumorigenic (407), we anticipated that co-staining with F4/80 and ARG1 would identify fewer M2 mononuclear cells in the *Mtgr1*$^{-/-}$ tumors. We were surprised to find increased M2 cells in the *Mtgr1*$^{-/-}$ tumors (15.8 ±2.6 positive cells/tumor HPF vs 7.2 ±1.3, *P*=0.003, Fig. 5.8A, B).

In situ hybridization indicated that *Mtgr1* was mainly expressed within the epithelium of developing AOM/DSS induced tumors (Fig. 5.1C). However, MTGR1 is present in many tissue types, including hematopoietic lineages (198). Given the dramatic

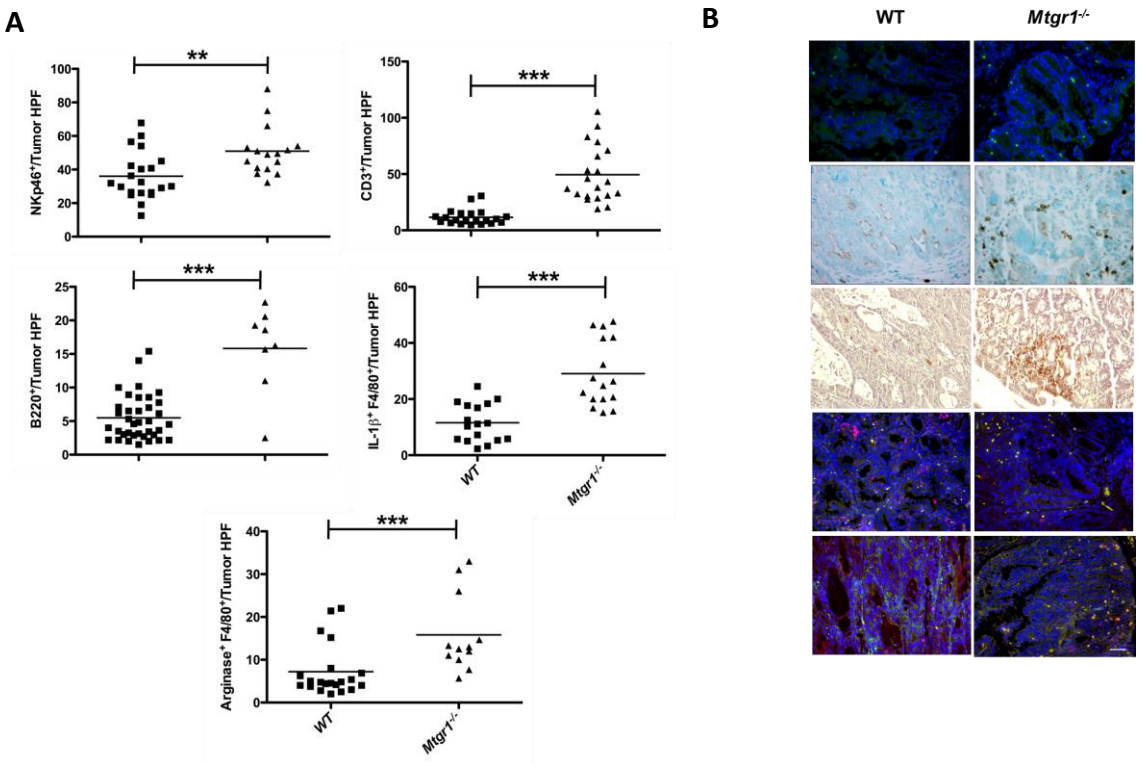

*Figure 5.8 Mtgr1$^{-/-}$ tumors have increased immune infiltration. A & B) WT or Mtgr1$^{-/-}$ tumors were stained with αNKp46(green), αCD3, αB220, αF4/80 (red), αIL-1β (green), and αARG1 (green) antibodies and positive cells/tumor HPF were counted showing increased immune infiltrate in Mtgr1$^{-/-}$ tumors in comparison to WT tumors (***P<0.001, **P<0.01). Scale bar is 5 μm.*

changes in inflammatory cell infiltration in the tumors, MTGR1 could be acting in a hematopoietic cell autonomous fashion to repress immune infiltration, or alternatively, MTGR1 could be acting in the stromal or epithelial compartment to repress immune cell recruitment. To test whether the MTGR1 effect is hematopoietic cell autonomous, we restored MTGR1 expression in hematopoietic cells in the *Mtgr1$^{-/-}$* mouse via bone marrow transplantation of WT marrow. In addition, WT mice were transplanted with *Mtgr1$^{-/-}$*

marrow and control transplants consisting of WT or *Mtgr1*$^{-/-}$ mice transplanted with WT or *Mtgr1*$^{-/-}$ marrow, respectively, were also performed (Fig. 5.9A, B). Non-transplanted controls did not survive two weeks post irradiation, indicating that the endogenous marrow was ablated. Transplanted animals were allowed to recover for three months prior to placing the animals on the AOM/DSS protocol.

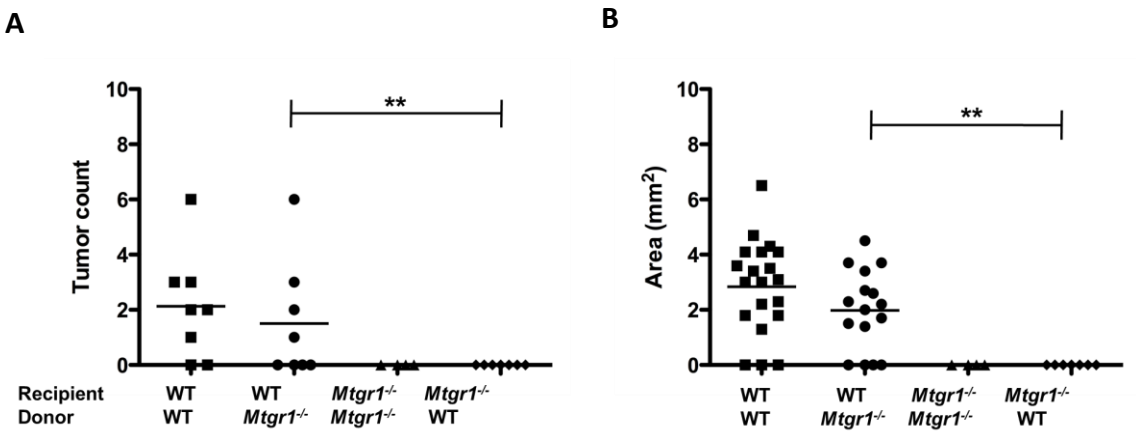

Figure 5.9 Autologous transfer of Mtgr1$^{+/+}$ *marrow does not reverse the Mtgr1*$^{-/-}$ *AOM/DSS phenotype. Bone marrow transplants were performed on WT and Mtgr1*$^{-/-}$ *mice as indicated. A) wild type mice given Mtgr1*$^{-/-}$ *bone marrow have more polyps per colon than Mtgr1*$^{-/-}$ *mice given WT bone marrow (**P<0.01). B) colonic polyps are larger in WT mice rescued with Mtgr1*$^{-/-}$ *bone marrow than in Mtgr1*$^{-/-}$ *mice rescued with WT marrow.*

WT mice rescued with either WT or *Mtgr1*$^{-/-}$ bone marrow had equivalent tumor burden (2.125 ± 0.693 and 1.5 ± 0.756, polyps/mouse, respectively). No tumors were observed in either of the *Mtgr1*$^{-/-}$ recipient groups. This indicates, at least in this model, that it is the absence of MTGR1 in non-hematopoietic cellular compartments that protects from AOM/DSS-induced tumorigenesis. This data coupled with increased epithelial apoptosis in the HCT-116 cells suggests that MTGR1 promotes tumorigenesis through its actions in the epithelium.

Discussion

Myeloid Translocation Genes (MTGs) are transcriptional co-repressors that were first identified in AML where the prototypic event is the 8:21 translocation (408). Considerable information has been gained from the creation of constitutional null alleles for each MTG family member. *Mtgr1*$^{-/-}$ mice have increased enterocyte proliferation, mainly localized to the lower 1/3 of the crypt, as well as the progressive depletion of the secretory lineage in the small intestine (217). The presence of MTGR1 is required for maintenance of epithelial integrity after DSS-mediated injury and chronic architectural changes occur after a solitary DSS-mediated injury (226).

In this report, we demonstrate that MTGR1 is required for efficient inflammatory-associated colonic carcinogenesis. AOM is a procarcinogen and is metabolically activated to a potent alkylating agent forming O^6-methyl-guanine (318). Its oncogenic potential is markedly augmented in the setting of chronic inflammation, such as that induced by repeated cycles of DSS treatment (319). The power of this model has recently been demonstrated in deciphering the epithelial versus myeloid cell contribution of IKKβ to polyp formation in the setting of inflammation (265), and the contributions of IL-6 and its downstream mediator, STAT-3 (33). IL-6 and MTGR1 are required for maintenance of mucosal integrity after injury (226), (33). Both *Mtgr1*$^{-/-}$ and *IL-6*$^{-/-}$ mice are protected from tumorigenesis in the AOM/DSS model. In the case of the *Mtgr1*$^{-/-}$ mice, higher levels of intra-tumoral apoptosis, with no appreciable difference in proliferation, may mediate the beneficial affect of MTGR1 deletion. Injury is required for the *Mtgr1*$^{-/-}$ protective effect, as there was no difference in tumor burden when mice were injected with AOM without

subsequent cycles of DSS. This suggests that MTGR1, similar to IL-6, protects initiated epithelial cells from apoptosis. In the case of IL-6, this is mediated via its production by lamina propria myeloid cells, and our data indicates that hematopoetic MTGR1 production does not modify tumorigenesis.

Alteration in Wnt signaling is a common initiating event in sporadic CRC (25); however, it is less common in colitis-associated carcinoma (CAC), and when it does occur, it typically does so as a late event (409). We were surprised to find evidence of low Wnt signaling in *Mtgr1*$^{-/-}$ tumors as it has previously been shown that MTGs bind to TCF4 and compete with β-catenin for occupancy; thus, at least in certain circumstances, antagonizing WNT transduced signals (209). One potential explanation for this apparent paradox is that MTGs are known to function as transcriptional co-repressors via diverse interactions with multiple transcription factors (i.e. PLZF, BCL6, GFI-1) in addition to TCF4. They also form bridging interactions with other transcriptional co-repressors such as N-CoR, SMRT, mSin3A and HDACs 1, 2, and 3 (176, 178, 187). Our results suggest that the effect of MTGR1 on WNT signaling may be less important than its ability to inhibit apoptosis via modulating other pathways.

Our data suggests that loss of MTGR1 shifts the inflammatory response towards an anti-tumorigenic state by increasing expression of tumoricidal immune cells such as natural killer cells and M1 macrophage subsets. Perplexingly, there is also a concomitant increase in "pro-tumorigenic" M2 polarized macrophages. It is theorized that there is a balance between M1 (anti-tumorigenic) and M2 (pro-tumorigenic) within the tumor microenvironment and it is proposed that this balance could have different net effects at

different stages of tumor progression (407). As the overall observed effect in the absence of MTGR1 was smaller and fewer tumors this observation suggests that MTGR1 could influence the balance between anti- and pro- tumorigenic macrophage function. Furthermore, the fact that WT marrow transplanted into *Mtgr1*$^{-/-}$ mice failed to prevent the reduction in tumorigenesis in the *Mtgr1*$^{-/-}$ AOM/DSS phenotype indicates that this process is not acting in a hematopoietic cell autonomous manner in this tumor model. This raises the possibility that MTGR1 suppresses inflammatory recruitment, perhaps via regulating production of epithelial derived chemokines and cytokines.

We observed decreased *Mmp-7* (Matrilysin), *-12*, *-13*, and *-14* in *Mtgr1*$^{-/-}$ tumors. These matrix metalloproteinases are overexpressed in human colorectal carcinomas with increased *Mmp7* observed early in malignant progression and in 85% of surveyed tumors (410). *Mmp7*$^{-/-}$ mice bred with *Apc*$^{Min/+}$ mice have a 50% decrease in polyposis (406, 411). MMP7 has pleiotropic effects promoting cancer progression via its proteolytic activity against the ectodomain of a number of cell surface proteins. For example, MMP7 cleavage of CD45 makes tumor cells resistant to apoptosis (412, 413), MMP7 mediated cleavage of proHB-EGF into mature HB-EGD promotes proliferation and angiogenesis (414), and E-cadherin is cleaved to soluble E-cadherin, promoting invasion (415). The tumor promoting effects of increased MMP expression could contribute to tumor growth differences and raises the intriguing possibility that MMPs may be important targets of MTGR1-mediated repression.

In conclusion, we demonstrate that removal of MTGR1 enhances inflammation, increases intra-tumoral apoptosis, and reduces production of proteins such as MMPs

known to be pivotal to tumor growth. Thus, MTGR1 appears to influence the tumor microenvironment and in addition to its effects on initiated cell survival may also suppress tumor immunosurvelliance. These studies provide insight into disease pathogenesis and implicate MTGR1 dysfunction in colitis-associated carcinoma and sporadic colorectal carcinoma, thus providing the substrate for translational investigations of MTGR1 in colitis-associated carcinoma.

Acknowledgements

This work was supported by NIH Grant K08 DK080221-01 (CSW), CA64140 (SWH), CA112005 (SWH) and HL088494 (SWH), NIH P50CA095103 (MKW), AT004821 (KTW), AT004821-S1 (KTW), a Merit Review Grant (KTW), P30DK058404, ACS-RSG 116552 (CSW). We thank Drs. Richard Peek, Robert Coffey, Baolin Zhang for thoughtful discussions regarding this research project. We also thank Frank Revetta for histologic support.

CHAPTER VI

KAISO DIRECTS THE TRANSCRIPTIONAL COREPRESSOR MTG16 TO THE KAISO BINDING SITE IN TARGET PROMOTERS[4]

Introduction

The myeloid translocation gene proteins (MTGs) are transcriptional corepressors, lacking both enzymatic and DNA-binding activities, that act as scaffolding proteins upon which other transcriptional corepressors (mSin3a, N-CoR, SMRT), histone deacetylases (HDACs), and transcription factors assemble (178, 190). Their modular nature permits contributions to multiple promoter-specific repressor complexes, making them master regulators of gene expression. MTG8 and MTG16 (CBFA2T3) were originally identified as targets of chromosomal translocations in acute myeloid leukemia (178, 190), suggesting an important role in cellular growth and development. MTG family proteins have since been implicated in the development of colon and breast cancers as well (227-229, 269). Because MTG repressive capabilities are dictated via protein-protein interactions with transcription factors and other co-repressors it is imperative to identify MTG-interacting proteins and understand their functions and specificities in the context of tumorigenesis. Zinc fingers, C_2H_2 and BTB domain containing (ZBTB) family members bind methylated or unmethylated DNA in a sequence-specific manner and repress target genes (416). A ZBTB

[4] This work has been published under Caitlyn W. Barrett, J. Joshua Smith, Lauren C. Lu, Nicholas Markham, Kristy R. Stengel, Sarah P. Short, Baolin Zhang, Aubrey A. Hunt, Barbara M. Fingleton, Robert H. Carnahan, Michael E. Engel, Xi Chen, R. Daniel Beauchamp, Keith T. Wilson, Scott W. Hiebert, Albert B. Reynolds, Christopher S. Williams (2012) Kaiso directs the transcriptional corepressor MTG16 to the Kaiso binding site in target promoters, *PLoS One*, 7, e51205 (12).

family member that has recently been studied in detail for its ability to modulate colorectal cancer, Kaiso (ZBTB33), utilizes all three zinc fingers for high affinity binding to DNA targets (417). All ZBTB family members likely share this method of DNA binding, as homology exists within their zinc finger motifs. Kaiso, like MTGs, forms repression complexes that include N-CoR and HDACs (190, 233) and plays a pivotal role in the repression of tumor suppression genes such as *CDKN2A* in colon cancer cell lines (247). Kaiso also represses matrix metalloproteinase gene *MMP*7 expression (241) in addition to canonical and non-canonical Wnt targets (418-420). Moreover, Kaiso expression is a prognostic indicator in non-small cell lung cancer (420) and its deletion suppresses intestinal tumorigenesis in mice (251). ZBTB4 also modulates the cellular responses to p53 activation (248) and is downregulated in breast cancer (421). Collectively, these data suggest ZBTB proteins, and Kaiso specifically, have multidimensional roles in cancer development.

Like the ZBTB family of transcription factors, the MTG family of transcriptional corepressors has disparate roles in cancer development. For example, MTGs associate with TCF4 to repress Wnt signaling (209) and mutations in both MTG8 and MTG16 were found in colon and breast cancer (228, 229). *Mtgr1* is required for tumorigenesis in a murine model of inflammatory carcinogenesis (269), and MTG16 has been identified as a putative tumor suppressor in human breast cancer (227). Given that ZBTB16 (also known as PLZF) and BCL6 (ZBTB27) associate with MTG8 (192, 199) and that Kaiso and MTG16 have similar influences in cancer development, we tested for a wider structure-function

relationship between the ZBTB and MTG families, which could provide insights into their roles in tumorigenesis.

Here, we identified the association of Kaiso, ZBTB4, and ZBTB38 with MTG16 in yeast two-hybrid assays, which suggests a direct physical interaction between these factors. The Kaiso-MTG16 complex specifically binds to Kaiso's established binding site (KBS) on DNA and enhances repression of a KBS-containing reporter and the Kaiso target, *MMP7* promoter. However, MTG family members did not influence methylation-based repression by Kaiso. These data suggest that Kaiso-MTG16 dependent transcriptional repression requires the interaction of this complex on the KBS. Moreover, the impact of MTG16 on repression of Kaiso target promoters depends on Kaiso DNA binding. Analysis of publicly available ChIP-seq datasets showed that MTG family members bind Kaiso-targeted promoters over 70% of the time, implicating this interaction in the regulation of over 100 genes. Lastly we examined a large multi-stage CRC expression array dataset and discovered an inverse relationship between *Kaiso* and *MTG16* expression and consistently elevated *MMP7* expression at all stages of tumorigenesis supporting the hypothesis that loss of either Kaiso or MTG16 de-regulates *MMP7* expression.

Materials and Methods

Yeast Two-Hybrid. ZBTB4 and *ZBTB38* prey and *MTG16* bait plasmids were obtained from Hybrigenics. pDONR201-*Kaiso* (clone ID: HsCD00082434, The ORFeome Collaboration) and pDONR221-*MTG16* (clone ID: HsCD00079915, HIP) plasmids were obtained from Harvard PlasmID and pGAD-GW and pGBT9-GW vectors were provided by ABR. Kaiso and

MTG16 were inserted into the pGAD-GW and pGBT9-GW plasmids using the Gateway Cloning procedure (422). In short, 150ng of entry vector (*Kaiso* or *MTG16*) was mixed with 150ng of destination vector (pGAD or pGBT9) and the volume was brought to 8µl with TE. 2µl of LR Clonase II enzyme mix (Invitrogen) was added and the reaction was incubated for 1 hour at 25°C. 1µl Proteinase K was then added to each sample and incubated at 37°C for 10 minutes. Kaiso was then truncated to include amino acids 298-573 by Agilent Quickchange II site-directed mutagenesis (Agilent) according to the manufacturer's protocol. The MTG16 constructs shown in Figure 1 were also developed using the Quickchange II site-directed mutagenesis kit. For the yeast two-hybrid, yeast at OD_{600} were transformed via the PEG-LiAc-TE method using a 42°C heat shock. Yeast at an OD_{600} of 0.6 were centrifuged at 3000 rpm for 5 minutes and resuspended in 10ml of LiAc-TE, centrifuged and resuspended in 1ml of LiAc-TE. Transformations were set up using 50ug of carrier DNA (sheared salmon sperm DNA, Ambion), 1ug of DNA for each construct (pGAD and pGBT9) and 100ul of competent yeast. 0.7ml of sterile 40%PEG-LiAc-TE was added and yeast were allowed to recover at 30°C for 30 minutes and then heat shocked at 42°C for 15 minutes. Cells were then washed with sterile TE and the reactions were plated on double-dropout selective media plates (-leu, -trp) and grown at 30°C for three days. Colonies were then plated on either triple- (for the Hybrigenics system) or quadruple-dropout (for the pGAD/pGBT9 system, -leu, -trp, -his, -ala) plates. Empty vector bait was used as a negative control.

Immunofluorescence and Colocalization. K562 human leukemia cells (ATCC CCL-243) were plated on poly-l-lysine (Sigma-Aldrich) coated cover slips and allowed to adhere for 30

minutes at room temperature. Cells were fixed with ice-cold 2% paraformaldehyde, pH7.4 for 10 minutes. After three washes, cells were blocked with 1% BSA and then stained with MTG16 antibody (1:1000 333, supplied by MEE) and a polyclonal Kaiso antibody (1:1000 supplied by ABR) overnight at 4°C. Cells were washed then stained with anti-rabbit-Cy3 and anti-mouse-FITC for 1 hour at room temperature and mounted using ProLong Gold antifade mounting medium with DAPI (Invitrogen). Slides were visualized using Deltavision software (Stress Photonics, Madison, WI) supplied by the Epithelial Biology Core (Vanderbilt).

Cell Culture. Human colon cancer cell lines HCT116 (ATCC CCL-247) and HT29 (ATCC HTB-38) were maintained in McCoy's 5A media supplemented with fetal bovine serum (FBS) and pen/strep (P/S). HCT116 cells were transfected with Lipofectamine LTX and Plus reagent (Invitrogen) and HT29 cells were transfected with Fugene HD (Promega) according to manufacturer's protocol. K562 cells were maintained in DMEM supplemented with FBS and P/S.

Coimmunoprecipitation. HCT116 cells were transfected with Kaiso and each of the Gal- or Myc-tagged MTG family members (provided by Mike Engel) using Lipofectamine LTX and Plus reagent (Invitrogen) according to manufacturer's protocol. 48 hours post-transfection, cells were lysed with coimmunoprecipitation buffer (0.5% Triton-X 100, 0.1% DOC, 0.1% SDS, and protease inhibitors in PBS), clarified by centrifugation, and pre-cleared with protein A/G agarose beads for 1 hour at 4°C. 2ug of either anti-Gal (Santa-Cruz, sc-510), anti-Myc (Santa-Cruz, sc-40) or anti-IgG (Cell Signaling, G3A1) control antibodies were then added to pre-cleared lysate and incubated overnight at 4°C with

rotation. Following removal of input, 40μl protein A/G agarose beads were added to each sample and incubated at 4°C for 1 hour with rotation. Western blotting for Kaiso (polyclonal Kaiso antibody supplied by ABR, 1:1000) was then performed.

Kaiso Knockdown. HEK293T packaging cells (ATCC CRL-11268) were transfected with Mission shRNA constructs (Sigma-Aldrich) specific for human Kaiso (clone ID: NM_006777.3-2600s1c1 and NM_006777.3-358s1c1) as well as the PAX2 and MDG2 plasmids using Superfect Transfection Reagent (Qiagen) according to the manufacturer's protocol. 24 hours post-transfection, media was removed from the HEK293T cells and passed through a 0.2 μM filter. 4μg/ml Polybrene (Millipore) was added to the filtered media. Growth medium was removed from HCT116 cells and replaced by infection medium. After 6 hours, the infection medium was replaced with normal growth medium and the infection process was repeated 24 hours later. Cells were selected for knockdown using 5μg/ml Puromycin (Invitrogen) over a 3-day period. Knockdown was analyzed by the delta-delta-CT method following RT-PCR using Kaiso-specific Taqman probes (Invitrogen) and by Western blotting using the polyclonal Kaiso antibody (1:1000, supplied by ABR).

Luciferase Reporter Assays. Kaiso and MTG family members were transiently expressed in HCT116 cells along with either the Kaiso binding site (4xKBS) reporter, which contains four consensus Kaiso binding sites and a luciferase reporter gene (gift from Juliet Daniel, McMaster University, Canada), or the mutant Kaiso binding site promoter which contains mutant forms of the KBS and a luciferase reporter gene (PGL3 control 4xKBSMT, gift from Juliet Daniel). A constitutive reporter plasmid expressing Renilla luciferase (pGL4 TK

hRluc) was included to normalize data generated from the Kaiso reporter constructs. Cell lysates were subjected to a dual-luciferase assay and presented as adjusted RLUs. For human *MMP7* (HMAT, gift from BMF) assays, Myc-tagged delta-MTG16 constructs (ME, Figure 1C) were co-transfected with activators PEA3, LEF1, C-JUN, and delta β-Catenin and the human *MMP7* promoter fused to the luciferase reporter gene (HMAT-2.3). Activation by enforced expression of PEA3, LEF1, C-JUN, and delta β-catenin was required to see repression by MTG family members because HCT116 cells express low levels of *MMP7* endogenously. *Mbd2*$^{-/-}$ cells (a gift from Pierre-Antoine Defossez) (232) were maintained in Advanced MEM supplemented with BCS and P/S and transfected with Superfect (Qiagen), according to manufacturer's protocol. For methylation-dependent studies, 5μg of pSV40Luc was methylated upon mixture of 1.5μl SAM, 30μl 10x NEB2, 1μl SssI methylase (New England Biolabs) and water to 300μl. The mixture was incubated at 37°C for 2 hours followed by addition of 1.5μl SAM and continued incubation for 1 hour. DNA was then purified using the Qiaquick PCR purification kit (Qiagen). *Mbd2*$^{-/-}$ cells (gift from Pierre-Antoine Defossez) were transfected with MTG family members and either methylated or unmethylated promoter according to previously published specifications (232). HMAT and KBS assays were performed as outlined in the Materials and Methods section in the main paper.

MMP7 Repression. HT29 cells were transfected with expression plasmids for Kaiso, an MTG family member, or a combination of the two. RNA was isolated using the Qiagen RNA Isolation Kit and cDNA was generated from 1 μg of total RNA using the iScript cDNA Synthesis Kit (BioRad). Taqman qPCR was performed using *MMP7*-specific probes

(Invitrogen), and expression was normalized to *GAPDH* (Invitrogen). Analysis was performed using the delta-delta Ct method. Transfected cells were also treated with Protein transport inhibitor containing Brefeldin A (BD GolgiPlug) for 3 hours before lysate was collected using RIPA buffer. Lysates were run on Western blots, probed with α-MMP7 (Santa-Cruz 1:1000) and α-β-actin (Sigma-Aldrich, 1:5000) as a loading control and developed using the Odyssey system.

Chromatin Immunoprecitation. HCT116 cells were fixed using 1% formaldehyde for 20 minutes at room temperature. Cells were then lysed and chromatin was sheared by sonication (4 watts, 10 seconds on, 1 minute off, on ice repeated ten times). Lysate was precleared with 20ul protein A/G agarose beads (Santa Cruz, sc-2003) and beads were blocked with 2ug sheared salmon sperm DNA (Ambion). Lysate was immunoprecipitated with either IgG (Cell Signaling, G3A1), polyclonal MTG16 (333, provided by MEE) or monoclonal MTG16 (2D1, provided by SWH) overnight at 4°C with rotation. Protein A/G agarose beads were then added for 1 hour at 4°C with rotation. Complexes were eluted and crosslinks reversed with NaCl at 65 degrees for 5 hours and DNA isolated using the Qiagen PCR purification kit. qRT-PCR was performed using Kaiso binding site-specific primers (241). Analysis was performed using the delta-delta Ct method.

Statistical Methods. Luciferase, ChIP, and expression analyses were analyzed using one-way ANOVA and a Newman-Keuls post-test in Graphpad Prism 5.0c, unless otherwise indicated.

Microarray experiments—human tissues and microarray platform. Representative sections of fresh tissue specimens were flash frozen in liquid nitrogen and stored at -80C

until RNA isolation. Quality assessment slides were obtained to verify the diagnosis of cancer or normal adjacent mucosa. Stage was assessed using American Joint Commission on Cancer guidelines for both cohorts of tumor samples. RNA for human tissue was purified using the RNeasy kit (Qiagen). Samples were hybridized to the Human Genome U133 Plus 2.0 GeneChip Expression Affymetrix array. The expression array data are deposited and the GEO accession number is GSE17538. Complete minimum information about a microarray experiment-compliant dataset for analysis are available (http://www.ncbi.nlm.nih.gov/geo/query/acc.cgi?acc=GSE17538).

Microarray Analysis and Statistics. Microarray data were normalized using the Robust MultiChip Averaging (RMA) algorithm as implemented in the Bioconductor package *Affy* as previously described (423-425). Wilcoxon Rank sum test was used to determine significance for the normal, adenoma and colorectal cancer comparisons. The gene expression data Spearman correlation coefficient was used to assess the association between *Kaiso* and *MTG16* (probes 214631_at and 208056_s_at respectively). We next compared the differential expression between normal samples and carcinoma samples for genes MTG16 and *MMP7* using a linear model with an interaction term. More specifically, our model included gene expression as the outcome variable, main effects group (normal, carcinoma) and gene (e.g., *Kaiso, MMP7*) as well as the group x gene interaction term. The significance of interaction term indicates that differential gene expression for normal vs. carcinoma is significantly different for the two genes. This test procedure was similarly applied to genes *Kaiso* versus *MMP7*.

Ethics Statement. The protocols and procedures for this study were approved by the Institutional Review Boards at University of Alabama-Birmingham Medical Center, Vanderbilt University Medical Center, Veterans Administration Hospital (Nashville, TN) and H. Lee Moffitt Cancer Center, and written informed consent was obtained from each subject per institutional protocol.

Results

ZBTB family members interact with MTG16.

In order to understand MTG16-mediated intracellular signaling we used yeast-two hybrid screening to identify MTG16 binding partners. This approach identified two members of a family of zinc-finger transcription factors that repress methylated and non-methylated DNA: ZBTB4 and ZBTB38. Another member of this family, Kaiso (ZBTB33), is of particular interest because, like MTG16, it has been previously linked to Wnt signaling and tumorigenesis in the gut (247, 251, 418). Kaiso was not identified in the initial yeast two-hybrid screen, likely due to limited expression in the murine brain library that was screened. However, the ZBTB4 and ZBTB38 clones that were identified consisted of the highly homologous zinc finger region shared by ZBTB family members (Fig. 6.1A) and suggested that Kaiso would likely be a third target for MTG16 binding. Directed yeast two-hybrid validation experiments demonstrated that ZBTB4, ZBTB38, and Kaiso each interact with MTG16 via a highly conserved zinc-finger domain (Fig. 6.1B) which is also required for ZBTB16 (PLZF) MTG16 interaction (192), but not with ZBTB27 (BCL6) which demonstrates MTG16 binding within the fourth zinc finger motif (199). Mapping of the

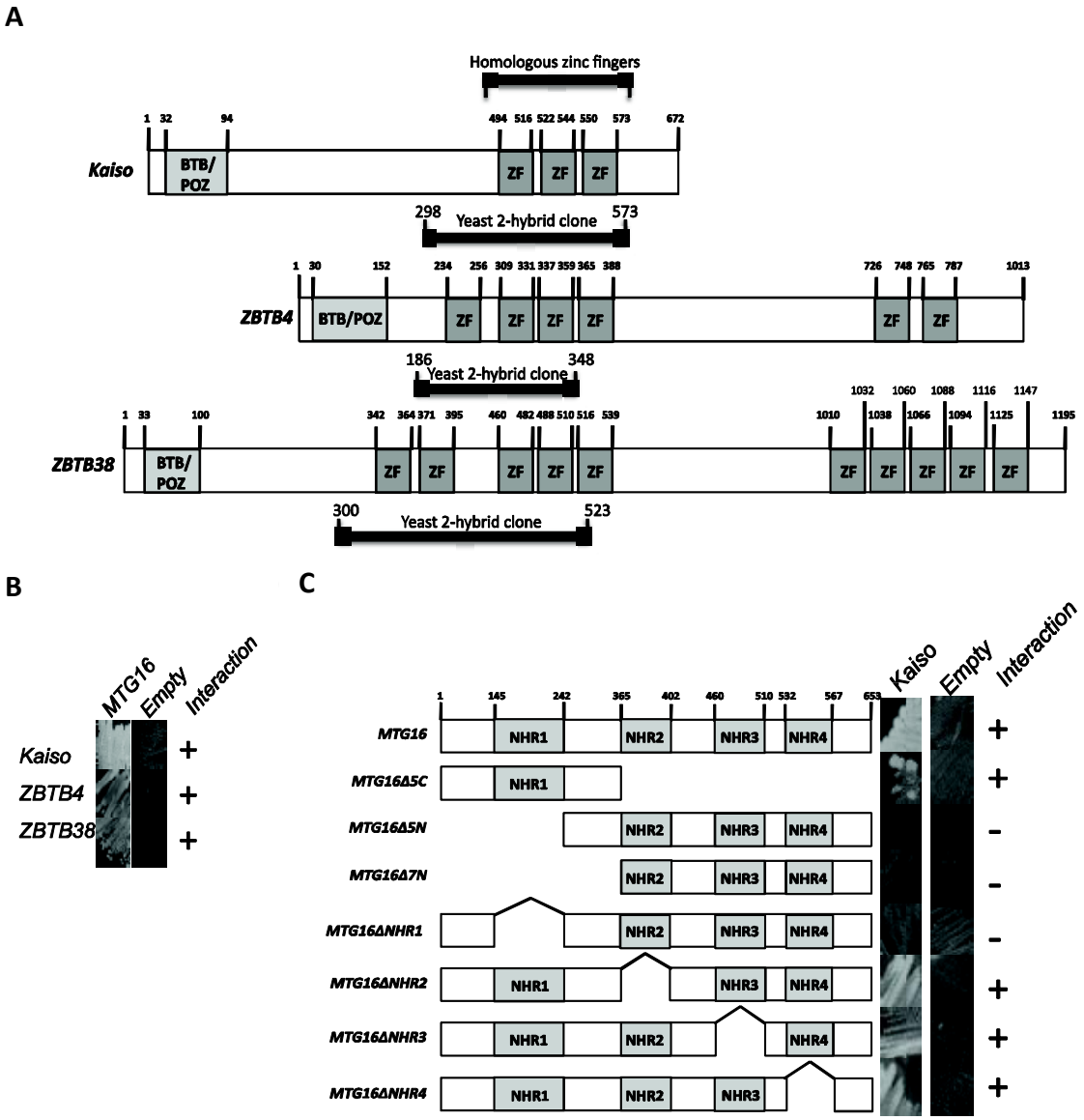

Figure 6.1 ZBTB family members interact with MTG16. A. ZBTB family member alignment based on homologous zinc fingers and identification of amino acids used in yeast-two hybrid experiments (yeast two-hybrid clones). B. Yeast-two hybrid assay for interactions between ZBTB family members and MTG16. C. Mapping of the Kaiso binding site on MTG16. Yeast two-hybrid assays were performed in triplicate.

MTG16 binding domain identified the nervy homology region 1 (NHR1) as the component of MTG16 that is required for binding to Kaiso as the three constructs lacking the NHR1 domain (Δ5N, Δ7N, and ΔNHR1) failed to demonstrate an interaction in the yeast two-hybrid assay (Fig. 6.1C).

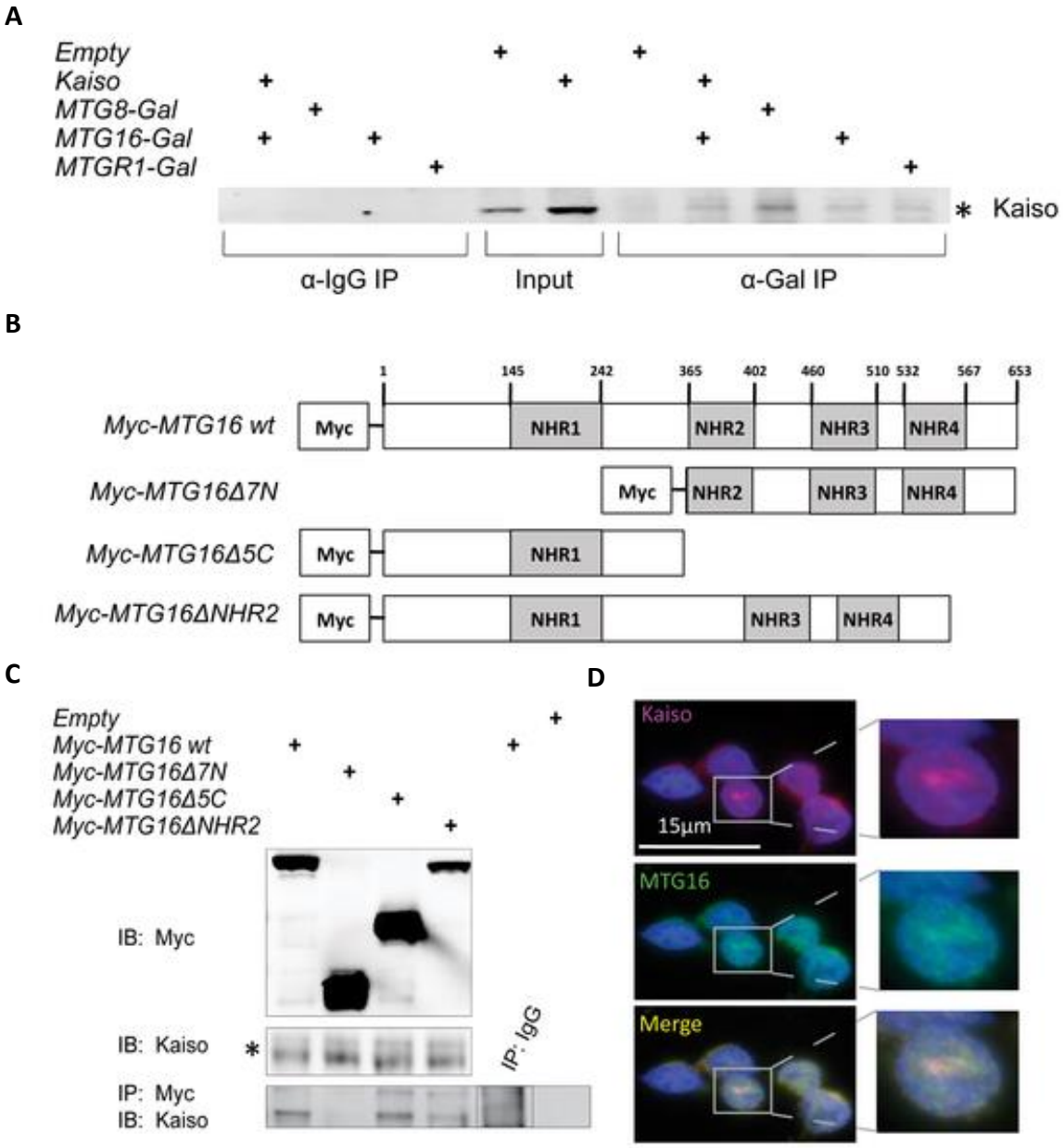

<u>Figure 6.2</u> Kaiso and MTG16 associate and co-localize. A. Immunoprecipitation of overexpressed Gal-tagged MTG family members in HCT116 cells. Cell lysates were fractionated and immunoprecipitated with anti-Gal or control IgG and analyzed by immunoblotting with Kaiso antibody. B. Myc-tagged MTG16 constructs used for immunoprecipitation mapping of MTG16 binding site. C. Immunoprecipitation of overexpressed Myc-tagged MTG family members in HCT116 cells. Cell lysates were fractionated and immunoprecipitated with anti-Myc or control IgG and analyzed by immunoblotting with Kaiso antibody. D. K562 cells costained for MTG16 (333, FITC) and Kaiso (polyclonal, ABR, Cy3) were imaged using the Deltavision system, and a correlation coefficient was determined for Kaiso and MTG16 colocalization (r=0.95±0.04, n=25 cells).

Using wild-type and selected mutant constructs for MTG16, we confirmed the Kaiso interaction in the HCT116 human colon cancer cell line which has endogenous Kaiso expression (Fig. 6.2A, r=0.95±0.04). We then mapped the binding interface to the N-terminus of MTG16 (Fig. 6.2B,C). We next used immunofluorescence to demonstrate endogenous co-localization of Kaiso and MTG16 in the K562 cells, a human leukemia cell line with high levels of expression of both proteins (Fig. 6.2D). Furthermore, *in silico* analysis of publicly available ChIP-seq data (UCSC Genome Browser, (426)) identified 101 promoters with intersecting Kaiso and MTG protein occupancy (Fig. 6.3A), providing further evidence that cooperativity between Kaiso and the MTG proteins may occur. Furthermore, three targets identified in the *in silico* ChIP-seq analysis, *ATF-2*, *ATF-7*, and *MAPK14* demonstrate altered expression in response to MTG16 overexpression. *ATF-2* and *MAPK14* are repressed by MTG16 (Fig. 6.3B, $P<0.0001$ *ATF-2* and $P=0.04$ *MAPK14*) while *ATF-7* expression is higher in response to MTG16 overexpression (Fig. 6.3C, $P<0.0001$). Though initially surprising, this result still points to a Kaiso and MTG16 complex binding the *ATF-7* promoter but suggests that either the proteins behave as activators, something Kaiso is capable of on this promoter, or that they are displacing another repressor complex that is a more potent repressor than the Kaiso-MTG16 complex. Collectively, these findings suggest a direct binding relationship between Kaiso and MTG16 with a shared impact in transcriptional control and tumorigenesis.

A

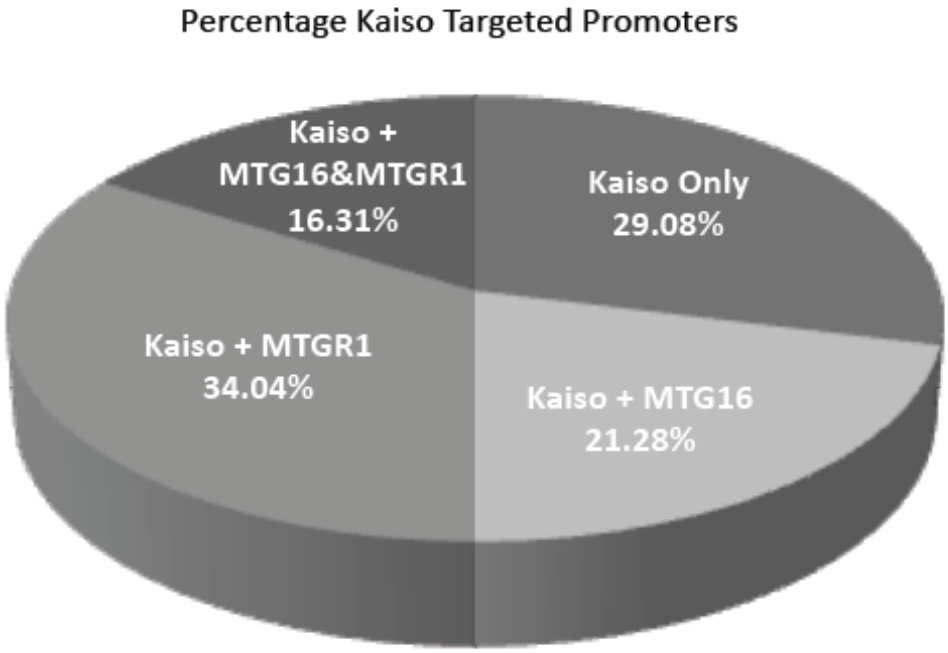

B

C

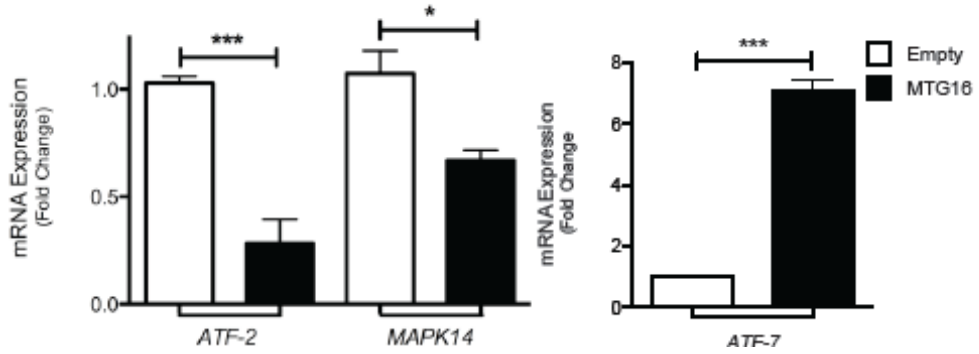

*Figure 6.3 Kaiso shares repression targets with MTG16 and MTGR1. A. The UCSC genome browser ChIP-seq data was used to identify Kaiso targets. Chip-seq data developed by Soler et al., 2011 (426) was used to identify MTG16 and MTGR1 targets that overlapped with Kaiso binding sites. B. ATF-2, MAPK14, and C. ATF-7 mRNA expression upon overexpression of MTG16. The graph shows the fold-change ($^{\Delta\Delta}$Ct) of mRNA compared to an empty vector control. Error bars represent the standard error for three replicate experiments performed in triplicate. *P<0.05, ***P<0.001.*

MTG family members repress the Kaiso binding site promoter.

In mammalian cells, Kaiso recognizes both the consensus sequence TCCTGCNA (Kaiso binding site, KBS) and methylated CpG dinucleotides (231, 232). We used a luciferase-based Kaiso binding site reporter (4xKBS), as well as a mutant form that contains a C→A transversion that abolishes both Kaiso binding and Kaiso-mediated repression (4xKBSMT) (231) to explore cooperation between Kaiso and MTG family proteins in transcriptional repression (Fig. 6.4A). We determined that MTGs were capable of repressing the 4xKBS reporter construct (Fig. 6.4B) and that this repression was specific as it was disrupted when the 4xKBSMT reporter was used in lieu of the 4xKBS reporter (Fig. 3C). Additionally, Kaiso knockdown (Fig. 6.4D, left) resulted i a dose-dependent loss of 4xKBS repression by MTG16 (Fig. 6.4D, right). Finally, knockdown of both MTG16 and Kaiso resulted in decreased repression of the KBS in the HCT 116 cell line that expresses high levels of both proteins (Fig. 6.5A & B, *P*=0.008).

Because we determined MTG family members are able to repress the sequence-specific Kaiso target, we also wanted to determine whether MTGs were able to repress the second common Kaiso target, methyl-CpG. We therefore assessed the ability of MTG family members to repress a methylated reporter plasmid (232). In this case, we saw little repression of the methylated reporter by MTG family members until very high levels of MTG8 or MTG16 were used (Fig. 6.4E). This indicates that Kaiso dependent MTG repression specificity is directed towards genes containing the KBS as opposed to methyl-CpG, and suggests a model where MTG16 cooperates with Kaiso in the repression of KBS targets, but not to methylated CpG targets (Fig. 6.4F).

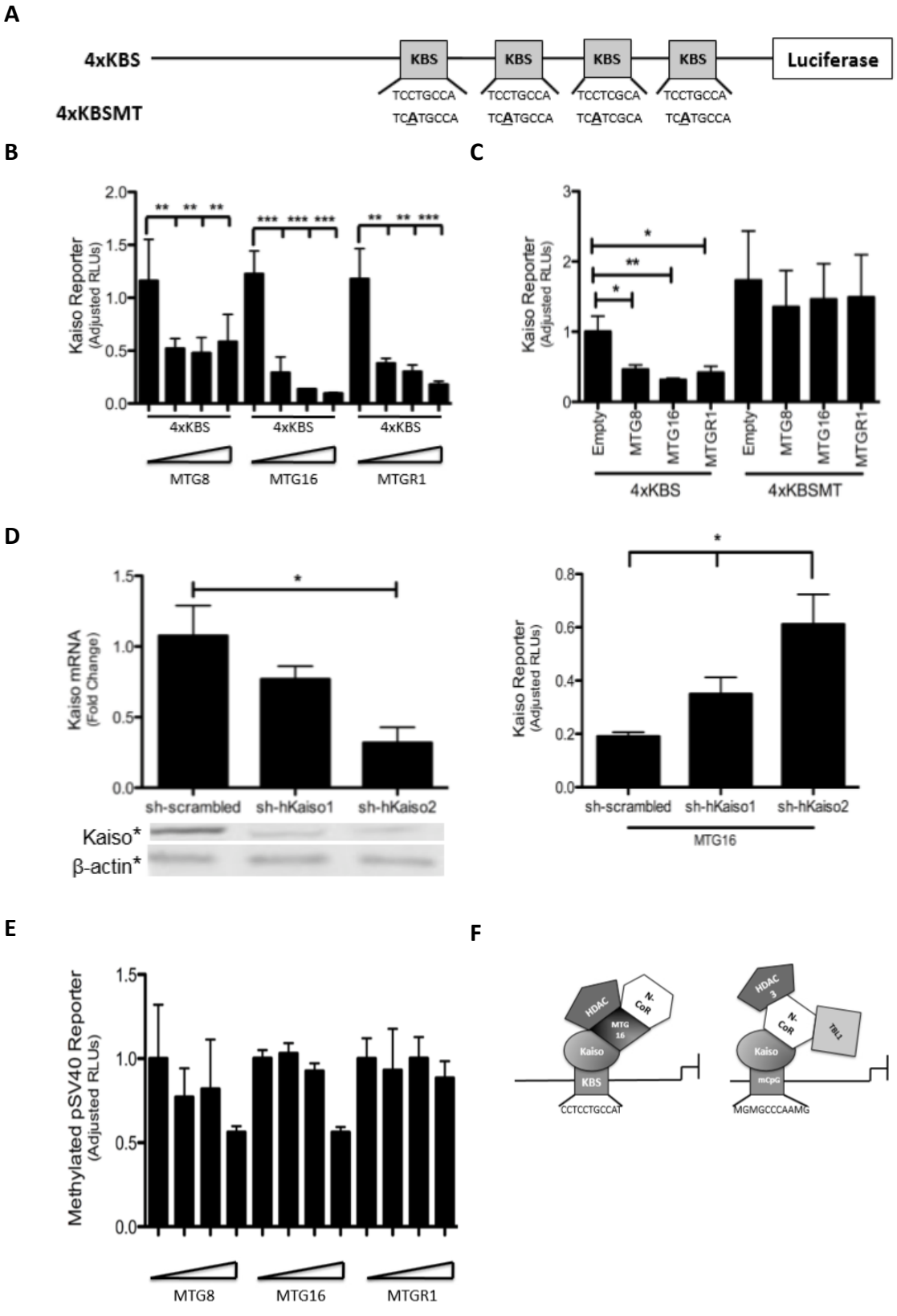
A
4xKBS
KBS
KBS
KBS
KBS
Luciferase
TCCTGCCA
TCCTGCCA
TCCTCGCA
TCCTGCCA
4xKBSMT
TCATGCCA
TCATGCCA
TCATCGCA
TCATGCCA
B
Kaiso Reporter (Adjusted RLUs)
4xKBS
4xKBS
4xKBS
MTG8
MTG16
MTGR1
C
Kaiso Reporter (Adjusted RLUs)
Empty
MTG8
MTG16
MTGR1
Empty
MTG8
MTG16
MTGR1
4xKBS
4xKBSMT
D
Kaiso mRNA (Fold Change)
sh-scrambled
sh-hKaiso1
sh-hKaiso2
Kaiso*
β-actin*
Kaiso Reporter (Adjusted RLUs)
sh-scrambled
sh-hKaiso1
sh-hKaiso2
MTG16
E
Methylated pSV40 Reporter (Adjusted RLUs)
MTG8
MTG16
MTGR1
F
HDAC
N. CoR
MTG 16
Kaiso
KBS
CCTCCTGCCAT
HDAC 3
N. CoR
TBL1
Kaiso
mCpG
MGMGCCCAAMG

*Figure 6.4 MTG family members repress the Kaiso binding site reporter (4xKBS). A. Composition of the KBS reporter constructs. The 4xKBS reporter contains four consensus Kaiso binding site sequences followed by a luciferase gene. The mutant reporter (4xKBSMT) contains a C→A transversion in the Kaiso binding sites which abolishes Kaiso binding. B. 4xKBS artificial promoter assays in HCT116 cells upon titration of MTG family members (0ng, 200ng, 400ng, 800ng). The graph shows the fold-change in luciferase activity relative to the control reporter, pGL4-TK hRLUC, after transfection of expression plasmids encoding MTG family members, MTG8, MTG16, and MTGR1. The error bars represent the standard error of the mean for 3 replicate experiments performed in triplicate. C. 4xKBS and 4xKBSMT artificial promoter assays in HCT116 cells after transfection of 500ng of the indicated MTG family member. The error bars represent the standard error of the mean for 4 replicate experiments performed in triplicate. D. Kaiso knockdown by two independent Kaiso shRNA constructs compared to a scrambled shRNA control (left). 4xKBS artificial promoter assay after knockdown of Kaiso and the transfection of 500ng of MTG16 (right). E. Methylated pSV40 artificial promoter assay in Mbd2$^{-/-}$ cells upon titration of MTG family members (0ng, 200ng, 400ng, 800ng). The graph shows the fold-change in luciferase activity relative to the control reporter, pGL4-TK hRLUC, after transfection of expression plasmids encoding MTG family members, MTG8, MTG16, and MTGR1. The error bars represent the standard error of the mean for 3 replicate experiments performed in triplicate. F. Model for Kaiso repression of Kaiso binding site (KBS) and methyl CpGs (mCpG) on target promoters. *P<0.05, **P<0.01, ***P<0.001.*

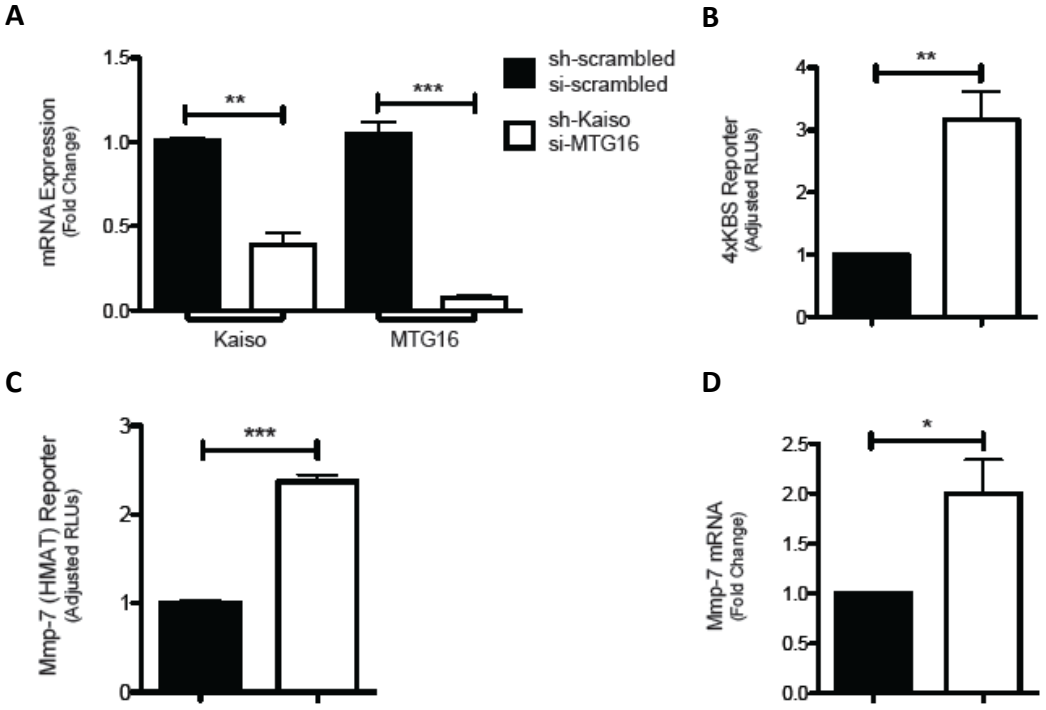

*Figure 6.5 Repression of 4xKBS, HMAT, and MMP7 is decreased with knockdown of MTG16 and Kaiso in HCT116 cells. A. Kaiso or MTG16 mRNA expression after knockdown of Kaiso (sh-Kaiso) and MTG16 (si-MTG16) in HCT116 cells. The graph shows the fold-change ($^{\Delta\Delta}$Ct) of mRNA compared to a scrambled control (sh-scrambled and si-scrambled). B. 4xKBS and C. HMAT reporter activity after knockdown of both Kaiso and MTG16. D. MMP7 expression in response to knockdown of Kaiso and MTG16. Error bars represent the standard error for three replicate experiments performed in triplicate. **P<0.01, ***P<0.001.*

MTG family members repress the MMP7 promoter.

MMP7 is an established tumor promoter in colon, prostate, pancreatic, and lung cancers (242, 243, 427, 428). It also contributes to tumor progression and metastasis (429). Interestingly, two Kaiso binding sites are present in the human *MMP7* promoter (Fig. 6.6A) that enable Kaiso-mediated repression of MMP7 expression (231). Our data suggests that MTGs may cooperate with Kaiso to repress Kaiso targets. Therefore, we hypothesized that MTGs would repress the *MMP7* promoter. Titration of each MTG family member with the full-length human *MMP7* reporter (HMAT-2.3, (231)) in the Kaiso-expressing HCT116 cells resulted in dose-dependent repression (Fig. 6.6B). This repression was lost when an MTG16 construct lacking the NHR1 domain (loss of affinity mutant) was used, further supporting an interaction with Kaiso that is dependent on the NHR1 domain of MTG16 (Fig. 6.6C). Also, Kaiso knockdown resulted in loss of HMAT repression, suggesting that Kaiso represses *MMP7* via MTG16 recruitment. Moreover, knockdown of both MTG16 and Kaiso in the HCT116 cell line resulted in decreased repression of the HMAT reporter (Fig. 6.5A & C, $P<0.0001$). Taken together, these data demonstrate that MTG16 and Kaiso repress *MMP7* promoter activity.

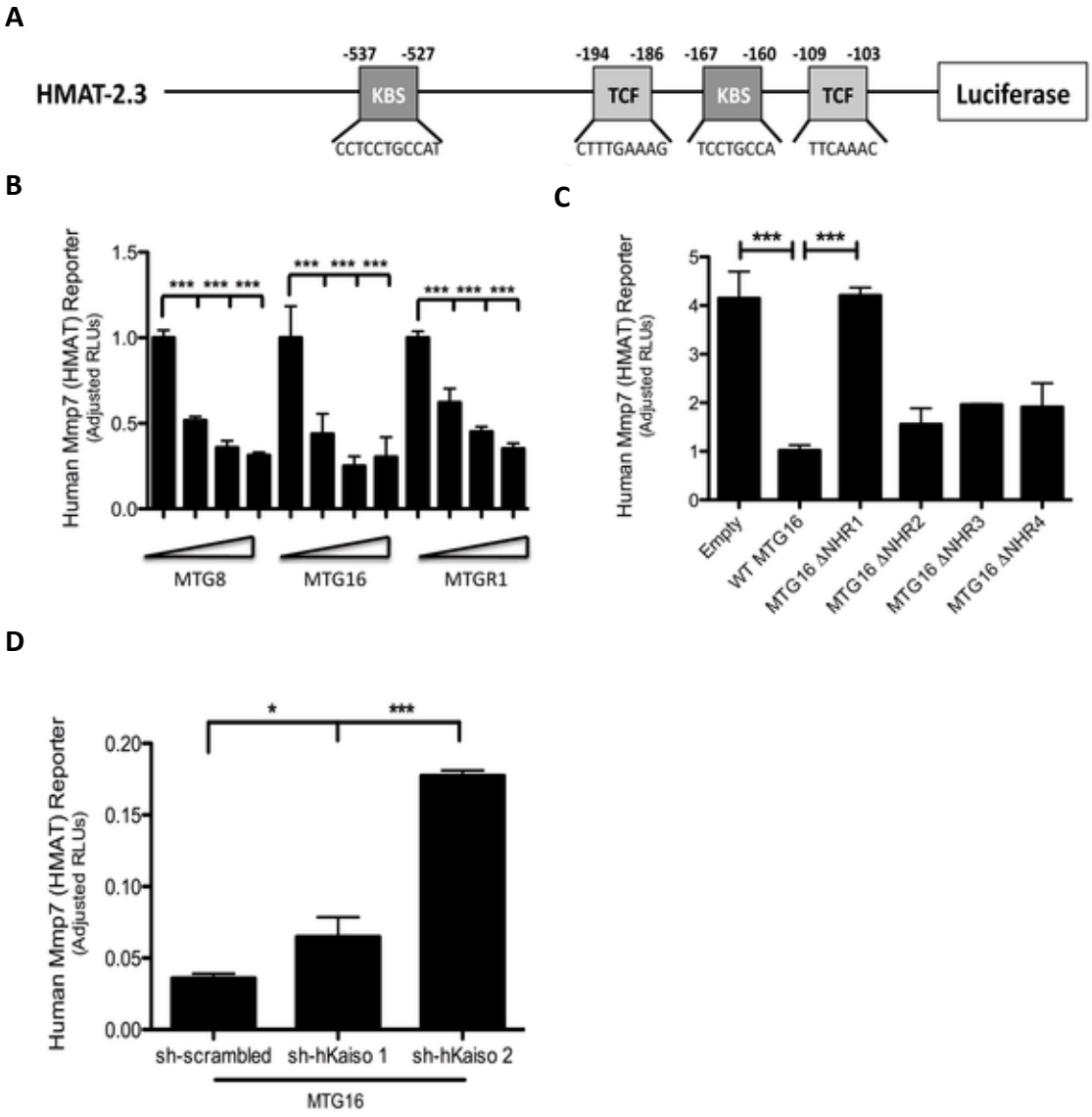

*<u>Figure 6.6</u> MTG family members depend on Kaiso to repress the human MMP7 promoter. A. The composition of the full-length MMP7 reporter (HMAT-2.3). The HMAT-2.3 reporter contains two Kaiso and two TCF binding sites followed by a luciferase gene. B. HMAT-2.3 artificial promoter assays in HCT116 cells upon titration of MTG family members (0ng, 200ng, 400ng, 800ng). The graph shows the fold-change in luciferase activity relative to the control reporter, pGL4-TK hRLUC, after transfection of expression plasmids encoding MTG family members, MTG8, MTG16, and MTGR1. The error bars represent the standard error of the mean for 3 replicate experiments performed in triplicate. C. HMAT-2.3 promoter assay utilizing MTG16 deletion constructs in which the indicated nervy homology region is removed. Error bars represent the standard deviation of triplicate samples. D. HMAT-2.3 artificial promoter assay after knockdown of Kaiso and the transfection of 500ng of MTG16. Error bars represent the standard deviation of triplicate samples. *P<0.05, ***P<0.001.*

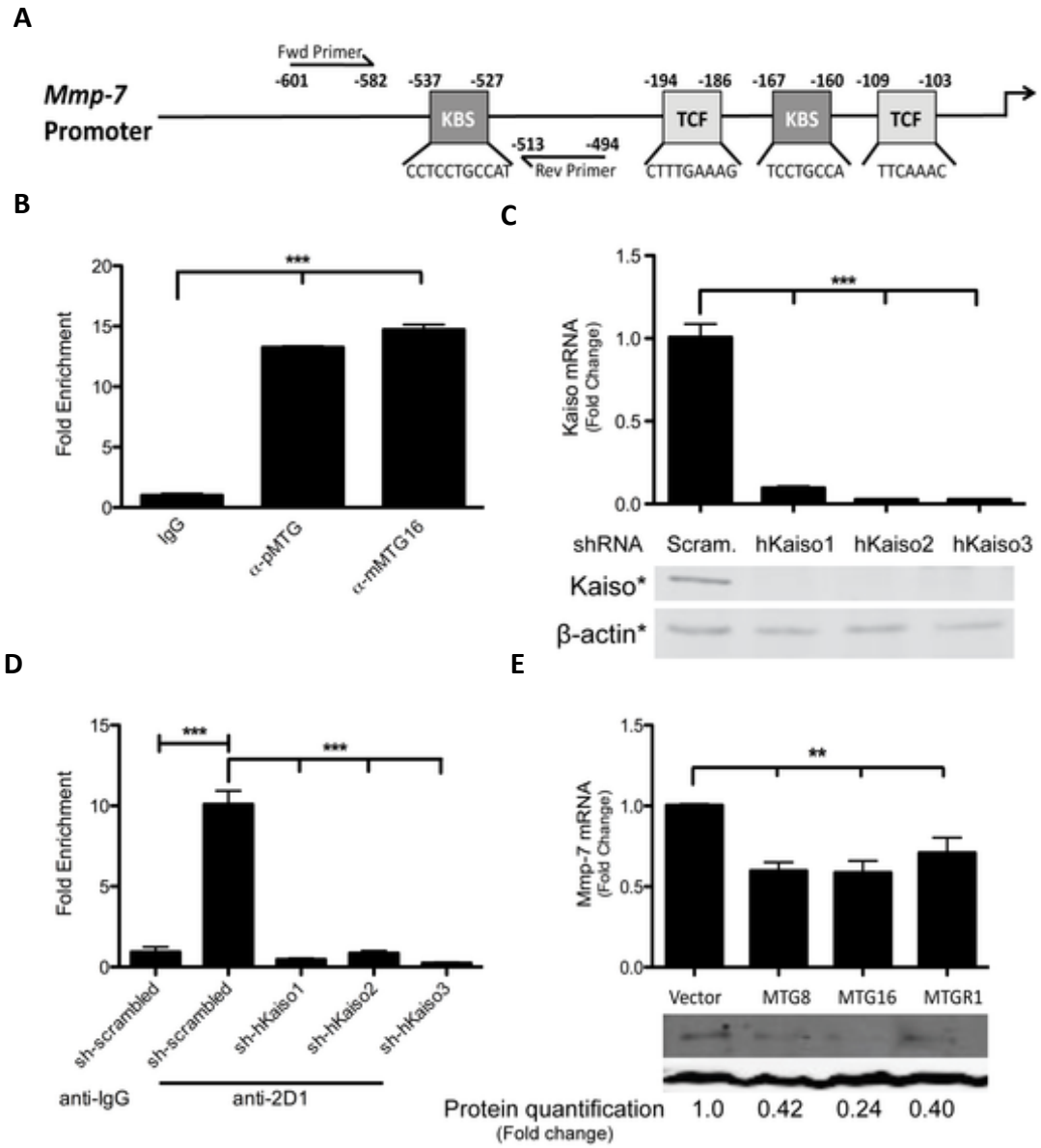

*Figure 6.7 MTG family members repress endogenous MMP7. A. Primers for the ChIP assay flank the -537 Kaiso binding site in the MMP7 promoter. B. ChIP assay performed in HCT116 cells using both polyclonal (333, pMTG) and monoclonal (2D1, mMTG16) antibodies for MTG16. The graph shows fold-enrichment compared to IgG control. C. Knockdown of Kaiso by three independent shRNA constructs compared to a scrambled sh-RNA control. D. Chromatin immunoprecipitation assay in HCT116 cells. The graph shows fold enrichment of the -537 Kaiso binding site after precipitation with the MTG16 2D1 antibody compared to the IgG control. E. MMP7 mRNA expression after transfection of the indicated MTG family member in HT29 cells. The graph shows the fold-change (ΔΔCt) of MMP7 mRNA compared to an empty control. Error bars represent the standard error for three replicate experiments performed in triplicate (top). Representative immunoblotting of MMP7 in HT29 cells after transfection of indicated family members and treatment with Brefeldin-A. Protein quantification was performed with the Odyssey Western blot developer system. **P<0.01, ***P<0.001.*

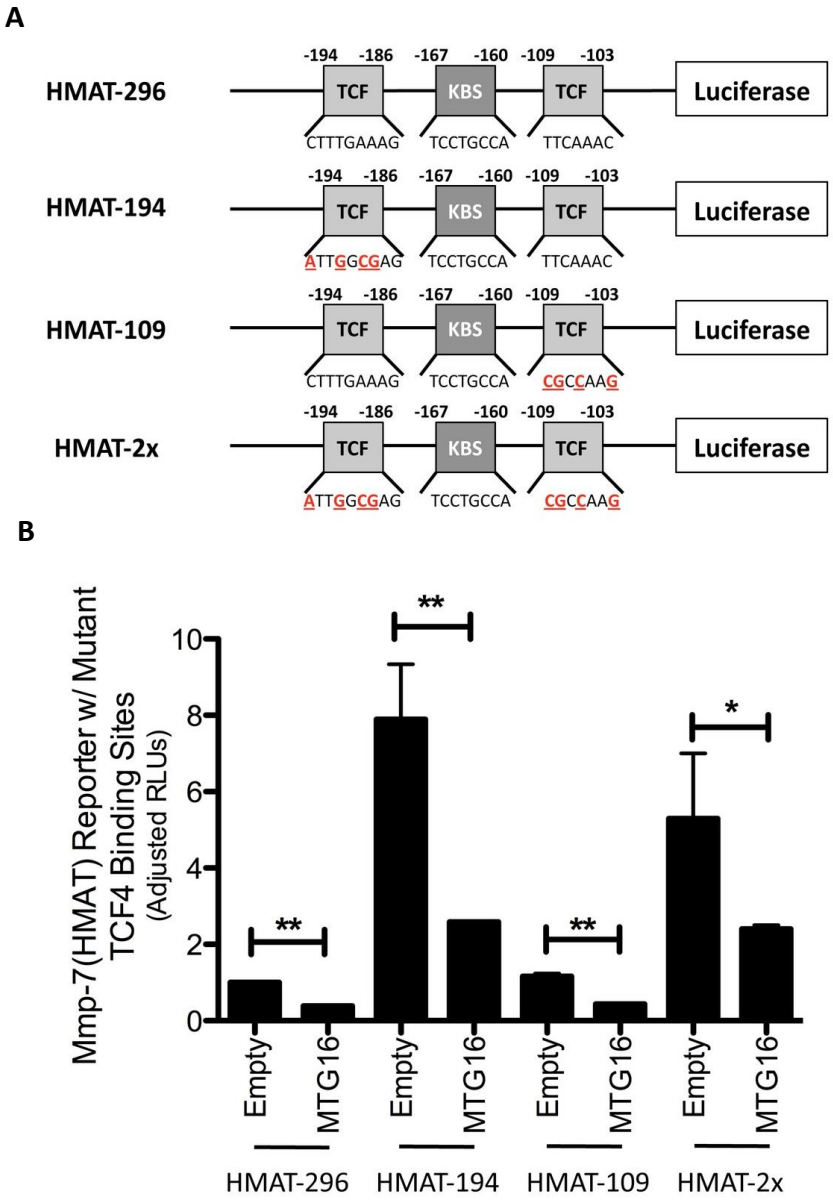

*Figure 6.8 MTG16 does not repress the MMP7 reporter via TCF binding sites. A. The composition of the truncated MMP7 reporter (HMAT-296) and TCF mutant reporters (HMAT-194, HMAT-109, and HMAT-2x). B. HMAT artificial promoter assays in HCT116 cells. HCT116 cells were transfected with either 500ng of MTG16 or 500ng of Empty vector as a control. The graph shows the fold-change in luciferase activity relative to the standard pGL4-TK hRLUC after transfection of expression plasmids. The error bars represent the standard error of four replicate experiments performed in triplicate. *P<0.05, **P<0.01.*

The human *MMP7* promoter also contains two TCF binding sites (Fig. 6.7A). MTGs also associate with TCF4 and repress TCF4 targets (209). Thus it was possible that in addition

to repressing via an interaction with Kaiso at the KBS, MTG16 could be recruited by TCF4 to repress *MMP7* via TCF response elements. To address this issue of MTG16 specificity for Kaiso or TCF binding sites, we performed repression assays using heterologous transcriptional reporters composed of minimal *MMP7* promoter elements where TCF binding sites were mutated individually or in combination (430) (Fig. 6.8A). Mutation of either or both of these sites had no effect on MTG16-mediated repression of *MMP7* (Fig. 6.8B). These data indicate that MTG16-dependent *MMP7* repression occurs independent of TCF binding sites. In concert, these results suggest that MTG16 recruitment by Kaiso to the *MMP7* KBS is responsible for MTG16:Kaiso mediated *MMP7* repression.

Both MTG16 and Kaiso have been implicated in breast, colon, and lung carcinoma (227-229, 247, 431, 432). Each can regulate Wnt signaling (209, 418), a pathway strongly associated with colon cancer development. Recently at least five MTG mutations have been identified in colon or breast cancer (228, 229), all are non-synonymous and predicted to influence MTG function. We therefore wanted to determine whether these mutations could influence Kaiso dependent repression of the 4xKBS and HMAT reporters. Overexpression of each MTG mutant resulted in no change in repression of either the 4xKBS (Fig. 6.9A) or HMAT reporters (Fig. 6.9B), indicating that these mutations do not influence MTG dependent Kaiso repression.

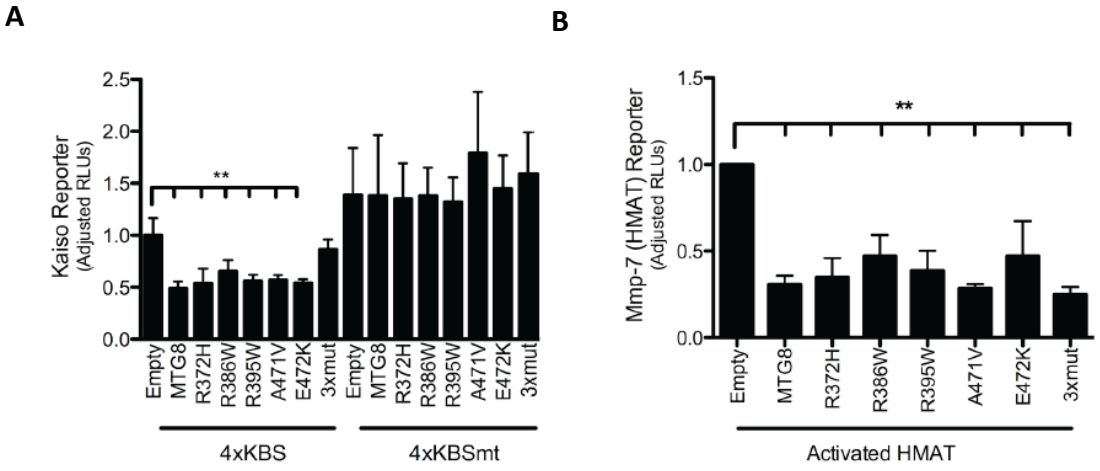

*Figure 6.9 Established MTG8 and MTG16 colorectal cancer mutations do not alter repression of Kaiso target promoters. A. 4xKBS artificial promoter assays in HCT116 cells. The graph shows the fold-change in luciferase activity relative to the standard pGL4-TK hRLUC after transfection of expression plasmids encoding the indicated MTG8 mutant constructs. B. HMAT-2.3 artificial promoter assays in HCT116 cells. The graph shows the fold-change in luciferase activity relative to the standard pGL4-TK hRLUC after transfection of expression plasmids encoding the indicated MTG8 mutant constructs. The error bars represent the standard error of three replicate experiments performed in triplicate. *P<0.05, **P<0.01.*

MTG family members repress endogenous MMP7 expression.

Based upon the transcriptional control data described above, we predicted that MTG16 should occupy the promoters of Kaiso-regulated genes. To address this hypothesis, we used ChIP to probe for MTG16 occupancy of the -537 Kaiso binding site in the endogenous *MMP7* promoter (Fig.7A). We observed 13.2 or 14.7 fold enrichment over IgG when either a polyclonal (333, pMTG) or monoclonal MTG16 (2D1, mMTG16) antibody was used ($P<0.001$, Fig. 6.7B). Importantly, Kaiso knockdown abrogated MTG16 binding to the *MMP7* promoter, showing that Kaiso is essential for MTG16 recruitment (Fig. 6.7C, D).

We next determined whether MTG16 was capable of regulating endogenous *MMP7* expression by analyzing *MMP7* mRNA and protein levels in the context of enforced expression of MTG family members. For this experiment, the colon cancer cell line HT29 was utilized. Overexpression of MTG8, MTG16, and MTGR1 resulted in decreased MMP7 both at the RNA and protein levels when compared to a vector control (fold-change mRNA expression: 0.60 S.E. 0.05 (MTG8), 0.59 S.E. 0.07 (MTG16), 0.71 S.E. 0.09 (MTGR1), $P<0.01$ for each, Fig. 6.7E). Considering that HT29 transfection efficiency in these experiments was 44.85% ± 6.553, the data likely under-represent the impact of MTGs on MMP7 expression. Moreover, knockdown of Kaiso and MTG16 in HCT116 cells resulted in derepression of endogenous MMP7 expression (Fig. 6.6D, $P=0.04$). These findings suggest that MTGs repress endogenous *MMP7* expression via interaction with Kaiso.

MMP7 increased expression is associated with decoupling of the MTG16 and Kaiso regulatory axis.

We next sought to compare the expression levels of *Kaiso*, *MMP7* and *MTG16* in patients with colorectal cancer compared with normal adjacent colon tissues and adenomas. We observed a significant up-regulation of *MMP7* and *Kaiso* (Fig. 6.10A, B, $P<0.001$ for all stages) while *MTG16* is significantly down-regulated for all stages of cancer compared with normal adjacent colon samples (Fig. 6.10C, $P<0.001$). Given the *in vitro* data demonstrating MTG16 played a key role and was required for maximal repression of Kaiso-regulated KBS-containing promoters, we reasoned that Kaiso and MTG16 expression would be inversely related on a per sample basis. We did in fact note a highly

significant inverse correlation (Fig. 6.10D, Rho=-0.29, *P*<0.001). The data presented in this paper suggests a model by which both Kaiso and MTG16 are necessary for *MMP7*

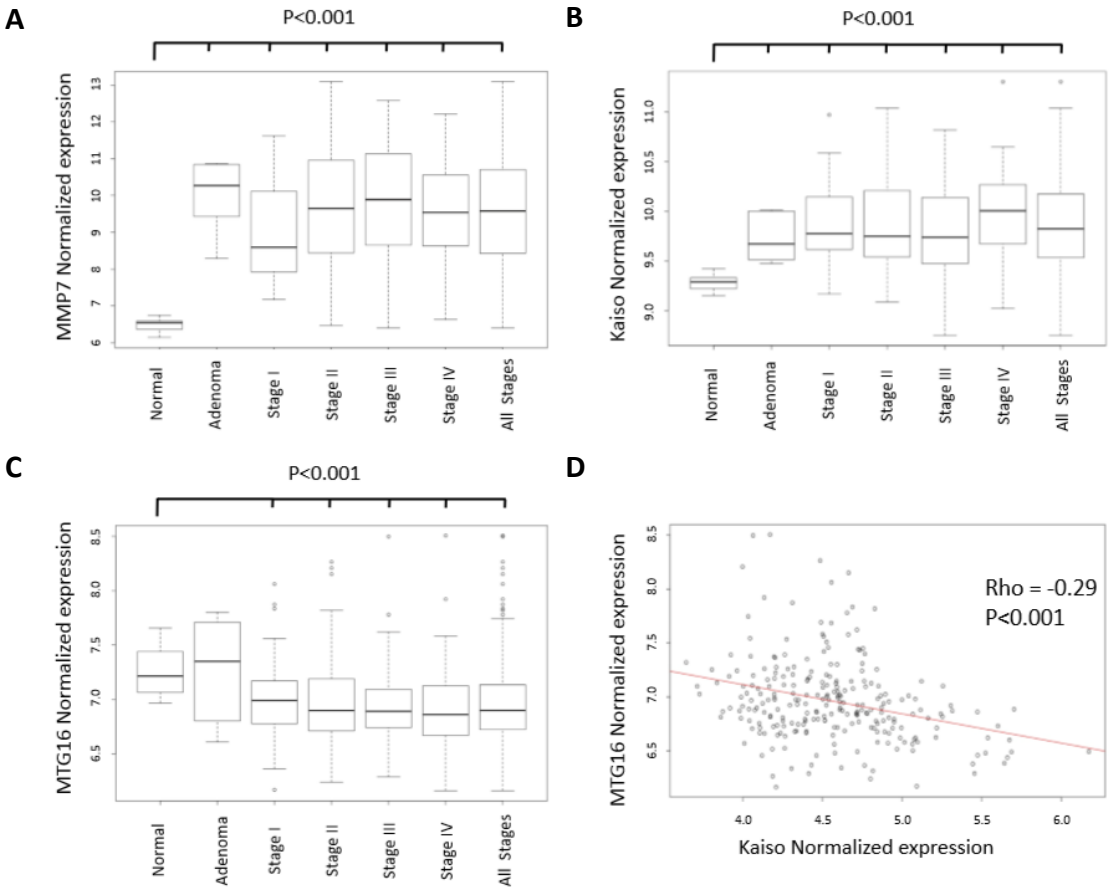

*<u>Figure 6.10</u> MTG16 and Kaiso are negatively correlated in human CRC patient samples and MMP7 is up-regulated. A) Kaiso expression is significantly up-regulated in adenomas and colorectal cancer patients compared with normal adjacent colon tissues (P<0.001, for all comparisons). B) MMP7 expression is significantly up-regulated in adenoma and colorectal cancer patients for each stage (P<0.001 for all comparisons). C) MTG16 expression is significantly down-regulated in colorectal cancers versus normal adjacent samples (P<0.001; *for all comparisons except adenoma). Wilcoxon Rank Sum test was used to determine significance for A-C. D) Normalized expression of both MTG16 and Kaiso probes (see Methods) were compared in human colorectal cancer patients. The graph demonstrates a significant inverse correlation for MTG16 versus Kaiso (rho = -0.29, P<0.001, inverse correlation depicted by red line, Spearman correlation coefficient).*

repression. This model likely applies to other Kaiso:MTG16 regulated KBS containing promoters.

Discussion

Kaiso and MTG16 share several functional similarities, including their abilities to repress Wnt signaling, bind co-repressors, and impact processes that influence tumorigenesis. Because of these similarities, we postulated that Kaiso and MTGs could form complexes and that Kaiso could target MTG repression functions to specific promoters. In testing this hypothesis we found that Kaiso and MTG16 interact and that this depends on the homologous zinc fingers in Kaiso and the NHR1 domain in MTG16. Furthermore, when MTG family members are overexpressed, they enhance repression of a KBS reporter. Studies with both heterologous KBS reporters and Kaiso knockdown showed that MTG-dependent transcriptional repression on Kaiso targets, such as the *MMP7* promoter, is Kaiso-dependent. ChIP experiments revealed that the Kaiso-MTG interaction occurs endogenously at the KBS in the *MMP7* promoter, and reduced MMP7 expression at both the RNA and protein level show the interaction to be functionally significant. Thus, we have linked two families of transcriptional repressors, both previously implicated in oncogenesis. Understanding the nature of this relationship is important in understanding transcriptional regulation by these complexes in normal biology and how this is perturbed in tumorigenesis.

Kaiso is a dual-specificity repressor that can recognize both a consensus sequence (KBS, TCCTGCNA) and methyl-CpG dinucleotides (231). Interestingly, though MTG16 is important for repression of KBS reporters, it does not repress a methylated reporter, suggesting that the Kaiso-MTG16 interaction is specific for promoters that contain the Kaiso binding site. Kaiso has been identified as the factor that recruits the N-CoR complex

to CpG-rich sequences in a methylation-dependent manner (235), our study demonstrates that there is a converse activity with interaction with MTG16, as it is a Kaiso cofactor that is dependent solely on Kaiso binding to the canonical KBS. This suggests that Kaiso might differentiate between target repression based on the availability of cofactors, making these cofactors key in understanding the regulation of Kaiso targets, be they methylated or the canonical consensus sequence. We think that this is biologically relevant as we noted a strong inverse correlation between *MTG16* and *Kaiso* levels in a large human CRC dataset. This could have important implications for the regulation of Kaiso:MTG16 targets and may influence the bimodal effect of Kaiso on carcinogenesis (247, 251, 418, 432).

This interaction is also of great importance as our data directly implicates MTG16:Kaiso complexes in the regulation of *MMP7* expression. MMP7 plays a significant role in all stages of tumor progression and is a key player in a wide variety of cancers including, but not limited to, colon, prostate, lung and ovarian (427, 433-436). Indeed, metalloproteinases are among the most common targets for anti-cancer drug development (437) so understanding their regulation will give insight into mechanisms by which their expression might be altered. We have determined that MTG16 binds Kaiso at the *MMP7* promoter and recruits transcriptional corepressors to attenuate *MMP7* expression. Furthermore, both *MTG16* and *Kaiso* demonstrate coordinate patterns of expression when compared with *MMP7* in human CRC samples vs. normal adjacent colon samples. Decreased repression upon loss of either protein within this complex could contribute to tumorigenesis.

In order to better understand the scope of the Kaiso-MTG interaction, we analyzed public-domain ChIP-seq datasets (UCSC Genome Browser, (426)) to determine the overlap of targets bound by Kaiso and the MTG family members MTG16 and MTGR1. Several targets relevant to cancer pathogenesis were revealed using this methodology. For example, Kaiso and MTG16 bind the Activating Transcription Factor *(ATF)-2* promoter, while Kaiso and MTGR1 bind the promoter for *ATF7*. The ATF family is composed of transcription factors that are involved in cellular stress response (438). Aside from being activated by the MAPK pathway in response to stress, ATFs 2 and 7 are also involved in oncogenesis, as they are able to dimerize with c-Jun to influence Jun-dependent survival, apoptosis, and cell cycle progression (439, 440). C-Jun pathway regulation is also seen with a third target of MTG-Kaiso binding, MAPK14. Mitogen-activated protein kinase (MAPK) p38α (MAPK14) suppresses cellular proliferation through inhibition of the JNK-c-Jun pathway (441) and plays an essential role in stem and progenitor cell proliferation and differentiation in the lung (442). Another MAPK family member, MAP3K7, was also identified in this screen. MAP3K7 plays an important role in the modulation of TGF-β signaling (443), a pathway highly related to oncogenesis. Importantly, overexpression of MTG16 in the HT29 cell line resulted in repression of both *ATF2* and *MAPK14*, consistent with MTG16 functioning as a repressor, but also overexpression of the target *ATF7*, suggesting that this target has more complex transcriptional regulation.

In summary, we identified an association between Kaiso and MTG family members. Because Kaiso is the prototypic ZBTB family member, we focused on understanding the contribution of MTG16 to Kaiso mediated repression. We determined

that the Kaiso-MTG16 complex specifically binds to the KBS and represses the Kaiso target, *MMP7*. We examined a large multi-stage CRC expression array dataset and discovered an inverse relationship between Kaiso and MTG16 expression and consistently elevated *MMP7* expression at all stages of tumorigenesis supporting the hypothesis that loss of either Kaiso or MTG16 de-regulates *MMP7* expression. Analysis of publicly available ChIP-seq datasets showed that MTG family members bind Kaiso-targeted promoters over 70% of the time, implicating this interaction in the regulation of over 100 genes, many of which are involved in cell cycle control and survival programs.

In conclusion, we report that Kaiso and MTGs interact in inhibitory complexes and identify a subset of target genes which are important in oncogenesis. Additional targets identified in the ChIP-seq screen include stress and oxidative damage response proteins potentially important in inflammatory carcinogenesis. Future experiments should be directed towards understanding the role of Kaiso and MTG16 in sporadic and inflammatory colon carcinogenesis.

Acknowledgements

This work was funded by National Center for Research Resources, Grant UL1 RR024975-01, and is now at the National Center for Advancing Translational Sciences, Grant 2 UL1 TR000445-06, the Cellular and Biochemical and Molecular Sciences Training Program (NIH T32 GM08554), an NCI sponsored fellowship (CWB 1F31CA167920), and NIDDK K-08 (CSW 5K08DK080221). Additional funding from the Veterans Administration (CSW & KTW) and the American Cancer Society ACS-RSG 116552 (CSW). Core Services performed through

Vanderbilt University Medical Center's Digestive Disease Research Center supported by NIH grant P30DK058404 (RMP) and the Vanderbilt Ingram Cancer Center shared resources P30CA068485. The content is solely the responsibility of the authors and does not necessarily represent the official views of the NIH. The funders had no role in study design, data collection and analysis, decision to publish, or preparation of the manuscript. We would like to thank members of the Williams lab and Paul Barrett for helpful comments regarding this manuscript and Joseph Roland for technical assistance with the Deltavision System. We thank Howard Crawford for the matrilysin reporter constructs and Juliet Daniel for her kind gift of the 4xKBS vectors. Finally, we would like to thank Brian Hendrich and Pierre-Antoine Defossez for providing the *Mbd2*$^{-/-}$ cells and technical advice regarding their use in methylation studies.

CHAPTER VII

KAISO IS REQUIRED FOR MTG16-DEPENDENT EFFECTS ON COLITIS-ASSOCIATED CARCINOMA

Introduction

Kaiso is a p120 catenin binding partner that represses DNA methylation-dependent targets including several tumor suppressor genes including *CDKN2A*, *HIC1*, and *MGMT* (247). As such, Kaiso dysfunction might play a key role in tumorigenesis. In fact, Kaiso knockout mice crossed with the tumor-susceptible $Apc^{Min/+}$ mouse model show resistance to intestinal tumorigenesis (251). Moreover, Kaiso represses several genes within the canonical WNT signaling pathway including the B-catenin/TCF target gene matrix metalloproteinase-7 (*Mmp7*) (241, 418) which has been implicated in stimulation of Wnt signaling as well as tumor progression in several solid malignancies (244, 406, 410, 428, 429).

Transcriptional co-repressors recruit other repressors, HDACs, and DNA binding transcription factors to repression complexes. The myeloid translocation genes are a three-member family of transcriptional corepressors that act as scaffolding proteins upon which other transcriptional corepressors, including mSin3a, N-CoR, SMRT, histone deacetylases (HDACs), and transcription factors assemble (178, 190). Kaiso is a myeloid translocation gene (MTG) family binding partner and the interaction occurs through the zinc finger domain of Kaiso and the NHR1 domain of MTG16. Target specificity is achieved

via Kaiso vectoring the complex to Kaiso Binding Site (KBS)-containing promoters. The functional relevance of the interaction is evident as loss of either protein leads to derepression of targets such as Mmp7 (444). MTG family members have been implicated in both hematologic and solid malignancies including leukemia and colon and breast cancers (227-229) and our lab has shown that MTGR1 is required for tumorigenesis and absence of MTG16 leads to increased tumorigenesis in a murine model of colitis-associated carcinoma, implicating the MTGs in inflammation-driven tumorigenesis (269).

The impact of Kaiso loss on inflammatory cancer has not yet been established. Because Kaiso and MTG16 form a repression complex and MTG16 loss greatly exacerbates injury and tumorigenesis in response to the AOM/DSS protocol, the purpose of this work was to determine whether Kaiso deficiency modified tumorigenesis and whether subsequent loss of MTG16 would modify the *Kaiso*$^{-/-}$ phenotype. Here, we determine that Kaiso deficiency does not lead to altered injury or tumorigenesis in response to the AOM/DSS inflammatory carcinogenesis protocol while *Mtg16*$^{-/-}$ mice, as expected, demonstrated increased injury and tumorigenesis in response to AOM/DSS. Perhaps most surprisingly, knockout of both MTG16 and Kaiso led to a similar phenotype as that seen in *WT* and *Kaiso*$^{-/-}$ mice, suggesting that Kaiso loss rescues the *Mtg16*$^{-/-}$ phenotype. Moreover, intratumoral proliferation and apoptosis indices support the alterations in tumorigenesis seen in each genotype and, consistent with a pro-tumorigenic microenvironment, only *Mtg16*$^{-/-}$ tumors demonstrate increased pro-tumorigenic M2 macrophages and increased chemokine and cytokine expression. This suggests that, though Kaiso and MTG16 share several targets, it is the transcriptional

targets that they do not share that distinguish their responses to the AOM/DSS protocol and that Kaiso targets are dominant to MTG16 targets where loss of Kaiso leads to rescue of the *Mtg16*$^{-/-}$ phenotype.

Materials and Methods

Murine inflammatory carcinogenesis protocol. 8-12 week old C57BL/6 wild type (WT) (n=14), *Mtg16*$^{-/-}$ (n=15), *Kaiso*$^{-/-}$ (n=14), or *Kaiso*$^{-/-}$*;Mtg16*$^{-/-}$ (*DKO*, n=8) mice were injected with 10 mg/kg of azoxymethane (AOM, Sigma-Aldrich, St. Louis, MO, USA) intraperitoneally as described by Greten, *et al.* (265). Three days post-injection, the animals were started on the first of two cycles of 2% DSS *ad libitum* (see schematic in Fig. 7.1A). Each cycle lasted 5 days and was followed by a 16-day recovery period. Weights were obtained throughout the treatment and recovery period and reported as the percentage of the original weight one day before DSS administration. In addition, stools were examined for consistency and the presence of blood during the treatment period: normal stools = 0 points, loose stool = 1 point, diarrhea = 2 points, presence of blood = 2 points, and excessive blood = 4 points. During the second cycle of recovery (day 29), colonoscopy (Karl Storz veterinary endoscopy, El Segundo, CA, USA) was performed to assess injury, tumor multiplicity, and tumor grade. Injury was evaluated based on the murine endoscopic index of colitis severity (MEICS) that includes thickening of the colon, changes in vasculature, presence of granularity, presence of exudate, and stool consistency (302, 358). Mice were subsequently sacrificed on day 40. Colons were removed, flushed with PBS, and opened longitudinally and tumor counts and diameter

were assessed using calipers. Sections of tumor and normal adjacent colon were collected and stored in RNAlater (Qiagen, Valencia, Santa Clarita, CA, USA) and a section of distal colon was collected and flash frozen in liquid nitrogen for protein analysis. The remainder of the colon was "Swiss Rolled", formalin fixed overnight, and sectioned for histological analysis. All *in vivo* procedures were carried out in accordance with protocols approved by the Vanderbilt Institutional Animal Care and Use Committee.

Immunohistochemistry and immunofluorescence staining. Five-micrometer sections of paraffin-embedded colons were cut and haematoxylin and eosin (H&E) staining was performed by the Vanderbilt University Translational Pathology Shared Resource. Cut sections were dewaxed, hydrated, and quenched of endogenous peroxidase activity with 0.03% hydrogen peroxide in methanol. Antigen retrieval was conducted using Antigen Unmasking Reagent (Vector Laboratories, Inc., Burlingame, CA, USA) according to manufacturer's instructions. After blocking, primary antibody was added [α-Ki67 (NeoMarkers, Fremont, CA, USA), 1:1,000; α-arginase I (ARG1, Santa Cruz, Dallas, TX, USA), 1:500; α-IL-1β (R&D Systems, Minneapolis, MN, USA), 1:40; α-F4/80 (AbD Serotec, Raleigh, NC, USA) 1:1000] and incubated overnight at 4°C. Isotype-matched antibodies were included as negative controls. Identification of intratumoral apoptotic cells was conducted using the ApopTag Plus Peroxidase *In Situ* Apoptosis Kit (Chemicon, Temecula, CA, USA) according to the manufacturer's protocol. Control slides were obtained by omitting the terminal transferase (TnT) enzyme. For immunofluorescence staining of proliferation and macrophages, slides were counterstained and mounted with ProLong Gold antifade including 4',6-diamidino-2-phenylindole (DAPI, Invitrogen, Grand Island,

NY, USA). Apoptosis, proliferation, and M1 and M2 macrophage indices were generated by counting either the number of positive cells per high-powered field (HPF; 40x objective) within each tumor or the number of positive cells per crypt in 20 crypts per mouse by a blinded observer. The average score was then calculated for each Swiss-rolled colon.

Wnt pathway analysis. Flash-frozen sections of colon (n=6 for each genotype) were lysed in RIPA buffer including 1x protease inhibitor cocktail (Sigma-Aldrich) using a rotor homogenizer (Janke & Kunkel IKA-Labortechnik Ultra-Turrax T25). Protein quantification was performed using a Pierce BCA Protein Assay Kit (Thermo, Hudson, NH, USA) according to manufacturer's instructions. Samples were treated with loading buffer, boiled, and 40 µg was run on an SDS-PAGE gel for western blot detection using the Odyssey western blot system (LI-COR, Lincoln, NE, USA). A Wnt/β-catenin Activated Targets Antibody Sampler Kit (Cell Signaling Technology, Boston, MA, USA) was used to probe for Wnt targets according to the manufacturer's protocol with the exception of using Odyssey-specific secondary antibodies for detection. Bands were quantified using Odyssey software and normalized to β-actin.

Cytokine array analysis. RNA from tumors of WT (n=4), *Kaiso*$^{-/-}$ (n=4), *Mtg16*$^{-/-}$ (n=4), and *DKO* (n=4) was isolated using the RNeasy Mini Kit (Qiagen). cDNA was synthesized using the iScript cDNA synthesis kit (Bio-rad, Hercules, CA, USA) and 1 µg of total RNA. 1 µl of the 20 µl cDNA produced through the iScript reaction was used as a template in each subsequent PCR reaction. SYBR green qRT-PCR was performed using mouse cytokine array libraries I and II from RealTimePrimers.com (Elkins Park, PA, USA) according to

manufacturer's instructions. Individual cytokines were analyzed using the delta-delta Ct method and those showing significant differences can be seen in Supplementary Figure 3. The networks were generated through the use of IPA (Ingenuity® Systems, www.ingenuity.com).

Statistical methods. Statistical analysis comparing all four groups was performed utilizing Graphpad Prism and analysis with the one-way ANOVA and Newman-Keuls Multiple Comparison post-test. Differences in stool scores and percentage weight loss were determined using two-way ANOVA for repeated measurements over time.

Results

Kaiso is required for enhanced mucosal injury in Mtg16$^{-/-}$ mice after AOM/DSS treatment.

Mtg16$^{-/-}$ mice demonstrate increased mucosal injury in response to the AOM/DSS protocol resulting in increased weight loss, stool scores, and morbidity (McDonough et al., submitted). Because we have determined that Kaiso and MTG16 form a repression complex, we wanted to determine whether absence of Kaiso influenced AOM/DSS-induced injury. We utilized 10mg/kg azoxymethane (AOM) in order to initiate DNA damage and treated mice with cyclical administration of 2% DSS for five days followed by 16 days of recovery (Figure 7.1A). Absence of MTG16 resulted in exacerbated injury as evidenced by increased stool scores which take into account stool consistency and presence of frank blood (P<0.0001 2-way ANOVA, Figure 7.1B) as well as increased weight loss (P<0.0001 2-way ANOVA, Figure 7.1C), both of which were most prominent during the second cycle of DSS administration. In support of these clinical metrics, endoscopy

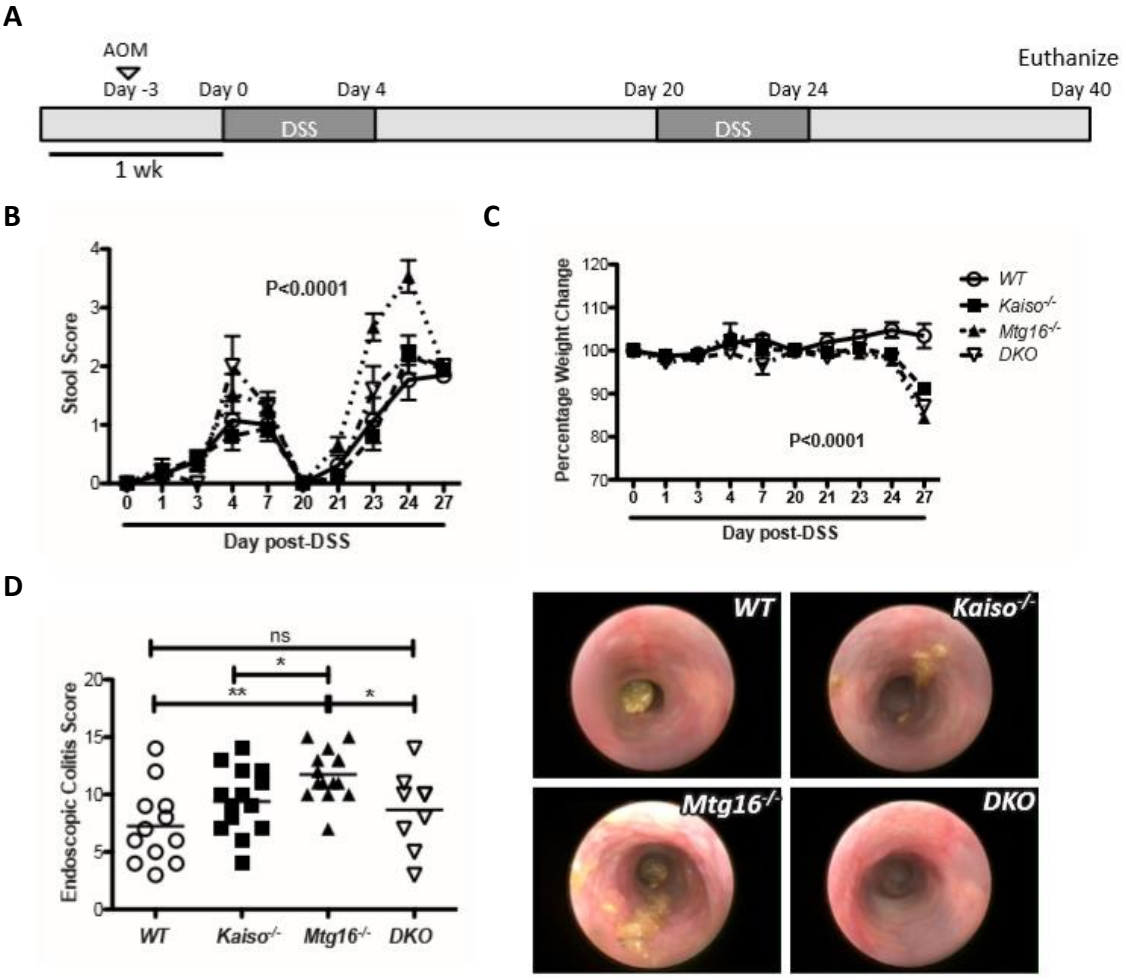

*Figure 7.1 Kaiso knockout rescues the Mtg16$^{-/-}$ injury phenotype observed in response to the AOM/DSS protocol. A. Schematic of AOM/DSS inflammatory carcinogenesis protocol. B. Stool scores as determined using the scoring system described in the "materials and methods" section and C. percent weight change throughout the course of the AOM/DSS protocol. D. Endoscopic colitis scoring (MEICS scale) determined at day 29 of the AOM/DSS protocol. *P<0.05, **P<0.01.*

performed at day 29 demonstrated an increase in colitis severity as measured by the MEICS scoring system (302) (*WT*: 7.3±1.0, *Mtg16*$^{-/-}$: 11.7±0.6, *P*<0.01, Figure 7.1D). *Kaiso*$^{-/-}$ mice, however, did not show increased injury in response to the AOM/DSS protocol above that of WT mice (*Kaiso*$^{-/-}$: 9.4±0.7). In fact, *Kaiso*$^{-/-}$*;Mtg16*$^{-/-}$ double knockout (DKO) mice demonstrated injury equivalent to that seen in *Kaiso*$^{-/-}$ mice (MEICS *DKO*: 8.7±1.1,

Figure 7.1) indicating Kaiso was required for this Mtg16-null phenotype. Thus *Mtg16*$^{-/-}$ mice have worse injury after AOM/DSS treatment, which is Kaiso dependent.

Knockout of Kaiso rescues Mtg16$^{-/-}$*-dependent increases in tumorigenesis.*

We next evaluated for modified tumor burden in *Mtg16*$^{-/-}$, *Kaiso*$^{-/-}$, or *DKO* mice compared to *WT* mice in response to the AOM/DSS CAC protocol. Tumor development tracked very closely with severity of injury with *Mtg16*$^{-/-}$ mice displaying increased tumor number (9.9±0.8 tumors/mouse, $P<0.001$) compared to both the *WT* (5.4±0.8 tumors/mouse) and *Kaiso*$^{-/-}$ (4.9±0.6 tumors/mouse) mice and the MTG16 effect on tumorigenesis was partially rescued by subsequent Kaiso knockout (7.5±1.1 tumors/mouse, Figure 7.2A & B). Furthermore, consistent with an increase in injury extent, an increased number of *Mtg16*$^{-/-}$ tumors were identified in the more proximal region within the colon compared to those seen in the other three genotypes (Figure 7.2C). These data suggest that, while MTG16 loss serves to promote tumorigenesis, at least in part through increasing mucosal injury and inflammation, Kaiso loss has no impact on inflammatory tumorigenesis by itself, but in fact, rescues the *Mtg16*$^{-/-}$ phenotype.

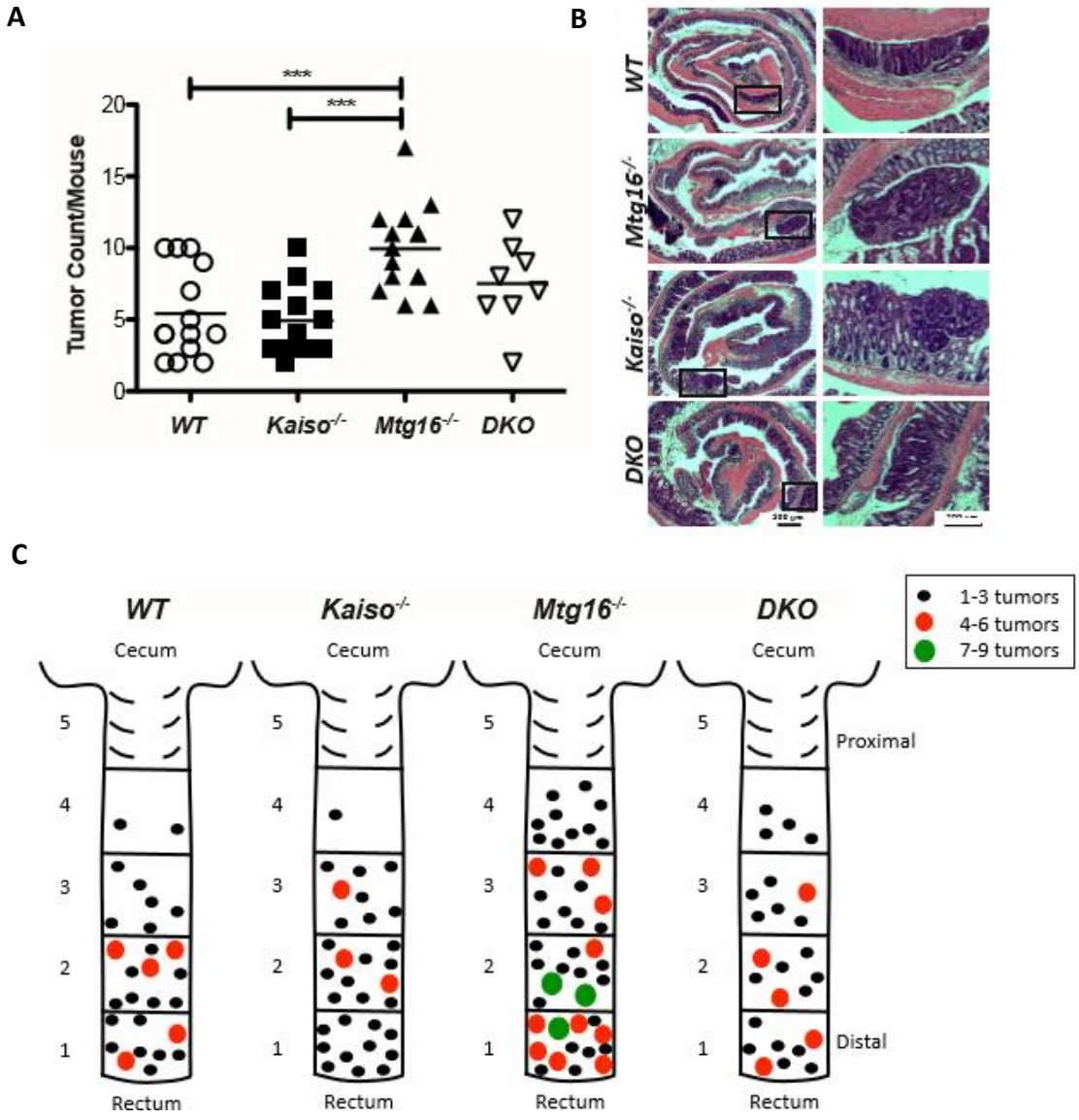

*Figure 7.2 Knockout of Kaiso rescues the Mtg16$^{-/-}$ tumor phenotype. A. Number of tumors within each mouse of the indicated genotypes. B. Representative images of Swiss rolled colons and tumors from WT, Mtg16$^{-/-}$, Kaiso$^{-/-}$, and DKO mice (left 25x, right 100x) C. Graphical depictions of tumor locations within mice post-AOM/DSS protocol. Each dot represents the number of tumors found within the given region of the colon in a single mouse. ***P<0.001.*

Crypt and intratumoral proliferation and apoptosis rates support alterations in tumorigenesis between the genotypes.

Alterations in proliferation and apoptosis, among other growth parameters, could contribute to differences in tumor size and number. As we identified increased tumor

multiplicity in *Mtg16*$^{-/-}$ mice, we wanted to determine whether crypt or intratumoral proliferation or apoptosis indices were altered in these mice and if Kaiso absence reversed any of these parameters. Proliferation, as determined by Ki67 staining, was only increased in crypts of *Mtg16*$^{-/-}$ mice (1.2±0.2 Ki67^{+}/crypt, P<0.01) compared to *WT* (0.7±0.02 Ki67^{+}/crypt), *Kaiso*$^{-/-}$ (0.6±0.07 Ki67^{+}/crypt), and *DKO* mice (0.7±0.06 Ki67^{+}/crypt, Figure 7.3A). Intratumoral proliferation, on the other hand, was increased in both *Mtg16*$^{-/-}$ (34.0±3.4 Ki67^{+}/tumor high-powered field (HPF)) and *Kaiso*$^{-/-}$ (25.0±4.3 Ki67^{+}/tumor HPF) mice compared to *WT* mice (8.7±1.3 Ki67^{+}/tumor HPF, Figure 7.3B). This increase in *Kaiso*$^{-/-}$ intratumoral proliferation was balanced by a marked increase in apoptosis (*WT*: 12.5±2.3, *Kaiso*$^{-/-}$: 25.7±3.5, P<0.01, *Mtg16*$^{-/-}$: 20.9±1.2, P<0.05, *DKO*: 15.3±2.7 TUNEL^{+}/tumor HPF, Figure 7.3D). Crypt apoptosis is increased in *Mtg16*$^{-/-}$ (0.8±0.04 TUNEL^{+}/crypt, P<0.05), *Kaiso*$^{-/-}$ (0.7±0.08 TUNEL^{+}/crypt, P<0.05), and *DKO* (0.7±0.08 TUNEL^{+}/crypt, P<0.05) mice compared to *WT* mice (0.5±0.03 TUNEL^{+}/crypt, Figure 7.3C), and thus does not likely contribute to alterations in tumorigenesis. Therefore, *Mtg16*$^{-/-}$ mice likely demonstrate increased tumorigenesis compared to the other genotypes due to an increase in proliferation and, though *Kaiso*$^{-/-}$ mice display increased proliferation as well, they do not display increased tumorigenesis because the effects of this proliferation are reversed by a concomitant increase in apoptosis.

Wnt target expression is increased in tumors lacking Kaiso, MTG16, or both proteins.

Kaiso and MTG16 repress canonical Wnt signaling (209, 418) and our lab has shown that Kaiso recruits MTG16 to the *Mmp7* promoter and represses its expression

(444). We, therefore, wanted to determine whether Kaiso and MTG16 contributed to Wnt repression *in vivo*. Tumor lysates from *WT*, *Kaiso*$^{-/-}$, *Mtg16*$^{-/-}$, and *DKO* mice were immunoblotted to determine expression of WNT pathway targets. As expected, absence of Kaiso, MTG16, or both resulted in an increase in Mmp7 protein levels (*WT*: 1.6±0.3, *Kaiso*$^{-/-}$: 3.2±0.8, $P<0.01$, *Mtg16*$^{-/-}$: 2.8±0.7, $P<0.05$, *DKO*: 2.4±0.3 relative fold change compared to WT and normalized to β-actin, $P<0.05$). Moreover, c-Myc was also increased with loss of these proteins *in vivo* (*WT*: 0.7±0.3, *Kaiso*$^{-/-}$: 3.6±1.5, $P<0.05$, *Mtg16*$^{-/-}$: 3.1±0.8, $P<0.05$, *DKO*: 2.5±0.5 relative fold change compared to WT and normalized to β-actin, $P<0.05$, Figure 7.4A & B). These data suggest that Kaiso and MTG16 cooperate to repress at least a component of Wnt signaling and the loss of either protein increases Mmp7 and c-Myc levels.

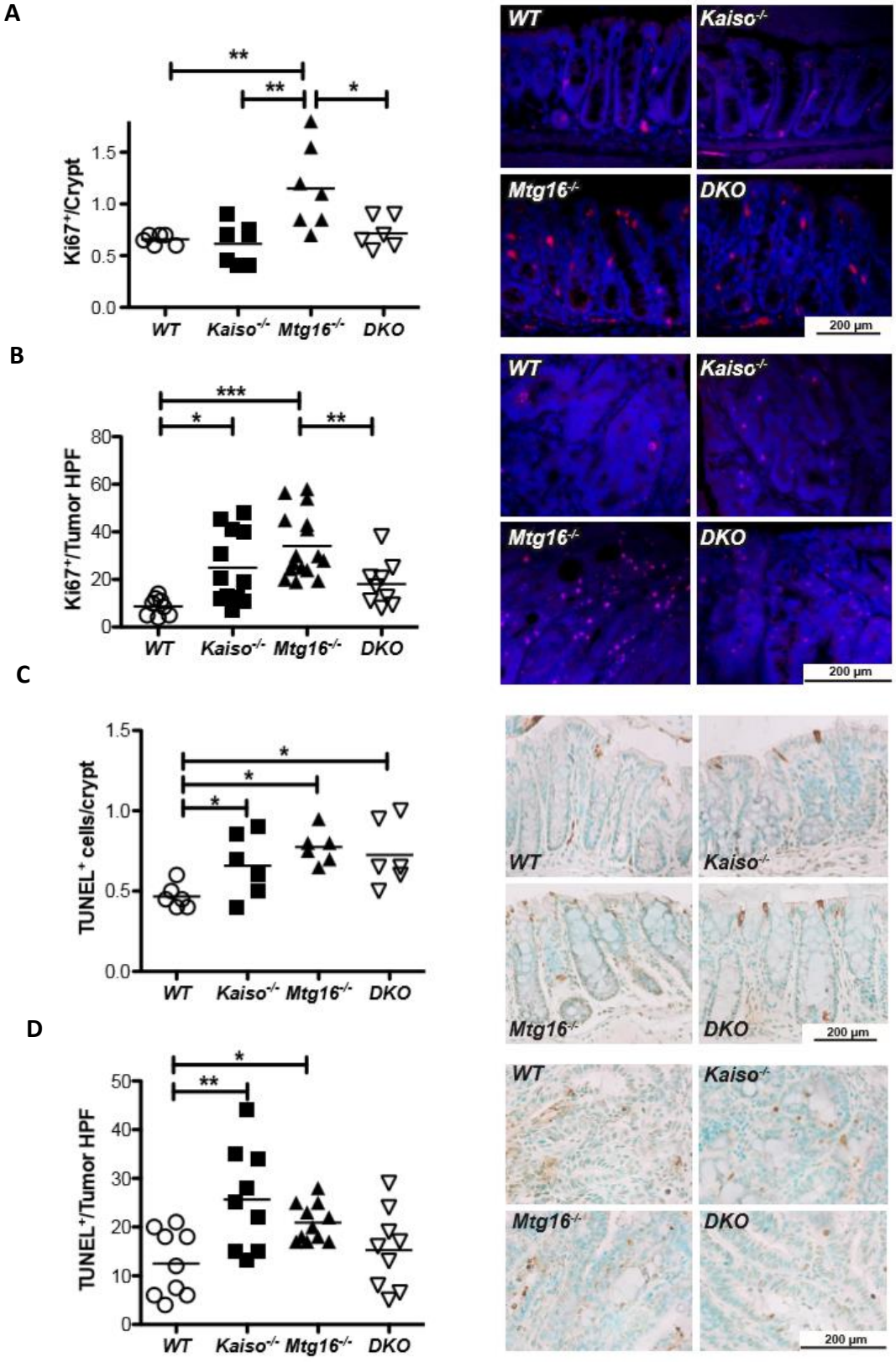
A
B
C
D
Ki67+/Crypt
Ki67+/Tumor HPF
TUNEL+ cells/crypt
TUNEL+/Tumor HPF
WT
Kaiso-/-
Mtg16-/-
DKO
200 μm

*Figure 7.3 Proliferation is increased in tumors and crypts of Mtg16$^{-/-}$ mice and apoptosis is increased in tumors of Kaiso$^{-/-}$ mice. α-Ki67 immunohistochemistry was conducted to identify actively proliferating cells and TUNEL staining was performed to identify apoptotic cells. A. Ki67^{+} cells/crypt determined as averaged positive cells/crypt within 20 crypts per mouse (left) and representative images shown for each genotype (right). B. Ki67^{+} cells/tumor high-powered field (HPF, 40x) averaged for each tumor (left) and representative images of each genotype (right) where red shows Ki67 staining and blue is DAPI nuclear stain. C. TUNEL^{+} cells/crypt determined as averaged positive cells/crypt within 20 crypts per mouse (left) and representative images shown for each genotype (right). D. TUNEL^{+} cells/tumor high-powered field (HPF, 40x) averaged for each tumor (left) and representative images of each genotype (right). *P<0.05, **P<0.01, ***P<0.001.*

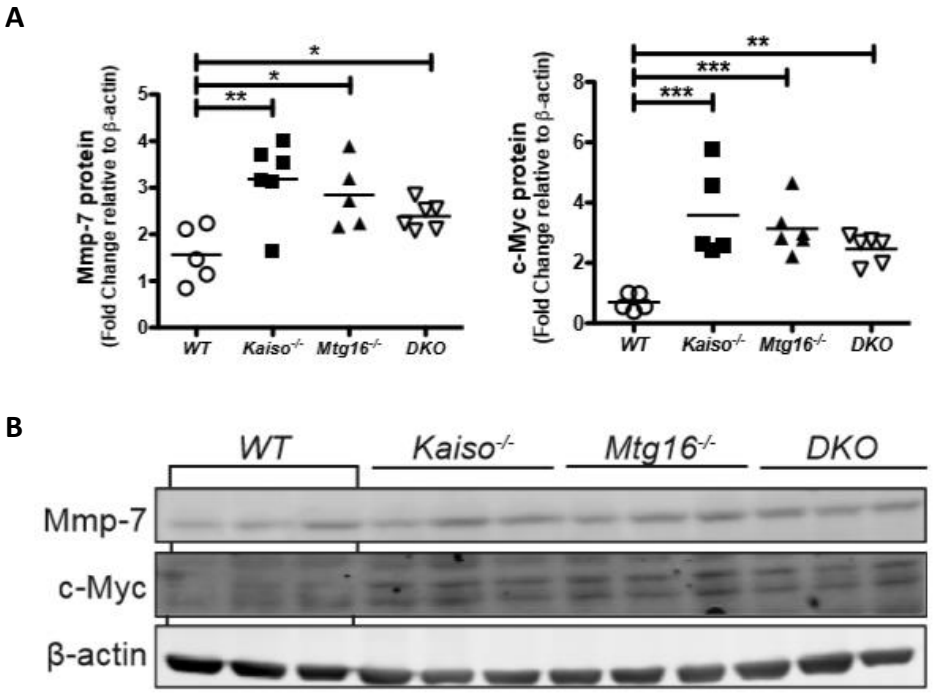

*Figure 7.4 Wnt targets are upregulated in Kaiso$^{-/-}$ and Mtg16$^{-/-}$ mice. A. Quantification of tumor protein expression of matrix metalloproteinase-7 (Mmp7) and c-Myc normalized to β-actin and B. representative western blots from three tumors within each genotype. *P<0.05, **P<0.01, ***P<0.001.*

Kaiso is required for recruitment of tumor-promoting M2 macrophages in Mtg16$^{-/-}$ tumors.

Macrophage polarization to the M2 phenotype is associated with a pro-tumorigenic microenvironment (368). Because we have previously identified an

upregulation of M2 macrophages in *Mtg16*$^{-/-}$ tumors (McDonough et al., submitted), we wanted to determine whether Kaiso was required for this phenotype. Co-staining for F4/80 and Arginase 1 revealed a relative paucity of M2 macrophages in *Kaiso*$^{-/-}$ (17.0±3.1 F4/80^{+}/Arginase I^{+}/tumor HPF) and *DKO* (13.3±1.2 F4/80^{+}/Arginase I^{+}/tumor HPF) tumors with their numbers equaling those of *WT* tumors (10.2±1.2 F4/80^{+}/Arginase I^{+}/tumor HPF), but a substantial increase in M2 macrophages in *Mtg16*$^{-/-}$ tumors (36.0±3.4 F4/80^{+}/Arginase I^{+}/tumor HPF, *P*<0.001, Figure 7.5 A & B) suggesting that the presence of Kaiso is required for recruitment or polarization of M2 macrophages in *Mtg16*$^{-/-}$ mice.

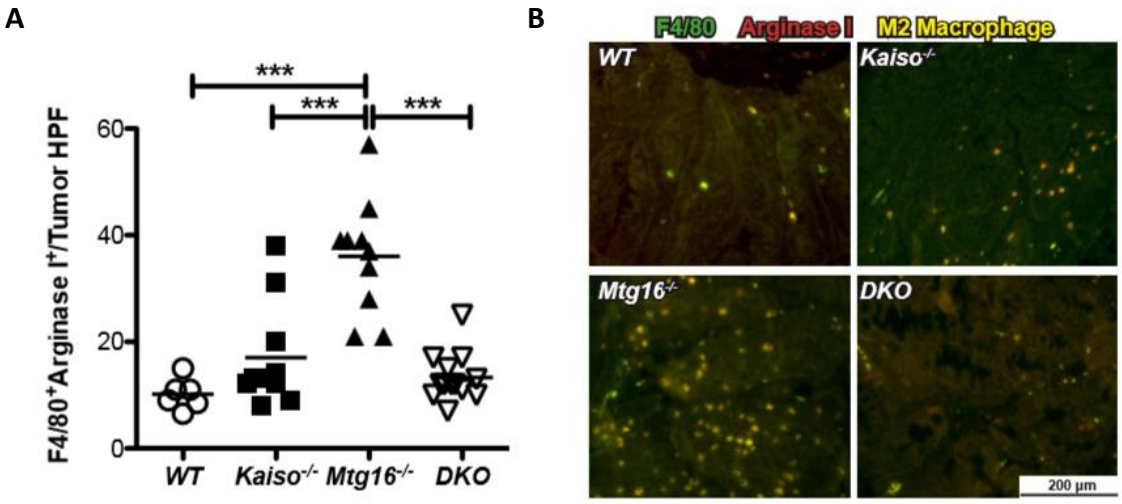

Figure 7.5 Pro-tumorigenic M2 macrophage infiltrate is increased in Mtg16$^{-/-}$ *tumors. α-F4/80 (green) and α-Arginase I (red) immunofluorescence was conducted to identify M2 macrophages. A. Intratumoral M2 macrophage index calculated from number of F4/80/Arginase I-double positive cells per high-powered field (HPF, 40x) and B. Representative images from tumors of each genotype. ***P<0.0001.*

Absence of Kaiso rescues increased tumor-promoting microenvironment seen in Mtg16$^{-/-}$ tumors.

Absence of MTG family members leads to an increase in pro-inflammatory and pro-tumorigenic cytokines in response to injury (269). We, therefore, performed cytokine and chemokine expression analysis from *WT*, *Kaiso*$^{-/-}$, *Mtg16*$^{-/-}$, and *DKO* colons after AOM/DSS treatment. Interestingly, we noted that the inflammatory microenvironment is

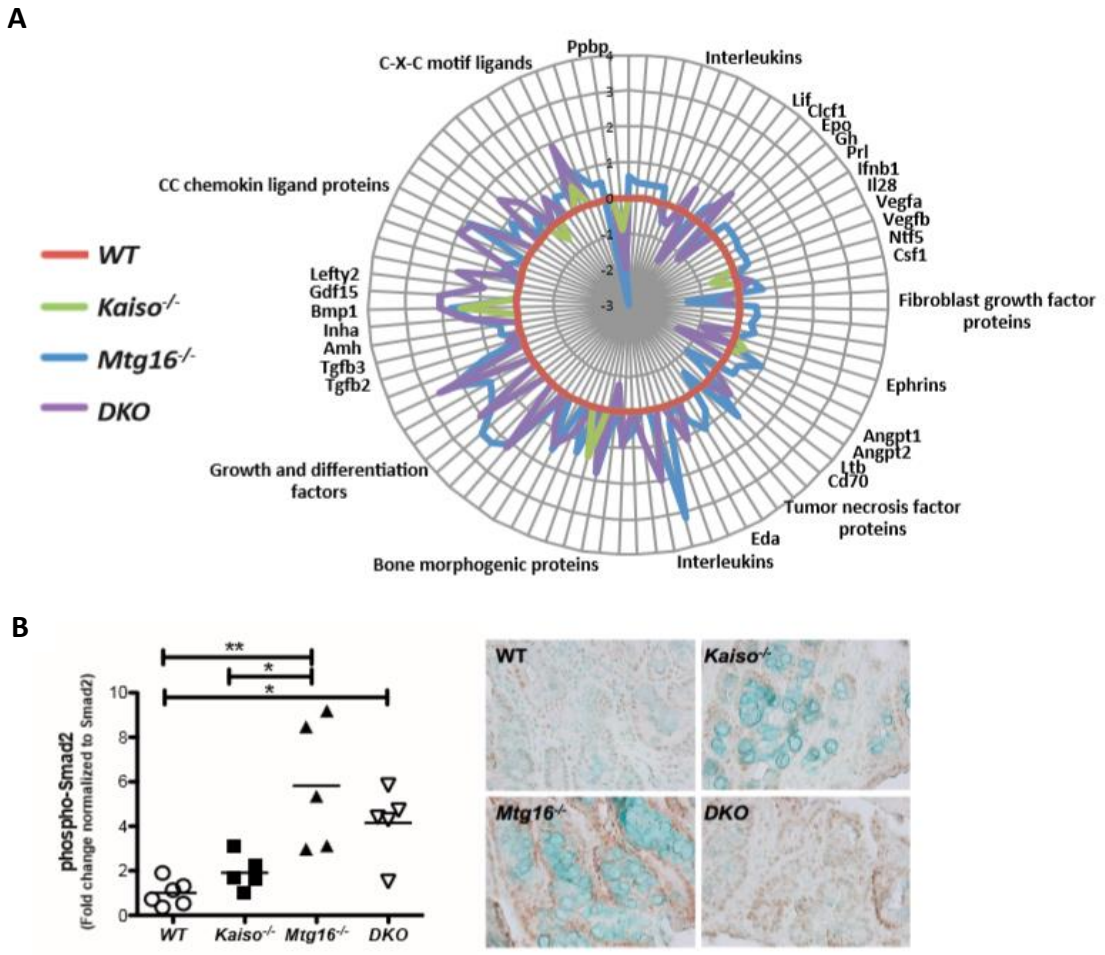

Figure 7.6 TGF and TNF signaling is increased in Mtg16$^{-/-}$ tumors but not in WT, Kaiso$^{-/-}$, or DKO tumors. A. Spider plot demonstrating alterations in cytokine and chemokine mRNA expression in WT (red), Kaiso$^{-/-}$ (green), Mtg16$^{-/-}$ (blue), and DKO (purple) tumors where each concentric circle represents the log fold change in expression for each gene. B. Quantification of tumor protein expression of phosphorylated Smad-2 normalized to total Smad-2 (left) and immunohistochemical staining of tumors from WT, Kaiso$^{-/-}$, Mtg16$^{-/-}$, and DKO mice for phosphorylated Smad-2.

very similar between *WT* and *DKO* mice (Figure 7.6A) with minimal alterations seen in chemokine and cytokine expression. Moreover, as has been demonstrated previously, the *Mtg16*$^{-/-}$ tumor inflammatory milieu is increased substantially compared to WT mice. Specifically, the fibroblast growth factor (FGF), transforming growth factor (TGF), bone morphogenic protein (BMP), and interleukin families are upregulated specifically in *Mtg16*$^{-/-}$ mice compared to *WT* and *Kaiso*$^{-/-}$ mice. Moreover, *DKO* mice show a partial rescue of the increased inflammation seen in *Mtg16*$^{-/-}$ mice (Figure 7.6A).

Because Ingenuity Pathway Analysis identified components of the TGF-β pathway as increased specifically in *Mtg16*$^{-/-}$ tumors compared to tumors from the other genotypes, we wanted to test the expression of a downstream TGF-β target, phosphorylated Smad-2. Analysis of phospho-Smad-2 by both western blot and IHC corroborated an increase in TGF-β signaling in *Mtg16*$^{-/-}$ tumors (*WT*: 1.0±0.2, *Kaiso*$^{-/-}$: 1.9±0.4, *Mtg16*$^{-/-}$: 5.8±1.3, $P<0.01$, *DKO*: 4.2±0.7, relative fold change compared to *WT* and normalized to total Smad-2, $P<0.05$, Figure 7.6B). Interestingly, based on immunohistochemical staining, this increase looks to be associated with the epithelial cells within the tumor and not the immune cells, suggesting that this is an epithelial cell-autonomous effect.

Discussion

Kaiso is a transcriptional repressor that recognizes both methylated DNA and a sequence-specific consensus sequence by utilizing its three zinc fingers for high-affinity

DNA binding (445). Moreover, the interaction between MTG16 and Kaiso has been mapped to this domain. MTG16 is a transcriptional co-repressor and serves as a scaffolding protein upon which repressor complexes are nucleated (444). As such, MTG16 and Kaiso are required for repression of several targets including Mmp7 (418, 444). A great deal has been learned about these proteins through the generation of *Kaiso*$^{-/-}$ and *Mtg16*$^{-/-}$ mice. Though Kaiso is reported to be a transcriptional repressor of S100A4, MTA2, Mmp7 (241, 446, 447), and an activator of Rapsyn (447) and is proposed to be a tumor modifier through its ability to repress tumor suppressor genes in a DNA methylation-dependent manner (247), *Kaiso*$^{-/-}$ mice demonstrate no overt phenotype. A phenotype is unmasked, though, when the mice are crossed with the *Apc*$^{Min/+}$ sporadic tumor model and resistance to intestinal polyposis is demonstrated (251). MTG16 knockout mice, on the other hand, display some very specific gut and stem cell phenotypes. *Mtg16*$^{-/-}$ mice demonstrate increased enterocyte proliferation at baseline and in response to DSS, *Mtg16*$^{-/-}$ mice demonstrate severe colitis (216), and display increased tumorigenesis when subjected to the AOM/DSS inflammatory tumorigenesis protocol (McDonough et al., submitted). Furthermore, *Mtg16*$^{-/-}$ mice also demonstrate hematopoietic stem cell defects (215). These data suggest that, though Kaiso and MTG16 share a subset of targets, loss of repression of exclusive, non-overlapping, targets of each might also influence tumorigenesis.

Because Kaiso and MTG16 cooperate in regulating Wnt signaling and have been implicated in intestinal tumorigenesis, we wanted to determine the requirement for Kaiso in the development of colitis-associated cancer in the absence of Mtg16. In this report,

we demonstrate that absence of Kaiso rescues the pro-injury and tumorigenesis phenotypes observed in *Mtg16*$^{-/-}$ mice after AOM/DSS treatment. This appears to occur via an increase in intratumoral apoptosis and a decrease in pro-inflammatory chemokines and cytokines that normally produce a pro-tumorigenic microenvironment. These data suggest that there is a subset of Kaiso targets that are normally repressed by Kaiso and block tumorigenesis an when Kaiso is lost these genes are activated, masking the Mtg16 phenotype.

Because MTG16 and Kaiso form a repression complex that binds the Mmp7 promoter and impacts its expression (444) and because both proteins have been implicated in Wnt regulation (209, 241), we analyzed Wnt targets Mmp7 and c-Myc for expression changes in the tumors of *WT*, *Kaiso*$^{-/-}$, *Mtg16*$^{-/-}$, and *DKO* mice. Wnt signaling is especially important in colitis-associated carcinoma as Wnt pathway gene methylation is an early event seen in IBD and methylation of several Wnt targets are proposed to serve as biomarkers for IBD-associated neoplasia (448). Interestingly, though, we have demonstrated that Kaiso-dependent methylation binding was not dependent on Mtg16 (444), suggesting differential methylation targets for the two proteins. As expected, we determined that knockout of either MTG16, Kaiso, or both resulted in an increase in Mmp7 and c-Myc expression in the tumors of the respective mice. Interestingly, these Wnt signaling changes do not contribute to the phenotypes seen in response to AOM and DSS administration as the expected increase in tumorigenesis with augmented Wnt signaling does not result in an increase in tumorigenesis in *Kaiso*$^{-/-}$ or *DKO* tumorigenesis

relative to *WT* mice. We therefore wanted to establish the role of injury and inflammation in the observed tumor phenotypes.

In order to analyze the pathways and genes that contribute most significantly to the injury phenotypes seen in *Kaiso*$^{-/-}$, *Mtg16*$^{-/-}$, and *DKO* mice we performed chemokine and cytokine expression analysis. Several interesting targets were increased in *Mtg16*$^{-/-}$ tumors but not tumors isolated from WT, *Kaiso*$^{-/-}$, or *DKO* mice. Ingenuity pathway analysis of these genes identified several pathways modified specifically in *Mtg16*$^{-/-}$ tumors. Amongst some of the most interesting targets were genes within a FGF, TGF, and IL18 signaling axis as well as genes within the BMP, TNF, and IFN signaling axis. Because of the complex role of TGF-β in tumor modulation as well as its central position in the signaling axis identified, we wanted to determine whether the canonical TGF-β target phosphorylated Smad-2 was altered in tumors of *Mtg16*$^{-/-}$ mice compared to *WT*, *Kaiso*$^{-/-}$, and *DKO* mice. Western blotting of tumors from *WT*, *Kaiso*$^{-/-}$, *Mtg16*$^{-/-}$, and *DKO* mice demonstrated that TGF-β signaling is significantly increased in *Mtg16*$^{-/-}$ mice and partially rescued in *DKO* tumors. Immunohistochemical staining corroborates Western blotting and suggests that increased TGF-β signaling is specific for the epithelial compartments of *Mtg16*$^{-/-}$ tumors. While TGF-β signaling has recently been implicated in tumor suppression, there are instances in which this pathway can contribute to tumorigenesis, especially in the context of severe inflammation as is seen in colitis-associated tumorigenesis. TGF-β is a key immunosuppressor and tumors often produce high levels in order to evade immune surveillance (449). TGF-β released by *Mtg16*$^{-/-}$ tumors, coupled with increased M2 macrophage infiltrate, may enable tumors to survive despite massive

inflammatory cytokine expression while also allowing for the pro-tumorigenic properties of that inflammation to contribute to tumorigenesis.

Kaiso and MTG16 interact within a repression complex and share a wide variety of targets, but they also target a separate set of genes. This is made clear by the fact that *Mtg16*$^{-/-}$ and *Kaiso*$^{-/-}$ mice display very different baseline phenotypes and, as reported here, demonstrate very different responses to the AOM/DSS initiation-promotion model. Moreover, knockout of both proteins leads to rescue of the increased tumorigenesis phenotype seen in *Mtg16*$^{-/-}$ mice. These data suggest that Kaiso targets act downstream or are dominant to MTG16 targets in this model system. This report is the first to establish the *Kaiso*$^{-/-}$ response to the AOM/DSS inflammatory carcinogenesis protocol and shows that Kaiso deficiency can rescue the *Mtg16*$^{-/-}$ phenotype.

Acknowledgments

This work was supported by the National Institutes of Health grants DK080221 (CSW), R01AT004821 (KTW), R01AT004821-S1 (KTW), R01DK053620 (KTW), P01CA028842 (KTW), P01CA116087 (KTW), 1F31CA167920 (CWB), and P30 DK058404 (Vanderbilt Digestive Disease Research Center), Merit Review Grants from the Office of Medical Research, Department of Veterans Affairs 1I01BX001426 (CSW) and 1I01BX001453 (KTW), and ACS-RSG 116552 (CSW). The authors thank members of the Williams and Reynolds laboratories for thoughtful discussions about this research project. We would also like to thank the Vanderbilt University Translational Pathology Shared Resource for cutting slides and performing H&E staining.

CHAPTER VIII

SUMMARY, CONCLUSIONS, AND IMPLICATIONS

Selenium as a potential therapeutic target in colitis-associated carcinoma

Amongst important considerations regarding the beneficial supplementation of Se is baseline Se status. Patients presenting with optimal Se levels, 124 ng/ml Se, are unlikely to benefit from Se supplementation. In fact, supranutritional Se levels can be detrimental. Importantly, patients with IBD demonstrate Se deficiency as measured by both plasma Se and Sepp1 levels. While healthy controls have plasma Se levels of 0.84 ± 0.13 mmol/L, patients with UC display Se levels of 0.63 ± 0.25 mmol/L and patients with CD have levels of 0.69 ± 0.25 mmol/L (283). Furthermore, the expression of Sepp1 in healthy controls is 3.4 ± 0.8 μg/ml while expression in patients with CD is 1.8 ± 0.5 μg/ml, a decrease of 53% in the most accurate determinant of Se status (274). This suggests that patients with IBD are Se deficient to an extent where Se supplementation would be beneficial should Se contribute to protection from inflammation, oxidative injury, and tumorigenesis in patients with IBD. It is for this reason that we tested the impact of dietary Se modulation as well as plasma selenoprotein loss in the development of colitis-associated carcinoma. We determine that Se and selenoproteins are protective against injury and tumor development in our model system suggesting that Se supplementation would be beneficial in patients with IBD that demonstrate low Se levels.

Selenium supplementation in reduction of inflammatory injury and cancer risk resulting from IBD.

We have shown that Se deficiency leads to increased morbidity, weight loss, stool scores, and colonic injury as well as increased DNA damage, likely resulting from increased oxidative stress, in response to DSS-induced injury compared to mice fed a Se-sufficient diet. This suggests that Se is protective against oxidative stress and inflammation. Moreover, it indicates that patients with IBD concomitant with low Se levels might have more severe colitis. Ultimately, the question that was posed was whether this increased injury, inflammation, and oxidative stress led to increased tumorigenesis. In response to the AOM/DSS protocol, we observed increased tumor number and progression to high-grade dysplasia. Taken together, these data indicate that Se supplementation could benefit patients with risk of CAC and Se-low status and, importantly, this supplementation might be able to not only decrease IBD disease severity, but also decrease risk of cancer. It is most likely through impact on selenoprotein expression that Se protects against inflammation and tumorigenesis, so we sought to determine the impact of loss of the plasma selenoproteins on development of CAC.

Selenoproteins in colitis-associated carcinoma

Sepp1 expression is decreased as much as 50% in IBD compared to healthy controls (274). We note that Sepp1 haploinsufficiency leads to a dramatic increase in tumorigenesis indicating that Se alterations already seen in patients with IBD could be actively contributing to CAC through the decreased expression of a single selenoprotein.

As we also note that Gpx3 loss leads to increased tumorigenesis and there is strong evidence to indicate that other selenoproteins contribute to tumor promotion, selenoprotein expression alterations could be significant contributors to CAC. Selenoproteins likely protect from tumorigenesis through protection from DNA damage, reduction of oxidative stress, and modulation of signaling pathways such as the Wnt pathway to which Sepp1 deficiency contributes significantly. A more detailed understanding of the impact of other selenoproteins on CAC or other cancers in which Se deficiency is commonplace would greatly benefit the design and development of intervention trials.

Contrary to expectations, complete Sepp1 loss leads to decreased tumor burden despite increased DNA damage and inflammatory injury. Because AOM-only experiments demonstrate that Sepp1 loss leads to increased ACF formation and DSS as a single modality leads to increased injury in *Sepp1*$^{-/-}$ mice, we predict that the decreased tumorigenesis observed in *Sepp1*$^{-/-}$ mice is the result of increased clearance of initiated epithelial cells. This indicates to us that complete Sepp1 loss is not necessarily detrimental to tumorigenesis, but instead overwhelms the antioxidant system making cell survival problematic in response to stress. We predict that, if there was a condition in humans in which Sepp1 was completely lost, the effects on cell survival in response to stress would be catastrophic. As decreased, but not completely lost, Sepp1 expression is observed in people with IBD and genetic variants, the *Sepp1*$^{+/-}$ phenotype is the more applicable model in this situation and best demonstrates the impact of Sepp1 loss on IBD and CAC.

Finally, we have noted an increase in Wnt signaling in mice lacking Sepp1 and a dependence upon Wnt signaling for the increased "stemness" that is seen in *Sepp1*$^{-/-}$ enteroids. This suggests that the Wnt pathway, a signaling pathway that is commonly upregulated in CRC and CAC, plays an integral role in the pro-tumorigenic phenotype in response to Sepp1 loss. It is possible that patients with SNPs in the promoter regions of *SEPP1* may not benefit from Se supplementation due to inability to promote transcription despite an influx of Se. In these cases, disruption of the signaling pathway that is activated might be beneficial. Unfortunately, until recently, the Wnt pathway has been a very difficult anti-cancer target. Pan-Wnt inhibitors inhibit both canonical and non-canonical Wnt signaling leading to far-reaching and detrimental non-specific effects. Even targeting some of the most downstream processes in Wnt signaling, such as inhibiting β-catenin, impact the binding of β-catenin to α-catenin and E-cadherin, disrupting cell adhesion (274). Notably, Gonsalves *et al*. have developed inhibitors of the β-catenin-TCF4 interaction that display minimal to no impact on non-canonical Wnt signaling or the Hedgehog, JAK/STAT, or Notch signaling pathways (450). Depending on the feasibility of use of these inhibitors on humans, they might preferentially benefit patients with IBD and *SEPP1* SNPs.

The impact of Mtgr1 on gut homeostasis and its misregulation in colitis-associated carcinoma

We have observed that Mtgr1 is expressed in the crypt base and overexpressed in the tumors of mice subjected to the AOM/DSS protocol compared to "normal" adjacent

tissue. Moreover, we note an increase in *MTGR1* expression in CRC samples compared to normal controls indicating that Mtgr1 expression might be tumor supportive. Interestingly, *Mtgr1*$^{-/-}$ mice are protected from inflammatory tumorigenesis, due at least in part to a significant increase in colonic apoptosis. This increase in cellular death is likely due to severe epithelial injury and inflammation typified by increased $CD3^{+}$ and natural killer T cells as well as macrophages. These phenotypes are dependent on epithelial injury as there is no difference in ACF when animals were treated with AOM as a single modality and the effect is not hematopoietic cell-autonomous because bone marrow transplantation does not impact the phenotype. Similar to results seen in *Sepp1*$^{-/-}$ mice, we predict that Mtgr1 is required for the survival of initiated epithelial cells in response to inflammation. Contrary to what is seen with complete loss of Sepp1, *Mtgr1* expression is increased in tumors of mice subjected to the AOM/DSS protocol as well as in human CRC samples. This suggests that, while at its core loss of Sepp1 expression is tumor-promoting, loss of Mtgr1 is tumor-suppressing. Thus, disruption of Mtgr1 skews the inflammatory microenvironment to the extent that anti-tumorigenic inflammatory cell recruitment is increased and damaged epithelial cells are destroyed. Through its potential impact on tumor immunosurveillance, Mtgr1 disruption could serve as a therapeutic approach in treatment of inflammatory cancers such as CAC.

The Kaiso-MTG16 interaction and how it modifies colitis-associated carcinoma

Kaiso and MTG16 share several functional similarities, including their abilities to repress Wnt signaling, bind co-repressors, and impact processes that influence

tumorigenesis. We, therefore, wanted to determine whether these two proteins could interact and, ultimately, whether this interaction had a functional impact on AOM/DSS-induced tumorigenesis. We found that Kaiso and MTGs interact in inhibitory complexes and target genes that are important in oncogenesis, including Mmp7. We expected knockout of either of the proteins alone or in tandem would result in similar AOM/DSS-induced tumor burdens as loss of either of the proteins in the complex should have destroyed the entire complex and released targets from repression.

Contrary to these expectations, knockout of either one or both of these proteins resulted in very different phenotypes suggesting that the Kaiso-MTG16 complex is not the only factor that controls tumorigenesis. Specifically, we see in this model system that, while *Mtg16*$^{-/-}$ mice display increased injury and tumorigenesis, Kaiso loss does not impact tumorigenesis in AOM/DSS mice relative to WT mice. Significantly, knockout of both Mtg16 and Kaiso results in rescue of the *Mtg16*$^{-/-}$ phenotype suggesting that, though Kaiso and Mtg16 share several targets, it is the transcriptional targets that they do not share that distinguish their responses to the AOM/DSS protocol. There is likely a subset of Kaiso targets that are normally repressed by Kaiso and block tumorigenesis which, when Kaiso is lost, are activated, masking the Mtg16 phenotype. Further exploration into these genes could provide important targets for anti-tumorigenic therapeutics, especially in people that express one of the 4 identified MTG mutations or demonstrate decreased intratumoral *MTG16* expression. These data establish a foundation for further research into the genes that may contribute to the protective effect of Kaiso in a subset of patients with decreased MTG16 expression or activity.

CHAPTER IX

FUTURE DIRECTIONS

Selenium and selenoproteins in modification of sporadic colorectal cancer

We hypothesized that, as important regulators of reactive oxygen species and inflammation, selenoproteins would play a critical role in protection against CAC. Interestingly, inflammation is not only important in the development of CAC, but it is also associated with pathogenesis of sporadic CRC (451). Moreover, our work has shown that Se and Sepp1 depletion induces Wnt signaling, a key contributor in colonic tumorigenesis. Both lines of evidence point toward a potential role for Se and selenoproteins in development of sporadic CRC. As Se and Sepp1 modulation of tumorigenesis is partially dependent on Wnt signaling, the commonly utilized *Apc*$^{min/+}$ model of sporadic tumorigenesis, which relies on mutagenesis of the murine homolog of the Apc gene, is not an ideal model as it could mask some of the impact of Se deficiency or Sepp1 loss. Recently, a genetic model of intestinal polyposis that is independent of dysregulated canonical Wnt signaling was developed by the lab of Robert Coffey utilizing the leucine-rich repeats and immunoglobin-like domains 1 (Lrig1) protein. Lrig1 is a transmembrane protein that inhibits ErbB signaling in an inducible manner (452). Lrig1 marks a subset of intestinal stem cells that are relatively quiescent until they are mobilized to repopulate the colonic crypt in response to tissue damage. The *Lrig1-CreERT2/CreERT2* mouse model results in low-grade adenomas within the duodenum by 5 to 6 months of age with 88%

penetrance (453). This model system is especially applicable to the analysis of phenotypes in response to dietary Se deficiency or Sepp1 knockout because, though it is not a model of CAC, the Lrig1 knockout mouse displays significant intratumoral inflammation (correspondence with Robert Coffey) which will model the inflammation commonly seen during the development of sporadic CRC. Monitoring the effect of dietary Se deficiency and Sepp1 depletion in this model will allow us to determine whether Se and Sepp1 can protect against sporadic CRC as well as inflammatory cancer, expanding the list of cancer types impacted by the essential micronutrient Se and one of the predominant plasma selenoproteins. In addition, this model system would allow other selenoproteins, such as Gpx3, to be studied, potentially establishing an important link between selenoproteins and CRC.

Hematopoietic and epithelial cell-autonomous effects of selenoprotein P modulation on cancer development

To our surprise, our data indicate that, despite the preponderance of hepatic Sepp1 within the body, liver-derived Sepp1 does not impact tumorigenesis in response to the AOM/DSS protocol. Studies in intestinal organoids suggest that epithelial Sepp1 loss has an effect on several tumorigenic properties, including increased stem cell characteristics, augmented proliferation, and increased ROS production in response to oxidative stress. Enteroid studies suggest that it might be through the epithelial compartment that Sepp1 loss is having an impact on tumorigenesis. It is for this reason

that epithelial-specific knockout models would benefit the understanding of the role of Sepp1 in CAC development.

The *villin-cre-ERT2* model of tissue-specific and inducible cre-mediated recombination allows for epithelial-specific knockout of genes of interest (454). Crossing the *Sepp1*$^{Fl/Fl}$ mouse onto this background will enable epithelial knockout of Sepp1. These mice could then be subjected to the AOM/DSS protocol and monitored for tumorigenesis, establishing the first evidence that non-hepatic Sepp1 is essential for tumor modification *in vivo*.

Sepp1 is one of the most highly induced genes in response to polarization of M2 and tumor –associated macrophages (375, 381) suggesting that Sepp1 may play a role in macrophage polarization. We identified a mild polarization defect in bone marrow macrophages isolated from *Sepp1*$^{+/-}$ mice, supporting the hypothesis that Sepp1 has an impact on macrophage activity. In addition, Sepp1 knockdown leads to amplified inflammation (172) which may be the result of more than just alterations in macrophage polarization. Sepp1 might be acting within the inflammatory compartment to modify tumorigenesis. In order to test this hypothesis, crossing the floxed Sepp1 mouse with the *Mx1-cre* mouse (455) would enable the cre-mediated inducible inactivation of Sepp1 in the bone marrow as well as several tissues including the liver, heart, spleen, and kidney. In order to avoid the complex effects of Sepp1 deletion in other tissues, bone marrow transplant could be used to insure that recombination only occurs within the bone marrow compartment, thus resulting in knockout of Sepp1 in the hematopoietic lineages. This tool will not only enable the analysis of the effects of Sepp1 loss in the hematopoietic

compartment on AOM/DSS carcinogenesis, but also allow for the characterization of immune cell function alterations *in vivo*.

Pathway alterations in response to modulation of selenoprotein P expression in normal physiology and response to oxidative stress

We have identified increased Wnt signaling in *Sepp1*$^{-/-}$ tumors and a potential dependence on Wnt signaling in the stem cell phenotype of *Sepp1*$^{-/-}$ enteroids. Wnt inhibitors will enable us to solidify the role of Wnt signaling in *Sepp1*$^{-/-}$ phenotypes. The monoclonal antibody OMP-18R5 binds to Frizzled, the receptor through which the Wnt/β-catenin pathway is initiated and can be utilized *in vivo* to inhibit Wnt signaling (456). The utilization of the OMP-18R5 inhibitor prior to and post-AOM/DSS protocol in *Sepp1*$^{+/-}$ and *Sepp1*$^{-/-}$ mice would enable the determination of the role of Wnt signaling in tumor initiation and promotion, respectively, in these genotypes. The use of this antibody would also establish a role for Wnt signaling in *Sepp1*$^{-/-}$ enteroid phenotypes, both during initiation of enteroids and upon establishment of fully differentiated enteroid cultures.

Enteroid experiments also suggest that Notch and EGF signaling may contribute to *Sepp1*$^{-/-}$ phenotypes. In order to gain unbiased insight into pathways modulated by Sepp1 loss, it would be beneficial to perform RNAseq analysis of enteroids isolated from *WT* and *Sepp1*$^{-/-}$ mice. We have performed this analysis in tumors from these mice, but the tumor microenvironment is incredibly complex, containing a plethora of cell types that might skew RNAseq results. The benefit of RNAseq analysis in enteroids is that it will analyze pathway changes in the epithelial compartment alone. Based on the pathway and

gene alterations identified, experiments can be designed that test for the impact of those pathways on *Sepp1*$^{-/-}$ phenotypes both *in vitro* and *in vivo* using either inhibitors or overexpression of essential pathway components, depending on the identified changes of the pathway of interest. Additionally, the enteroid system allows for the analysis of gene changes in response to events such as oxidative stress. RNAseq analysis if hydrogen peroxide or diquat-treated enteroids could establish pathways that are altered in *Sepp1*$^{-/-}$ epithelial cells in response to oxidative stress compared to *WT* epithelial cells.

Myeloid translocation gene modulation in intestinal organoids: stem cell properties and mechanisms for altered cellular activities

The identification of MTGs in leukemia translocations suggests that the MTGs play roles in stem cell properties. In addition, we have noted alterations in apoptosis and proliferation in cells with MTG knockdown. While we have dismissed a hematopoetic cell-autonomous effect of MTG knockout on CAC development, we have not established that the effect is epithelial in nature. The intestinal organoid model that we have leveraged to establish a role for Sepp1 in epithelial phenotypes will be an exceptional system with which to monitor the effects of Mtgr1 loss on epithelial phenotypes. Monitoring of stem cell properties including plating efficiency, stem spheroid percentage, percentage of branching enteroids and number of branches per enteroid will establish a role for Mtgr1 in stem cell fitness and/or characteristics. Moreover, analysis of cell types within the fully differentiated enteroid will confirm the effect of Mtgr1 on lineage allocation when microenvironmental influence is no longer a contributing factor in cellular differentiation.

Finally, enteroids will be used to monitor proliferation and apoptosis as well as pathway dependence in *Mtgr1*$^{-/-}$ epithelial cells. Taken together, these analyses will determine the mechanisms by which Mtgr1 loss is able to suppress tumorigenesis or, if upon taking the severe inflammation resulting from DSS out of the equation, Mtgr1 loss actually promotes tumorigenic properties.

Absence of Mtgr1 in the AOM/DSS model results in a multilineage inflammatory cell infiltrate. This influx of inflammatory cells is not due to a hematopoietic cell autonomous effect, suggesting that it is recruitment that controls this phenotype. To date, there have been no attempts to culture enteroids with immune cell subtypes, but the enteroid culturing parameters make this a feasible option. For one, immune cells, like enteroids, can be plated in Matrigel and monitored for alterations in motility and activity. Secondly, as enteroids are isolated from mice, immune cells can also be isolated from mice of the same strain, or even the same mouse from which the enteroids are derived, and cross-species immunity can be avoided. Finally, enteroids and immune cells can be isolated from *WT* or knockout mice, again of the same background, and mixed to monitor how loss of the protein of interest in either compartment contributes to the observed phenotypes. Co-culturing a combination of *WT* and *Mtgr1*$^{-/-}$ enteroids and immune cells, such as naïve macrophages, will give significant insight into the mechanism of increased infiltration and altered macrophage polarization in *Mtgr1*$^{-/-}$ tumors.

Mtgr1 in sporadic colorectal cancer

We have shown that *Mtgr1*$^{-/-}$ mice are protected from tumorigenesis in response to the AOM/DSS inflammatory carcinogenesis protocol, and that this protection is likely the result of clearance of initiated cells by an anti-tumorigenic microenvironment. Furthermore, we have identified an increase in *Mtgr1* expression in human CRC. These data beg the question, what is the impact of Mtgr1 loss on development of sporadic CRC? Similar to *Sepp1*$^{-/-}$ experiments outlined above, the *Lrig1-CreERT2/CreERT2* mouse will serve as an optimal background for the *Mtgr1*$^{-/-}$ cross. For one, the MTGs are repressors of canonical Wnt signaling making the *Apc*$^{Min/+}$ model less than ideal as it relies on augmented Wnt signaling for the development of intestinal polyps. If MTGs repress Wnt, knockout of Mtgr1 will result in increased Wnt signaling which will be masked by the Apc mutational activation of Wnt signaling. Lrig1 knockout, on the other hand, will allow for the induction of tumorigenesis in a Wnt-independent manner with the added benefit of smoldering inflammation. The determination of a *Mtgr1*$^{-/-}$ phenotype in a sporadic CRC model will expand the role of Mtgr1 into a realm beyond just CAC and will add insight into the role of DSS-induced injury in the *Mtgr1*$^{-/-}$ AOM/DSS phenotype.

The impacts of MTG colorectal cancer mutations on cancer risk and cellular properties

As mentioned in the Introduction, there are several non-synonymous mutations that have been identified in MTG8 and MTG16 in colorectal and breast cancer (228, 229). Preliminary work in our lab has demonstrated decreased TCF4 binding and decreased TOPFLASH Wnt inhibition with several of these MTG mutations, indicating severe

functional abnormalities in the repression capabilities of these mutants. It will be very interesting to develop a transgenic mouse model expressing the most severe mutation based on Wnt repressive capabilities, but in the short term, enteroids will serve as a great model for MTG mutant analysis. Overexpression of the *Mtg16* mutants in *Mtg16*$^{-/-}$ enteroids will enable analysis of epithelial phenotypes including lineage allocation, proliferation, apoptosis, and stem cell characteristics in response to abnormal Mtg16 function. Importantly, this will give insight into the mechanisms by which these mutations might be beneficial to tumorigenesis within a closed and well-controlled system. An understanding of the molecular mechanisms by which these mutations promote tumorigenesis will likely open avenues for specific therapeutic interventions in patients with MTG mutations.

Additional future directions

- Determine the receptor for Sepp1 in enterocytes.
- Establish the isoforms of Sepp1 made within enterocytes and hematopoietic cells. Subsequently, determine the activity/roles of each isoform in enteroids.
- Develop *Gpx3*$^{-/-}$*;Sepp1*$^{-/-}$ double knockout mice so that there is complete absence of plasma selenoproteins. Analyze mice and enteroids at baseline and in response to stress for intestinal phenotypes including proliferation changes, DNA damage, apoptosis, and macrophage polarization.

- Irradiate enteroids from *Sepp1*$^{-/-}$ mice and determine DNA damage and establish alterations in repair pathways.
- Treat *Sepp1*$^{-/-}$ enteroids with H_2O_2 or diquat. Determine if this alters DNA damage and, if so, perform RNAseq to determine genes mutated and the functional significance of these mutations (i.e. overexpression, underexpression).
- Isolate enteroids from *Sepp1*^{U40S} and *Sepp1*$^{\Delta 240\text{-}361}$ mice and establish which domains are important for the identified *Sepp1*$^{-/-}$ phenotypes in enteroids.
- We have found that the truncation of Sepp1 leads to alterations in tumorigenesis in response to AOM and DSS but that loss of the liver-specific form of Sepp1 does not show a phenotype, suggesting that the selenium-rich C-terminal domain serves a function aside from delivery of selenium to enterocytes and that this function is important for the inhibition of inflammatory tumorigenesis. Utilize *Sepp1*$^{\Delta 240\text{-}361}$ enteroids to determine pathway and functional changes that result from truncation. These enteroids can also be compared with *Sepp1*$^{-/-}$ enteroids by RNAseq to identify the pathway alterations that are dependent upon the selenium-rich region as opposed to the other domain of Sepp1.

REFERENCES

1. Jemal A, Siegel R, Ward E, Hao Y, Xu J, Murray T, et al. Cancer statistics, 2008. CA Cancer J Clin. 2008;58(2):71-96. Epub 2008/02/22. doi: 10.3322/CA.2007.0010. PubMed PMID: 18287387.

2. Quante M, Wang TC. Inflammation and stem cells in gastrointestinal carcinogenesis. Physiology (Bethesda). 2008;23:350-9. Epub 2008/12/17. doi: 10.1152/physiol.00031.2008. PubMed PMID: 19074742; PubMed Central PMCID: PMC2705777.

3. Loftus EV, Jr., Sandborn WJ. Epidemiology of inflammatory bowel disease. Gastroenterol Clin North Am. 2002;31(1):1-20. Epub 2002/07/19. PubMed PMID: 12122726.

4. Abraham C, Cho JH. Inflammatory bowel disease. N Engl J Med. 2009;361(21):2066-78. Epub 2009/11/20. doi: 10.1056/NEJMra0804647. PubMed PMID: 19923578; PubMed Central PMCID: PMC3491806.

5. Nieminen U, Jussila A, Nordling S, Mustonen H, Farkkila MA. Inflammation and disease duration have a cumulative effect on the risk of dysplasia and carcinoma in IBD: A case-control observational study based on registry data. Int J Cancer. 2013. Epub 2013/06/26. doi: 10.1002/ijc.28346. PubMed PMID: 23797639.

6. Beaugerie L, Svrcek M, Seksik P, Bouvier AM, Simon T, Allez M, et al. Risk of colorectal high-grade dysplasia and cancer in a prospective observational cohort of patients with inflammatory bowel disease. Gastroenterology. 2013;145(1):166-75 e8. Epub 2013/04/02. doi: 10.1053/j.gastro.2013.03.044. PubMed PMID: 23541909.

7. Jess T, Gamborg M, Matzen P, Munkholm P, Sorensen TI. Increased risk of intestinal cancer in Crohn's disease: a meta-analysis of population-based cohort studies. Am J Gastroenterol. 2005;100(12):2724-9. Epub 2006/01/06. doi: 10.1111/j.1572-0241.2005.00287.x. PubMed PMID: 16393226.

8. Jess T, Rungoe C, Peyrin-Biroulet L. Risk of colorectal cancer in patients with ulcerative colitis: a meta-analysis of population-based cohort studies. Clin Gastroenterol Hepatol. 2012;10(6):639-45. Epub 2012/02/01. doi: 10.1016/j.cgh.2012.01.010. PubMed PMID: 22289873.

9. Jess T, Simonsen J, Jorgensen KT, Pedersen BV, Nielsen NM, Frisch M. Decreasing risk of colorectal cancer in patients with inflammatory bowel disease over 30 years. Gastroenterology. 2012;143(2):375-81 e1; quiz e13-4. Epub 2012/04/24. doi: 10.1053/j.gastro.2012.04.016. PubMed PMID: 22522090.

10. Herrinton LJ, Liu L, Levin TR, Allison JE, Lewis JD, Velayos F. Incidence and mortality of colorectal adenocarcinoma in persons with inflammatory bowel disease from 1998 to 2010. Gastroenterology. 2012;143(2):382-9. Epub 2012/05/23. doi: 10.1053/j.gastro.2012.04.054. PubMed PMID: 22609382.

11. Neumann H, Vieth M, Langner C, Neurath MF, Mudter J. Cancer risk in IBD: how to diagnose and how to manage DALM and ALM. World J Gastroenterol. 2011;17(27):3184-91. Epub 2011/09/14. doi: 10.3748/wjg.v17.i27.3184. PubMed PMID: 21912466; PubMed Central PMCID: PMC3158393.

12. Nguyen GC, Bressler B. A tale of two cohorts: are we overestimating the risk of colorectal cancer in inflammatory bowel disease? Gastroenterology. 2012;143(2):288-90. Epub 2012/06/26. doi: 10.1053/j.gastro.2012.06.027. PubMed PMID: 22727998.

13. Rubin DT, Cruz-Correa MR, Gasche C, Jass JR, Lichtenstein GR, Montgomery EA, et al. Colorectal cancer prevention in inflammatory bowel disease and the role of 5-aminosalicylic acid: a clinical review and update. Inflamm Bowel Dis. 2008;14(2):265-74. Epub 2007/10/13. doi: 10.1002/ibd.20297. PubMed PMID: 17932965.

14. Quante M, Varga J, Wang TC, Greten FR. The gastrointestinal tumor microenvironment. Gastroenterology. 2013;145(1):63-78. Epub 2013/04/16. doi: 10.1053/j.gastro.2013.03.052. PubMed PMID: 23583733.

15. Itzkowitz SH, Yio X. Inflammation and cancer IV. Colorectal cancer in inflammatory bowel disease: the role of inflammation. Am J Physiol Gastrointest Liver Physiol. 2004;287(1):G7-17. Epub 2004/06/15. doi: 10.1152/ajpgi.00079.2004

287/1/G7 [pii]. PubMed PMID: 15194558.

16. Karin M, Lawrence T, Nizet V. Innate immunity gone awry: linking microbial infections to chronic inflammation and cancer. Cell. 2006;124(4):823-35. Epub 2006/02/25. doi: 10.1016/j.cell.2006.02.016. PubMed PMID: 16497591.

17. Allen IC, TeKippe EM, Woodford RM, Uronis JM, Holl EK, Rogers AB, et al. The NLRP3 inflammasome functions as a negative regulator of tumorigenesis during colitis-associated cancer. J Exp Med. 2010;207(5):1045-56. Epub 2010/04/14. doi: 10.1084/jem.20100050. PubMed PMID: 20385749; PubMed Central PMCID: PMC2867287.

18. Hussain SP, Hofseth LJ, Harris CC. Radical causes of cancer. Nat Rev Cancer. 2003;3(4):276-85. Epub 2003/04/03. doi: 10.1038/nrc1046. PubMed PMID: 12671666.

19. Mangerich A, Knutson CG, Parry NM, Muthupalani S, Ye W, Prestwich E, et al. Infection-induced colitis in mice causes dynamic and tissue-specific changes in stress response and DNA damage leading to colon cancer. Proc Natl Acad Sci U S A. 2012;109(27):E1820-9. Epub 2012/06/13. doi: 10.1073/pnas.1207829109. PubMed PMID: 22689960; PubMed Central PMCID: PMC3390855.

20. Meira LB, Bugni JM, Green SL, Lee CW, Pang B, Borenshtein D, et al. DNA damage induced by chronic inflammation contributes to colon carcinogenesis in mice. J Clin Invest. 2008;118(7):2516-25. Epub 2008/06/04. doi: 10.1172/JCI35073. PubMed PMID: 18521188; PubMed Central PMCID: PMC2423313.

21. Olipitz W, Wiktor-Brown D, Shuga J, Pang B, McFaline J, Lonkar P, et al. Integrated molecular analysis indicates undetectable change in DNA damage in mice after continuous irradiation at ~ 400-fold natural background radiation. Environ Health Perspect. 2012;120(8):1130-6. Epub 2012/04/28. doi: 10.1289/ehp.1104294. PubMed PMID: 22538203; PubMed Central PMCID: PMC3440074.

22. Kraus S, Arber N. Inflammation and colorectal cancer. Current opinion in pharmacology. 2009;9(4):405-10. Epub 2009/07/11. doi: 10.1016/j.coph.2009.06.006. PubMed PMID: 19589728.

23. Colotta F, Allavena P, Sica A, Garlanda C, Mantovani A. Cancer-related inflammation, the seventh hallmark of cancer: links to genetic instability. Carcinogenesis. 2009;30(7):1073-81. Epub 2009/05/27. doi: 10.1093/carcin/bgp127. PubMed PMID: 19468060.

24. Cummins JM, He Y, Leary RJ, Pagliarini R, Diaz LA, Jr., Sjoblom T, et al. The colorectal microRNAome. Proc Natl Acad Sci U S A. 2006;103(10):3687-92. Epub 2006/03/01. doi: 10.1073/pnas.0511155103. PubMed PMID: 16505370; PubMed Central PMCID: PMC1450142.

25. Grady WM, Carethers JM. Genomic and epigenetic instability in colorectal cancer pathogenesis. Gastroenterology. 2008;135(4):1079-99. Epub 2008/09/09. doi: S0016-5085(08)01451-0 [pii]

10.1053/j.gastro.2008.07.076. PubMed PMID: 18773902; PubMed Central PMCID: PMC2866182.

26. Oving IM, Clevers HC. Molecular causes of colon cancer. Eur J Clin Invest. 2002;32(6):448-57. Epub 2002/06/13. PubMed PMID: 12059991.

27. Perucho M. Tumors with microsatellite instability: many mutations, targets and paradoxes. Oncogene. 2003;22(15):2223-5. Epub 2003/04/18. doi: 10.1038/sj.onc.1206580. PubMed PMID: 12700658.

28. Sabates-Bellver J, Van der Flier LG, de Palo M, Cattaneo E, Maake C, Rehrauer H, et al. Transcriptome profile of human colorectal adenomas. Molecular cancer research : MCR. 2007;5(12):1263-75. Epub 2008/01/04. doi: 10.1158/1541-7786.MCR-07-0267. PubMed PMID: 18171984.

29. Grivennikov SI. Inflammation and colorectal cancer: colitis-associated neoplasia. Seminars in immunopathology. 2013;35(2):229-44. Epub 2012/11/20. doi: 10.1007/s00281-012-0352-6. PubMed PMID: 23161445; PubMed Central PMCID: PMC3568220.

30. Karin M, Greten FR. NF-kappaB: linking inflammation and immunity to cancer development and progression. Nat Rev Immunol. 2005;5(10):749-59. Epub 2005/09/22. doi: 10.1038/nri1703. PubMed PMID: 16175180.

31. Li J, Liu Y, Wang B, Xu Y, Ma A, Zhang F, et al. Myeloid TGF-beta signaling contributes to colitis-associated tumorigenesis in mice. Carcinogenesis. 2013. Epub 2013/05/23. doi: 10.1093/carcin/bgt172. PubMed PMID: 23695722.

32. Bollrath J, Phesse TJ, von Burstin VA, Putoczki T, Bennecke M, Bateman T, et al. gp130-mediated Stat3 activation in enterocytes regulates cell survival and cell-cycle progression during colitis-associated tumorigenesis. Cancer Cell. 2009;15(2):91-102. Epub 2009/02/03. doi: 10.1016/j.ccr.2009.01.002. PubMed PMID: 19185844.

33. Grivennikov S, Karin E, Terzic J, Mucida D, Yu GY, Vallabhapurapu S, et al. IL-6 and Stat3 are required for survival of intestinal epithelial cells and development of colitis-associated cancer. Cancer Cell. 2009;15(2):103-13. Epub 2009/02/03. doi: S1535-6108(09)00002-6 [pii]

10.1016/j.ccr.2009.01.001. PubMed PMID: 19185845; PubMed Central PMCID: PMC2667107.

34. Langowski JL, Zhang X, Wu L, Mattson JD, Chen T, Smith K, et al. IL-23 promotes tumour incidence and growth. Nature. 2006;442(7101):461-5. Epub 2006/05/12. doi: 10.1038/nature04808. PubMed PMID: 16688182.

35. Yen D, Cheung J, Scheerens H, Poulet F, McClanahan T, McKenzie B, et al. IL-23 is essential for T cell-mediated colitis and promotes inflammation via IL-17 and IL-6. J Clin Invest. 2006;116(5):1310-6. Epub 2006/05/04. doi: 10.1172/JCI21404. PubMed PMID: 16670770; PubMed Central PMCID: PMC1451201.

36. Gupta RA, Dubois RN. Colorectal cancer prevention and treatment by inhibition of cyclooxygenase-2. Nat Rev Cancer. 2001;1(1):11-21. Epub 2002/03/20. doi: 10.1038/35094017. PubMed PMID: 11900248.

37. Salcedo R, Worschech A, Cardone M, Jones Y, Gyulai Z, Dai RM, et al. MyD88-mediated signaling prevents development of adenocarcinomas of the colon: role of

interleukin 18. J Exp Med. 2010;207(8):1625-36. Epub 2010/07/14. doi: 10.1084/jem.20100199. PubMed PMID: 20624890; PubMed Central PMCID: PMC2916129.

38. Terzic J, Grivennikov S, Karin E, Karin M. Inflammation and colon cancer. Gastroenterology. 2010;138(6):2101-14 e5. Epub 2010/04/28. doi: 10.1053/j.gastro.2010.01.058. PubMed PMID: 20420949.

39. Wu Y, Zhou BP. Inflammation: a driving force speeds cancer metastasis. Cell Cycle. 2009;8(20):3267-73. Epub 2009/09/23. PubMed PMID: 19770594; PubMed Central PMCID: PMC3702728.

40. Klampfer L. The role of signal transducers and activators of transcription in colon cancer. Front Biosci. 2008;13:2888-99. Epub 2007/11/06. PubMed PMID: 17981761.

41. Wang S, Liu Z, Wang L, Zhang X. NF-kappaB signaling pathway, inflammation and colorectal cancer. Cell Mol Immunol. 2009;6(5):327-34. Epub 2009/11/06. doi: 10.1038/cmi.2009.43. PubMed PMID: 19887045.

42. Wu Y, Deng J, Rychahou PG, Qiu S, Evers BM, Zhou BP. Stabilization of snail by NF-kappaB is required for inflammation-induced cell migration and invasion. Cancer Cell. 2009;15(5):416-28. Epub 2009/05/05. doi: 10.1016/j.ccr.2009.03.016. PubMed PMID: 19411070; PubMed Central PMCID: PMC2881229.

43. Luo JL, Maeda S, Hsu LC, Yagita H, Karin M. Inhibition of NF-kappaB in cancer cells converts inflammation- induced tumor growth mediated by TNFalpha to TRAIL-mediated tumor regression. Cancer Cell. 2004;6(3):297-305. Epub 2004/09/24. doi: 10.1016/j.ccr.2004.08.012. PubMed PMID: 15380520.

44. Zucker S, Vacirca J. Role of matrix metalloproteinases (MMPs) in colorectal cancer. Cancer Metastasis Rev. 2004;23(1-2):101-17. Epub 2004/03/06. PubMed PMID: 15000152.

45. Emsley J. Nature's building blocks: an A-Z guide to te elements. Oxford, UK: Oxford University Press; 2011 2011. 720 p.

46. Rotruck JT, Pope AL, Ganther HE, Swanson AB, Hafeman DG, Hoekstra WG. Selenium: biochemical role as a component of glutathione peroxidase. Science. 1973;179(4073):588-90. Epub 1973/02/09. PubMed PMID: 4686466.

47. Hawkes WC, Wilhelmsen EC, Tappel AL. Abundance and tissue distribution of selenocysteine-containing proteins in the rat. J Inorg Biochem. 1985;23(2):77-92. Epub 1985/02/01. PubMed PMID: 3156209.

48. Kryukov GV, Castellano S, Novoselov SV, Lobanov AV, Zehtab O, Guigo R, et al. Characterization of mammalian selenoproteomes. Science. 2003;300(5624):1439-43. Epub 2003/05/31. doi: 10.1126/science.1083516. PubMed PMID: 12775843.

49. Driscoll DM, Copeland PR. Mechanism and regulation of selenoprotein synthesis. Annu Rev Nutr. 2003;23:17-40. Epub 2003/01/14. doi: 10.1146/annurev.nutr.23.011702.073318

011702.073318 [pii]. PubMed PMID: 12524431.

50. Heider J, Baron C, Bock A. Coding from a distance: dissection of the mRNA determinants required for the incorporation of selenocysteine into protein. EMBO J. 1992;11(10):3759-66. Epub 1992/10/01. PubMed PMID: 1396569; PubMed Central PMCID: PMC556836.

51. Berry MJ, Banu L, Harney JW, Larsen PR. Functional characterization of the eukaryotic SECIS elements which direct selenocysteine insertion at UGA codons. EMBO J. 1993;12(8):3315-22. Epub 1993/08/01. PubMed PMID: 8344267; PubMed Central PMCID: PMC413599.

52. Hill KE, Lloyd RS, Burk RF. Conserved nucleotide sequences in the open reading frame and 3' untranslated region of selenoprotein P mRNA. Proc Natl Acad Sci U S A. 1993;90(2):537-41. Epub 1993/01/15. PubMed PMID: 8421687; PubMed Central PMCID: PMC45698.

53. Martin GW, 3rd, Harney JW, Berry MJ. Selenocysteine incorporation in eukaryotes: insights into mechanism and efficiency from sequence, structure, and spacing proximity studies of the type 1 deiodinase SECIS element. RNA. 1996;2(2):171-82. Epub 1996/02/01. PubMed PMID: 8601283; PubMed Central PMCID: PMC1369361.

54. Lee BJ, Rajagopalan M, Kim YS, You KH, Jacobson KB, Hatfield D. Selenocysteine tRNA[Ser]Sec gene is ubiquitous within the animal kingdom. Mol Cell Biol. 1990;10(5):1940-9. Epub 1990/05/01. PubMed PMID: 2139169; PubMed Central PMCID: PMC360540.

55. Leinfelder W, Forchhammer K, Zinoni F, Sawers G, Mandrand-Berthelot MA, Bock A. Escherichia coli genes whose products are involved in selenium metabolism. J Bacteriol. 1988;170(2):540-6. Epub 1988/02/01. PubMed PMID: 2962989; PubMed Central PMCID: PMC210687.

56. Low SC, Harney JW, Berry MJ. Cloning and functional characterization of human selenophosphate synthetase, an essential component of selenoprotein synthesis. J Biol Chem. 1995;270(37):21659-64. Epub 1995/09/15. PubMed PMID: 7665581.

57. Squires JE, Berry MJ. Eukaryotic selenoprotein synthesis: mechanistic insight incorporating new factors and new functions for old factors. IUBMB Life. 2008;60(4):232-5. Epub 2008/03/18. doi: 10.1002/iub.38. PubMed PMID: 18344183.

58. Low SC, Grundner-Culemann E, Harney JW, Berry MJ. SECIS-SBP2 interactions dictate selenocysteine incorporation efficiency and selenoprotein hierarchy. EMBO J. 2000;19(24):6882-90. Epub 2000/12/16. doi: 10.1093/emboj/19.24.6882. PubMed PMID: 11118223; PubMed Central PMCID: PMC305907.

59. Fradejas N, Carlson BA, Rijntjes E, Becker NP, Tobe R, Schweizer U. Mammalian Trit1 is a tRNA([Ser]Sec)-isopentenyl transferase required for full selenoprotein expression. Biochem J. 2013;450(2):427-32. Epub 2013/01/08. doi: 10.1042/BJ20121713. PubMed PMID: 23289710.

60. Esaki N, Nakamura T, Tanaka H, Soda K. Selenocysteine lyase, a novel enzyme that specifically acts on selenocysteine. Mammalian distribution and purification and properties of pig liver enzyme. J Biol Chem. 1982;257(8):4386-91. Epub 1982/04/25. PubMed PMID: 6461656.

61. Kobayashi Y, Ogra Y, Ishiwata K, Takayama H, Aimi N, Suzuki KT. Selenosugars are key and urinary metabolites for selenium excretion within the required to low-toxic range. Proc Natl Acad Sci U S A. 2002;99(25):15932-6. Epub 2002/11/21. doi: 10.1073/pnas.252610699. PubMed PMID: 12441402; PubMed Central PMCID: PMC138542.

62. Bopp BA, Sonders RC, Kesterson JW. Metabolic fate of selected selenium compounds in laboratory animals and man. Drug metabolism reviews. 1982;13(2):271-318. Epub 1982/01/01. doi: 10.3109/03602538209030000. PubMed PMID: 7047128.

63. Hill KE, Zhou J, Austin LM, Motley AK, Ham AJ, Olson GE, et al. The selenium-rich C-terminal domain of mouse selenoprotein P is necessary for the supply of selenium to brain and testis but not for the maintenance of whole body selenium. J Biol Chem. 2007;282(15):10972-80. Epub 2007/02/22. doi: M700436200 [pii]

10.1074/jbc.M700436200. PubMed PMID: 17311913.

64. Olson GE, Winfrey VP, Nagdas SK, Hill KE, Burk RF. Apolipoprotein E receptor-2 (ApoER2) mediates selenium uptake from selenoprotein P by the mouse testis. J Biol Chem. 2007;282(16):12290-7. Epub 2007/02/23. doi: 10.1074/jbc.M611403200. PubMed PMID: 17314095.

65. Burk RF, Hill KE, Olson GE, Weeber EJ, Motley AK, Winfrey VP, et al. Deletion of apolipoprotein E receptor-2 in mice lowers brain selenium and causes severe neurological dysfunction and death when a low-selenium diet is fed. J Neurosci.

2007;27(23):6207-11. Epub 2007/06/08. doi: 10.1523/JNEUROSCI.1153-07.2007. PubMed PMID: 17553992.

66. Hill KE, Wu S, Motley AK, Stevenson TD, Winfrey VP, Capecchi MR, et al. Production of selenoprotein P (Sepp1) by hepatocytes is central to selenium homeostasis. J Biol Chem. 2012;287(48):40414-24. Epub 2012/10/06. doi: 10.1074/jbc.M112.421404. PubMed PMID: 23038251; PubMed Central PMCID: PMC3504756.

67. Kim JY, Carlson BA, Xu XM, Zeng Y, Chen S, Gladyshev VN, et al. Inhibition of selenocysteine tRNA[Ser]Sec aminoacylation provides evidence that aminoacylation is required for regulatory methylation of this tRNA. Biochem Biophys Res Commun. 2011;409(4):814-9. Epub 2011/06/01. doi: 10.1016/j.bbrc.2011.05.096. PubMed PMID: 21624347; PubMed Central PMCID: PMC3124823.

68. Brigelius-Flohe R. Tissue-specific functions of individual glutathione peroxidases. Free Radic Biol Med. 1999;27(9-10):951-65. Epub 1999/11/24. doi: S0891-5849(99)00173-2 [pii]. PubMed PMID: 10569628.

69. Burk RF, Hill KE. Selenoprotein P-expression, functions, and roles in mammals. Biochim Biophys Acta. 2009;1790(11):1441-7. Epub 2009/04/07. doi: 10.1016/j.bbagen.2009.03.026. PubMed PMID: 19345254; PubMed Central PMCID: PMC2763998.

70. Chen J. An original discovery: selenium deficiency and Keshan disease (an endemic heart disease). Asia Pacific journal of clinical nutrition. 2012;21(3):320-6. Epub 2012/06/19. PubMed PMID: 22705420.

71. Yao Y, Pei F, Kang P. Selenium, iodine, and the relation with Kashin-Beck disease. Nutrition. 2011;27(11-12):1095-100. Epub 2011/10/05. doi: 10.1016/j.nut.2011.03.002. PubMed PMID: 21967994.

72. Schoenmakers E, Agostini M, Mitchell C, Schoenmakers N, Papp L, Rajanayagam O, et al. Mutations in the selenocysteine insertion sequence-binding protein 2 gene lead to a multisystem selenoprotein deficiency disorder in humans. J Clin Invest. 2010;120(12):4220-35. Epub 2010/11/19. doi: 10.1172/JCI43653. PubMed PMID: 21084748; PubMed Central PMCID: PMC2993594.

73. Rayman MP. The importance of selenium to human health. Lancet. 2000;356(9225):233-41. Epub 2000/08/30. doi: 10.1016/S0140-6736(00)02490-9. PubMed PMID: 10963212.

74. Ashrafi MR, Shams S, Nouri M, Mohseni M, Shabanian R, Yekaninejad MS, et al. A probable causative factor for an old problem: selenium and glutathione peroxidase appear to play important roles in epilepsy pathogenesis. Epilepsia. 2007;48(9):1750-5. Epub 2007/06/09. doi: 10.1111/j.1528-1167.2007.01143.x. PubMed PMID: 17555528.

75. Zhang S, Rocourt C, Cheng WH. Selenoproteins and the aging brain. Mechanisms of ageing and development. 2010;131(4):253-60. Epub 2010/03/12. doi: 10.1016/j.mad.2010.02.006. PubMed PMID: 20219520.

76. Marcocci C, Kahaly GJ, Krassas GE, Bartalena L, Prummel M, Stahl M, et al. Selenium and the course of mild Graves' orbitopathy. N Engl J Med. 2011;364(20):1920-31. Epub 2011/05/20. doi: 10.1056/NEJMoa1012985. PubMed PMID: 21591944.

77. Fairweather-Tait SJ, Bao Y, Broadley MR, Collings R, Ford D, Hesketh JE, et al. Selenium in human health and disease. Antioxidants & redox signaling. 2011;14(7):1337-83. Epub 2010/09/04. doi: 10.1089/ars.2010.3275. PubMed PMID: 20812787.

78. Huang Z, Rose AH, Hoffmann PR. The role of selenium in inflammation and immunity: from molecular mechanisms to therapeutic opportunities. Antioxidants & redox signaling. 2012;16(7):705-43. Epub 2011/10/01. doi: 10.1089/ars.2011.4145. PubMed PMID: 21955027; PubMed Central PMCID: PMC3277928.

79. Steinbrenner H, Sies H. Protection against reactive oxygen species by selenoproteins. Biochim Biophys Acta. 2009;1790(11):1478-85. Epub 2009/03/10. doi: S0304-4165(09)00043-9 [pii]

10.1016/j.bbagen.2009.02.014. PubMed PMID: 19268692.

80. Nuttall KL. Evaluating selenium poisoning. Annals of clinical and laboratory science. 2006;36(4):409-20. Epub 2006/11/28. PubMed PMID: 17127727.

81. Stranges S, Marshall JR, Natarajan R, Donahue RP, Trevisan M, Combs GF, et al. Effects of long-term selenium supplementation on the incidence of type 2 diabetes: a randomized trial. Ann Intern Med. 2007;147(4):217-23. Epub 2007/07/11. PubMed PMID: 17620655.

82. Steinbrenner H, Speckmann B, Pinto A, Sies H. High selenium intake and increased diabetes risk: experimental evidence for interplay between selenium and carbohydrate metabolism. J Clin Biochem Nutr. 2011;48(1):40-5. Epub 2011/02/08. doi: 10.3164/jcbn.11-002FR. PubMed PMID: 21297910; PubMed Central PMCID: PMC3022062.

83. Czech MP, Lawrence JC, Jr., Lynn WS. Evidence for the involvement of sulfhydryl oxidation in the regulation of fat cell hexose transport by insulin. Proc Natl Acad Sci U S A. 1974;71(10):4173-7. Epub 1974/10/01. PubMed PMID: 4372610; PubMed Central PMCID: PMC434352.

84. Mahadev K, Zilbering A, Zhu L, Goldstein BJ. Insulin-stimulated hydrogen peroxide reversibly inhibits protein-tyrosine phosphatase 1b in vivo and enhances

the early insulin action cascade. J Biol Chem. 2001;276(24):21938-42. Epub 2001/04/12. doi: 10.1074/jbc.C100109200. PubMed PMID: 11297536.

85. Misu H, Takamura T, Takayama H, Hayashi H, Matsuzawa-Nagata N, Kurita S, et al. A liver-derived secretory protein, selenoprotein P, causes insulin resistance. Cell Metab. 2010;12(5):483-95. Epub 2010/11/03. doi: 10.1016/j.cmet.2010.09.015. PubMed PMID: 21035759.

86. Pinto A, Speckmann B, Heisler M, Sies H, Steinbrenner H. Delaying of insulin signal transduction in skeletal muscle cells by selenium compounds. J Inorg Biochem. 2011;105(6):812-20. Epub 2011/04/19. doi: 10.1016/j.jinorgbio.2011.03.010. PubMed PMID: 21497580.

87. Speckmann B, Walter PL, Alili L, Reinehr R, Sies H, Klotz LO, et al. Selenoprotein P expression is controlled through interaction of the coactivator PGC-1alpha with FoxO1a and hepatocyte nuclear factor 4alpha transcription factors. Hepatology. 2008;48(6):1998-2006. Epub 2008/10/31. doi: 10.1002/hep.22526. PubMed PMID: 18972406.

88. Gromadzinska J, Reszka E, Bruzelius K, Wasowicz W, Akesson B. Selenium and cancer: biomarkers of selenium status and molecular action of selenium supplements. Eur J Nutr. 2008;47 Suppl 2:29-50. Epub 2008/06/17. doi: 10.1007/s00394-008-2005-z. PubMed PMID: 18458833.

89. Chiang EC, Shen S, Kengeri SS, Xu H, Combs GF, Morris JS, et al. Defining the Optimal Selenium Dose for Prostate Cancer Risk Reduction: Insights from the U-Shaped Relationship between Selenium Status, DNA Damage, and Apoptosis. Dose-response : a publication of International Hormesis Society. 2009;8(3):285-300. Epub 2009/01/01. doi: 10.2203/dose-response.09-036.Chiang. PubMed PMID: 20877485; PubMed Central PMCID: PMC2939616.

90. Monsen ER. Dietary reference intakes for the antioxidant nutrients: vitamin C, vitamin E, selenium, and carotenoids. J Am Diet Assoc. 2000;100(6):637-40. Epub 2000/06/23. doi: 10.1016/S0002-8223(00)00189-9. PubMed PMID: 10863565.

91. Rayman MP. Food-chain selenium and human health: emphasis on intake. Br J Nutr. 2008;100(2):254-68. Epub 2008/03/19. doi: 10.1017/S0007114508939830. PubMed PMID: 18346308.

92. Duffield AJ, Thomson CD, Hill KE, Williams S. An estimation of selenium requirements for New Zealanders. Am J Clin Nutr. 1999;70(5):896-903. Epub 1999/10/28. PubMed PMID: 10539752.

93. Hurst R, Armah CN, Dainty JR, Hart DJ, Teucher B, Goldson AJ, et al. Establishing optimal selenium status: results of a randomized, double-blind, placebo-controlled trial. Am J Clin Nutr. 2010;91(4):923-31. Epub 2010/02/26. doi:

10.3945/ajcn.2009.28169. PubMed PMID: 20181815; PubMed Central PMCID: PMC2844680.

94. Xia Y, Hill KE, Byrne DW, Xu J, Burk RF. Effectiveness of selenium supplements in a low-selenium area of China. Am J Clin Nutr. 2005;81(4):829-34. Epub 2005/04/09. PubMed PMID: 15817859.

95. Xia Y, Hill KE, Li P, Xu J, Zhou D, Motley AK, et al. Optimization of selenoprotein P and other plasma selenium biomarkers for the assessment of the selenium nutritional requirement: a placebo-controlled, double-blind study of selenomethionine supplementation in selenium-deficient Chinese subjects. Am J Clin Nutr. 2010;92(3):525-31. Epub 2010/06/25. doi: 10.3945/ajcn.2010.29642. PubMed PMID: 20573787; PubMed Central PMCID: PMC2921536.

96. Hu Y, McIntosh GH, Le Leu RK, Upton JM, Woodman RJ, Young GP. The influence of selenium-enriched milk proteins and selenium yeast on plasma selenium levels and rectal selenoprotein gene expression in human subjects. Br J Nutr. 2011;106(4):572-82. Epub 2011/04/01. doi: 10.1017/S0007114511000420. PubMed PMID: 21450115.

97. Karunasinghe N, Han DY, Zhu S, Yu J, Lange K, Duan H, et al. Serum selenium and single-nucleotide polymorphisms in genes for selenoproteins: relationship to markers of oxidative stress in men from Auckland, New Zealand. Genes Nutr. 2012;7(2):179-90. Epub 2011/12/06. doi: 10.1007/s12263-011-0259-1. PubMed PMID: 22139612; PubMed Central PMCID: PMC3316745.

98. Al-Taie OH, Seufert J, Mork H, Treis H, Mentrup B, Thalheimer A, et al. A complex DNA-repeat structure within the Selenoprotein P promoter contains a functionally relevant polymorphism and is genetically unstable under conditions of mismatch repair deficiency. Eur J Hum Genet. 2002;10(9):499-504. Epub 2002/08/13. doi: 10.1038/sj.ejhg.5200811. PubMed PMID: 12173025.

99. Meplan C, Hughes DJ, Pardini B, Naccarati A, Soucek P, Vodickova L, et al. Genetic variants in selenoprotein genes increase risk of colorectal cancer. Carcinogenesis. 2010;31(6):1074-9. Epub 2010/04/10. doi: 10.1093/carcin/bgq076. PubMed PMID: 20378690.

100. Sutherland A, Kim DH, Relton C, Ahn YO, Hesketh J. Polymorphisms in the selenoprotein S and 15-kDa selenoprotein genes are associated with altered susceptibility to colorectal cancer. Genes Nutr. 2010;5(3):215-23. Epub 2010/11/06. doi: 10.1007/s12263-010-0176-8. PubMed PMID: 21052528; PubMed Central PMCID: PMC2935533.

101. Zhang J, Dhakal IB, Lang NP, Kadlubar FF. Polymorphisms in inflammatory genes, plasma antioxidants, and prostate cancer risk. Cancer Causes Control. 2010;21(9):1437-44. Epub 2010/05/01. doi: 10.1007/s10552-010-9571-0. PubMed PMID: 20431935; PubMed Central PMCID: PMC3207491.

102. Zhuo P, Goldberg M, Herman L, Lee BS, Wang H, Brown RL, et al. Molecular consequences of genetic variations in the glutathione peroxidase 1 selenoenzyme. Cancer Res. 2009;69(20):8183-90. Epub 2009/10/15. doi: 10.1158/0008-5472.CAN-09-1791. PubMed PMID: 19826042; PubMed Central PMCID: PMC2763328.

103. Steinbrenner H, Speckmann B, Sies H. Toward understanding success and failures in the use of selenium for cancer prevention. Antioxidants & redox signaling. 2013;19(2):181-91. Epub 2013/02/21. doi: 10.1089/ars.2013.5246. PubMed PMID: 23421468; PubMed Central PMCID: PMC3689159.

104. Stadtman TC. Selenium biochemistry. Mammalian selenoenzymes. Ann N Y Acad Sci. 2000;899:399-402. Epub 2000/06/23. PubMed PMID: 10863556.

105. Stadtman TC. Selenocysteine. Annual review of biochemistry. 1996;65:83-100. Epub 1996/01/01. doi: 10.1146/annurev.bi.65.070196.000503. PubMed PMID: 8811175.

106. Brozmanova J, Manikova D, Vlckova V, Chovanec M. Selenium: a double-edged sword for defense and offence in cancer. Archives of toxicology. 2010;84(12):919-38. Epub 2010/09/28. doi: 10.1007/s00204-010-0595-8. PubMed PMID: 20871980.

107. Dennert G, Zwahlen M, Brinkman M, Vinceti M, Zeegers MP, Horneber M. Selenium for preventing cancer. Cochrane Database Syst Rev. 2011(5):CD005195. Epub 2011/05/13. doi: 10.1002/14651858.CD005195.pub2. PubMed PMID: 21563143; PubMed Central PMCID: PMC3692366.

108. Jaworska K, Gupta S, Durda K, Muszynska M, Sukiennicki G, Jaworowska E, et al. A low selenium level is associated with lung and laryngeal cancers. PLoS One. 2013;8(3):e59051. Epub 2013/03/22. doi: 10.1371/journal.pone.0059051. PubMed PMID: 23516596; PubMed Central PMCID: PMC3596323.

109. Meyer HA, Endermann T, Stephan C, Stoedter M, Behrends T, Wolff I, et al. Selenoprotein P status correlates to cancer-specific mortality in renal cancer patients. PLoS One. 2012;7(10):e46644. Epub 2012/10/12. doi: 10.1371/journal.pone.0046644. PubMed PMID: 23056383; PubMed Central PMCID: PMC3467258.

110. Jung HJ, Seo YR. Current issues of selenium in cancer chemoprevention. Biofactors. 2010;36(2):153-8. Epub 2010/03/25. doi: 10.1002/biof.81. PubMed PMID: 20333751.

111. Mugesh G, du Mont WW, Sies H. Chemistry of biologically important synthetic organoselenium compounds. Chemical reviews. 2001;101(7):2125-79. Epub 2001/11/17. PubMed PMID: 11710243.

112. Wang D, Taylor EW, Wang Y, Wan X, Zhang J. Encapsulated nanoepigallocatechin-3-gallate and elemental selenium nanoparticles as paradigms for nanochemoprevention. International journal of nanomedicine. 2012;7:1711-21. Epub 2012/05/24. doi: 10.2147/IJN.S29341. PubMed PMID: 22619522; PubMed Central PMCID: PMC3356175.

113. Clark LC, Dalkin B, Krongrad A, Combs GF, Jr., Turnbull BW, Slate EH, et al. Decreased incidence of prostate cancer with selenium supplementation: results of a double-blind cancer prevention trial. Br J Urol. 1998;81(5):730-4. Epub 1998/06/20. PubMed PMID: 9634050.

114. Duffield-Lillico AJ, Dalkin BL, Reid ME, Turnbull BW, Slate EH, Jacobs ET, et al. Selenium supplementation, baseline plasma selenium status and incidence of prostate cancer: an analysis of the complete treatment period of the Nutritional Prevention of Cancer Trial. BJU Int. 2003;91(7):608-12. Epub 2003/04/18. PubMed PMID: 12699469.

115. Jacobs ET, Jiang R, Alberts DS, Greenberg ER, Gunter EW, Karagas MR, et al. Selenium and colorectal adenoma: results of a pooled analysis. J Natl Cancer Inst. 2004;96(22):1669-75. Epub 2004/11/18. doi: 10.1093/jnci/djh310. PubMed PMID: 15547179.

116. Fernandez-Banares F, Cabre E, Esteve M, Mingorance MD, Abad-Lacruz A, Lachica M, et al. Serum selenium and risk of large size colorectal adenomas in a geographical area with a low selenium status. Am J Gastroenterol. 2002;97(8):2103-8. Epub 2002/08/23. doi: 10.1111/j.1572-0241.2002.05930.x. PubMed PMID: 12190184.

117. Peters U, Chatterjee N, Church TR, Mayo C, Sturup S, Foster CB, et al. High serum selenium and reduced risk of advanced colorectal adenoma in a colorectal cancer early detection program. Cancer Epidemiol Biomarkers Prev. 2006;15(2):315-20. Epub 2006/02/24. doi: 10.1158/1055-9965.EPI-05-0471. PubMed PMID: 16492922.

118. Klein EA, Thompson IM, Jr., Tangen CM, Crowley JJ, Lucia MS, Goodman PJ, et al. Vitamin E and the risk of prostate cancer: the Selenium and Vitamin E Cancer Prevention Trial (SELECT). JAMA. 2011;306(14):1549-56. Epub 2011/10/13. doi: 10.1001/jama.2011.1437. PubMed PMID: 21990298.

119. Wallace K, Byers T, Morris JS, Cole BF, Greenberg ER, Baron JA, et al. Prediagnostic serum selenium concentration and the risk of recurrent colorectal adenoma: a nested case-control study. Cancer Epidemiol Biomarkers Prev. 2003;12(5):464-7. Epub 2003/05/17. PubMed PMID: 12750244.

120. Papaioannou D, Cooper KL, Carroll C, Hind D, Squires H, Tappenden P, et al. Antioxidants in the chemoprevention of colorectal cancer and colorectal adenomas in the general population: a systematic review and meta-analysis. Colorectal Dis.

2011;13(10):1085-99. Epub 2010/04/24. doi: 10.1111/j.1463-1318.2010.02289.x. PubMed PMID: 20412095.

121. Lee EH, Myung SK, Jeon YJ, Kim Y, Chang YJ, Ju W, et al. Effects of selenium supplements on cancer prevention: meta-analysis of randomized controlled trials. Nutr Cancer. 2011;63(8):1185-95. Epub 2011/10/19. doi: 10.1080/01635581.2011.607544. PubMed PMID: 22004275.

122. Zhang J, Wang L, Li G, Anderson LB, Xu Y, Witthuhn B, et al. Mouse prostate proteomes are differentially altered by supranutritional intake of four selenium compounds. Nutr Cancer. 2011;63(5):778-89. Epub 2011/05/27. doi: 10.1080/01635581.2011.563029. PubMed PMID: 21614726.

123. Brigelius-Flohe R, Kipp A. Glutathione peroxidases in different stages of carcinogenesis. Biochim Biophys Acta. 2009;1790(11):1555-68. Epub 2009/03/18. doi: 10.1016/j.bbagen.2009.03.006. PubMed PMID: 19289149.

124. Muller M, Banning A, Brigelius-Flohe R, Kipp A. Nrf2 target genes are induced under marginal selenium-deficiency. Genes Nutr. 2010;5(4):297-307. Epub 2010/12/31. doi: 10.1007/s12263-010-0168-8. PubMed PMID: 21189866; PubMed Central PMCID: PMC2989369.

125. Burk RF, Hill KE, Nakayama A, Mostert V, Levander XA, Motley AK, et al. Selenium deficiency activates mouse liver Nrf2-ARE but vitamin E deficiency does not. Free Radic Biol Med. 2008;44(8):1617-23. Epub 2008/02/19. doi: S0891-5849(08)00038-5 [pii]

10.1016/j.freeradbiomed.2008.01.016. PubMed PMID: 18279678; PubMed Central PMCID: PMC2346531.

126. Burk RF, Lawrence RA, Lane JM. Liver necrosis and lipid peroxidation in the rat as the result of paraquat and diquat administration. Effect of selenium deficiency. J Clin Invest. 1980;65(5):1024-31. Epub 1980/05/01. doi: 10.1172/JCI109754. PubMed PMID: 7364936; PubMed Central PMCID: PMC371432.

127. Burk RF, Hill KE, Awad JA, Morrow JD, Kato T, Cockell KA, et al. Pathogenesis of diquat-induced liver necrosis in selenium-deficient rats: assessment of the roles of lipid peroxidation and selenoprotein P. Hepatology. 1995;21(2):561-9. Epub 1995/02/01. doi: S0270913995000760 [pii]. PubMed PMID: 7843731.

128. Hill KE, McCollum GW, Boeglin ME, Burk RF. Thioredoxin reductase activity is decreased by selenium deficiency. Biochem Biophys Res Commun. 1997;234(2):293-5. Epub 1997/05/19. doi: 10.1006/bbrc.1997.6618. PubMed PMID: 9177261.

129. Ferguson LR, Karunasinghe N, Zhu S, Wang AH. Selenium and its' role in the maintenance of genomic stability. Mutat Res. 2012;733(1-2):100-10. Epub 2012/01/12. doi: 10.1016/j.mrfmmm.2011.12.011. PubMed PMID: 22234051.

130. Brigelius-Flohe R, Kipp AP. Selenium in the redox regulation of the nrf2 and the wnt pathway. Methods Enzymol. 2013;527:65-86. Epub 2013/07/09. doi: 10.1016/B978-0-12-405882-8.00004-0. PubMed PMID: 23830626.

131. Halliwell B. Free radicals and antioxidants - quo vadis? Trends Pharmacol Sci. 2011;32(3):125-30. Epub 2011/01/11. doi: 10.1016/j.tips.2010.12.002. PubMed PMID: 21216018.

132. Kim TH, Hur EG, Kang SJ, Kim JA, Thapa D, Lee YM, et al. NRF2 blockade suppresses colon tumor angiogenesis by inhibiting hypoxia-induced activation of HIF-1alpha. Cancer Res. 2011;71(6):2260-75. Epub 2011/02/01. doi: 10.1158/0008-5472.CAN-10-3007. PubMed PMID: 21278237.

133. Chang LC, Fan CW, Tseng WK, Chen JR, Chein HP, Hwang CC, et al. Immunohistochemical Study of the Nrf2 Pathway in Colorectal Cancer: Nrf2 Expression is Closely Correlated to Keap1 in the Tumor and Bach1 in the Normal Tissue. Appl Immunohistochem Mol Morphol. 2013. Epub 2013/03/05. doi: 10.1097/PAI.0b013e318282ac20. PubMed PMID: 23455180.

134. Reya T, Clevers H. Wnt signalling in stem cells and cancer. Nature. 2005;434(7035):843-50. Epub 2005/04/15. doi: 10.1038/nature03319. PubMed PMID: 15829953.

135. Kipp AP, Muller MF, Goken EM, Deubel S, Brigelius-Flohe R. The selenoproteins GPx2, TrxR2 and TrxR3 are regulated by Wnt signalling in the intestinal epithelium. Biochim Biophys Acta. 2012;1820(10):1588-96. Epub 2012/06/12. doi: 10.1016/j.bbagen.2012.05.016. PubMed PMID: 22683372.

136. Bera S, De Rosa V, Rachidi W, Diamond AM. Does a role for selenium in DNA damage repair explain apparent controversies in its use in chemoprevention? Mutagenesis. 2013;28(2):127-34. Epub 2012/12/04. doi: 10.1093/mutage/ges064. PubMed PMID: 23204505; PubMed Central PMCID: PMC3570792.

137. Jiang C, Jiang W, Ip C, Ganther H, Lu J. Selenium-induced inhibition of angiogenesis in mammary cancer at chemopreventive levels of intake. Mol Carcinog. 1999;26(4):213-25. Epub 1999/11/24. doi: 10.1002/(SICI)1098-2744(199912)26:4<213::AID-MC1>3.0.CO;2-Z [pii]. PubMed PMID: 10569799.

138. Chen YC, Prabhu KS, Mastro AM. Is selenium a potential treatment for cancer metastasis? Nutrients. 2013;5(4):1149-68. Epub 2013/04/10. doi: 10.3390/nu5041149. PubMed PMID: 23567478; PubMed Central PMCID: PMC3705340.

139. Kasaikina MV, Turanov AA, Avanesov A, Schweizer U, Seeher S, Bronson RT, et al. Contrasting roles of dietary selenium and selenoproteins in chemically induced hepatocarcinogenesis. Carcinogenesis. 2013;34(5):1089-95. Epub 2013/02/08. doi: 10.1093/carcin/bgt011. PubMed PMID: 23389288; PubMed Central PMCID: PMC3643414.

140. Moustafa ME, Carlson BA, Anver MR, Bobe G, Zhong N, Ward JM, et al. Selenium and selenoprotein deficiencies induce widespread pyogranuloma formation in mice, while high levels of dietary selenium decrease liver tumor size driven by TGFalpha. PLoS One. 2013;8(2):e57389. Epub 2013/03/06. doi: 10.1371/journal.pone.0057389. PubMed PMID: 23460847; PubMed Central PMCID: PMC3583866.

141. Krehl S, Loewinger M, Florian S, Kipp AP, Banning A, Wessjohann LA, et al. Glutathione peroxidase-2 and selenium decreased inflammation and tumors in a mouse model of inflammation-associated carcinogenesis whereas sulforaphane effects differed with selenium supply. Carcinogenesis.33(3):620-8. Epub 2011/12/20. doi: bgr288 [pii]

10.1093/carcin/bgr288. PubMed PMID: 22180572; PubMed Central PMCID: PMC3291858.

142. Tsuji PA, Carlson BA, Naranjo-Suarez S, Yoo MH, Xu XM, Fomenko DE, et al. Knockout of the 15 kDa selenoprotein protects against chemically-induced aberrant crypt formation in mice. PLoS One. 2012;7(12):e50574. Epub 2012/12/12. doi: 10.1371/journal.pone.0050574. PubMed PMID: 23226526; PubMed Central PMCID: PMC3514276.

143. Hu Y, Benya RV, Carroll RE, Diamond AM. Allelic loss of the gene for the GPX1 selenium-containing protein is a common event in cancer. J Nutr. 2005;135(12 Suppl):3021S-4S. Epub 2005/12/01. PubMed PMID: 16317164.

144. Hu YJ, Diamond AM. Role of glutathione peroxidase 1 in breast cancer: loss of heterozygosity and allelic differences in the response to selenium. Cancer Res. 2003;63(12):3347-51. Epub 2003/06/18. PubMed PMID: 12810669.

145. Hu YJ, Dolan ME, Bae R, Yee H, Roy M, Glickman R, et al. Allelic loss at the GPx-1 locus in cancer of the head and neck. Biol Trace Elem Res. 2004;101(2):97-106. Epub 2004/11/24. doi: 10.1385/BTER:101:2:097. PubMed PMID: 15557674.

146. Lee OJ, Schneider-Stock R, McChesney PA, Kuester D, Roessner A, Vieth M, et al. Hypermethylation and loss of expression of glutathione peroxidase-3 in Barrett's tumorigenesis. Neoplasia. 2005;7(9):854-61. Epub 2005/10/19. PubMed PMID: 16229808; PubMed Central PMCID: PMC1501938.

147. Lodygin D, Epanchintsev A, Menssen A, Diebold J, Hermeking H. Functional epigenomics identifies genes frequently silenced in prostate cancer. Cancer Res.

2005;65(10):4218-27. Epub 2005/05/19. doi: 10.1158/0008-5472.CAN-04-4407. PubMed PMID: 15899813.

148. Papp LV, Lu J, Holmgren A, Khanna KK. From selenium to selenoproteins: synthesis, identity, and their role in human health. Antioxidants & redox signaling. 2007;9(7):775-806. Epub 2007/05/19. doi: 10.1089/ars.2007.1528. PubMed PMID: 17508906.

149. Speckmann B, Bidmon HJ, Pinto A, Anlauf M, Sies H, Steinbrenner H. Induction of Glutathione Peroxidase 4 Expression during Enterocytic Cell Differentiation. J Biol Chem.286(12):10764-72. Epub 2011/01/22. doi: M110.216028 [pii]

10.1074/jbc.M110.216028. PubMed PMID: 21252226; PubMed Central PMCID: PMC3060527.

150. Davis CD, Tsuji PA, Milner JA. Selenoproteins and cancer prevention. Annu Rev Nutr. 2012;32:73-95. Epub 2012/03/13. doi: 10.1146/annurev-nutr-071811-150740. PubMed PMID: 22404120.

151. Meplan C, Hesketh J. The influence of selenium and selenoprotein gene variants on colorectal cancer risk. Mutagenesis.27(2):177-86. Epub 2012/02/02. doi: ger058 [pii]

10.1093/mutage/ger058. PubMed PMID: 22294765.

152. Meplan C, Crosley LK, Nicol F, Horgan GW, Mathers JC, Arthur JR, et al. Functional effects of a common single-nucleotide polymorphism (GPX4c718t) in the glutathione peroxidase 4 gene: interaction with sex. Am J Clin Nutr. 2008;87(4):1019-27. Epub 2008/04/11. PubMed PMID: 18400727.

153. Bermano G, Pagmantidis V, Holloway N, Kadri S, Mowat NA, Shiel RS, et al. Evidence that a polymorphism within the 3'UTR of glutathione peroxidase 4 is functional and is associated with susceptibility to colorectal cancer. Genes Nutr. 2007;2(2):225-32. Epub 2008/10/14. doi: 10.1007/s12263-007-0052-3. PubMed PMID: 18850177; PubMed Central PMCID: PMC2474949.

154. Udler M, Maia AT, Cebrian A, Brown C, Greenberg D, Shah M, et al. Common germline genetic variation in antioxidant defense genes and survival after diagnosis of breast cancer. J Clin Oncol. 2007;25(21):3015-23. Epub 2007/07/20. doi: 10.1200/JCO.2006.10.0099. PubMed PMID: 17634480.

155. Bermano G, Smyth E, Goua M, Heys SD, Wahle KW. Impaired expression of glutathione peroxidase-4 gene in peripheral blood mononuclear cells: a biomarker of increased breast cancer risk. Cancer biomarkers : section A of Disease markers. 2010;7(1):39-46. Epub 2010/11/04. doi: 10.3233/CBM-2010-0146. PubMed PMID: 21045263.

156. Sengupta A, Lichti UF, Carlson BA, Cataisson C, Ryscavage AO, Mikulec C, et al. Targeted disruption of glutathione peroxidase 4 in mouse skin epithelial cells impairs postnatal hair follicle morphogenesis that is partially rescued through inhibition of COX-2. J Invest Dermatol. 2013;133(7):1731-41. Epub 2013/02/01. doi: 10.1038/jid.2013.52. PubMed PMID: 23364477; PubMed Central PMCID: PMC3652900.

157. Liu J, Du J, Zhang Y, Sun W, Smith BJ, Oberley LW, et al. Suppression of the malignant phenotype in pancreatic cancer by overexpression of phospholipid hydroperoxide glutathione peroxidase. Hum Gene Ther. 2006;17(1):105-16. Epub 2006/01/18. doi: 10.1089/hum.2006.17.105. PubMed PMID: 16409129.

158. Heirman I, Ginneberge D, Brigelius-Flohe R, Hendrickx N, Agostinis P, Brouckaert P, et al. Blocking tumor cell eicosanoid synthesis by GP x 4 impedes tumor growth and malignancy. Free Radic Biol Med. 2006;40(2):285-94. Epub 2006/01/18. doi: 10.1016/j.freeradbiomed.2005.08.033. PubMed PMID: 16413410.

159. Saito Y, Hayashi T, Tanaka A, Watanabe Y, Suzuki M, Saito E, et al. Selenoprotein P in human plasma as an extracellular phospholipid hydroperoxide glutathione peroxidase. Isolation and enzymatic characterization of human selenoprotein p. J Biol Chem. 1999;274(5):2866-71. Epub 1999/01/23. PubMed PMID: 9915822.

160. Burk RF, Hill KE. Selenoprotein P: an extracellular protein with unique physical characteristics and a role in selenium homeostasis. Annu Rev Nutr. 2005;25:215-35. Epub 2005/07/14. doi: 10.1146/annurev.nutr.24.012003.132120. PubMed PMID: 16011466.

161. Dreher I, Schmutzler C, Jakob F, Kohrle J. Expression of selenoproteins in various rat and human tissues and cell lines. J Trace Elem Med Biol. 1997;11(2):83-91. Epub 1997/06/01. doi: 10.1016/S0946-672X(97)80031-4. PubMed PMID: 9285888.

162. Al-Taie OH, Uceyler N, Eubner U, Jakob F, Mork H, Scheurlen M, et al. Expression profiling and genetic alterations of the selenoproteins GI-GPx and SePP in colorectal carcinogenesis. Nutr Cancer. 2004;48(1):6-14. Epub 2004/06/19. doi: 10.1207/s15327914nc4801_2. PubMed PMID: 15203372.

163. Calvo A, Xiao N, Kang J, Best CJ, Leiva I, Emmert-Buck MR, et al. Alterations in gene expression profiles during prostate cancer progression: functional correlations to tumorigenicity and down-regulation of selenoprotein-P in mouse and human tumors. Cancer Res. 2002;62(18):5325-35. Epub 2002/09/18. PubMed PMID: 12235003.

164. Steinbrecher A, Meplan C, Hesketh J, Schomburg L, Endermann T, Jansen E, et al. Effects of selenium status and polymorphisms in selenoprotein genes on prostate cancer risk in a prospective study of European men. Cancer Epidemiol Biomarkers

Prev. 2010;19(11):2958-68. Epub 2010/09/21. doi: 10.1158/1055-9965.EPI-10-0364. PubMed PMID: 20852007.

165. Peters U, Chatterjee N, Hayes RB, Schoen RE, Wang Y, Chanock SJ, et al. Variation in the selenoenzyme genes and risk of advanced distal colorectal adenoma. Cancer Epidemiol Biomarkers Prev. 2008;17(5):1144-54. Epub 2008/05/17. doi: 10.1158/1055-9965.EPI-07-2947. PubMed PMID: 18483336.

166. Gonzalez-Moreno O, Boque N, Redrado M, Milagro F, Campion J, Endermann T, et al. Selenoprotein-P is down-regulated in prostate cancer, which results in lack of protection against oxidative damage. Prostate. 2011;71(8):824-34. Epub 2011/04/02. doi: 10.1002/pros.21298. PubMed PMID: 21456065.

167. Bellone G, Carbone A, Tibaudi D, Mauri F, Ferrero I, Smirne C, et al. Differential expression of transforming growth factors-beta1, -beta2 and -beta3 in human colon carcinoma. Eur J Cancer. 2001;37(2):224-33. Epub 2001/02/13. PubMed PMID: 11166150.

168. Mostert V, Dreher I, Kohrle J, Abel J. Transforming growth factor-beta1 inhibits expression of selenoprotein P in cultured human liver cells. FEBS Lett. 1999;460(1):23-6. Epub 1999/11/26. doi: S0014-5793(99)01298-3 [pii]. PubMed PMID: 10571054.

169. Dreher I, Jakobs TC, Kohrle J. Cloning and characterization of the human selenoprotein P promoter. Response of selenoprotein P expression to cytokines in liver cells. J Biol Chem. 1997;272(46):29364-71. Epub 1997/11/20. PubMed PMID: 9361018.

170. Rock C, Moos PJ. Selenoprotein P regulation by the glucocorticoid receptor. Biometals. 2009;22(6):995-1009. Epub 2009/06/11. doi: 10.1007/s10534-009-9251-2. PubMed PMID: 19513589; PubMed Central PMCID: PMC3039700.

171. Speckmann B, Pinto A, Winter M, Forster I, Sies H, Steinbrenner H. Proinflammatory cytokines down-regulate intestinal selenoprotein P biosynthesis via NOS2 induction. Free Radic Biol Med.49(5):777-85. Epub 2010/06/15. doi: S0891-5849(10)00354-0 [pii]

10.1016/j.freeradbiomed.2010.05.035. PubMed PMID: 20542496.

172. Zhang Y, Chen X. Reducing selenoprotein P expression suppresses adipocyte differentiation as a result of increased preadipocyte inflammation. Am J Physiol Endocrinol Metab.300(1):E77-85. Epub 2010/10/21. doi: ajpendo.00380.2010 [pii]

10.1152/ajpendo.00380.2010. PubMed PMID: 20959537; PubMed Central PMCID: PMC3023214.

173. Look AT. Oncogenic transcription factors in the human acute leukemias. Science. 1997;278(5340):1059-64. Epub 1997/11/14. PubMed PMID: 9353180.

174. Miyoshi H, Shimizu K, Kozu T, Maseki N, Kaneko Y, Ohki M. t(8;21) breakpoints on chromosome 21 in acute myeloid leukemia are clustered within a limited region of a single gene, AML1. Proc Natl Acad Sci U S A. 1991;88(23):10431-4. Epub 1991/12/01. PubMed PMID: 1720541; PubMed Central PMCID: PMC52942.

175. Rhoades KL, Hetherington CJ, Harakawa N, Yergeau DA, Zhou L, Liu LQ, et al. Analysis of the role of AML1-ETO in leukemogenesis, using an inducible transgenic mouse model. Blood. 2000;96(6):2108-15. Epub 2000/09/09. PubMed PMID: 10979955.

176. Wang J, Hoshino T, Redner RL, Kajigaya S, Liu JM. ETO, fusion partner in t(8;21) acute myeloid leukemia, represses transcription by interaction with the human N-CoR/mSin3/HDAC1 complex. Proc Natl Acad Sci U S A. 1998;95(18):10860-5. Epub 1998/09/02. PubMed PMID: 9724795; PubMed Central PMCID: PMC27986.

177. Lutterbach B, Sun D, Schuetz J, Hiebert SW. The MYND motif is required for repression of basal transcription from the multidrug resistance 1 promoter by the t(8;21) fusion protein. Mol Cell Biol. 1998;18(6):3604-11. Epub 1998/06/20. PubMed PMID: 9584201; PubMed Central PMCID: PMC108942.

178. Lutterbach B, Westendorf JJ, Linggi B, Patten A, Moniwa M, Davie JR, et al. ETO, a target of t(8;21) in acute leukemia, interacts with the N-CoR and mSin3 corepressors. Mol Cell Biol. 1998;18(12):7176-84. Epub 1998/11/20. PubMed PMID: 9819404; PubMed Central PMCID: PMC109299.

179. Miyoshi H, Kozu T, Shimizu K, Enomoto K, Maseki N, Kaneko Y, et al. The t(8;21) translocation in acute myeloid leukemia results in production of an AML1-MTG8 fusion transcript. EMBO J. 1993;12(7):2715-21. Epub 1993/07/01. PubMed PMID: 8334990; PubMed Central PMCID: PMC413521.

180. Fracchiolla NS, Colombo G, Finelli P, Maiolo AT, Neri A. EHT, a new member of the MTG8/ETO gene family, maps on 20q11 region and is deleted in acute myeloid leukemias. Blood. 1998;92(9):3481-4. Epub 1998/10/27. PubMed PMID: 9787195.

181. Gamou T, Kitamura E, Hosoda F, Shimizu K, Shinohara K, Hayashi Y, et al. The partner gene of AML1 in t(16;21) myeloid malignancies is a novel member of the MTG8(ETO) family. Blood. 1998;91(11):4028-37. Epub 1998/05/30. PubMed PMID: 9596646.

182. Kitabayashi I, Ida K, Morohoshi F, Yokoyama A, Mitsuhashi N, Shimizu K, et al. The AML1-MTG8 leukemic fusion protein forms a complex with a novel member of

the MTG8(ETO/CDR) family, MTGR1. Mol Cell Biol. 1998;18(2):846-58. Epub 1998/02/03. PubMed PMID: 9447981; PubMed Central PMCID: PMC108796.

183. Davis JN, Williams BJ, Herron JT, Galiano FJ, Meyers S. ETO-2, a new member of the ETO-family of nuclear proteins. Oncogene. 1999;18(6):1375-83. Epub 1999/02/18. doi: 10.1038/sj.onc.1202412. PubMed PMID: 10022820.

184. McGhee L, Bryan J, Elliott L, Grimes HL, Kazanjian A, Davis JN, et al. Gfi-1 attaches to the nuclear matrix, associates with ETO (MTG8) and histone deacetylase proteins, and represses transcription using a TSA-sensitive mechanism. J Cell Biochem. 2003;89(5):1005-18. Epub 2003/07/23. doi: 10.1002/jcb.10548. PubMed PMID: 12874834.

185. Hoey T, Weinzierl RO, Gill G, Chen JL, Dynlacht BD, Tjian R. Molecular cloning and functional analysis of Drosophila TAF110 reveal properties expected of coactivators. Cell. 1993;72(2):247-60. Epub 1993/01/29. PubMed PMID: 7678780.

186. Wei Y, Liu S, Lausen J, Woodrell C, Cho S, Biris N, et al. A TAF4-homology domain from the corepressor ETO is a docking platform for positive and negative regulators of transcription. Nat Struct Mol Biol. 2007;14(7):653-61. Epub 2007/06/19. doi: 10.1038/nsmb1258. PubMed PMID: 17572682.

187. Amann JM, Nip J, Strom DK, Lutterbach B, Harada H, Lenny N, et al. ETO, a target of t(8;21) in acute leukemia, makes distinct contacts with multiple histone deacetylases and binds mSin3A through its oligomerization domain. Mol Cell Biol. 2001;21(19):6470-83. Epub 2001/09/05. PubMed PMID: 11533236; PubMed Central PMCID: PMC99794.

188. Hildebrand D, Tiefenbach J, Heinzel T, Grez M, Maurer AB. Multiple regions of ETO cooperate in transcriptional repression. J Biol Chem. 2001;276(13):9889-95. Epub 2001/01/21. doi: 10.1074/jbc.M010582200. PubMed PMID: 11150306.

189. Gelmetti V, Zhang J, Fanelli M, Minucci S, Pelicci PG, Lazar MA. Aberrant recruitment of the nuclear receptor corepressor-histone deacetylase complex by the acute myeloid leukemia fusion partner ETO. Mol Cell Biol. 1998;18(12):7185-91. Epub 1998/11/20. PubMed PMID: 9819405; PubMed Central PMCID: PMC109300.

190. Davis JN, McGhee L, Meyers S. The ETO (MTG8) gene family. Gene. 2003;303:1-10. PubMed PMID: 12559562.

191. Sacchi N, Tamanini F, Willemsen R, Denis-Donini S, Campiglio S, Hoogeveen AT. Subcellular localization of the oncoprotein MTG8 (CDR/ETO) in neural cells. Oncogene. 1998;16(20):2609-15. Epub 1998/06/19. doi: 10.1038/sj.onc.1201824. PubMed PMID: 9632137.

192. Melnick AM, Westendorf JJ, Polinger A, Carlile GW, Arai S, Ball HJ, et al. The ETO protein disrupted in t(8;21)-associated acute myeloid leukemia is a

corepressor for the promyelocytic leukemia zinc finger protein. Mol Cell Biol. 2000;20(6):2075-86. Epub 2000/02/25. PubMed PMID: 10688654; PubMed Central PMCID: PMC110824.

193. Fukuyama T, Sueoka E, Sugio Y, Otsuka T, Niho Y, Akagi K, et al. MTG8 proto-oncoprotein interacts with the regulatory subunit of type II cyclic AMP-dependent protein kinase in lymphocytes. Oncogene. 2001;20(43):6225-32. Epub 2001/10/11. doi: 10.1038/sj.onc.1204794. PubMed PMID: 11593431.

194. Wolford JK, Prochazka M. Structure and expression of the human MTG8/ETO gene. Gene. 1998;212(1):103-9. Epub 1998/07/14. PubMed PMID: 9661669.

195. Erickson PF, Dessev G, Lasher RS, Philips G, Robinson M, Drabkin HA. ETO and AML1 phosphoproteins are expressed in CD34+ hematopoietic progenitors: implications for t(8;21) leukemogenesis and monitoring residual disease. Blood. 1996;88(5):1813-23. Epub 1996/09/01. PubMed PMID: 8781439.

196. Okumura AJ, Peterson LF, Lo MC, Zhang DE. Expression of AML/Runx and ETO/MTG family members during hematopoietic differentiation of embryonic stem cells. Experimental hematology. 2007;35(6):978-88. Epub 2007/05/30. doi: 10.1016/j.exphem.2007.03.002. PubMed PMID: 17533052.

197. Calabi F, Cilli V. CBFA2T1, a gene rearranged in human leukemia, is a member of a multigene family. Genomics. 1998;52(3):332-41. Epub 1998/10/29. doi: 10.1006/geno.1998.5429. PubMed PMID: 9790752.

198. Morohoshi F, Mitani S, Mitsuhashi N, Kitabayashi I, Takahashi E, Suzuki M, et al. Structure and expression pattern of a human MTG8/ETO family gene, MTGR1. Gene. 2000;241(2):287-95. Epub 2000/02/16. doi: S0378111999004813 [pii]. PubMed PMID: 10675041.

199. Chevallier N, Corcoran CM, Lennon C, Hyjek E, Chadburn A, Bardwell VJ, et al. ETO protein of t(8;21) AML is a corepressor for Bcl-6 B-cell lymphoma oncoprotein. Blood. 2004;103(4):1454-63. Epub 2003/10/11. doi: 10.1182/blood-2003-06-2081

2003-06-2081 [pii]. PubMed PMID: 14551142.

200. Fischer MA, Moreno-Miralles I, Hunt A, Chyla BJ, Hiebert SW. Myeloid translocation gene 16 is required for maintenance of haematopoietic stem cell quiescence. EMBO J.31(6):1494-505. Epub 2012/01/24. doi: emboj2011500 [pii]

10.1038/emboj.2011.500. PubMed PMID: 22266796; PubMed Central PMCID: PMC3321173.

201. Allenspach EJ, Maillard I, Aster JC, Pear WS. Notch signaling in cancer. Cancer Biol Ther. 2002;1(5):466-76. Epub 2002/12/24. PubMed PMID: 12496471.

202. Artavanis-Tsakonas S, Rand MD, Lake RJ. Notch signaling: cell fate control and signal integration in development. Science. 1999;284(5415):770-6. Epub 1999/04/30. PubMed PMID: 10221902.

203. Aster JC, Pear WS, Blacklow SC. Notch signaling in leukemia. Annual review of pathology. 2008;3:587-613. Epub 2007/11/28. doi: 10.1146/annurev.pathmechdis.3.121806.154300. PubMed PMID: 18039126.

204. Gridley T. Notch signaling and inherited disease syndromes. Hum Mol Genet. 2003;12 Spec No 1:R9-13. Epub 2003/04/02. PubMed PMID: 12668592.

205. Jundt F, Schwarzer R, Dorken B. Notch signaling in leukemias and lymphomas. Current molecular medicine. 2008;8(1):51-9. Epub 2008/02/22. PubMed PMID: 18289013.

206. Miele L, Golde T, Osborne B. Notch signaling in cancer. Current molecular medicine. 2006;6(8):905-18. Epub 2006/12/16. PubMed PMID: 17168741.

207. Engel ME, Nguyen HN, Mariotti J, Hunt A, Hiebert SW. Myeloid translocation gene 16 (MTG16) interacts with Notch transcription complex components to integrate Notch signaling in hematopoietic cell fate specification. Mol Cell Biol. 2010;30(7):1852-63. Epub 2010/02/04. doi: 10.1128/MCB.01342-09. PubMed PMID: 20123979; PubMed Central PMCID: PMC2838074.

208. Kumar P, Sharoyko VV, Spegel P, Gullberg U, Mulder H, Olsson I, et al. The transcriptional co-repressor myeloid translocation gene 16 inhibits glycolysis and stimulates mitochondrial respiration. PLoS One. 2013;8(7):e68502. Epub 2013/07/11. doi: 10.1371/journal.pone.0068502. PubMed PMID: 23840896; PubMed Central PMCID: PMC3698176.

209. Moore AC, Amann JM, Williams CS, Tahinci E, Farmer TE, Martinez JA, et al. Myeloid translocation gene family members associate with T-cell factors (TCFs) and influence TCF-dependent transcription. Mol Cell Biol. 2008;28(3):977-87. PubMed PMID: 18039847.

210. Costa FF. Non-coding RNAs: lost in translation? Gene. 2007;386(1-2):1-10. Epub 2006/11/23. doi: 10.1016/j.gene.2006.09.028. PubMed PMID: 17113247.

211. Mattick JS, Makunin IV. Non-coding RNA. Hum Mol Genet. 2006;15 Spec No 1:R17-29. Epub 2006/05/03. doi: 10.1093/hmg/ddl046. PubMed PMID: 16651366.

212. Storz G. An expanding universe of noncoding RNAs. Science. 2002;296(5571):1260-3. Epub 2002/05/23. doi: 10.1126/science.1072249. PubMed PMID: 12016301.

213. Rossetti S, van Unen L, Sacchi N, Hoogeveen AT. Novel RNA-binding properties of the MTG chromatin regulatory proteins. BMC Mol Biol. 2008;9:93.

Epub 2008/10/28. doi: 10.1186/1471-2199-9-93. PubMed PMID: 18950503; PubMed Central PMCID: PMC2579434.

214. Calabi F, Pannell R, Pavloska G. Gene targeting reveals a crucial role for MTG8 in the gut. Mol Cell Biol. 2001;21(16):5658-66. Epub 2001/07/21. doi: 10.1128/MCB.21.16.5658-5666.2001. PubMed PMID: 11463846; PubMed Central PMCID: PMC87286.

215. Chyla BJ, Moreno-Miralles I, Steapleton MA, Thompson MA, Bhaskara S, Engel M, et al. Deletion of Mtg16, a target of t(16;21), alters hematopoietic progenitor cell proliferation and lineage allocation. Mol Cell Biol. 2008;28(20):6234-47. Epub 2008/08/20. doi: 10.1128/MCB.00404-08. PubMed PMID: 18710942; PubMed Central PMCID: PMC2577421.

216. Williams CS, Bradley AM, Chaturvedi R, Singh K, Piazuelo MB, Chen X, et al. MTG16 contributes to colonic epithelial integrity in experimental colitis. Gut. 2012. Epub 2012/07/27. doi: 10.1136/gutjnl-2011-301439. PubMed PMID: 22833394; PubMed Central PMCID: PMC3663894.

217. Amann JM, Chyla BJ, Ellis TC, Martinez A, Moore AC, Franklin JL, et al. Mtgr1 is a transcriptional corepressor that is required for maintenance of the secretory cell lineage in the small intestine. Mol Cell Biol. 2005;25(21):9576-85. Epub 2005/10/18. doi: 25/21/9576 [pii]

10.1128/MCB.25.21.9576-9585.2005. PubMed PMID: 16227606; PubMed Central PMCID: PMC1265807.

218. Erickson P, Gao J, Chang KS, Look T, Whisenant E, Raimondi S, et al. Identification of breakpoints in t(8;21) acute myelogenous leukemia and isolation of a fusion transcript, AML1/ETO, with similarity to Drosophila segmentation gene, runt. Blood. 1992;80(7):1825-31. Epub 1992/10/01. PubMed PMID: 1391946.

219. Acute myelogenous leukemia with an 8;21 translocation. A report on 148 cases from the Groupe Francais de Cytogenetique Hematologique. Cancer Genet Cytogenet. 1990;44(2):169-79. Epub 1990/02/01. PubMed PMID: 2297675.

220. Nucifora G, Rowley JD. AML1 and the 8;21 and 3;21 translocations in acute and chronic myeloid leukemia. Blood. 1995;86(1):1-14. Epub 1995/07/01. PubMed PMID: 7795214.

221. Langabeer SE, Walker H, Rogers JR, Burnett AK, Wheatley K, Swirsky D, et al. Incidence of AML1/ETO fusion transcripts in patients entered into the MRC AML trials. MRC Adult Leukaemia Working Party. Br J Haematol. 1997;99(4):925-8. Epub 1998/01/31. PubMed PMID: 9432044.

222. Goardon N, Lambert JA, Rodriguez P, Nissaire P, Herblot S, Thibault P, et al. ETO2 coordinates cellular proliferation and differentiation during erythropoiesis.

EMBO J. 2006;25(2):357-66. Epub 2006/01/13. doi: 10.1038/sj.emboj.7600934. PubMed PMID: 16407974; PubMed Central PMCID: PMC1383517.

223. Zhang J, Kalkum M, Yamamura S, Chait BT, Roeder RG. E protein silencing by the leukemogenic AML1-ETO fusion protein. Science. 2004;305(5688):1286-9. Epub 2004/08/31. doi: 10.1126/science.1097937. PubMed PMID: 15333839.

224. Hiebert SW, Lutterbach B, Amann J. Role of co-repressors in transcriptional repression mediated by the t(8;21), t(16;21), t(12;21), and inv(16) fusion proteins. Curr Opin Hematol. 2001;8(4):197-200. Epub 2001/09/19. PubMed PMID: 11561155.

225. Wang J, Saunthararajah Y, Redner RL, Liu JM. Inhibitors of histone deacetylase relieve ETO-mediated repression and induce differentiation of AML1-ETO leukemia cells. Cancer Res. 1999;59(12):2766-9. Epub 1999/06/26. PubMed PMID: 10383127.

226. Martinez JA, Williams CS, Amann JM, Ellis TC, Moreno-Miralles I, Washington MK, et al. Deletion of Mtgr1 sensitizes the colonic epithelium to dextran sodium sulfate-induced colitis. Gastroenterology. 2006;131(2):579-88. Epub 2006/08/08. doi: S0016-5085(06)01238-8 [pii]

10.1053/j.gastro.2006.06.009. PubMed PMID: 16890610.

227. Kochetkova M, McKenzie OL, Bais AJ, Martin JM, Secker GA, Seshadri R, et al. CBFA2T3 (MTG16) is a putative breast tumor suppressor gene from the breast cancer loss of heterozygosity region at 16q24.3. Cancer Res. 2002;62(16):4599-604. Epub 2002/08/17. PubMed PMID: 12183414.

228. Wood LD, Parsons DW, Jones S, Lin J, Sjoblom T, Leary RJ, et al. The genomic landscapes of human breast and colorectal cancers. Science. 2007;318(5853):1108-13. Epub 2007/10/13. doi: 1145720 [pii]

10.1126/science.1145720. PubMed PMID: 17932254.

229. Sjoblom T, Jones S, Wood LD, Parsons DW, Lin J, Barber TD, et al. The consensus coding sequences of human breast and colorectal cancers. Science. 2006;314(5797):268-74. PubMed PMID: 16959974.

230. Jaenisch R, Bird A. Epigenetic regulation of gene expression: how the genome integrates intrinsic and environmental signals. Nat Genet. 2003;33 Suppl:245-54. Epub 2003/03/01. doi: 10.1038/ng1089. PubMed PMID: 12610534.

231. Daniel JM, Spring CM, Crawford HC, Reynolds AB, Baig A. The p120(ctn)-binding partner Kaiso is a bi-modal DNA-binding protein that recognizes both a sequence-specific consensus and methylated CpG dinucleotides. Nucleic Acids Res.

2002;30(13):2911-9. Epub 2002/06/28. PubMed PMID: 12087177; PubMed Central PMCID: PMC117053.

232. Prokhortchouk A, Hendrich B, Jorgensen H, Ruzov A, Wilm M, Georgiev G, et al. The p120 catenin partner Kaiso is a DNA methylation-dependent transcriptional repressor. Genes Dev. 2001;15(13):1613-8. Epub 2001/07/11. doi: 10.1101/gad.198501. PubMed PMID: 11445535; PubMed Central PMCID: PMC312733.

233. Filion GJ, Zhenilo S, Salozhin S, Yamada D, Prokhortchouk E, Defossez PA. A family of human zinc finger proteins that bind methylated DNA and repress transcription. Mol Cell Biol. 2006;26(1):169-81. Epub 2005/12/16. doi: 26/1/169 [pii]

10.1128/MCB.26.1.169-181.2006. PubMed PMID: 16354688; PubMed Central PMCID: PMC1317629.

234. Daniel JM, Reynolds AB. The catenin p120(ctn) interacts with Kaiso, a novel BTB/POZ domain zinc finger transcription factor. Mol Cell Biol. 1999;19(5):3614-23. Epub 1999/04/17. PubMed PMID: 10207085; PubMed Central PMCID: PMC84161.

235. Yoon HG, Chan DW, Reynolds AB, Qin J, Wong J. N-CoR mediates DNA methylation-dependent repression through a methyl CpG binding protein Kaiso. Mol Cell. 2003;12(3):723-34. Epub 2003/10/07. PubMed PMID: 14527417.

236. Futamura M, Nishimori H, Shiratsuchi T, Saji S, Nakamura Y, Tokino T. Molecular cloning, mapping, and characterization of a novel human gene, MTA1-L1, showing homology to a metastasis-associated gene, MTA1. J Hum Genet. 1999;44(1):52-6. Epub 1999/02/04. doi: 10.1007/s100380050107. PubMed PMID: 9929979.

237. Luo J, Su F, Chen D, Shiloh A, Gu W. Deacetylation of p53 modulates its effect on cell growth and apoptosis. Nature. 2000;408(6810):377-81. Epub 2000/12/01. doi: 10.1038/35042612. PubMed PMID: 11099047.

238. Defossez PA, Kelly KF, Filion GJ, Perez-Torrado R, Magdinier F, Menoni H, et al. The human enhancer blocker CTC-binding factor interacts with the transcription factor Kaiso. J Biol Chem. 2005;280(52):43017-23. Epub 2005/10/19. doi: 10.1074/jbc.M510802200. PubMed PMID: 16230345.

239. Fiorentino FP, Giordano A. The tumor suppressor role of CTCF. J Cell Physiol. 2012;227(2):479-92. Epub 2011/04/06. doi: 10.1002/jcp.22780. PubMed PMID: 21465478.

240. Iioka H, Doerner SK, Tamai K. Kaiso is a bimodal modulator for Wnt/beta-catenin signaling. FEBS Lett. 2009;583(4):627-32. Epub 2009/01/27. doi: 10.1016/j.febslet.2009.01.012. PubMed PMID: 19166851.

241. Spring CM, Kelly KF, O'Kelly I, Graham M, Crawford HC, Daniel JM. The catenin p120ctn inhibits Kaiso-mediated transcriptional repression of the beta-catenin/TCF target gene matrilysin. Exp Cell Res. 2005;305(2):253-65. Epub 2005/04/09. doi: 10.1016/j.yexcr.2005.01.007. PubMed PMID: 15817151.

242. Adachi Y, Yamamoto H, Itoh F, Hinoda Y, Okada Y, Imai K. Contribution of matrilysin (MMP-7) to the metastatic pathway of human colorectal cancers. Gut. 1999;45(2):252-8. Epub 1999/07/14. PubMed PMID: 10403738; PubMed Central PMCID: PMC1727600.

243. Bloomston M, Zervos EE, Rosemurgy AS, 2nd. Matrix metalloproteinases and their role in pancreatic cancer: a review of preclinical studies and clinical trials. Ann Surg Oncol. 2002;9(7):668-74. Epub 2002/08/09. PubMed PMID: 12167581.

244. Crawford HC, Fingleton BM, Rudolph-Owen LA, Goss KJ, Rubinfeld B, Polakis P, et al. The metalloproteinase matrilysin is a target of beta-catenin transactivation in intestinal tumors. Oncogene. 1999;18(18):2883-91. Epub 1999/06/11. doi: 10.1038/sj.onc.1202627. PubMed PMID: 10362259.

245. Del Valle-Perez B, Casagolda D, Lugilde E, Valls G, Codina M, Dave N, et al. Wnt controls the transcriptional activity of Kaiso through CK1epsilon-dependent phosphorylation of p120-catenin. J Cell Sci. 2011;124(Pt 13):2298-309. Epub 2011/06/15. doi: 10.1242/jcs.082693. PubMed PMID: 21670201.

246. Kelly KF, Daniel JM. POZ for effect--POZ-ZF transcription factors in cancer and development. Trends Cell Biol. 2006;16(11):578-87. Epub 2006/09/26. doi: 10.1016/j.tcb.2006.09.003. PubMed PMID: 16996269.

247. Lopes EC, Valls E, Figueroa ME, Mazur A, Meng FG, Chiosis G, et al. Kaiso contributes to DNA methylation-dependent silencing of tumor suppressor genes in colon cancer cell lines. Cancer Res. 2008;68(18):7258-63. Epub 2008/09/17. doi: 10.1158/0008-5472.CAN-08-0344. PubMed PMID: 18794111.

248. Weber A, Marquardt J, Elzi D, Forster N, Starke S, Glaum A, et al. Zbtb4 represses transcription of P21CIP1 and controls the cellular response to p53 activation. EMBO J. 2008;27(11):1563-74. Epub 2008/05/03. doi: emboj200885 [pii]

10.1038/emboj.2008.85. PubMed PMID: 18451802; PubMed Central PMCID: PMC2426723.

249. Soubry A, van Hengel J, Parthoens E, Colpaert C, Van Marck E, Waltregny D, et al. Expression and nuclear location of the transcriptional repressor Kaiso is

regulated by the tumor microenvironment. Cancer Res. 2005;65(6):2224-33. Epub 2005/03/23. doi: 10.1158/0008-5472.CAN-04-2020. PubMed PMID: 15781635.

250. Jiang G, Wang Y, Dai S, Liu Y, Stoecker M, Wang E. P120-catenin isoforms 1 and 3 regulate proliferation and cell cycle of lung cancer cells via beta-catenin and Kaiso respectively. PLoS One. 2012;7(1):e30303. Epub 2012/01/26. doi: 10.1371/journal.pone.0030303. PubMed PMID: 22276175; PubMed Central PMCID: PMC3262806.

251. Prokhortchouk A, Sansom O, Selfridge J, Caballero IM, Salozhin S, Aithozhina D, et al. Kaiso-deficient mice show resistance to intestinal cancer. Mol Cell Biol. 2006;26(1):199-208. Epub 2005/12/16. doi: 26/1/199 [pii]

10.1128/MCB.26.1.199-208.2006. PubMed PMID: 16354691; PubMed Central PMCID: PMC1317619.

252. Vermeulen JF, van de Ven RA, Ercan C, van der Groep P, van der Wall E, Bult P, et al. Nuclear Kaiso expression is associated with high grade and triple-negative invasive breast cancer. PLoS One. 2012;7(5):e37864. Epub 2012/06/05. doi: 10.1371/journal.pone.0037864. PubMed PMID: 22662240; PubMed Central PMCID: PMC3360634.

253. Yan Y, Kolachala V, Dalmasso G, Nguyen H, Laroui H, Sitaraman SV, et al. Temporal and spatial analysis of clinical and molecular parameters in dextran sodium sulfate induced colitis. PLoS One. 2009;4(6):e6073. Epub 2009/06/30. doi: 10.1371/journal.pone.0006073. PubMed PMID: 19562033; PubMed Central PMCID: PMC2698136.

254. Rogler G, Andus T. Cytokines in inflammatory bowel disease. World J Surg. 1998;22(4):382-9. Epub 1998/04/02. PubMed PMID: 9523521.

255. Kennedy RJ, Hoper M, Deodhar K, Erwin PJ, Kirk SJ, Gardiner KR. Interleukin 10-deficient colitis: new similarities to human inflammatory bowel disease. Br J Surg. 2000;87(10):1346-51. Epub 2000/10/24. doi: 10.1046/j.1365-2168.2000.01615.x. PubMed PMID: 11044159.

256. Steidler L, Hans W, Schotte L, Neirynck S, Obermeier F, Falk W, et al. Treatment of murine colitis by Lactococcus lactis secreting interleukin-10. Science. 2000;289(5483):1352-5. Epub 2000/08/26. PubMed PMID: 10958782.

257. Hofstetter C, Kleen M, Habler O, Allmeling AM, Krombach F, Zwissler B. Recombinant human interleukin-10 attenuates TNFalpha production by porcine monocytes. European journal of medical research. 1998;3(6):299-303. Epub 1998/06/11. PubMed PMID: 9620892.

258. Kim IW, Myung SJ, Do MY, Ryu YM, Kim MJ, Do EJ, et al. Western-style diets induce macrophage infiltration and contribute to colitis-associated carcinogenesis. J

Gastroenterol Hepatol. 2010;25(11):1785-94. Epub 2010/11/03. doi: 10.1111/j.1440-1746.2010.06332.x. PubMed PMID: 21039842.

259. Miyazawa F, Olijnyk OR, Tilley CJ, Tamaoki T. Interactions between dextran sulfate and Escherichia coli ribosomes. Biochim Biophys Acta. 1967;145(1):96-104. Epub 1967/08/22. PubMed PMID: 4861264.

260. Fellig J, Wiley CE. The inhibition of pancreatic ribonuclease by anionic polymers. Arch Biochem Biophys. 1959;85:313-6. Epub 1959/12/01. PubMed PMID: 13822112.

261. Philipson L, Zetterqvist O. The Presence of DNA in Human Erythrocyte Membranes. Biochim Biophys Acta. 1964;91:171-3. Epub 1964/09/11. PubMed PMID: 14227268.

262. Laroui H, Ingersoll SA, Liu HC, Baker MT, Ayyadurai S, Charania MA, et al. Dextran sodium sulfate (DSS) induces colitis in mice by forming nano-lipocomplexes with medium-chain-length fatty acids in the colon. PLoS One. 2012;7(3):e32084. Epub 2012/03/20. doi: 10.1371/journal.pone.0032084. PubMed PMID: 22427817; PubMed Central PMCID: PMC3302894.

263. Okayasu I, Yamada M, Mikami T, Yoshida T, Kanno J, Ohkusa T. Dysplasia and carcinoma development in a repeated dextran sulfate sodium-induced colitis model. J Gastroenterol Hepatol. 2002;17(10):1078-83. Epub 2002/08/31. PubMed PMID: 12201867.

264. Tanaka T, Kohno H, Suzuki R, Yamada Y, Sugie S, Mori H. A novel inflammation-related mouse colon carcinogenesis model induced by azoxymethane and dextran sodium sulfate. Cancer Sci. 2003;94(11):965-73. Epub 2003/11/13. PubMed PMID: 14611673.

265. Greten FR, Eckmann L, Greten TF, Park JM, Li ZW, Egan LJ, et al. IKKbeta links inflammation and tumorigenesis in a mouse model of colitis-associated cancer. Cell. 2004;118(3):285-96. Epub 2004/08/06. doi: 10.1016/j.cell.2004.07.013

S0092867404006713 [pii]. PubMed PMID: 15294155.

266. Fukata M, Chen A, Vamadevan AS, Cohen J, Breglio K, Krishnareddy S, et al. Toll-like receptor-4 promotes the development of colitis-associated colorectal tumors. Gastroenterology. 2007;133(6):1869-81. Epub 2007/12/07. doi: S0016-5085(07)01649-6 [pii]

10.1053/j.gastro.2007.09.008. PubMed PMID: 18054559; PubMed Central PMCID: PMC2180834.

267. Lowe EL, Crother TR, Rabizadeh S, Hu B, Wang H, Chen S, et al. Toll-like receptor 2 signaling protects mice from tumor development in a mouse model of

colitis-induced cancer. PLoS One.5(9):e13027. Epub 2010/10/05. doi: 10.1371/journal.pone.0013027. PubMed PMID: 20885960; PubMed Central PMCID: PMC2946405.

268. Barrett CW, Ning W, Chen X, Smith JJ, Washington MK, Hill KE, et al. Tumor suppressor function of the plasma glutathione peroxidase gpx3 in colitis-associated carcinoma. Cancer Res. 2013;73(3):1245-55. Epub 2012/12/12. doi: 10.1158/0008-5472.CAN-12-3150. PubMed PMID: 23221387; PubMed Central PMCID: PMC3563732.

269. Barrett CW, Fingleton B, Williams A, Ning W, Fischer MA, Washington MK, et al. MTGR1 is required for tumorigenesis in the murine AOM/DSS colitis-associated carcinoma model. Cancer Res.71(4):1302-12. Epub 2011/02/10. doi: 0008-5472.CAN-10-3317 [pii]

10.1158/0008-5472.CAN-10-3317. PubMed PMID: 21303973; PubMed Central PMCID: PMC3150168.

270. Kuroki F, Matsumoto T, Iida M. Selenium is depleted in Crohn's disease on enteral nutrition. Dig Dis. 2003;21(3):266-70. Epub 2003/10/23. doi: 73346. PubMed PMID: 14571102.

271. Hoffenberg EJ, Deutsch J, Smith S, Sokol RJ. Circulating antioxidant concentrations in children with inflammatory bowel disease. Am J Clin Nutr. 1997;65(5):1482-8. Epub 1997/05/01. PubMed PMID: 9129480.

272. Rannem T, Ladefoged K, Hylander E, Hegnhoj J, Jarnum S. Selenium status in patients with Crohn's disease. Am J Clin Nutr. 1992;56(5):933-7. Epub 1992/11/01. PubMed PMID: 1415013.

273. Reimund JM, Hirth C, Koehl C, Baumann R, Duclos B. Antioxidant and immune status in active Crohn's disease. A possible relationship. Clin Nutr. 2000;19(1):43-8. Epub 2000/03/04. doi: 10.1054/clnu.1999.0073. PubMed PMID: 10700533.

274. Andoh A, Hirashima M, Maeda H, Hata K, Inatomi O, Tsujikawa T, et al. Serum selenoprotein-P levels in patients with inflammatory bowel disease. Nutrition. 2005;21(5):574-9. Epub 2005/04/27. doi: 10.1016/j.nut.2004.08.025. PubMed PMID: 15850963.

275. Loftus EV, Jr. Clinical epidemiology of inflammatory bowel disease: Incidence, prevalence, and environmental influences. Gastroenterology. 2004;126(6):1504-17. Epub 2004/05/29. PubMed PMID: 15168363.

276. Kirsner JB. Inflammatory bowel disease. Part II: Clinical and therapeutic aspects. Disease-a-month : DM. 1991;37(11):669-746. Epub 1991/11/01. PubMed PMID: 1935537.

277. Kirsner JB. Inflammatory bowel disease. Part I: Nature and pathogenesis. Disease-a-month : DM. 1991;37(10):605-66. Epub 1991/10/01. PubMed PMID: 1893828.

278. Vatn MH. Natural history and complications of IBD. Current gastroenterology reports. 2009;11(6):481-7. Epub 2009/11/12. PubMed PMID: 19903424.

279. Kirsner JB. The local and systemic complications of inflammatory bowel disease. JAMA. 1979;242(11):1177-83. Epub 1979/09/14. PubMed PMID: 470073.

280. Ringstad J, Kildebo S, Thomassen Y. Serum selenium, copper, and zinc concentrations in Crohn's disease and ulcerative colitis. Scand J Gastroenterol. 1993;28(7):605-8. Epub 1993/07/01. PubMed PMID: 8362213.

281. Han PD, Burke A, Baldassano RN, Rombeau JL, Lichtenstein GR. Nutrition and inflammatory bowel disease. Gastroenterol Clin North Am. 1999;28(2):423-43, ix. Epub 1999/06/18. PubMed PMID: 10372275.

282. Sturniolo GC, Mestriner C, Lecis PE, D'Odorico A, Venturi C, Irato P, et al. Altered plasma and mucosal concentrations of trace elements and antioxidants in active ulcerative colitis. Scand J Gastroenterol. 1998;33(6):644-9. Epub 1998/07/21. PubMed PMID: 9669638.

283. Ojuawo A, Keith L. The serum concentrations of zinc, copper and selenium in children with inflammatory bowel disease. The Central African journal of medicine. 2002;48(9-10):116-9. Epub 2003/10/18. PubMed PMID: 14562534.

284. Mannick EE, Bonomolo JC, Horswell R, Lentz JJ, Serrano MS, Zapata-Velandia A, et al. Gene expression in mononuclear cells from patients with inflammatory bowel disease. Clin Immunol. 2004;112(3):247-57. Epub 2004/08/17. doi: 10.1016/j.clim.2004.03.014. PubMed PMID: 15308118.

285. Denson LA, Long MD, McGovern DP, Kugathasan S, Wu GD, Young VB, et al. Challenges in IBD research: update on progress and prioritization of the CCFA's research agenda. Inflamm Bowel Dis. 2013;19(4):677-82. Epub 2013/03/02. doi: 10.1097/MIB.0b013e31828134b3. PubMed PMID: 23448796.

286. Kipp A, Banning A, van Schothorst EM, Meplan C, Schomburg L, Evelo C, et al. Four selenoproteins, protein biosynthesis, and Wnt signalling are particularly sensitive to limited selenium intake in mouse colon. Mol Nutr Food Res. 2009;53(12):1561-72. Epub 2009/10/08. doi: 10.1002/mnfr.200900105. PubMed PMID: 19810021.

287. Yin F, Sancheti H, Cadenas E. Mitochondrial thiols in the regulation of cell death pathways. Antioxidants & redox signaling. 2012;17(12):1714-27. Epub 2012/04/26. doi: 10.1089/ars.2012.4639. PubMed PMID: 22530585; PubMed Central PMCID: PMC3474184.

288. Clark LC, Cantor KP, Allaway WH. Selenium in forage crops and cancer mortality in U.S. counties. Arch Environ Health. 1991;46(1):37-42. Epub 1991/01/01. doi: 10.1080/00039896.1991.9937427. PubMed PMID: 1992931.

289. Combs GF, Jr., Gray WP. Chemopreventive agents: selenium. Pharmacol Ther. 1998;79(3):179-92. Epub 1998/10/17. PubMed PMID: 9776375.

290. Jaworska K, Gupta S, Durda K, Muszynska M, Sukiennicki G, Jaworowska E, et al. A low selenium level is associated with lung and laryngeal cancers. PLoS One. 2013;8(3):e59051. Epub 2013/03/22. doi: 10.1371/journal.pone.0059051. PubMed PMID: 23516596; PubMed Central PMCID: PMC3596323.

291. Schrauzer GN. Trace elements, nutrition and cancer: perspectives of prevention. Adv Exp Med Biol. 1977;91:323-44. Epub 1977/01/01. PubMed PMID: 605853.

292. Irons R, Carlson BA, Hatfield DL, Davis CD. Both selenoproteins and low molecular weight selenocompounds reduce colon cancer risk in mice with genetically impaired selenoprotein expression. J Nutr. 2006;136(5):1311-7. Epub 2006/04/15. doi: 136/5/1311 [pii]. PubMed PMID: 16614422.

293. Florian S, Wingler K, Schmehl K, Jacobasch G, Kreuzer OJ, Meyerhof W, et al. Cellular and subcellular localization of gastrointestinal glutathione peroxidase in normal and malignant human intestinal tissue. Free Radic Res. 2001;35(6):655-63. Epub 2002/01/29. PubMed PMID: 11811519.

294. Mork H, al-Taie OH, Bahr K, Zierer A, Beck C, Scheurlen M, et al. Inverse mRNA expression of the selenocysteine-containing proteins GI-GPx and SeP in colorectal adenomas compared with adjacent normal mucosa. Nutr Cancer. 2000;37(1):108-16. Epub 2000/08/31. doi: 10.1207/S15327914NC3701_14. PubMed PMID: 10965527.

295. Lin YM, Furukawa Y, Tsunoda T, Yue CT, Yang KC, Nakamura Y. Molecular diagnosis of colorectal tumors by expression profiles of 50 genes expressed differentially in adenomas and carcinomas. Oncogene. 2002;21(26):4120-8. Epub 2002/05/31. doi: 10.1038/sj.onc.1205518. PubMed PMID: 12037668.

296. Chu FF, Esworthy RS, Chu PG, Longmate JA, Huycke MM, Wilczynski S, et al. Bacteria-induced intestinal cancer in mice with disrupted Gpx1 and Gpx2 genes. Cancer Res. 2004;64(3):962-8. Epub 2004/02/12. PubMed PMID: 14871826.

297. Krehl S, Loewinger M, Florian S, Kipp AP, Banning A, Wessjohann LA, et al. Glutathione peroxidase-2 and selenium decreased inflammation and tumors in a mouse model of inflammation-associated carcinogenesis whereas sulforaphane effects differed with selenium supply. Carcinogenesis. 2012;33(3):620-8. Epub 2011/12/20. doi: 10.1093/carcin/bgr288. PubMed PMID: 22180572; PubMed Central PMCID: PMC3291858.

298. Murawaki Y, Tsuchiya H, Kanbe T, Harada K, Yashima K, Nozaka K, et al. Aberrant expression of selenoproteins in the progression of colorectal cancer. Cancer Lett. 2008;259(2):218-30. Epub 2007/12/07. doi: 10.1016/j.canlet.2007.10.019. PubMed PMID: 18054426.

299. Dincer Y, Erzin Y, Himmetoglu S, Gunes KN, Bal K, Akcay T. Oxidative DNA damage and antioxidant activity in patients with inflammatory bowel disease. Dig Dis Sci. 2007;52(7):1636-41. Epub 2007/03/30. doi: 10.1007/s10620-006-9386-8. PubMed PMID: 17393334.

300. Ekbom A, Helmick C, Zack M, Adami HO. Ulcerative colitis and colorectal cancer. A population-based study. N Engl J Med. 1990;323(18):1228-33. Epub 1990/11/01. PubMed PMID: 2215606.

301. Hill KE, Zhou J, McMahan WJ, Motley AK, Burk RF. Neurological dysfunction occurs in mice with targeted deletion of the selenoprotein P gene. J Nutr. 2004;134(1):157-61. Epub 2004/01/06. PubMed PMID: 14704310.

302. Becker C, Fantini MC, Wirtz S, Nikolaev A, Kiesslich R, Lehr HA, et al. In vivo imaging of colitis and colon cancer development in mice using high resolution chromoendoscopy. Gut. 2005;54(7):950-4. Epub 2005/06/14. doi: 10.1136/gut.2004.061283. PubMed PMID: 15951540; PubMed Central PMCID: PMC1774595.

303. Washington MK, Powell AE, Sullivan R, Sundberg JP, Wright N, Coffey RJ, et al. Pathology of rodent models of intestinal cancer: progress report and recommendations. Gastroenterology. 2013;144(4):705-17. Epub 2013/02/19. doi: 10.1053/j.gastro.2013.01.067. PubMed PMID: 23415801; PubMed Central PMCID: PMC3660997.

304. Boivin GP, Washington K, Yang K, Ward JM, Pretlow TP, Russell R, et al. Pathology of mouse models of intestinal cancer: consensus report and recommendations. Gastroenterology. 2003;124(3):762-77. Epub 2003/03/04. doi: 10.1053/gast.2003.50094. PubMed PMID: 12612914.

305. Koh TS, Benson TH. Critical re-appraisal of fluorometric method for determination of selenium in biological materials. J Assoc Off Anal Chem. 1983;66(4):918-26. Epub 1983/07/01. PubMed PMID: 6885699.

306. Sheehan TM, Gao M. Simplified fluorometric assay of total selenium in plasma and urine. Clin Chem. 1990;36(12):2124-6. Epub 1990/12/01. PubMed PMID: 2253359.

307. Lawrence RA, Burk RF. Glutathione peroxidase activity in selenium-deficient rat liver. Biochem Biophys Res Commun. 1976;71(4):952-8. Epub 1976/08/23. doi: 0006-291X(76)90747-6 [pii]. PubMed PMID: 971321.

308. Paglia DE, Valentine WN. Studies on the quantitative and qualitative characterization of erythrocyte glutathione peroxidase. J Lab Clin Med. 1967;70(1):158-69. Epub 1967/07/01. PubMed PMID: 6066618.

309. Milne GL, Sanchez SC, Musiek ES, Morrow JD. Quantification of F2-isoprostanes as a biomarker of oxidative stress. Nat Protoc. 2007;2(1):221-6. Epub 2007/04/03. doi: 10.1038/nprot.2006.375. PubMed PMID: 17401357.

310. Koller FL, Dozier EA, Nam KT, Swee M, Birkland TP, Parks WC, et al. Lack of MMP10 exacerbates experimental colitis and promotes development of inflammation-associated colonic dysplasia. Lab Invest. 2012;92(12):1749-59. Epub 2012/10/10. doi: 10.1038/labinvest.2012.141. PubMed PMID: 23044923; PubMed Central PMCID: PMC3510327.

311. Gentschew L, Bishop KS, Han DY, Morgan AR, Fraser AG, Lam WJ, et al. Selenium, selenoprotein genes and Crohn's disease in a case-control population from Auckland, New Zealand. Nutrients. 2012;4(9):1247-59. Epub 2012/11/01. doi: 10.3390/nu4091247. PubMed PMID: 23112913; PubMed Central PMCID: PMC3475235.

312. Circu ML, Aw TY. Intestinal redox biology and oxidative stress. Semin Cell Dev Biol. 2012;23(7):729-37. Epub 2012/04/10. doi: 10.1016/j.semcdb.2012.03.014. PubMed PMID: 22484611; PubMed Central PMCID: PMC3396776.

313. Thomas PD, Campbell MJ, Kejariwal A, Mi H, Karlak B, Daverman R, et al. PANTHER: a library of protein families and subfamilies indexed by function. Genome Res. 2003;13(9):2129-41. Epub 2003/09/04. doi: 10.1101/gr.772403. PubMed PMID: 12952881; PubMed Central PMCID: PMC403709.

314. Beckett GJ, Arthur JR. Selenium and endocrine systems. J Endocrinol. 2005;184(3):455-65. Epub 2005/03/08. doi: 10.1677/joe.1.05971. PubMed PMID: 15749805.

315. Seril DN, Liao J, Yang GY, Yang CS. Oxidative stress and ulcerative colitis-associated carcinogenesis: studies in humans and animal models. Carcinogenesis. 2003;24(3):353-62. Epub 2003/03/29. PubMed PMID: 12663492.

316. Kadiiska MB, Gladen BC, Baird DD, Germolec D, Graham LB, Parker CE, et al. Biomarkers of oxidative stress study II: are oxidation products of lipids, proteins, and DNA markers of CCl4 poisoning? Free Radic Biol Med. 2005;38(6):698-710. Epub 2005/02/22. doi: 10.1016/j.freeradbiomed.2004.09.017. PubMed PMID: 15721980.

317. Ferguson LR, Karunasinghe N, Zhu S, Wang AH. Selenium and its' role in the maintenance of genomic stability. Mutat Res.733(1-2):100-10. Epub 2012/01/12. doi: S0027-5107(11)00325-3 [pii]

10.1016/j.mrfmmm.2011.12.011. PubMed PMID: 22234051.

318. Pegg AE. Methylation of the O6 position of guanine in DNA is the most likely initiating event in carcinogenesis by methylating agents. Cancer Invest. 1984;2(3):223-31. Epub 1984/01/01. PubMed PMID: 6733565.

319. Okayasu I, Ohkusa T, Kajiura K, Kanno J, Sakamoto S. Promotion of colorectal neoplasia in experimental murine ulcerative colitis. Gut. 1996;39(1):87-92. Epub 1996/07/01. PubMed PMID: 8881816; PubMed Central PMCID: PMC1383238.

320. Okayasu I, Hatakeyama S, Yamada M, Ohkusa T, Inagaki Y, Nakaya R. A novel method in the induction of reliable experimental acute and chronic ulcerative colitis in mice. Gastroenterology. 1990;98(3):694-702. Epub 1990/03/01. PubMed PMID: 1688816.

321. Hong MY, Turner ND, Carroll RJ, Chapkin RS, Lupton JR. Differential response to DNA damage may explain different cancer susceptibility between small and large intestine. Exp Biol Med (Maywood). 2005;230(7):464-71. Epub 2005/06/30. PubMed PMID: 15985621.

322. Chang SH, Reynolds JM, Pappu BP, Chen G, Martinez GJ, Dong C. Interleukin-17C promotes Th17 cell responses and autoimmune disease via interleukin-17 receptor E. Immunity. 2011;35(4):611-21. Epub 2011/10/11. doi: 10.1016/j.immuni.2011.09.010. PubMed PMID: 21982598.

323. Neurath MF. IL-23: a master regulator in Crohn disease. Nat Med. 2007;13(1):26-8. Epub 2007/01/09. doi: 10.1038/nm0107-26. PubMed PMID: 17206128.

324. Damiani CR, Benetton CA, Stoffel C, Bardini KC, Cardoso VH, Di Giunta G, et al. Oxidative stress and metabolism in animal model of colitis induced by dextran sulfate sodium. J Gastroenterol Hepatol. 2007;22(11):1846-51. Epub 2007/05/11. doi: 10.1111/j.1440-1746.2007.04890.x. PubMed PMID: 17489966.

325. Trivedi PP, Jena GB. Ulcerative colitis-induced hepatic damage in mice: studies on inflammation, fibrosis, oxidative DNA damage and GST-P expression. Chem Biol Interact. 2013;201(1-3):19-30. Epub 2012/12/25. doi: 10.1016/j.cbi.2012.12.004. PubMed PMID: 23261717.

326. Stucchi AF, Shofer S, Leeman S, Materne O, Beer E, McClung J, et al. NK-1 antagonist reduces colonic inflammation and oxidative stress in dextran sulfate-induced colitis in rats. Am J Physiol Gastrointest Liver Physiol. 2000;279(6):G1298-306. Epub 2000/11/30. PubMed PMID: 11093954.

327. Carrier J, Aghdassi E, Cullen J, Allard JP. Iron supplementation increases disease activity and vitamin E ameliorates the effect in rats with dextran sulfate

sodium-induced colitis. J Nutr. 2002;132(10):3146-50. Epub 2002/10/09. PubMed PMID: 12368409.

328. Ying Y, Liu XM, Marble A, Lawson KA, Zhao GQ. Requirement of Bmp8b for the generation of primordial germ cells in the mouse. Mol Endocrinol. 2000;14(7):1053-63. Epub 2000/07/14. PubMed PMID: 10894154.

329. Frierson HF, Jr., El-Naggar AK, Welsh JB, Sapinoso LM, Su AI, Cheng J, et al. Large scale molecular analysis identifies genes with altered expression in salivary adenoid cystic carcinoma. Am J Pathol. 2002;161(4):1315-23. Epub 2002/10/09. doi: 10.1016/S0002-9440(10)64408-2. PubMed PMID: 12368205; PubMed Central PMCID: PMC1867312.

330. Langenskiold M, Holmdahl L, Falk P, Angenete E, Ivarsson ML. Increased TGF-beta 1 protein expression in patients with advanced colorectal cancer. J Surg Oncol. 2008;97(5):409-15. Epub 2008/01/08. doi: 10.1002/jso.20961. PubMed PMID: 18176914.

331. Saltzman BS, Yamamoto JF, Decker R, Yokochi L, Theriault AG, Vogt TM, et al. Association of genetic variation in the transforming growth factor beta-1 gene with serum levels and risk of colorectal neoplasia. Cancer Res. 2008;68(4):1236-44. Epub 2008/02/19. doi: 10.1158/0008-5472.CAN-07-2144. PubMed PMID: 18281501.

332. Rhodes DR, Yu J, Shanker K, Deshpande N, Varambally R, Ghosh D, et al. ONCOMINE: a cancer microarray database and integrated data-mining platform. Neoplasia. 2004;6(1):1-6. Epub 2004/04/08. PubMed PMID: 15068665; PubMed Central PMCID: PMC1635162.

333. Skrzypczak M, Goryca K, Rubel T, Paziewska A, Mikula M, Jarosz D, et al. Modeling oncogenic signaling in colon tumors by multidirectional analyses of microarray data directed for maximization of analytical reliability. PLoS One. 2010;5(10). Epub 2010/10/20. doi: 10.1371/journal.pone.0013091. PubMed PMID: 20957034; PubMed Central PMCID: PMC2948500.

334. Modjtahedi H, Dean C. The receptor for EGF and its ligands - expression, prognostic value and target for therapy in cancer (review). Int J Oncol. 1994;4(2):277-96. Epub 1994/02/01. PubMed PMID: 21566922.

335. Pasquale EB. Eph receptors and ephrins in cancer: bidirectional signalling and beyond. Nat Rev Cancer. 2010;10(3):165-80. Epub 2010/02/25. doi: 10.1038/nrc2806. PubMed PMID: 20179713; PubMed Central PMCID: PMC2921274.

336. Hill KE, Zhou J, McMahan WJ, Motley AK, Atkins JF, Gesteland RF, et al. Deletion of selenoprotein P alters distribution of selenium in the mouse. J Biol Chem. 2003;278(16):13640-6. Epub 2003/02/08. doi: 10.1074/jbc.M300755200

M300755200 [pii]. PubMed PMID: 12574155.

337. Schrauzer GN, White DA, Schneider CJ. Cancer mortality correlation studies--III: statistical associations with dietary selenium intakes. Bioinorg Chem. 1977;7(1):23-31. Epub 1977/01/01. PubMed PMID: 856291.

338. Rachmilewitz D, Stamler JS, Bachwich D, Karmeli F, Ackerman Z, Podolsky DK. Enhanced colonic nitric oxide generation and nitric oxide synthase activity in ulcerative colitis and Crohn's disease. Gut. 1995;36(5):718-23. Epub 1995/05/01. PubMed PMID: 7541008; PubMed Central PMCID: PMC1382676.

339. Hudson TS, Carlson BA, Hoeneroff MJ, Young HA, Sordillo L, Muller WJ, et al. Selenoproteins reduce susceptibility to DMBA-induced mammary carcinogenesis. Carcinogenesis. Epub 2012/03/23. doi: bgs129 [pii]

10.1093/carcin/bgs129. PubMed PMID: 22436612.

340. Maiorino M, Aumann KD, Brigelius-Flohe R, Doria D, van den Heuvel J, McCarthy J, et al. Probing the presumed catalytic triad of selenium-containing peroxidases by mutational analysis of phospholipid hydroperoxide glutathione peroxidase (PHGPx). Biol Chem Hoppe Seyler. 1995;376(11):651-60. Epub 1995/11/01. PubMed PMID: 8962674.

341. Olson GE, Whitin JC, Hill KE, Winfrey VP, Motley AK, Austin LM, et al. Extracellular glutathione peroxidase (Gpx3) binds specifically to basement membranes of mouse renal cortex tubule cells. Am J Physiol Renal Physiol.298(5):F1244-53. Epub 2009/12/18. doi: 00662.2009 [pii]

10.1152/ajprenal.00662.2009. PubMed PMID: 20015939; PubMed Central PMCID: PMC2867408.

342. Maeda K, Okubo K, Shimomura I, Mizuno K, Matsuzawa Y, Matsubara K. Analysis of an expression profile of genes in the human adipose tissue. Gene. 1997;190(2):227-35. Epub 1997/05/06. doi: S0378-1119(96)00730-5 [pii]. PubMed PMID: 9197538.

343. Chu FF, Esworthy RS, Doroshow JH, Doan K, Liu XF. Expression of plasma glutathione peroxidase in human liver in addition to kidney, heart, lung, and breast in humans and rodents. Blood. 1992;79(12):3233-8. Epub 1992/06/15. PubMed PMID: 1339300.

344. Tham DM, Whitin JC, Kim KK, Zhu SX, Cohen HJ. Expression of extracellular glutathione peroxidase in human and mouse gastrointestinal tract. Am J Physiol. 1998;275(6 Pt 1):G1463-71. Epub 1998/12/09. PubMed PMID: 9843785.

345. Avissar N, Ornt DB, Yagil Y, Horowitz S, Watkins RH, Kerl EA, et al. Human kidney proximal tubules are the main source of plasma glutathione peroxidase. Am J Physiol. 1994;266(2 Pt 1):C367-75. Epub 1994/02/01. PubMed PMID: 8141250.

346. Burk RF, Olson GE, Winfrey VP, Hill KE, Yin D. Glutathione peroxidase-3 produced by the kidney binds to a population of basement membranes in the gastrointestinal tract and in other tissues. Am J Physiol Gastrointest Liver Physiol.301(1):G32-8. Epub 2011/04/16. doi: ajpgi.00064.2011 [pii]

10.1152/ajpgi.00064.2011. PubMed PMID: 21493731; PubMed Central PMCID: PMC3280860.

347. Chen B, Rao X, House MG, Nephew KP, Cullen KJ, Guo Z. GPx3 promoter hypermethylation is a frequent event in human cancer and is associated with tumorigenesis and chemotherapy response. Cancer Lett.309(1):37-45. Epub 2011/06/21. doi: S0304-3835(11)00279-5 [pii]

10.1016/j.canlet.2011.05.013. PubMed PMID: 21684681.

348. Zhang X, Yang JJ, Kim YS, Kim KY, Ahn WS, Yang S. An 8-gene signature, including methylated and down-regulated glutathione peroxidase 3, of gastric cancer. Int J Oncol.36(2):405-14. Epub 2010/01/01. PubMed PMID: 20043075.

349. Yu YP, Yu G, Tseng G, Cieply K, Nelson J, Defrances M, et al. Glutathione peroxidase 3, deleted or methylated in prostate cancer, suppresses prostate cancer growth and metastasis. Cancer Res. 2007;67(17):8043-50. Epub 2007/09/07. doi: 67/17/8043 [pii]

10.1158/0008-5472.CAN-07-0648. PubMed PMID: 17804715.

350. Esworthy RS, Aranda R, Martin MG, Doroshow JH, Binder SW, Chu FF. Mice with combined disruption of Gpx1 and Gpx2 genes have colitis. Am J Physiol Gastrointest Liver Physiol. 2001;281(3):G848-55. Epub 2001/08/24. PubMed PMID: 11518697.

351. Chu FF, Esworthy RS, Doroshow JH. Role of Se-dependent glutathione peroxidases in gastrointestinal inflammation and cancer. Free Radic Biol Med. 2004;36(12):1481-95. Epub 2004/06/09. doi: 10.1016/j.freeradbiomed.2004.04.010

S0891584904003132 [pii]. PubMed PMID: 15182851.

352. D'Odorico A, D'Inca R, Mestriner C, Di Leo V, Ferronato A, Sturniolo GC. Influence of disease site and activity on peripheral neutrophil function in inflammatory bowel disease. Dig Dis Sci. 2000;45(8):1594-600. Epub 2000/09/28. PubMed PMID: 11007111.

353. Eaden J. Review article: colorectal carcinoma and inflammatory bowel disease. Aliment Pharmacol Ther. 2004;20 Suppl 4:24-30. Epub 2004/09/09. doi: 10.1111/j.1365-2036.2004.02046.x

APT2046 [pii]. PubMed PMID: 15352890.

354. Mayer R, Wong WD, Rothenberger DA, Goldberg SM, Madoff RD. Colorectal cancer in inflammatory bowel disease: a continuing problem. Dis Colon Rectum. 1999;42(3):343-7. Epub 1999/05/01. PubMed PMID: 10223754.

355. Popivanova BK, Kitamura K, Wu Y, Kondo T, Kagaya T, Kaneko S, et al. Blocking TNF-alpha in mice reduces colorectal carcinogenesis associated with chronic colitis. J Clin Invest. 2008;118(2):560-70. Epub 2008/01/26. doi: 10.1172/JCI32453. PubMed PMID: 18219394; PubMed Central PMCID: PMC2213370.

356. Uronis JM, Muhlbauer M, Herfarth HH, Rubinas TC, Jones GS, Jobin C. Modulation of the intestinal microbiota alters colitis-associated colorectal cancer susceptibility. PLoS One. 2009;4(6):e6026. Epub 2009/06/25. doi: 10.1371/journal.pone.0006026. PubMed PMID: 19551144; PubMed Central PMCID: PMC2696084.

357. Dieleman LA, Palmen MJ, Akol H, Bloemena E, Pena AS, Meuwissen SG, et al. Chronic experimental colitis induced by dextran sulphate sodium (DSS) is characterized by Th1 and Th2 cytokines. Clin Exp Immunol. 1998;114(3):385-91. Epub 1998/12/09. PubMed PMID: 9844047; PubMed Central PMCID: PMC1905133.

358. Becker C, Fantini MC, Neurath MF. High resolution colonoscopy in live mice. Nat Protoc. 2006;1(6):2900-4. Epub 2007/04/05. doi: nprot.2006.446 [pii]

10.1038/nprot.2006.446. PubMed PMID: 17406549.

359. Chaturvedi R, Asim M, Romero-Gallo J, Barry DP, Hoge S, de Sablet T, et al. Spermine oxidase mediates the gastric cancer risk associated with Helicobacter pylori CagA. Gastroenterology.141(5):1696-708 e1-2. Epub 2011/08/16. doi: S0016-5085(11)01080-8 [pii]

10.1053/j.gastro.2011.07.045. PubMed PMID: 21839041; PubMed Central PMCID: PMC3202654.

360. Carlson BA, Yoo MH, Sano Y, Sengupta A, Kim JY, Irons R, et al. Selenoproteins regulate macrophage invasiveness and extracellular matrix-related gene expression. BMC Immunol. 2009;10:57. Epub 2009/10/30. doi: 1471-2172-10-57 [pii]

10.1186/1471-2172-10-57. PubMed PMID: 19863805; PubMed Central PMCID: PMC2774298.

361. Yasui Y, Tanaka T. Protein expression analysis of inflammation-related colon carcinogenesis. J Carcinog. 2009;8:10. Epub 2009/06/06. doi: JCarcinog_2009_8_1_10_51851 [pii]

10.4103/1477-3163.51851. PubMed PMID: 19491504; PubMed Central PMCID: PMC2699605.

362. Bartsch H, Nair J. Potential role of lipid peroxidation derived DNA damage in human colon carcinogenesis: studies on exocyclic base adducts as stable oxidative stress markers. Cancer Detect Prev. 2002;26(4):308-12. Epub 2002/11/15. PubMed PMID: 12430635.

363. Fridovich I. Fundamental aspects of reactive oxygen species, or what's the matter with oxygen? Ann N Y Acad Sci. 1999;893:13-8. Epub 2000/02/15. PubMed PMID: 10672226.

364. Muscoli C, Cuzzocrea S, Riley DP, Zweier JL, Thiemermann C, Wang ZQ, et al. On the selectivity of superoxide dismutase mimetics and its importance in pharmacological studies. Br J Pharmacol. 2003;140(3):445-60. Epub 2003/10/03. doi: 10.1038/sj.bjp.0705430

140/3/445 [pii]. PubMed PMID: 14522841; PubMed Central PMCID: PMC1574047.

365. Dix TA, Hess KM, Medina MA, Sullivan RW, Tilly SL, Webb TL. Mechanism of site-selective DNA nicking by the hydrodioxyl (perhydroxyl) radical. Biochemistry. 1996;35(14):4578-83. Epub 1996/04/09. doi: 10.1021/bi952010w

bi952010w [pii]. PubMed PMID: 8605208.

366. Cheng KC, Cahill DS, Kasai H, Nishimura S, Loeb LA. 8-Hydroxyguanine, an abundant form of oxidative DNA damage, causes G----T and A----C substitutions. J Biol Chem. 1992;267(1):166-72. Epub 1992/01/05. PubMed PMID: 1730583.

367. Hussain SP, Harris CC. Molecular epidemiology of human cancer: contribution of mutation spectra studies of tumor suppressor genes. Cancer Res. 1998;58(18):4023-37. Epub 1998/09/29. PubMed PMID: 9751603.

368. Sica A, Bronte V. Altered macrophage differentiation and immune dysfunction in tumor development. J Clin Invest. 2007;117(5):1155-66. Epub 2007/05/04. doi: 10.1172/JCI31422. PubMed PMID: 17476345; PubMed Central PMCID: PMC1857267.

369. Kiremidjian-Schumacher L, Roy M, Wishe HI, Cohen MW, Stotzky G. Regulation of cellular immune responses by selenium. Biol Trace Elem Res. 1992;33:23-35. Epub 1992/04/01. PubMed PMID: 1379457.

370. Kiremidjian-Schumacher L, Roy M, Wishe HI, Cohen MW, Stotzky G. Supplementation with selenium and human immune cell functions. II. Effect on cytotoxic lymphocytes and natural killer cells. Biol Trace Elem Res. 1994;41(1-2):115-27. Epub 1994/04/01. PubMed PMID: 7946899.

371. Burk RF, Hill KE. Selenoprotein P. A selenium-rich extracellular glycoprotein. J Nutr. 1994;124(10):1891-7. Epub 1994/10/01. PubMed PMID: 7931697.

372. Schomburg L, Schweizer U, Holtmann B, Flohe L, Sendtner M, Kohrle J. Gene disruption discloses role of selenoprotein P in selenium delivery to target tissues. Biochem J. 2003;370(Pt 2):397-402. Epub 2003/01/11. doi: 10.1042/BJ20021853

BJ20021853 [pii]. PubMed PMID: 12521380; PubMed Central PMCID: PMC1223208.

373. Arteel GE, Mostert V, Oubrahim H, Briviba K, Abel J, Sies H. Protection by selenoprotein P in human plasma against peroxynitrite-mediated oxidation and nitration. Biol Chem. 1998;379(8-9):1201-5. Epub 1998/10/29. PubMed PMID: 9792455.

374. Shamberger RJ, Willis CE. Selenium distribution and human cancer mortality. CRC Crit Rev Clin Lab Sci. 1971;2(2):211-21. Epub 1971/06/01. PubMed PMID: 4950948.

375. Bosschaerts T, Guilliams M, Noel W, Herin M, Burk RF, Hill KE, et al. Alternatively activated myeloid cells limit pathogenicity associated with African trypanosomiasis through the IL-10 inducible gene selenoprotein P. J Immunol. 2008;180(9):6168-75. Epub 2008/04/22. PubMed PMID: 18424738.

376. Lee SR, Yon JM, Baek IJ, Kim MR, Park CG, Lee BJ, et al. Spatiotemporal expression of the selenoprotein P gene in postimplantational mouse embryos. Int J Dev Biol. 2008;52(7):1005-11. Epub 2008/10/29. doi: 082656sl [pii]

10.1387/ijdb.082656sl. PubMed PMID: 18956332.

377. Olson GE, Winfrey VP, Hill KE, Burk RF. Megalin mediates selenoprotein P uptake by kidney proximal tubule epithelial cells. J Biol Chem. 2008;283(11):6854-60. Epub 2008/01/05. doi: 10.1074/jbc.M709945200. PubMed PMID: 18174160.

378. Zhang X, Goncalves R, Mosser DM. The isolation and characterization of murine macrophages. Curr Protoc Immunol. 2008;Chapter 14:Unit 14 1. Epub 2008/11/20. doi: 10.1002/0471142735.im1401s83. PubMed PMID: 19016445; PubMed Central PMCID: PMC2834554.

379. Mosser DM, Zhang X. Activation of murine macrophages. Curr Protoc Immunol. 2008;Chapter 14:Unit 14 2. Epub 2008/11/20. doi: 10.1002/0471142735.im1402s83. PubMed PMID: 19016446; PubMed Central PMCID: PMC2822273.

380. Read R, Bellew T, Yang JG, Hill KE, Palmer IS, Burk RF. Selenium and amino acid composition of selenoprotein P, the major selenoprotein in rat serum. J Biol Chem. 1990;265(29):17899-905. Epub 1990/10/15. PubMed PMID: 2211667.

381. Solinas G, Schiarea S, Liguori M, Fabbri M, Pesce S, Zammataro L, et al. Tumor-conditioned macrophages secrete migration-stimulating factor: a new marker for M2-polarization, influencing tumor cell motility. J Immunol.185(1):642-52. Epub 2010/06/10. doi: jimmunol.1000413 [pii]

10.4049/jimmunol.1000413. PubMed PMID: 20530259.

382. Ghassabeh GH, De Baetselier P, Brys L, Noel W, Van Ginderachter JA, Meerschaut S, et al. Identification of a common gene signature for type II cytokine-associated myeloid cells elicited in vivo in different pathologic conditions. Blood. 2006;108(2):575-83. Epub 2006/03/25. doi: 10.1182/blood-2005-04-1485. PubMed PMID: 16556895.

383. Connelly-Frost A, Poole C, Satia JA, Kupper LL, Millikan RC, Sandler RS. Selenium, folate, and colon cancer. Nutr Cancer. 2009;61(2):165-78. Epub 2009/02/24. doi: 10.1080/01635580802404188. PubMed PMID: 19235033; PubMed Central PMCID: PMC2743456.

384. Barrett CW, Singh K, Motley AK, Lintel MK, Matafonova E, Bradley AM, et al. Dietary Selenium Deficiency Exacerbates DSS-Induced Epithelial Injury and AOM/DSS-Induced Tumorigenesis. PLoS One. 2013;8(7):e67845. Epub 2013/07/19. doi: 10.1371/journal.pone.0067845. PubMed PMID: 23861820; PubMed Central PMCID: PMC3701622.

385. Renko K, Werner M, Renner-Muller I, Cooper TG, Yeung CH, Hollenbach B, et al. Hepatic selenoprotein P (SePP) expression restores selenium transport and prevents infertility and motor-incoordination in Sepp-knockout mice. Biochem J. 2008;409(3):741-9. Epub 2007/10/27. doi: 10.1042/BJ20071172. PubMed PMID: 17961124.

386. Xiao W, Zhu Y, Sarsour EH, Kalen AL, Aykin-Burns N, Spitz DR, et al. Selenoprotein P regulates 1-(4-Chlorophenyl)-benzo-2,5-quinone-induced oxidative stress and toxicity in human keratinocytes. Free Radic Biol Med. 2013;65C:70-7. Epub 2013/06/19. doi: 10.1016/j.freeradbiomed.2013.06.010. PubMed PMID: 23770201.

387. Sampson N, Koziel R, Zenzmaier C, Bubendorf L, Plas E, Jansen-Durr P, et al. ROS signaling by NOX4 drives fibroblast-to-myofibroblast differentiation in the diseased prostatic stroma. Mol Endocrinol. 2011;25(3):503-15. Epub 2011/01/29. doi: 10.1210/me.2010-0340. PubMed PMID: 21273445.

388. Sato T, Clevers H. Growing self-organizing mini-guts from a single intestinal stem cell: mechanism and applications. Science. 2013;340(6137):1190-4. Epub 2013/06/08. doi: 10.1126/science.1234852. PubMed PMID: 23744940.

389. Fuller MK, Faulk DM, Sundaram N, Shroyer NF, Henning SJ, Helmrath MA. Intestinal crypts reproducibly expand in culture. J Surg Res. 2012;178(1):48-54. Epub 2012/05/09. doi: 10.1016/j.jss.2012.03.037. PubMed PMID: 22564827; PubMed Central PMCID: PMC3654833.

390. Murawaki Y, Tsuchiya H, Kanbe T, Harada K, Yashima K, Nozaka K, et al. Aberrant expression of selenoproteins in the progression of colorectal cancer. Cancer Lett. 2008;259(2):218-30. Epub 2007/12/07. doi: 10.1016/j.canlet.2007.10.019. PubMed PMID: 18054426.

391. Steinbrenner H, Alili L, Bilgic E, Sies H, Brenneisen P. Involvement of selenoprotein P in protection of human astrocytes from oxidative damage. Free Radic Biol Med. 2006;40(9):1513-23. Epub 2006/04/25. doi: S0891-5849(05)00759-8 [pii]

10.1016/j.freeradbiomed.2005.12.022. PubMed PMID: 16632112.

392. Gu P, Goodwin B, Chung AC, Xu X, Wheeler DA, Price RR, et al. Orphan nuclear receptor LRH-1 is required to maintain Oct4 expression at the epiblast stage of embryonic development. Mol Cell Biol. 2005;25(9):3492-505. Epub 2005/04/16. doi: 10.1128/MCB.25.9.3492-3505.2005. PubMed PMID: 15831456; PubMed Central PMCID: PMC1084298.

393. Danielson PB. The cytochrome P450 superfamily: biochemistry, evolution and drug metabolism in humans. Current drug metabolism. 2002;3(6):561-97. Epub 2002/10/09. PubMed PMID: 12369887.

394. Robertson G, Leclercq I, Farrell GC. Nonalcoholic steatosis and steatohepatitis. II. Cytochrome P-450 enzymes and oxidative stress. Am J Physiol Gastrointest Liver Physiol. 2001;281(5):G1135-9. Epub 2001/10/23. PubMed PMID: 11668021.

395. Kan Z, Jaiswal BS, Stinson J, Janakiraman V, Bhatt D, Stern HM, et al. Diverse somatic mutation patterns and pathway alterations in human cancers. Nature.466(7308):869-73. Epub 2010/07/30. doi: nature09208 [pii]

10.1038/nature09208. PubMed PMID: 20668451.

396. Chyla B, Moreno-Miralles I, Steapleton M, Thompson M, Bhaskara S, Engel M, et al. Deletion of Mtg16, a target of the t(16;21), alters hematopoietic progenitor cell proliferation and lineage allocation. Mol Cell Biol. 2008. doi: MCB.00404-08 [pii]

10.1128/MCB.00404-08. PubMed PMID: 18710942.

397. Ostrand-Rosenberg S, Sinha P. Myeloid-derived suppressor cells: linking inflammation and cancer. J Immunol. 2009;182(8):4499-506. Epub 2009/04/04. doi: 182/8/4499 [pii]

10.4049/jimmunol.0802740. PubMed PMID: 19342621; PubMed Central PMCID: PMC2810498.

398. Berasain C, Castillo J, Perugorria MJ, Latasa MU, Prieto J, Avila MA. Inflammation and liver cancer: new molecular links. Ann N Y Acad Sci. 2009;1155:206-21. Epub 2009/03/03. doi: NYAS03704 [pii]

10.1111/j.1749-6632.2009.03704.x. PubMed PMID: 19250206.

399. Swann JB, Smyth MJ. Immune surveillance of tumors. J Clin Invest. 2007;117(5):1137-46. Epub 2007/05/04. doi: 10.1172/JCI31405. PubMed PMID: 17476343; PubMed Central PMCID: PMC1857231.

400. Greten FR, Eckmann L, Greten TF, Park JM, Li Z-W, Egan LJ, et al. IKKbeta links inflammation and tumorigenesis in a mouse model of colitis-associated cancer. Cell. 2004;118(3):285-96. doi: 10.1016/j.cell.2004.07.013. PubMed PMID: 15294155.

401. Popivanova B, Kitamura K, Wu Y, Kondo T, Kagaya T, Kaneko S, et al. Blocking TNF-alpha in mice reduces colorectal carcinogenesis associated with chronic colitis. J Clin Invest. 2008;118(2):560-70. doi: 10.1172/JCI32453. PubMed PMID: 18219394.

402. Grivennikov S, Karin E, Terzic J, Mucida D, Yu G-Y, Vallabhapurapu S, et al. IL-6 and Stat3 are required for survival of intestinal epithelial cells and development of colitis-associated cancer. Cancer Cell. 2009;15(2):103-13. doi: 10.1016/j.ccr.2009.01.001. PubMed PMID: 19185845.

403. Uronis JM, Mühlbauer M, Herfarth HH, Rubinas TC, Jones GS, Jobin C, et al. Modulation of the Intestinal Microbiota Alters Colitis-Associated Colorectal Cancer Susceptibility. PLoS ONE. 2009;4(6):e6026. doi: 10.1371/journal.pone.0006026.g007.

404. Fingleton B, Powell WC, Crawford HC, Couchman JR, Matrisian LM. A rat monoclonal antibody that recognizes pro- and active MMP-7 indicates polarized expression in vivo. Hybridoma (Larchmt). 2007;26(1):22-7. Epub 2007/02/24. doi: 10.1089/hyb.2006.028. PubMed PMID: 17316082.

405. Cotta CV, Zhang Z, Kim HG, Klug CA. Pax5 determines B- versus T-cell fate and does not block early myeloid-lineage development. Blood. 2003;101(11):4342-6. Epub 2003/02/01. doi: 10.1182/blood-2002-10-3139

2002-10-3139 [pii]. PubMed PMID: 12560221.

406. Wilson CL, Heppner KJ, Labosky PA, Hogan BL, Matrisian LM. Intestinal tumorigenesis is suppressed in mice lacking the metalloproteinase matrilysin. Proc Natl Acad Sci U S A. 1997;94(4):1402-7. Epub 1997/02/18. PubMed PMID: 9037065; PubMed Central PMCID: PMC19803.

407. Allavena P, Sica A, Garlanda C, Mantovani A. The Yin-Yang of tumor-associated macrophages in neoplastic progression and immune surveillance. Immunol Rev. 2008;222:155-61. doi: 10.1111/j.1600-065X.2008.00607.x. PubMed PMID: 18364000.

408. Kozu T, Komori A, Sueoka E, Fujiki H, Kaneko Y, Matsui T, et al. Significance of MTG8 in leukemogenesis. Leukemia. 1997;11 Suppl 3:297-8. Epub 1997/04/01. PubMed PMID: 9209371.

409. Feagins LA, Souza RF, Spechler SJ. Carcinogenesis in IBD: potential targets for the prevention of colorectal cancer. Nat Rev Gastroenterol Hepatol. 2009;6(5):297-305. Epub 2009/05/01. doi: nrgastro.2009.44 [pii]

10.1038/nrgastro.2009.44. PubMed PMID: 19404270.

410. Wagenaar-Miller RA, Gorden L, Matrisian LM. Matrix metalloproteinases in colorectal cancer: is it worth talking about? Cancer Metastasis Rev. 2004;23(1-2):119-35. Epub 2004/03/06. PubMed PMID: 15000153.

411. Sinnamon MJ, Carter KJ, Fingleton B, Matrisian LM. Matrix metalloproteinase-9 contributes to intestinal tumourigenesis in the adenomatous polyposis coli multiple intestinal neoplasia mouse. Int J Exp Pathol. 2008;89(6):466-75. Epub 2009/01/13. doi: IEP621 [pii]

10.1111/j.1365-2613.2008.00621.x. PubMed PMID: 19134056; PubMed Central PMCID: PMC2669608.

412. Fingleton B, Vargo-Gogola T, Crawford HC, Matrisian LM. Matrilysin [MMP-7] expression selects for cells with reduced sensitivity to apoptosis. Neoplasia. 2001;3(6):459-68. Epub 2002/01/05. doi: 10.1038/sj/neo/7900190. PubMed PMID: 11774028; PubMed Central PMCID: PMC1506562.

413. Powell WC, Fingleton B, Wilson CL, Boothby M, Matrisian LM. The metalloproteinase matrilysin proteolytically generates active soluble Fas ligand and potentiates epithelial cell apoptosis. Curr Biol. 1999;9(24):1441-7. Epub 1999/12/23. doi: S0960-9822(00)80113-X [pii]. PubMed PMID: 10607586.

414. Yu WH, Woessner JF, Jr., McNeish JD, Stamenkovic I. CD44 anchors the assembly of matrilysin/MMP-7 with heparin-binding epidermal growth factor precursor and ErbB4 and regulates female reproductive organ remodeling. Genes Dev. 2002;16(3):307-23. Epub 2002/02/05. doi: 10.1101/gad.925702. PubMed PMID: 11825873; PubMed Central PMCID: PMC155329.

415. Noe V, Fingleton B, Jacobs K, Crawford HC, Vermeulen S, Steelant W, et al. Release of an invasion promoter E-cadherin fragment by matrilysin and stromelysin-1. J Cell Sci. 2001;114(Pt 1):111-8. Epub 2000/12/12. PubMed PMID: 11112695.

416. Sasai N, Nakao M, Defossez PA. Sequence-specific recognition of methylated DNA by human zinc-finger proteins. Nucleic Acids Res.38(15):5015-22. Epub 2010/04/21. doi: gkq280 [pii]

10.1093/nar/gkq280. PubMed PMID: 20403812; PubMed Central PMCID: PMC2926618.

417. Bethany A. Buck-Koehntop MAM-Y, H. Jane Dyson, Peter E. Wright. Kaiso uses all three zinc fingers and adjacent sequence motifs for high affinity binding to sequence-specific and methyl-CpG DNA targets. FEBS J. 2012;586:734-9. Epub 30 January 2012.

418. Park JI, Kim SW, Lyons JP, Ji H, Nguyen TT, Cho K, et al. Kaiso/p120-catenin and TCF/beta-catenin complexes coordinately regulate canonical Wnt gene targets. Dev Cell. 2005;8(6):843-54. Epub 2005/06/07. doi: S1534-5807(05)00141-3 [pii]

10.1016/j.devcel.2005.04.010. PubMed PMID: 15935774.

419. Del Valle-Perez B, Casagolda D, Lugilde E, Valls G, Codina M, Dave N, et al. Wnt controls the transcriptional activity of Kaiso through CK1epsilon-dependent phosphorylation of p120-catenin. J Cell Sci.124(Pt 13):2298-309. Epub 2011/06/15. doi: 124/13/2298 [pii]

10.1242/jcs.082693. PubMed PMID: 21670201.

420. Dai SD, Wang Y, Zhang JY, Zhang D, Zhang PX, Jiang GY, et al. Upregulation of delta-catenin is associated with poor prognosis and enhances transcriptional activity through Kaiso in non-small-cell lung cancer. Cancer Sci.102(1):95-103. Epub 2010/11/13. doi: 10.1111/j.1349-7006.2010.01766.x. PubMed PMID: 21070476.

421. Kim K, Chadalapaka G, Lee SO, Yamada D, Sastre-Garau X, Defossez PA, et al. Identification of oncogenic microRNA-17-92/ZBTB4/specificity protein axis in breast cancer. Oncogene.31(8):1034-44. Epub 2011/07/19. doi: onc2011296 [pii]

10.1038/onc.2011.296. PubMed PMID: 21765466; PubMed Central PMCID: PMC3288192.

422. Hartley JL, Temple, G.F., Brasch, M.A. DNA Cloning Using In Vitro Site-Specific Recombination. Genome Res. 2000(10):1788-95. doi: 10.1101/gr.143000.

423. Smith JJ, Deane NG, Wu F, Merchant NB, Zhang B, Jiang A, et al. Experimentally derived metastasis gene expression profile predicts recurrence and

death in patients with colon cancer. Gastroenterology.138(3):958-68. Epub 2009/11/17. doi: S0016-5085(09)01964-7 [pii]

10.1053/j.gastro.2009.11.005. PubMed PMID: 19914252.

424. Williams CS, Zhang B, Smith JJ, Jayagopal A, Barrett CW, Pino C, et al. BVES regulates EMT in human corneal and colon cancer cells and is silenced via promoter methylation in human colorectal carcinoma. J Clin Invest.121(10):4056-69. Epub 2011/09/14. doi: 44228 [pii]

10.1172/JCI44228. PubMed PMID: 21911938; PubMed Central PMCID: PMC3195453.

425. Singh AB, Sharma A, Smith JJ, Krishnan M, Chen X, Eschrich S, et al. Claudin-1 up-regulates the repressor ZEB-1 to inhibit E-cadherin expression in colon cancer cells. Gastroenterology.141(6):2140-53. Epub 2011/09/01. doi: S0016-5085(11)01221-2 [pii]

10.1053/j.gastro.2011.08.038. PubMed PMID: 21878201.

426. Soler E, Andrieu-Soler C, de Boer E, Bryne JC, Thongjuea S, Stadhouders R, et al. The genome-wide dynamics of the binding of Ldb1 complexes during erythroid differentiation. Genes Dev.24(3):277-89. Epub 2010/02/04. doi: 24/3/277 [pii]

10.1101/gad.551810. PubMed PMID: 20123907; PubMed Central PMCID: PMC2811829.

427. Lynch CC, Hikosaka A, Acuff HB, Martin MD, Kawai N, Singh RK, et al. MMP-7 promotes prostate cancer-induced osteolysis via the solubilization of RANKL. Cancer Cell. 2005;7(5):485-96. Epub 2005/05/17. doi: S1535-6108(05)00124-8 [pii]

10.1016/j.ccr.2005.04.013. PubMed PMID: 15894268.

428. Liu D, Nakano J, Ishikawa S, Yokomise H, Ueno M, Kadota K, et al. Overexpression of matrix metalloproteinase-7 (MMP-7) correlates with tumor proliferation, and a poor prognosis in non-small cell lung cancer. Lung Cancer. 2007;58(3):384-91. Epub 2007/08/31. doi: S0169-5002(07)00414-X [pii]

10.1016/j.lungcan.2007.07.005. PubMed PMID: 17728005.

429. Westermarck J, Kahari VM. Regulation of matrix metalloproteinase expression in tumor invasion. FASEB J. 1999;13(8):781-92. Epub 1999/05/04. PubMed PMID: 10224222.

430. Crawford HC, Fingleton B, Gustavson MD, Kurpios N, Wagenaar RA, Hassell JA, et al. The PEA3 subfamily of Ets transcription factors synergizes with beta-

catenin-LEF-1 to activate matrilysin transcription in intestinal tumors. Mol Cell Biol. 2001;21(4):1370-83. PubMed PMID: 11158322.

431. Jiang G, Wang Y, Dai S, Liu Y, Stoecker M, Wang E. P120-catenin isoforms 1 and 3 regulate proliferation and cell cycle of lung cancer cells via beta-catenin and Kaiso respectively. PLoS One.7(1):e30303. Epub 2012/01/26. doi: 10.1371/journal.pone.0030303

PONE-D-11-19390 [pii]. PubMed PMID: 22276175; PubMed Central PMCID: PMC3262806.

432. van Roy FM, McCrea PD. A role for Kaiso-p120ctn complexes in cancer? Nat Rev Cancer. 2005;5(12):956-64. Epub 2005/11/19. doi: nrc1752 [pii]

10.1038/nrc1752. PubMed PMID: 16294216.

433. Brabletz T, Jung A, Dag S, Hlubek F, Kirchner T. beta-catenin regulates the expression of the matrix metalloproteinase-7 in human colorectal cancer. Am J Pathol. 1999;155(4):1033-8. Epub 1999/10/09. doi: S0002-9440(10)65204-2 [pii]. PubMed PMID: 10514384; PubMed Central PMCID: PMC1867011.

434. Kim EJ, Lee SY, Woo MK, Choi SI, Kim TR, Kim MJ, et al. Fibulin-3 promoter methylation alters the invasive behavior of non-small cell lung cancer cell lines via MMP-7 and MMP-2 regulation. Int J Oncol.40(2):402-8. Epub 2011/09/09. doi: 10.3892/ijo.2011.1191. PubMed PMID: 21901248.

435. Chang MC, Chen CA, Chen PJ, Chiang YC, Chen YL, Mao TL, et al. Mesothelin enhances invasion of ovarian cancer by inducing MMP-7 through MAPK/ERK and JNK pathways. Biochem J.442(2):293-302. Epub 2011/10/18. doi: BJ20110282 [pii]

10.1042/BJ20110282. PubMed PMID: 21999204.

436. Stetler-Stevenson WG. Dynamics of matrix turnover during pathologic remodeling of the extracellular matrix. Am J Pathol. 1996;148(5):1345-50. Epub 1996/05/01. PubMed PMID: 8623905; PubMed Central PMCID: PMC1861572.

437. Coussens LM, Fingleton B, Matrisian LM. Matrix metalloproteinase inhibitors and cancer: trials and tribulations. Science. 2002;295(5564):2387-92. Epub 2002/03/30. doi: 10.1126/science.1067100

295/5564/2387 [pii]. PubMed PMID: 11923519.

438. Hai T, Hartman MG. The molecular biology and nomenclature of the activating transcription factor/cAMP responsive element binding family of transcription factors: activating transcription factor proteins and homeostasis. Gene. 2001;273(1):1-11. Epub 2001/08/03. doi: S0378-1119(01)00551-0 [pii]. PubMed PMID: 11483355.

439. van Dam H, Castellazzi M. Distinct roles of Jun : Fos and Jun : ATF dimers in oncogenesis. Oncogene. 2001;20(19):2453-64. Epub 2001/06/13. doi: 10.1038/sj.onc.1204239. PubMed PMID: 11402340.

440. Kaszubska W, Hooft van Huijsduijnen R, Ghersa P, DeRaemy-Schenk AM, Chen BP, Hai T, et al. Cyclic AMP-independent ATF family members interact with NF-kappa B and function in the activation of the E-selectin promoter in response to cytokines. Mol Cell Biol. 1993;13(11):7180-90. Epub 1993/11/01. PubMed PMID: 7692236; PubMed Central PMCID: PMC364779.

441. Hui L, Bakiri L, Mairhorfer A, Schweifer N, Haslinger C, Kenner L, et al. p38alpha suppresses normal and cancer cell proliferation by antagonizing the JNK-c-Jun pathway. Nat Genet. 2007;39(6):741-9. Epub 2007/05/01. doi: ng2033 [pii]

10.1038/ng2033. PubMed PMID: 17468757.

442. Ventura JJ, Tenbaum S, Perdiguero E, Huth M, Guerra C, Barbacid M, et al. p38alpha MAP kinase is essential in lung stem and progenitor cell proliferation and differentiation. Nat Genet. 2007;39(6):750-8. Epub 2007/05/01. doi: ng2037 [pii]

10.1038/ng2037. PubMed PMID: 17468755.

443. Kajino T, Omori E, Ishii S, Matsumoto K, Ninomiya-Tsuji J. TAK1 MAPK kinase kinase mediates transforming growth factor-beta signaling by targeting SnoN oncoprotein for degradation. J Biol Chem. 2007;282(13):9475-81. Epub 2007/02/06. doi: M700875200 [pii]

10.1074/jbc.M700875200. PubMed PMID: 17276978; PubMed Central PMCID: PMC2175395.

444. Barrett CW, Smith JJ, Lu LC, Markham N, Stengel KR, Short SP, et al. Kaiso directs the transcriptional corepressor MTG16 to the Kaiso binding site in target promoters. PLoS One. 2012;7(12):e51205. Epub 2012/12/20. doi: 10.1371/journal.pone.0051205. PubMed PMID: 23251453; PubMed Central PMCID: PMC3521008.

445. . !!! INVALID CITATION !!!

446. Kim SW, Park JI, Spring CM, Sater AK, Ji H, Otchere AA, et al. Non-canonical Wnt signals are modulated by the Kaiso transcriptional repressor and p120-catenin. Nat Cell Biol. 2004;6(12):1212-20. Epub 2004/11/16. doi: 10.1038/ncb1191. PubMed PMID: 15543138.

447. Rodova M, Kelly KF, VanSaun M, Daniel JM, Werle MJ. Regulation of the rapsyn promoter by kaiso and delta-catenin. Mol Cell Biol. 2004;24(16):7188-96. Epub 2004/07/30. doi: 10.1128/MCB.24.16.7188-7196.2004. PubMed PMID: 15282317; PubMed Central PMCID: PMC479716.

448. Dhir M, Montgomery EA, Glockner SC, Schuebel KE, Hooker CM, Herman JG, et al. Epigenetic regulation of WNT signaling pathway genes in inflammatory bowel disease (IBD) associated neoplasia. Journal of gastrointestinal surgery : official journal of the Society for Surgery of the Alimentary Tract. 2008;12(10):1745-53. Epub 2008/08/22. doi: 10.1007/s11605-008-0633-5. PubMed PMID: 18716850.

449. Massague J. A very private TGF-beta receptor embrace. Mol Cell. 2008;29(2):149-50. Epub 2008/02/05. doi: 10.1016/j.molcel.2008.01.006. PubMed PMID: 18243107.

450. Gonsalves FC, Klein K, Carson BB, Katz S, Ekas LA, Evans S, et al. An RNAi-based chemical genetic screen identifies three small-molecule inhibitors of the Wnt/wingless signaling pathway. Proc Natl Acad Sci U S A. 2011;108(15):5954-63. Epub 2011/03/12. doi: 10.1073/pnas.1017496108. PubMed PMID: 21393571; PubMed Central PMCID: PMC3076864.

451. Moossavi S, Bishehsari F. Inflammation in sporadic colorectal cancer. Arch Iran Med. 2012;15(3):166-70. Epub 2012/03/01. doi: 012153/AIM.0012. PubMed PMID: 22369306.

452. Laederich MB, Funes-Duran M, Yen L, Ingalla E, Wu X, Carraway KL, 3rd, et al. The leucine-rich repeat protein LRIG1 is a negative regulator of ErbB family receptor tyrosine kinases. J Biol Chem. 2004;279(45):47050-6. Epub 2004/09/04. doi: 10.1074/jbc.M409703200. PubMed PMID: 15345710.

453. Powell AE, Wang Y, Li Y, Poulin EJ, Means AL, Washington MK, et al. The pan-ErbB negative regulator Lrig1 is an intestinal stem cell marker that functions as a tumor suppressor. Cell. 2012;149(1):146-58. Epub 2012/04/03. doi: 10.1016/j.cell.2012.02.042. PubMed PMID: 22464327; PubMed Central PMCID: PMC3563328.

454. el Marjou F, Janssen KP, Chang BH, Li M, Hindie V, Chan L, et al. Tissue-specific and inducible Cre-mediated recombination in the gut epithelium. Genesis. 2004;39(3):186-93. Epub 2004/07/30. doi: 10.1002/gene.20042. PubMed PMID: 15282745.

455. Kuhn R, Schwenk F, Aguet M, Rajewsky K. Inducible gene targeting in mice. Science. 1995;269(5229):1427-9. Epub 1995/09/08. PubMed PMID: 7660125.

456. Gurney A, Axelrod F, Bond CJ, Cain J, Chartier C, Donigan L, et al. Wnt pathway inhibition via the targeting of Frizzled receptors results in decreased growth and tumorigenicity of human tumors. Proc Natl Acad Sci U S A. 2012;109(29):11717-22. Epub 2012/07/04. doi: 10.1073/pnas.1120068109. PubMed PMID: 22753465; PubMed Central PMCID: PMC3406803.